

**Controls on coalbed methane potential and gas sorption characteristics
of high-volatile bituminous coals in Indiana**

Wilfrido Solano-Acosta

Submitted to the faculty of the University Graduate School
in partial fulfillment of the requirements for the degree
Doctor of Philosophy
in the Department of Geological Sciences,
Indiana University
July 2007

Accepted by the Graduate Faculty, Indiana University, in partial fulfillment of the requirements for the degree of Doctor of Philosophy

Arndt Schimmelmann, Ph.D. (Chair)

Maria Mastalerz, Ph.D. (Co-Chair)

Doctoral Committee

Juergen Schieber, Ph.D.

July 23rd, 2007

Greg. A. Olyphant, Ph.D. (Minor Advisor)

© Copyright, 2007

Wilfrido Solano-Acosta

ALL RIGHTS RESERVED

Al amor de mi vida:

Ilusión y sueños
Razón para continuar
Esperanza
Necesidad
Estímulo constante

Acknowledgments

I thank all members of my doctoral committee, and especially Maria Mastalerz, Arndt Schimmelmann, and Greg A. Olyphant for their guidance, direction, dedication friendship, and constant support.

Thanks to my colleagues and friends of the Indiana Geological Survey, especially John A. Rupp for his friendship, leadership, and encouragement to further my education, Charly (and Martha) Zuppann for their friendship and for adopting me during the final stages of my dissertation (you were my home away from home), John C. Steinmetz, Deb DeChurch, Brian Keith, Richard (Dick) Powell, Kathleen Griffin, and all the IGS personnel that remains and that has left the Survey during this past 6 years for their friendship.

Thanks to Arindam Sarkar, Ed Ripley, David Bish, John Fong, and Peter Sauer for their helpful suggestions and advice at different stages of this work. I would also thank Gary Fleener (Director of mechanical instrument services and his crew at the Chemistry machine shop) and Tim Johnson for their ideas and precision work during construction of the small-volume high-pressure volumetric adsorption apparatus.

I especially thank my parents for their love and support throughout all my life, my siblings, spouses and their beautiful children who make my life more pleasant when I have them around; the Arango family for their moral support, love, friendship, and especially for bringing to this world the most special person I could ever meet, my wife Irene, without whom I'd be a broken compass, not knowing where to point.

Funding from this work included the John Patton Award from the Indiana Geological Survey and multiple other grants awarded to M. Mastalerz, A. Schimmelmann, and John A. Rupp. I would also like to thank Agnieszka Drobniak, Grzegorz Lis, and Dariusz Strapoć for their assistance in the field, as well as Phil Ames, Matt Atkins, and Chris Hutchison for providing access to several coal mines in southwestern Indiana, USA.

Abstract

The increasing demand for energy and a growing concern for global warming, owing in part to the steep rise in anthropogenic greenhouse gas emissions, have sparked worldwide interest in clean coal technologies. Although the energy potential of coal is large, there are many environmental concerns associated with its large-scale utilization. An alternative solution to increasing demand for energy is the recovery of coalbed methane (CBM), an efficient and clean fossil fuel associated with extensive coal deposits. CBM today represents nearly 10 percent of the energy consumed in the United States. From an environmental perspective, coal beds that are too deep or that contain low-quality coal are being investigated as potential sites for permanently sequestering carbon dioxide emissions (CO₂ sequestration).

Methane has been documented in coals of various ranks. The occurrence and distribution of economically recoverable quantities of CBM result from the interplay between stratigraphy, tectonics, and hydrology. This study evaluates geologic factors that control the occurrence of CBM in Indiana coals, ranging from large-scale processes (i.e., burial and fracturing) to molecular interactions between CBM and the physical structure of coal (i.e., gas adsorption). This study investigates the role of tectonics and burial in the formation of coal fracture sets (cleats) that are critical for CBM extraction. Based on field data, I investigate the role of fracturing with regard to gas occurrence and CBM producibility. The timing of cleat formation is evaluated via carbon and oxygen isotopic signatures of cleat-filling minerals. In addition to field-scale observations, this study includes an experimental component that, based on a multitude of laboratory data, constrains optimum conditions for coal-sample preservation prior to laboratory analyses for exploration. Chemical analyses, petrography, grain-size distributions, Fourier transform infra-red (FTIR) spectroscopy, pore distribution, and adsorption experiments at high

and low gas pressures are employed to estimate reservoir gas capacity and to characterize high volatile bituminous coals of Indiana for potential future CO₂ sequestration.

Understanding the mechanisms and geologic conditions that control the occurrence of gas in coal allows us to better characterize: (1) CBM reservoirs for their potential economic use, and (2) coal seams as future receptacles of anthropogenic carbon dioxide.

Table of contents

	page
Title page _____	i
Signature page _____	ii
Copyright notice _____	iii
Dedication _____	iv
Acknowledgments _____	v
Abstract _____	vi
Table of contents _____	viii
List of tables _____	xi
List of figures _____	xiv
 Chapter 1 – Introduction _____	 1
1.1. Objectives and significance _____	2
1.2. Coalbed methane (CBM) _____	5
1.3. CO ₂ sequestration _____	7
 Chapter 2 – Methods and data acquisition _____	 11
2.1. Field data collection _____	12
2.1.1. Coalbed methane exploratory drillings _____	12
2.1.2. Cleats and fracture measurements and coal sampling _____	14
2.2. Laboratory analyses _____	14
2.2.1. Stable isotope analyses and X-ray diffraction _____	15
2.2.2. Petrographic and chemical analyses _____	15
2.2.3. Fourier Transform Infrared Spectroscopy (FTIR) _____	16
2.2.4. Surface area, pore size distribution, and grain size analyses _____	16
2.2.5. High-pressure adsorption analyses _____	17
2.3. Practical definitions _____	18
 Chapter 3 – Geology and coalbed methane potential of the Illinois Basin and Indiana _____	 20
3.1. The Illinois Basin _____	21

3.1.1. The Pennsylvanian System _____	23
3.1.2. Coalbed methane potential of the Illinois Basin _____	26
3.1.3. Coalbed methane potential of Indiana _____	27
Chapter 4 – Coal-bed gas potential in Pennsylvanian coal beds of Indiana _____	30
4.1. Introduction _____	32
4.2. Pennsylvanian coal stratigraphy _____	33
4.3. Previous studies _____	37
4.4. Coal distribution _____	37
4.5. Gas content _____	49
4.6. Gas origin _____	54
4.7. Conclusions _____	58
Chapter 5 - Cleats and their relation to geologic lineaments, and coalbed methane potential in Pennsylvanian coals in Indiana _____	62
5.1. Introduction _____	65
5.2. Geologic framework _____	66
5.3. Methods _____	71
5.3.1. Measurements of macro- and mesocleats _____	71
5.3.2. Microcleat analysis _____	81
5.3.3. Lineament analysis _____	82
5.4. Results _____	83
5.4.1. Macro- and mesocleats data _____	83
5.4.2. Microcleat data _____	88
5.4.3. Lineament data _____	95
5.5. Discussion _____	97
5.5.1. Mechanisms of cleat formation _____	97
5.5.2. Cleat spacing _____	103
5.5.3. Cleats and geologic lineaments _____	113
5.5.4. Cleats and permeability _____	117
5.5.5. Cleats and coalbed methane potential _____	122
5.6. Conclusions _____	124

Chapter 6 - Diagenetic mineralization in Pennsylvanian coals from Indiana, USA: $^{13}\text{C}/^{12}\text{C}$ and $^{18}\text{O}/^{16}\text{O}$ implications for cleat origin and coalbed methane generation	136
6.1. Introduction	138
6.2. Materials and methods	143
6.2.1. Sample origin	143
6.2.2. X-ray diffraction	145
6.2.3. Oxygen and carbon stable isotope ratios	145
6.2.4. Temperature corrections	146
6.3. Results	147
6.4. Discussion	151
6.4.1. Thermal history of the Illinois basin	151
6.4.2. Isotopic equilibrium between oxygen in minerals and water during mineralization	151
6.4.3. Significance of $^{18}\text{O}/^{16}\text{O}$ ratio of water for paleotemperature estimates	154
6.4.3.1. Mineralization scenario A: low temperature and $\delta^{18}\text{O}_{\text{water}} \sim -6.2\text{‰}$	156
6.4.3.2. Mineralization scenario B: intermediate temperature and $\delta^{18}\text{O}_{\text{water}} \sim$ -1.25‰	163
6.4.3.3. Mineralization scenario C: intermediate temperature and $\delta^{18}\text{O}_{\text{water}} \sim 3\text{‰}$	166
6.4.3.4. Mineralization scenario D: high temperature and $\delta^{18}\text{O}_{\text{water}} \sim 7.5\text{‰}$	167
6.4.4. Implications for coalbed methane occurrence	168
6.5. Conclusions	172
Chapter 7 – Effects of coal storage in air on physical and chemical coal properties and on gas adsorption at low pressure	181
7.1. Introduction	182
7.2. Methods	186
7.2.1. Sample preparation	187
7.2.2. Proximate and ultimate coal chemical analyses	188
7.2.3. Petrographic analyses	188
7.2.4. Surface area and pore size distribution	189

7.2.5. Fourier transform infrared (FTIR) spectroscopy _____	193
7.2.6. Outline of experimental strategy _____	194
7.3. Results _____	196
7.3.1. Proximate and ultimate chemical coal analyses _____	196
7.3.2. Petrographic analyses _____	199
7.3.3. Mesopore characteristics constrained by low-pressure N ₂ adsorption ____	199
7.3.4. Micropore characteristics constrained by low-pressure CO ₂ adsorption ____	206
7.3.5. Fourier transform infra-red (FTIR) analyses _____	215
7.4. Discussion _____	221
7.4.1. Elemental chemistry and petrographic changes _____	221
7.4.2. Changes in physical properties _____	222
7.4.3. Effects of air exposure on gas adsorption characteristics in coal _____	224
7.4.4. Changes in the abundance of chemical functional groups _____	224
7.4.5. Implications for CO ₂ sequestration in coal _____	226
7.4. Conclusions _____	228

Chapter 8 – Effects of grain size, maceral composition, and moisture content

on adsorption characteristics of bituminous coals _____	235
8.1. Introduction _____	236
8.1.1. Influence of particle size on CO ₂ and CH ₄ sorption _____	240
8.1.2. Influence of coal type on CO ₂ and CH ₄ sorption _____	241
8.1.3. Effects of moisture content on gas sorption in coal _____	243
8.2. Methods _____	244
8.2.1. Experimental approach, sample selection, and sample preparation _____	244
8.2.2. Preparation of grain size fractions and petrographic characterization _____	248
8.2.3. High-pressure adsorption analysis _____	248
8.2.3.1. Instrumentation _____	248
8.2.3.2. Data acquisition _____	252
8.2.4. Low-pressure gas adsorption measurements _____	255
8.3. Results and Discussion _____	259
8.3.1. High-pressure CH ₄ adsorption of CH ₄ on coal _____	259

8.3.1.1. CH ₄ adsorption capacity of dry versus moisture-equilibrated coals _____	259
8.3.1.2. Changes in CH ₄ adsorption capacity with increasing time of exposure to air _____	261
8.3.2. High-pressure CO ₂ adsorption of CO ₂ on coal _____	264
8.3.2.1. CO ₂ adsorption capacity of dry versus moisture-equilibrated coals _____	264
8.3.2.2. Changes in CO ₂ adsorption capacity with increasing time of exposure to air _____	266
8.3.3. Effects of moisture loss on high-pressure gas adsorption in coal _____	272
8.3.4. Influence of particle size on gas adsorption: results from a large-volume high-pressure volumetric adsorption apparatus _____	277
8.3.5. Petrographic data, ash content, and equilibrium moisture content _____	281
8.3.6. Grain size analyses _____	283
8.3.7. Mesopore characteristics constrained by low-pressure N ₂ adsorption _____	285
8.3.8. Micropore characteristics constrained by low-pressure CO ₂ adsorption _____	291
8.3.9. Effects of grain size and maceral composition on gas adsorption _____	299
8.4. Conclusions _____	302
Chapter 9 - Summary _____	313
Appendix _____	318
Vitae	

List of tables

	page
Chapter 4	
Table 1. Minimum and maximum depths and gas contents measured from canister desorption on Indiana coal samples ($1 \text{ cm}^3/\text{g} \approx 32 \text{ scf/ton}$).	50
Table 2. Carbon and hydrogen isotope ratios of CBM from the Illinois Basin.	56
Chapter 5	
Table 1. Populations of endogenic cleats.	73
Table 2. Measured macrocleat direction, spacing, and abundances in coals from various coal mines in southwestern Indiana. Macrocleats correspond to Group 2 of Ammosov and Eremin's (1963) classification.	76
Table 3. Indiana macro- and mesocleat data collected prior to this study (Mastalerz, personal database).	78
Table 4. Mesocleat measurements on hand specimens for selected coals. Mesocleats correspond to Group 3 of Ammosov and Eremin's (1963) classification.	78
Table 5. Average microcleat apertures and spacing measured under the microscope. Microcleats correspond to Group 4 of Ammosov and Eremin's (1963) classification. Slit aperture and spacing measurements are also reported.	80
Chapter 6	
Table 1. Carbon- and oxygen-stable isotope ratios of diagenetic calcites from coal cleats, and carbon-stable isotope ratios of carbon dioxide (CO_2) from coalbed gases. $\delta^{13}\text{C}$ and $\delta^{18}\text{O}$ values are expressed in ‰ relative to Vienna Pee Dee Belemnite (VPDB) and Vienna Standard Mean Ocean Water (VSMOW), respectively. The sequence of data entries within each data set is relative to stratigraphic position, from top to bottom.	149
Table 2. Oxygen-stable isotope ratios of diagenetic kaolinites from coal cleats. $\delta^{18}\text{O}$ values are expressed in ‰ relative to Vienna Standard Mean Ocean Water (VSMOW). The sequence of data entries within each data set is relative to stratigraphic position, from top to bottom. Three data of Shieh and Suter (1979) derive from Illinois (IL). Averages of isotope ratios are indicated by asterisks next to the county when more than one data point is available from Ambers (1993) and Shieh and Suter (1979).	150
Table 3. Four scenarios of paleotemperatures in coals during mineralization based on published data and estimates of the oxygen isotopic signature of coalbed waters in equilibrium with precipitated authigenic minerals in coal cleats.	155
Table 4. Measured $\delta^{18}\text{O}_{\text{kaolinite}}$ values and calculated formation temperatures of diagenetic kaolinites, according to four scenarios A, B, C, and D where isotopically different waters are in isotopic equilibrium with growing	

kaolinite. $\delta^{18}\text{O}_{\text{kaolinite}}$ values are reported in ‰ relative to Vienna Standard Mean Ocean Water (VSMOW). The equilibrium equation of Zheng (1993) was used for temperature calculations. The sequence of data entries within each data set is relative to stratigraphic position, from top to bottom. Averages of isotope ratios and of calculated temperatures are indicated by asterisks next to the county when more than one data point is available from Ambers (1993) and Shieh and Suter (1979).

Table 5. Measured $\delta^{18}\text{O}_{\text{calcite}}$ values and calculated formation temperatures of diagenetic calcites, according to four scenarios A, B, C, and D where isotopically different waters are in isotopic equilibrium with growing calcite. $\delta^{18}\text{O}_{\text{calcite}}$ values are reported in ‰ relative to Vienna Standard Mean Ocean Water (VSMOW). The equilibrium equation of Kim and O'Neil (1997) was used for temperature calculations. The sequence of data entries within each data set is relative to stratigraphic position, from top to bottom.	158
	161

Chapter 7

Table 1. Proximate and ultimate analyses of coal samples exposed to laboratory air from zero to 13 months in Experiment 1. The first row of data describes the original “zero exposure coal”.	197
Table 2. Petrographic analyses of samples exposed to oxidizing air in the laboratory for 13 months in Experiment 1. Data normalized to 100% by volume (vol. %). Experiment 1 resulted in no changes in vitrinite reflectance (R_o). The first row of data describes the original “zero exposure coal”.	201
Table 3. Low-pressure N_2 adsorption data. Note the changes in surface area and mesopore characteristics resulting from isothermal oxidation in air at increasing temperatures.	201
Table 4. Low-pressure CO_2 adsorption data. Note the changes in surface area and micropore characteristics resulting from isothermal oxidation in air at increasing temperatures.	207
Table 5. Selected ratios of FTIR-identified functional groups in coals that were exposed to laboratory air at room temperature for up to 9 months in Experiment 1. No particular trends can be discerned from collected data and their ratios. Data from coal that was heated in air for 10 days at 75°C (Experiment 2) are presented in the last row for comparison.	217

Chapter 8

Table 1. High-pressure adsorption analyses performed on coal samples to investigate the effects of moisture content and exposure to air at room temperature on adsorption capacity.	247
Table 2. Inventory of laboratory analyses that were performed on selected Indiana coal samples. The sequence of samples is arranged by coal member in stratigraphic order.	247

Table 3a. Gas adsorption data of moisture-equilibrated coal samples at gas pressures 2.07 MPa (300 psi) and 2.8 MPa (400 psi). Data are reported ‘as received’ and on a dry, ash-free basis (daf). CO ₂ /CH ₄ volume ratios (daf) were calculated for both pressures. Equilibrium moisture and ash contents are expressed as weight %; n.d. = no data.	268
Table 3b. Gas adsorption data of moisture-equilibrated coal samples at gas pressures 300 psi (2.07 MPa) and 400 psi (2.8 MPa). Data are reported ‘as received’ and on a dry, ash-free basis (daf). CO ₂ /CH ₄ volume ratios (daf) were calculated for both pressures. Equilibrium moisture and ash contents are expressed as weight %; n.d. = no data. Data are presented in U.S. industry standard units. The same data in SI units are listed in Table 3a. Unit conversion: 1 cm ³ /g ≈ 32 scf/ton.	269
Table 4a. Gas adsorption data of dry coal samples at 2.07 and 2.8 MPa (300 and 400 psi). The same data in U.S. industry standard units are listed in Table 4b. Data reported on dry, ash-free basis (daf); n.d. = no data. CO ₂ /CH ₄ volume ratios (daf) were calculated for both pressures.	270
Table 4b. Gas adsorption data of dry coal samples at 300 and 400 psi (2.07 and 2.8 MPa). Data are presented in U.S. industry standard units. The same data in SI units are listed in Table 4a. Data reported on dry, ash-free basis (daf); n.d. = no data. CO ₂ /CH ₄ volume ratios (daf) were calculated for both pressures.	270
Table 5a. Calculated adsorption volume ratios between dry and moisture-equilibrated coal samples at gas pressures 2.07 MPa (300 psi) and 2.8 MPa (400 psi). The same data in U.S. industry standard units are listed in Table 5b. n.d. = no data.	271
Table 5b. Calculated adsorption volume ratios between dry and moisture-equilibrated coal samples (ash included) at gas pressures 300 psi (2.07 MPa) and 400 psi (2.8 MPa). Data are presented in U.S. industry standard units. The same data in SI units are listed in Table 5a. n.d. = no data.	271
Table 6. Petrographic characteristics (vol. %) and ash yield and moisture content of coals (wt. %). V = vitrinite, L = liptinite, I = inertinite, MM = mineral matter, R _o = vitrinite reflectance (%), H ₂ O _{eq} = equilibrium moisture content (wt. %). Coal samples are listed in stratigraphic order by Coal Member. Ash yield reported in wt. % as received (a.r.) and dry basis.	282
Table 7. Particle size distribution of crushed and sieved Indiana coals. The data are presented in stratigraphic order by Coal Member.	284
Table 8. Low-pressure N ₂ adsorption data collected for various coal seams in southwestern Indiana using the Micromeritics ASAP-2020 instrument described in section 8.2.4. The samples are presented in stratigraphic order by Coal Member.	286
Table 9. Low-pressure CO ₂ adsorption data collected for various coal seams in southwestern Indiana. The samples are grouped in stratigraphic order by Coal Member.	293

List of figures

	page
Chapter 1	
Figure 1. Coalbed methane production in the U.S. 1000 Bcf are approximately 28.3 km ³ (~28.3*10 ⁶ m ³). Source: U.S. Energy Information Administration. (1 Bcf = 10 ⁹ ft ³).	6
Figure 2. Geological CO ₂ sequestration options.	9
Chapter 3	
Figure 1. Structural configuration of the Illinois basin and extent of the Pennsylvanian System.	22
Figure 2. Generalized stratigraphic sequence of the coal-bearing units in the Pennsylvanian System of Indiana.	25
Chapter 4	
Figure 1. Geographic and stratigraphic distribution of Pennsylvanian coals of Desmoinesian age (Carbondale Group) in Indiana. Circled in gray and highlighted are the coal seams evaluated in this study.	36
Figure 2a. Map showing depth of the Danville Coal Member in southwestern Indiana.	40
Figure 2b. Thickness map of the Danville Coal Member in southwestern Indiana.	41
Figure 3a. Map showing depth of the Springfield Coal Member in southwestern Indiana.	42
Figure 3b. Thickness map of the Springfield Coal Member in southwestern Indiana.	43
Figure 4a. Map showing depth of the Houchin Creek Coal Member in southwestern Indiana.	45
Figure 4b. Thickness map of the Houchin Creek Coal Member in southwestern Indiana.	46
Figure 5a. Map showing depth of the Seelyville Coal Member in southwestern Indiana.	47
Figure 5b. Thickness map of the Seelyville Coal Member in southwestern Indiana.	48
Figure 6. Depth vs. gas content data from canister desorption. No significant correlation observed for all available data.	51
Figure 7. Data from Sullivan and Gibson Counties suggesting a general increase in gas content with depth.	51
Figure 8. Data for Springfield coal in Gibson County suggest a very good correlation between gas content and depth ($R^2 = 0.93$). Only one value plotted outside the observed trend. When all data is included, the correlation drops ($R^2 = 0.29$)	52
Figure 9. Data for Seelyville coals in Vanderburgh County showing a good correlation between gas content and depth ($R^2 = 0.73$)	53

Figure 10. Carbon and hydrogen isotopes for available gas samples from coals in Indiana, Illinois, and Kentucky (isotopic ranges after Whiticar, 1999).	53
---	----

Chapter 5

Figure 1. Structural configuration of the Illinois basin and extent of the Pennsylvanian System.	69
Figure 2. Generalized stratigraphic sequence of the coal-bearing units in the Pennsylvanian System of Indiana.	70
Figure 3. Photolinear interpretation of geological lineaments and faults in southwestern Indiana. Data compiled and modified from Wier <i>et al.</i> , (1974a, b).	75
Figure 4. Distribution and average macrocleat spacing for all measurements collected from nine coal members in Indiana. Average value for all measurements is 8 ± 2.6 cm.	85
Figure 5. Power-law distribution of face mesocleats in relation with abundance (cumulative fracture intensity) and kinematic aperture.	87
Figure 6. Photomicrograph showing microcleats and microfractures in a vitrinite-rich layer.	90
Figure 7a. Distribution of microcleats and microfractures in relation with abundance (cumulative fracture intensity) and kinematic aperture.	91
Figure 7b. Power-law distribution of face and oblique-face microcleats in relation with abundance (cumulative fracture intensity) and kinematic aperture.	92
Figure 7c. Power-law distribution of butt and oblique-butt microcleats in relation with abundance (cumulative fracture intensity) and kinematic aperture.	93
Figure 7d. Power-law distribution of microfractures in relation with abundance (cumulative fracture intensity) and kinematic aperture.	94
Figure 8. Rose diagrams depicting orientation patterns of cleats, fractures, and geologic lineaments. The size of the rose diagram is proportional to the density of data analyzed on a 20 km radius grid.	96
Figure 9. Changes in azimuth direction of face cleats near the axis of a small syncline. Photo from the Danville Coal Member in Vigo County, Indiana.	98
Figure 10. Small syncline depicted by sandstone facies overlying the Danville Coal Member in Vigo County, Indiana.	100
Figure 11. Slickensides and slickenlines on a kaolinite-filled cleat from Gibson County, Indiana.	102
Figure 12. Ammosov and Eremin's (1963) original data are plotted with a modified grade classification. An envelope around all mesocleats in lustrous coals depicts the relation between coal rank and cleat abundance. The average value of all mesocleats abundance measurements from Indiana coals is represented by a gray-filled pentagon.	105
Figure 13. Ammosov and Eremin's (1963) original data are plotted with an ASTM rank classification. The average value of all microcleat abundance measurements from Indiana coals is represented by a gray-filled pentagon.	108

Figure 14. Cleat abundance in coals versus rank, adapted from Pashin et al. (1999). The average values of all cleat abundance measurements from Indiana coals from macro-, meso-, and microcleats (Groups 2, 3, and 4 of Ammosov and Eremin, 1963) are indicated by solid triangles.	111
Figure 15. Distribution of cleat abundance versus cleat scale for Indiana coals. The average data for all measurements within each cleat category was used to calculate the exponential relationship presented.	112
Figure 16. Kaolinite-filled cleats in bright coal of the Lower Block Coal Member. Collected in Daviess County, Indiana.	112
Figure 17. Relation between cleat abundance, cleat aperture, and resulting permeability in milidarcys (md). Bold horizontal grey lines correspond to maximum and minimum values measured for cleat abundance in Indiana coals. Microcleat aperture measurements were used to define the microcleat domain. The boundary between cleat domains is not very well constrained. Internal box corresponds to the permeability range of highly productive wells (0.5 – 100 md) and was used to delineate the mesocleats domain. Higher permeabilities are generally associated with macrocleats (adapted from Scott, 2002).	121

Chapter 6

Figure 1. Map of southwestern Indiana showing the distribution of isotope data from calcite, kaolinite, and CO ₂ from various sources. The expanded area corresponds to the gray-shaded counties in the index map of Indiana (top left).	142
Figure 2. Generalized stratigraphic column of the Pennsylvanian section in Indiana identifying the coals from which calcite and kaolinite samples were collected.	144
Figure 3. X-ray diffraction pattern of cleat-filling kaolinite from the Lower Block Coal Member in Danville, Indiana. The titanium signal derives from the mounting media.	148
Figure 4. Empirical relationships of mineral-water fractionation factors for kaolinite (Zheng, 1993) and calcite (Kim and O'Neil, 1997). Averages of measured $\Delta^{18}\text{O}_{\text{mineral-water}}$ values are plotted for the proposed A, B, C, and D scenarios using estimated $\delta^{18}\text{O}_{\text{water}}$ values from Table 3; the isotopic standard deviation is smaller than the size of symbols.	153
Figure 5. Measured $\delta^{18}\text{O}_{\text{calcite}}$ and $\delta^{18}\text{O}_{\text{kaolinite}}$ values and hypothetical $\delta^{18}\text{O}_{\text{water}}$ values from scenarios A, B, C, and D define temperatures of crystallization for (a) kaolinite and (b) calcite. Filled circles with error bars represent mean values and standard deviations from each data set.	157

- Figure 6. The observed carbon isotopic differences $\Delta^{13}\text{C}_{\text{CO}_2\text{-calcite}}$ (horizontal dashed lines) between calcites from cleats and carbon dioxide from coalbed gases from Gibson and Sullivan Counties in Indiana are not compatible with the equilibrium isotope fractionation of the CO_2 -calcite system (Bottinga, 1968) within the temperature range of scenarios A, B, C, and D (gray vertical bars). The widths of the gray bars correspond to the standard deviations around the mean values of each scenario. 162
- Figure 7. Distribution of $\delta^{13}\text{C}_{\text{calcite}}$ vs. $\delta^{18}\text{O}_{\text{calcite}}$ values from calcites recovered from coal cleats. Data from the Indiana section of the Illinois Basin (● new data from this study; Δ Ambers, 1993) are distinctly different from the Black Warrior Basin, Alabama, where calcites reflect ^{13}C -enrichment of residual carbon dioxide as a result of preferential utilization of $^{12}\text{CO}_2$ during microbial methanogenesis via CO_2 -reduction (□ Pitman *et al.*, 2003). 170

Chapter 7

- Figure 1. Low-pressure volumetric adsorption apparatus (Micromeritics ASAP-2020). 192
- Figure 2A. Long-term experiments up to 13 months. 195
- Figure 2B. Short-term experiments lasting for 10 days. 195
- Figure 3. Proximate chemical analyses showing changes in moisture, ash, and sulfur contents in coal during the exposure to air over 13 months in Experiment 1. Observed variations in ash reflect heterogeneity within coal samples. 198
- Figure 4. Ultimate chemical analyses showing changes in O, N, H, S, and C contents during the 13 months exposure of Experiment 1. Elemental data are reported in weight % on a dry, ash-free basis. 198
- Figure 5. Low-pressure nitrogen adsorption data versus temperature. A: Consistent decrease in mesopore surface area with temperature increase. B: No clear trend in cumulative mesopore volume with temperature increase. C: Consistent increase in mesopore width with increasing temperature. 203
- Figure 6. Low-pressure nitrogen isotherm adsorption data for Experiment 1. Note the decrease in adsorption capacity with exposure time. Data graphed at standard temperature and pressure (STP) conditions (0°C and 0.101 MPa). 204
- Figure 7. Decrease in cumulative mesopore volume with increasing exposure of coal in Experiment 1. The X-axis has a logarithmic scale. 204
- Figure 8. Low-pressure nitrogen isotherm adsorption data from Experiment 2. A significant decrease in adsorption capacity occurred when coal was heated in air to 75°C for 10 days. Data graphed at standard temperature and pressure (STP) conditions (0°C and 0.101 MPa). 205
- Figure 9. Low-pressure nitrogen isotherm adsorption data from Experiment 3. A decrease in adsorption capacity of coals resulted from isothermal heating at different temperatures for 10 days. Data graphed at standard temperature and pressure (STP) conditions (0°C and 0.101 MPa). 205

Figure 10. Low-pressure CO ₂ adsorption data versus temperature. Diagrams A, B, and C show that micropore surface area and monolayer capacity increase with increasing temperature of exposure.	209
Figure 11. Low-pressure CO ₂ adsorption data versus temperature of exposure to air. No consistent trends are observed for the limiting micropore volume (A) and the micropore size (B) with increasing temperature.	210
Figure 12. Low-pressure carbon dioxide adsorption isotherm for Experiment 1. No significant difference is observed with time of exposure of coal to laboratory air at room temperature. Data expressed at standard temperature and pressure (STP) conditions (0°C and 0.101 MPa).	211
Figure 13. Minimal changes in micropore surface area are observed with increasing time of exposure of coal to laboratory air at room temperature in Experiment 1.	211
Figure 14. Low-pressure carbon dioxide adsorption isotherms for Experiment 2. A large increase in adsorption capacity occurred during heating in laboratory air at 75°C for 10 days.	213
Figure 15. Small increases in adsorption capacity were observed for coals that were isothermally exposed to laboratory air at increasing temperatures for 10 days in Experiment 3.	213
Figure 16. Small increases in cumulative micropore surface area were observed for coals that were isothermally exposed to laboratory air at increasing temperatures for 10 days in Experiment 3.	214
Figure 17. FTIR band assignments and approximate peak locations of functional groups of a high-volatile C bituminous coal from the Lower Block Coal Member, Billings Mine, Indiana, that was used in this study.	216
Figure 18. Fourier self-deconvolution of the aliphatic stretching region (2800-3000 cm ⁻¹) in the sample illustrated above.	216
Figure 19. FTIR spectra of a coal sample exposed to laboratory air at room temperature for up to 9 months in Experiment 1. No long-term distinct changes are observed in functional group abundance through time.	219
Figure 20. A differential spectrum (A - B, bottom) was obtained by subtracting the FTIR spectrum of coal that had been heated in air at 75°C for 10 days (Experiment 2, spectrum A, top) from the FTIR spectrum of the original “zero exposure” coal (spectrum B, middle). The negative peak near 1600 cm ⁻¹ in the differential spectrum suggests partial loss of aromatic carbon from coal during heat exposure in air, whereas a well-developed peak near 1700 cm ⁻¹ suggests the generation of carbonyl/carboxyl groups.	220
Figure 21. Oxidation indices from FTIR-derived ratios of functional groups for Experiments 1 and 2. No distinct long-term trends are observed with increasing exposure (Experiment 1). The shaded area represents the coal sample heated in air at 75°C (Experiment 2). No change is observed between the original “zero exposure coal” and coal that was exposed to 75°C.	220

Chapter 8

- Figure 1. Experimental adsorption isotherm classification according to Sing *et al.* (1985). Type I isotherms are characteristic of microporous adsorbents for subcritical, near-critical, and supercritical conditions. Type II represents adsorption on non-porous or macroporous adsorbents with strong gas adsorption affinities. Type III (not common) represents the adsorption on macroporous adsorbents with weak gas adsorption affinities. Types IV and V represent adsorption on mesoporous adsorbents with strong (for mesoporous industrial adsorbents) and weak (uncommon) gas adsorption affinities. Both types exhibit adsorption hysteresis at low temperatures. Type VI is characteristic for multilayer adsorption on a uniform non-porous surface. 239
- Figure 2. Experimental design of the small-volume high-pressure volumetric adsorption apparatus that uses crushed coal in two test cells (1, 3) in comparison with two calibrated reference cells (2, 4). 251
- Figure 3a. Photograph of the small-volume high-pressure volumetric adsorption apparatus. The illustration shows four pressure cells inside a temperature-controlled water bath. Each pressure cell is connected to a high-pressure transducer. 256
- Figure 3b. Photograph of the large-volume high-pressure volumetric adsorption apparatus. The instrument is housed in a fume hood for safety compliance with Indiana University. A high-pressure ISCO pump capable of injecting pressures up to 70 MPa (10,000 psi) is connected to the instrument. The high-pressure test cell was built to potentially reach a maximum pressure of 31.5 MPa (4,500 psi). 258
- Figure 4. Compressibility factors derived experimentally using our small-volume high-pressure volumetric adsorption apparatus. The data are compatible with theoretical compressibility factors from the National Institute for Standards (NIST) database. 254
- Figure 5. Methane adsorption isotherms determined at 17°C from selected Indiana coals using our small-volume high-pressure volumetric adsorption apparatus. Dry coal samples express significantly larger adsorption capacities for CH₄ than the same coals after moisture-equilibration. Data presented in scientific (SI) and U.S. industry standard units. 260
- Figure 6. Methane adsorption isotherms collected at 17°C from moisture-equilibrated coal samples. The samples were exposed to air in the laboratory for up to ~13 months, followed by moisture-equilibration and measurement at RMB Earth Science Consultants, Ltd. Although all coals were moisture-equilibrated before measurements, coals exposed longer to air were less able to become re-hydrated. The observed decrease in equilibrium-moisture content translates into an increase in adsorption capacity. 263

Figure 7. Carbon dioxide isotherms measured at 17°C from selected Indiana coals using our small-volume high-pressure volumetric adsorption apparatus. Dry samples show significantly larger adsorption capacities than moisture-equilibrated samples. Data are presented in scientific (SI) and U.S. industry standard units.	265
Figure 8. Carbon dioxide adsorption isotherms collected at 17°C from moisture-equilibrated coal samples that had been exposed to air in the laboratory for up to ~13 months, followed by moisture-equilibration and measurement at RMB Earth Science Consultants, Ltd. Although all coals were moisture-equilibrated before measurements, the more exposed coals were less able to become re-hydrated. The observed decrease in moisture content translates into an increase in adsorption capacity.	267
Figure 9. Comparison between carbon dioxide and methane adsorption isotherms determined at 17°C from moisture-equilibrated coal samples. Solid lines correspond to high-pressure methane (black) and carbon dioxide (gray) isotherms measured with our small-volume high-pressure volumetric adsorption apparatus. Dashed lines correspond to high-pressure methane (black) and carbon dioxide (gray) adsorption isotherms determined at RMB Earth Science Consultants, Ltd. CO ₂ /CH ₄ adsorption volume ratios vary between 2.3 and 5.5 for 2.07 and 2.8 MPa (300 and 400 psi, respectively).	276
Figure 10. Particle size distributions of coal samples that were crushed to various degrees. The green bar represents a grain size that is typically used for conventional adsorption isotherm work by commercial laboratories.	279
Figure 11. CO ₂ adsorption isotherms of crushed coals with distinct particle size distributions. Experiments at Indiana University were conducted at 21°C, whereas data from the commercial laboratory were gathered at 17°C. Note that the adsorption capacity increases with decreasing grain size of crushed coal. Experiment 4 shows a sudden increase in CO ₂ adsorption capacity above 2.8 MPa (400 psi) that is expressed as a straight line and is probably due to a leak in the adsorption apparatus.	280
Figure 12. Maceral compositions of selected coal samples.	282
Figure 13. Weight percent distribution of measured coal size fractions from crushed and sieved Indiana coals.	284
Figure 14. Low-pressure nitrogen adsorption isotherms from coal samples of the Springfield Coal Member from Gibson and Warrick Counties, southwest Indiana. Data graphed at standard temperature and pressure (STP) conditions (0°C and 0.101 MPa).	288
Figure 15. Low-pressure nitrogen adsorption isotherms from coal samples of the Buffaloville Coal Member in Daviess County, Indiana. Data graphed at standard temperature and pressure (STP) conditions (0°C and 0.101 MPa).	288
Figure 16. Low-pressure nitrogen adsorption isotherms from coal samples of the Upper Block Coal Member in Daviess County, Indiana. Data graphed at standard temperature and pressure (STP) conditions (0°C and 0.101 MPa).	289

Figure 17. Low-pressure nitrogen adsorption isotherms from coal samples of the Lower Block Coal Member in Daviess County, Indiana. Data graphed at standard temperature and pressure (STP) conditions (0°C and 0.101 MPa).	289
Figure 18. Low-pressure nitrogen adsorption isotherms from coal samples of the Seelyville Coal Member in Sullivan County, Indiana. Data graphed at standard temperature and pressure (STP) conditions (0°C and 0.101 MPa).	290
Figure 19. Comparison of low-pressure nitrogen adsorption isotherms from selected coal samples across several coal members and counties in Indiana. Data graphed at standard temperature and pressure (STP) conditions (0°C and 0.101 MPa).	290
Figure 20. Low-pressure carbon dioxide adsorption isotherms from coal samples of the Springfield Coal Member in Gibson and Warrick Counties, Indiana. Data are graphed at standard temperature and pressure (STP) conditions (0°C and 0.101 MPa).	294
Figure 21. Low-pressure carbon dioxide adsorption isotherms from coal samples of the Buffaloville Coal Member in Daviess County, Indiana. Data are graphed at standard temperature and pressure (STP) conditions (0°C and 0.101 MPa).	294
Figure 22. Low-pressure carbon dioxide adsorption isotherms from coal samples of the Upper Block Coal Member in Daviess County, Indiana. Data are graphed at standard temperature and pressure (STP) conditions (0°C and 0.101 MPa).	295
Figure 23. Low-pressure carbon dioxide adsorption isotherms from coal samples of the Lower Block Coal Member in Daviess County, Indiana. Data are graphed at standard temperature and pressure (STP) conditions (0°C and 0.101 MPa).	295
Figure 24. Low-pressure carbon dioxide adsorption isotherm from a coal sample from the Seelyville Coal Member in Sullivan County, Indiana. Data are graphed at standard temperature and pressure (STP) conditions (0°C and 0.101 MPa).	296
Figure 25. Comparison of low-pressure carbon dioxide adsorption isotherms from selected coal samples across several coal members and counties in Indiana. Data are graphed at standard temperature and pressure (STP) conditions (0°C and 0.101 MPa).	296
Figure 26. Comparison of cumulative surface areas versus pore widths calculated from low-pressure CO ₂ adsorption data for selected coal samples across several coal members and counties in Indiana.	298
Figure 27. Comparison of cumulative pore volumes versus pore widths calculated from low-pressure CO ₂ adsorption data for selected coal samples across several coal members and counties in Indiana.	298

CHAPTER 1

Introduction

1.1. Objectives and significance

The increasing demand for energy sources, particularly natural gas, and the growing concerns for global warming owing in part to the steep rise in anthropogenic greenhouse gas emissions, have awakened interest in the once and almost forgotten coal resources worldwide. Special attention is now being paid to coal seams, not only because of their huge potential for providing reliable energy in the future, but also because of their possible utilization for sequestering anthropogenic carbon dioxide emissions in an effort to mitigate the increase in CO₂ concentration in the atmosphere. Despite the enormous amount of previous studies devoted to understanding the characteristics of coal and its utilization, new technologies are revealing that our understanding of coal remains incomplete. Coal, in general, is a complex macromolecular network that owes its characteristics in part to the paleoenvironment of deposition, which in turn, imparts distinctive properties to coal and makes it unique from a research perspective.

Current technology is inadequate to obtain in situ gas sorption data on coal. To quantify gas adsorption in coal, laboratory experiments are designed to approximate in situ conditions of coal in the natural environment. Although reservoir pressure and temperature are changed with coal extraction, these can be re-established and thus simulated in the laboratory. Other factors that affect adsorption (e.g., oxidation, moisture, and storage time) are not as easily mimicked and require clever laboratory procedures that allow us to quantify or estimate their effects.

Numerous studies have attempted to quantify the gas adsorption potential of coals. At low pressures, coal adsorption properties are investigated to understand the nature of

porosity and surface areas. At high pressures, research aims to understand the gas saturation capacity of coals and their potential for trapping or releasing gas for further utilization. Although there is limited consensus about the main parameters controlling gas adsorption characteristics in coals, the following questions address needed additional research: 1) Are experimental conditions able to mimic reservoir conditions? 2) What is the effect of reduced grain size during laboratory analyses when coal is crushed in order to minimize diffusion time through the coal matrix? 3) Does oxidation of coal during storage and exposure to air oxygen affect adsorption characteristics over time? 4) Do various sampling procedures introduce artifacts in the measured gas adsorption behavior in coal?

Several processes are relevant for gas sorption in coal beds. Physical adsorption (“physisorption”) is a reversible process based on weak intermolecular “van der Waals” attraction forces. Chemical absorption (“chemisorption”, sometimes incorrectly termed ‘adsorption’) is based on the chemical removal of gas components where a large reaction enthalpy makes a reaction irreversible. Biochemical utilization of gas components, such as the reductive conversion of carbon dioxide to methane by microbial consortia, is a special case of chemical absorption.

Most interaction between gas and coal is due to reversible physical adsorption that is intricately linked with the pressure regime of the reservoir. Methane in coal is generally present in two forms, (1) as a free gas phase in the open pore spaces of coal and within natural cleats and fractures, and (2) gas that is adsorbed by van der Waals forces to coal’s interior surface area. The weak bonding between adsorbed gas and coal surfaces must be overcome (e.g., by applying a pressure gradient) before gas can migrate out of the coal

matrix. The loss of adsorbed gas is termed desorption. Gas in the free gas phase migrates out of the reservoir following Darcy's law (Harpalani and Schraufnagel, 1990), while adsorbed bound gas more slowly leaves the coal matrix obeying Fick's law of diffusion and pressure gradients (Scott, 2002).

This study investigates geologic controls on coalbed methane potential on a wide range of scales, from large-scale phenomena involving geologic lineaments, faults, and other tectonic controls, to the behavior of micrometer-sized pores in coal controlling the adsorption characteristic of coalbed gases in a reservoir. The field study component of this dissertation is represented by chapters 4, 5 and 6 providing data from drillings, cleat and fracture orientations, and mineralization in cleats. These data are discussed in relation to geologic controls for coalbed methane potential in Indiana. The experimental component of this dissertation is presented in chapters 7 and 8 describing the effects of oxidation and storage time on adsorption (Chapter 7), and the effects of coal composition, moisture, and grain size from a custom-built apparatus for determining the high-pressure adsorption characteristics of coal (Chapter 8). The resulting adsorption and desorption data are used to quantify the gas saturation capacity of high volatile bituminous coals from Indiana. Natural reservoir conditions are simulated by maintaining coal samples at a constant temperature and within a range of pressures that are reasonable assuming that Indiana coals are under hydrostatic conditions.

1.2. Coalbed methane

Gas in coal is largely composed of methane with relatively small amounts of other gas species. Coalbed methane (CBM) is a widely used term that refers to methane-rich natural gas in coals, or produced from coals. Compressed CBM requires little or no processing after production, making it ideal for retail. The quantity and geochemical composition of CBM in coal are linked to (1) coal composition, (2) coal rank, (3) coal thickness, (4) burial history of the basin, (5) structural configuration of the basin, (6) tectonic history, (7) lithology adjacent to coal beds, (8) and basin hydrology. All these geologic factors control the potential accumulation of gas and determine its suitability for economic extraction. Various geologic factors conspire to make the occurrence of economic accumulations of CBM critically dependent on the physical and chemical characteristics of coal, e.g., adsorption potential, moisture content, and degree of oxidation.

In the United States, CBM contributes to nearly 10% of the yearly production of natural gas and its use is projected to increase in the future (Figure 1). In contrast to conventional coal energy, CBM is considered one of the unconventional energy resources. New techniques, including horizontal drilling, are being developed to extract CBM more efficiently and its use is gaining worldwide acceptance. An increasing number of studies are being conducted on coal basins to improve our understanding of this commodity and to maximize the economic return for its utilization.

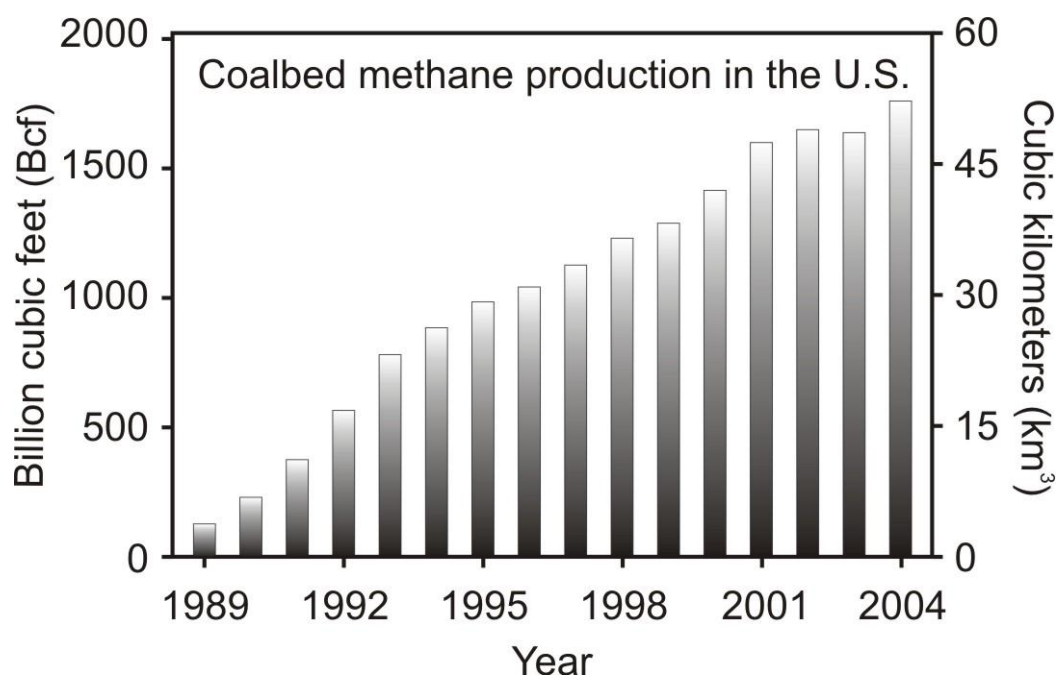


Figure 1. Coalbed methane production in the U.S. 1000 Bcf are approximately 28.3 km^3 ($\sim 28.3 \times 10^6 \text{ m}^3$). Source: U.S. Energy Information Administration. (1 Bcf = 10^9 ft^3).

1.3. CO₂ sequestration

Growing concerns of the negative effects of anthropogenic greenhouse gas emissions released to the atmosphere have prompted several nations to sign agreements to reduce their carbon dioxide (CO₂) emissions to a level that would theoretically stabilize or even reduce atmospheric greenhouse gas concentrations (i.e., Kyoto Protocol). Although the United States decided not to sign the Kyoto agreement over political and economic concerns, the USA is developing alternative ways to minimize or curtail CO₂ emissions.

CO₂ sequestration stands for capturing/trapping of carbon dioxide and is often abbreviated to 'carbon sequestration'. Natural biological sequestration involves the utilization of CO₂ by terrestrial plants and phytoplankton, but its potential is limited and jeopardized by deforestation, desertification, and a CO₂-related lowering of pH of ocean water that reduces marine algal populations. Industrial sequestration of CO₂ has been considered a more feasible approach, especially if applied to point sources of CO₂ such as coal-fired power plants, ethanol plants, refineries, etc. Presently the capture of CO₂ from anthropogenic point sources still requires cost-prohibitive measures and the construction of new facilities, but sequestration of CO₂ in gas or liquid form in geological formations and even the chemical absorption by mineral reactions at depth in geological formations are being evaluated in experimental approaches and in field pilot projects.

At present, geological sequestration is given more attention because gas injection underground is a proven technology that has been developed by the petroleum industry for re-pressurizing oilfields, and also because the cost of capturing CO₂ may be offset by the recovery of additional oil and gas that otherwise could not be recovered. CO₂

sequestration is being viewed as a potential mechanism for reducing anthropogenic CO₂ emissions provided that booming economies such as India and China develop similar mechanisms to control their emissions, thus preventing a second “industrial revolution” with profoundly negative consequences for the global biosphere.

Geological carbon sequestration currently focuses on four types of potential receptacles: (1) deep saline aquifers, (2) abandoned and nearly depleted oil fields, (3) coal seams, and (4) shales (Figure 2). Deep saline aquifers have been utilized in the past for the disposal of hazardous wastes and are accessible with proven technology that is available for the capture of CO₂. Few examples have shown the benefit of capturing carbon dioxide in geological formations (e.g., Sleipner Field in the North Sea).

Geochemical and geophysical interactions between CO₂ and deep environments are being investigated to better constrain the long-term consequences and possible hazards of this technology. Capturing CO₂ in mature oil fields is tested at the Wayburn oil field in Canada. The use of carbon dioxide for enhanced oil recovery has been tested and proven successful for many years (e.g., west Texas).

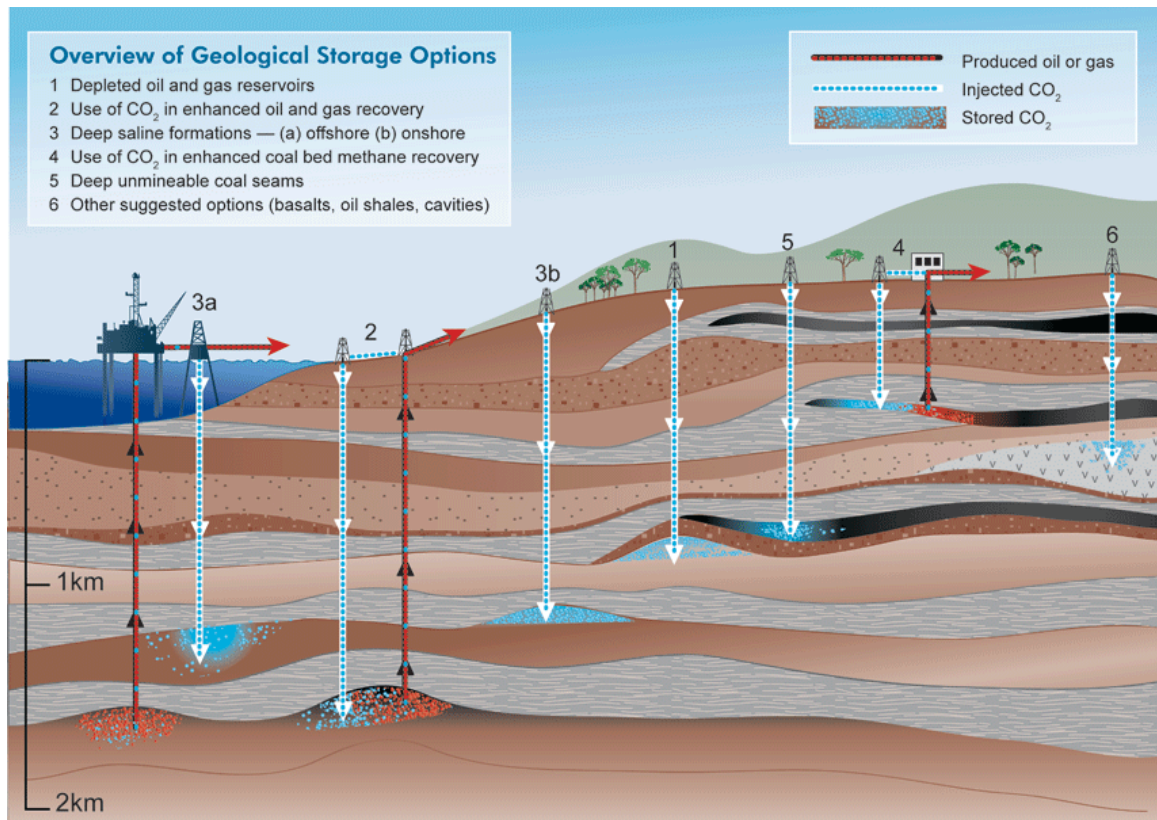


Figure 2. Geological CO₂ sequestration options.

Sequestration of CO₂ in coal requires more investigation. Experimental data suggest that CO₂ sequestration in coal can be induced through artificial injection. Gas composition plays an important role since different gas components have different adsorption affinities in coal. Experimental gas adsorption in coal shows that not all gases can access all available pore space. The controlled adsorption of nitrogen, for example, is used to measure the volume of mesopores (2nm – 50 μm), while CO₂ can access pores smaller than 2 nm. Because of the preferential affinity of coal to adsorb carbon dioxide, CO₂ injection is being investigated as a mechanism for displacement of methane, which will offset the cost of sequestration. Knowledge of the gas saturation capacity of coals is critical for the estimation of potential capture volumes. This information, at present, can only be obtained experimentally.

References

- Harpalani, S., Schraufnagel, R.A., 1990. Shrinkage of coal matrix with release of gas and its impact on permeability of coal. *Fuel* 69, 551-556.
- Scott, A.R., 2002. Hydrogeologic factors affecting gas content distribution in coal beds. *International Journal of Coal Geology* 50, 363-387.

CHAPTER 2

Methods and data acquisition

This chapter outlines the various types of field and laboratory analyses that were performed to generate data for this thesis. Field analyses include sampling of coal from drillings and coal mines and measurements of fracture and cleat orientations in coal mines. The analysis of these data is presented in Chapters 4 and 5. Laboratory analyses included carbon and oxygen stable isotopes, X-ray diffraction, chemical data, FTIR measurements, low-pressure adsorption measurements, and high-pressure adsorption measurements. The analysis of laboratory data is presented in Chapters 6, 7 and 8.

Each chapter contains a methods section where analytical techniques are presented in more detail. This chapter provides a brief description of the techniques used, with their applications in this project.

2.1. Field data collection

2.1.1. Coalbed methane exploratory drillings

Only few coalbed methane operations have been actively pursued in the Illinois Basin, in part because of preconceived and uncritically extrapolated notions on the occurrence and distribution of coalbed gas from other basins. It has been commonly assumed that low rank coals are unable to generate economic quantities of gas. Although that is undoubtedly the case with regard to thermogenically-derived gas, the occurrence of large accumulations of biogenically-derived gas has also proven economically feasible, for example in the Powder River Basin. In Indiana, only one field is economically producing biogenically-derived coalbed gas.

To improve our understanding on the occurrence of Indiana coalbed gas and to complement the existing regional data, three test sites in Indiana were selected at the beginning of this project to assess the coalbed methane potential in areas where net coal thicknesses and gas accumulations were thought to be the most appropriate for future exploration and production. Drilling was made possible in part with funding from the U.S. Department of Energy. Our project also benefited from ‘in-kind’ collaboration with mining operators in two of the three locations. Two of the coalbed methane exploratory wells were drilled in Gibson County and one well was drilled in Knox County in Indiana. Selection of target exploratory well locations followed standard isopach and structural mapping techniques based on available geophysical well-logs from petroleum operations in southwestern Indiana. The relationships observed from the analysis of gas content vs. depth were used as screening criteria for selecting the exploratory well locations. Another criterion in site selection was the scarcity of data in certain areas prompting us to improve the understanding of the regional geologic distribution of coal units.

With regard to coalbed gas exploration, the main reason for drilling the three specific wells was the collection of coal cores from the thickest coal seams available at each location to determine gas content based on standard canister desorption techniques. In addition to supplying data on coalbed gas potential, a complete suite of logs was gathered for each location to document lithologies around the coals. Geophysical log data were obtained across the entire drilled depths from all three locations. Coring was limited to selected coal intervals because continuous coring would have been cost-prohibitive. The drilling results were integrated into updated structure and thickness maps for the

Danville, Springfield, Houchin Creek, and Seelyville Coal Members (presented in Chapter 4).

2.1.2. Cleats and fracture measurements and coal sampling

Cleats and fractures in coal are some of the most important parameters controlling gas production in coalbed methane reservoirs. Intensity of fracturing (abundance), spacing, and aperture define permeability, fluid transmissibility, and access of microbes into coal. Although several studies have qualitatively described the occurrence of cleats in coals, only few studies have presented quantitative analyses. Cleat and fracture data from other basins may not necessarily give an adequate picture of the distribution of similar features in Indiana coals because fracturing is specific to coal composition and maturity and closely relates to a basin's tectonic and burial history. Chapter 5 utilizes nearly 1,600 new cleat measurements to investigate the distribution of cleats and fractures in Indiana coals at scales ranging from macroscopic to microscopic. The study constrains the relation of cleats and fractures to geologic lineaments and coalbed methane occurrence.

2.2. Laboratory analyses

Laboratory analyses were conducted to complement data collected in the field. These analyses include X-ray analysis, carbon and oxygen stable isotope ratios, and the microscopic study of fractures in selected samples. Additionally, laboratory analyses were conducted to study the effects of oxidation, grain size, and maceral composition on

the adsorption characteristics of coals. Petrographic analysis was employed to quantify maceral composition and vitrinite reflectance. Coals were further analyzed with regard to their elemental chemical compositions, Fourier-Transform Infra-Red (FTIR) spectral properties, grain size distributions of crushed coals, surface areas, microporosimetric responses from low-pressure adsorption, and high-pressure adsorption responses describing the maximum gas retention capacity of coals under simulated ‘in situ’ reservoir conditions.

2.2.1. Stable isotope analyses and X-ray diffraction

Isotopic analyses of oxygen and carbon were conducted to constrain the timing, temperature, and burial depth during crystallization of diagenetic minerals along cleats and fractures in coals. X-ray diffraction (XRD) data were collected for selected samples to determine the mineralogic composition. Details of the methodological procedures followed to gather X-ray and stable isotopic data are described in Chapter 6.

2.2.2. Petrographic and chemical analyses

Petrographic analyses yielded vitrinite reflectance data and maceral compositions of Indiana coals to establish possible correlations between coal petrographic parameters and experimental gas adsorption data.

Chemical analyses (proximate and ultimate analyses: see definitions at the end of this chapter) were performed routinely on all coal samples by Standard Laboratories, Inc., Evansville, Indiana. Data from proximate analyses includes moisture content, ash, fixed carbon, and sulfur weight percentages, in addition to calorific value of coals (BTU/lb;

kcal/kg; MJ/kg). Data obtained from ultimate analyses include elemental composition in terms of weight percent hydrogen, carbon, nitrogen, sulfur, and oxygen, and the percentage of ash (i.e., mineral matter). Chemical compositional data were tabulated and normalized to 100 percent for comparison among the different samples. Petrographic and chemical data are presented in Chapters 7 and 8.

2.2.3. Fourier Transform Infrared Spectroscopy (FTIR)

FTIR spectroscopy was applied to study the changes in the molecular structure of coals due to oxidation with storage time. Aliquots of a freshly ground and homogenized coal sample were exposed to oxidizing air in the laboratory for different time intervals and directly compared against the original coal stored in an inert gas. FTIR measurements were collected at the Center for Applied Coal Research at the University of Kentucky in Lexington, KY. FTIR data are discussed in Chapter 7.

2.2.4. Surface area, pore size distribution, and grain size analyses

To accelerate gas adsorption and reach equilibrium conditions between coal and gas within hours, coal was routinely crushed and homogenized. Crushed coal was sieved to separate grain size fractions in order to deepen our understanding of possible relationships between adsorption, particle size, and pore distribution. Chapter 8 describes the methodology used to analyze grain size data.

Low-pressure adsorption measurements collected on a Micromeritics ASAP 2020 surface area analyzer with nitrogen gas provide information about mesopores (2 – 50 nm) with regard to surface area, adsorbed volumes, and pore width. Similar low-pressure

adsorption experiments with carbon dioxide gas yield information about the microporous (<2 nm) structure of coals, in particular about the saturation capacity of the monomolecular layer (monolayer capacity), the total surface area of coal, and the average micropore size (Chapter 7).

2.2.5. High-pressure adsorption analyses

High-pressure adsorption isotherms are routinely used to quantify the gas adsorption capacity in coal. Crushed and sieved coal samples (<60 mesh; particle diameter ~250 μm) are typically used in volumetric or gravimetric apparatuses for measuring high-pressure adsorption isotherms (Goodman *et al.*, 2004; Goodman *et al.*, 2007, in press). The high cost of obtaining these data from commercial laboratories made it advantageous to design and custom-build our own apparatus. Chapter 8 describes the design and implementation of instrumentation.

High pressure isotherms were determined on selected samples that were split in two sets: the first split represented a dry coal sample, whereas the second split was moisture equilibrated. These analyses constrained the effects of moisture loading in relation to adsorption behavior in coal. For quality control, comparison, and calibration of our own instrument, selected samples were also sent to a commercial laboratory that specializes in the generation of high-pressure isotherm data. Chapter 8 presents and discusses adsorption data and compares them with grain size distributions.

2.3. Practical definitions (sources: Thomas, 1992; ASTM, 2006)

Proximate analysis: this analysis is considered the most fundamental of all coal analyses and is of great importance in the practical use of coal. In this analysis, the amounts of moisture, volatile matter, ash, and fixed carbon are determined.

Moisture: various terms describe the occurrence of moisture in coal (surface moisture, ‘as received’ moisture, total moisture, air-dried moisture, and equilibrium moisture). The coal industry has developed techniques to estimate moisture content, and the use of equilibrium moisture has gained wide acceptance for multiple usage.

Volatile matter: with the exception of moisture, volatile matter represents the coal components liberated at high temperature in the absence of air.

Ash: this term corresponds to the inorganic residue that remains after combustion. Ash represents the bulk of the mineral matter in the coal after losing the volatile components.

Fixed carbon: corresponds to the carbon content of coal that is found in the residue after the volatile matter has been liberated. Fixed carbon is the organic fraction (wt. %) of coal determined by subtracting the total percentages of other components (i.e. moisture, ash, and volatile matter) from 100%.

Ultimate analysis: consists of the determination of carbon and hydrogen as gaseous products of its complete combustion, determination of sulfur, nitrogen and ash in the material as a whole, and the estimation of oxygen by difference.

Calorific value: amount of heat produced per unit mass when combusted. Different units are used worldwide, the most common being BTU/lb, kcal/kg, and MJ/kg.

References

- ASTM, 2006. Annual book of ASTM standards. Section five: Petroleum Products, Lubricants, and Fossil Fuels. Gaseous fuels; coal and coke. West Conshohocken, PA, 05.06, 705 pp.
- Goodman, A.L., Busch, A., Duffy, G.J., Fitzgerald, J.E., Gasem, K.A.M., Gensterblum, Y., Krooss, B.M., Levy, J., Ozdemir, E., Pan, Z., Robinson Jr., R.L., Schroeder, K., Sudibandriyo, M., White, C.M., 2004. An inter-laboratory comparison of CO₂ isotherms measured on Argonne Premium coal samples. *Energy & Fuels* 18, 1175-1182.
- Goodman, A.L., Busch, A., Bustin, R.M., Chikatamarla, L., Day, S., Duffy, G.J., Fitzgerald, J.E., Gasem, K.A.M., Gensterblum, Y., Hartman, C., Jing, C., Krooss B.M., Mohammed, S., Pratt, T., Robinson Jr., R.L. Romanov, V., Sakurovs, R., Schroeder, K., White, C.M., in press. Inter-laboratory comparison II: CO₂ isotherms measured on moisture-equilibrated Argonne premium coals at 55°C and up to 15 MPa. *International Journal of Coal Geology*, doi:10.1016/j.coal.2007.01.005
- Thomas, L., 1992. Handbook of Practical Coal Geology. John Wiley and Sons, Inc., New York.

CHAPTER 3

Geology and coalbed methane potential of the Illinois Basin and Indiana

3.1. The Illinois Basin

The Illinois Basin is a spoon-shaped depression that began its development as a rhyolitic caldera in the Proterozoic (McBride *et al.*, 2003) and was progressively filled by sediments derived from the Canadian Shield and the Appalachian Mountains. The Paleozoic sedimentary sequence of the Illinois Basin is characterized by more than 7 km in thickness at the deepest part of the basin (Collinson *et al.*, 1988). The stratigraphy of the basin can be subdivided into four megasequences that have been identified as the Cambro-Ordovician Sauk, Ordovician-Devonian Tippecanoe, Devonian-Mississippian Kaskasia, and Pennsylvanian-Permian Absaroka sequences. These sequences are separated by major unconformities revealing the cyclic sedimentation in response to sea-level fluctuations. Most of the sediments deposited in the basin developed before the development of the Pascola Arch that closed the basin to the south. In general, the sedimentary units thicken towards the center of the basin in southeastern Illinois (Archer and Kirr, 1984). The Illinois Basin is bounded by broad structural features such as the Cincinnati Arch to the east, the Kankakee and Wisconsin Arches to the north and northeast, the Mississippi River Arch to the northwest, the Ozark Dome to the west, and the Pascola Arch to the south. Within the basin, the major structural features correspond to high-angle basement faults and their associated features (i.e. anticlines and monoclines). Only the major faults have significant vertical and lateral displacement, e.g. Shawneetown - Rough Creek fault zone (Archer and Kirr, 1984). Figure 1 shows the structural configuration of the Illinois Basin boundaries and the approximate area where Pennsylvanian sediments are present in the basin.

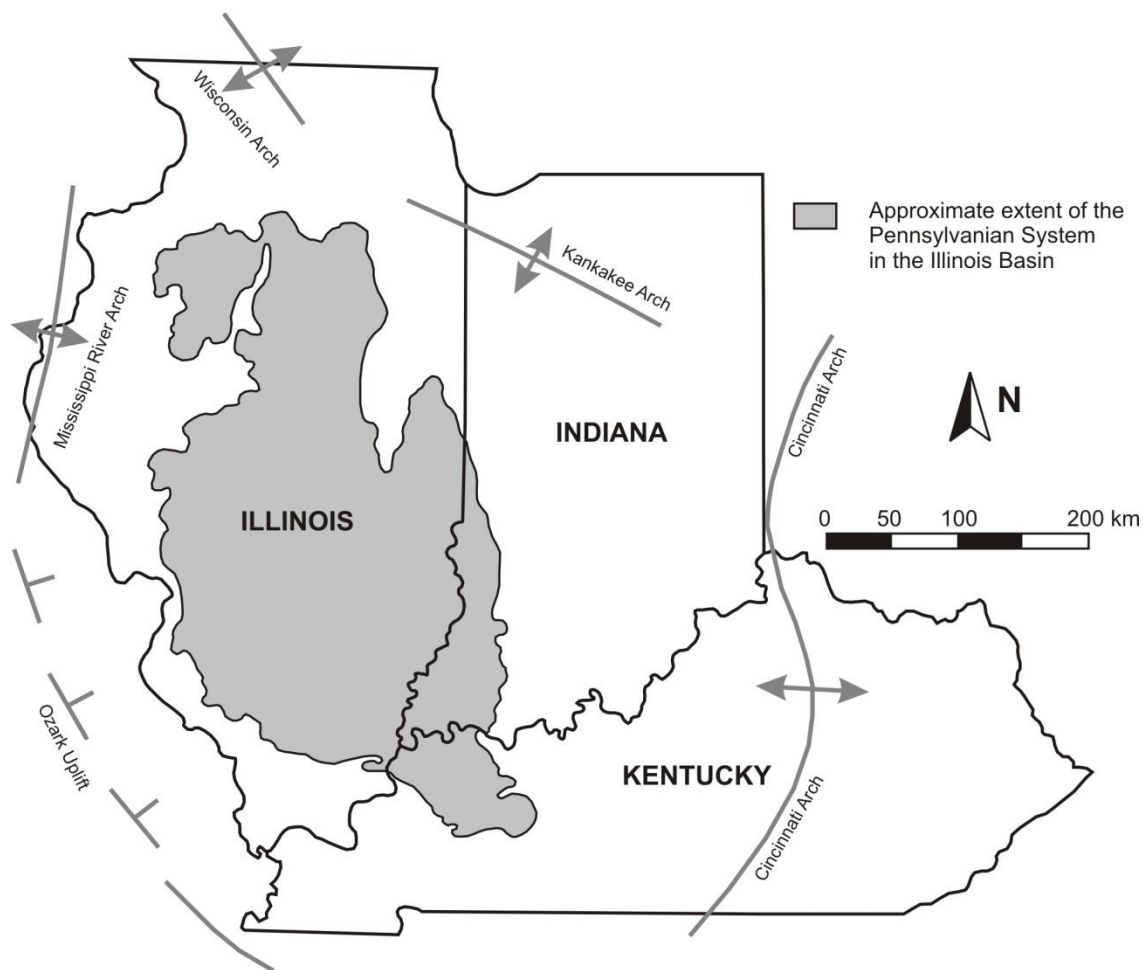


Figure 1. Structural configuration of the Illinois Basin and extent of the Pennsylvanian System.

3.1.1. The Pennsylvanian System

The Pennsylvanian system in the Illinois Basin developed as sediments transported mainly from the northeast (and from the northwest for western Illinois) progressively filled this shallow elongated depression (Potter, 1963; Wanless, 1975). Major erosion and uplift at the end of the Mississippian Period created an unconformable surface upon which Pennsylvanian sediments sourced from the Canadian Shield and the Appalachian Mountains were deposited (Archer and Kirr, 1984).

Pennsylvanian rocks in southwestern Indiana are represented by a clastic sequence of shale, siltstone, and sandstone, with intercalated coals and limestones (Gray, 1979). This sequence of interbedded terrigenous and marine facies resulted from fluctuations in sea level (cyclothems). Deposition occurred along paralic and deltaic environments and was influenced by tidal regimes (Kvale and Archer, 1990; Kvale and Mastalerz, 1998; Kvale *et al.*, 2004). As a result, extensive development of swamps, marshes, and deposition of alternating open marine (black shales and limestones) and continental facies (sandstones, siltstones, and associated coal deposits) occurred.

Pennsylvanian coal-bearing strata in Indiana are subdivided into three main intervals that span from Morrowan to Desmoinesian epochs (i.e. Raccoon Creek, Carbondale, and McLeansboro Groups). Figure 2 shows a generalized stratigraphic column for the Pennsylvanian System in Indiana. In the lower interval (Raccoon Creek Group), there are several coal seams, some of which are considered of economic importance due to their low sulfur contents. However, most of them are not very thick and their extent is somewhat limited (Mastalerz and Harper, 1998). The intermediate Carbondale Group is stratigraphically divided into three Formations (Linton, Petersburg, and Dugger) and

contains widespread coals that account for most of the mining operations in Indiana (Mastalerz and Harper, 1998). Sulfur content of Carbondale coals is generally higher than that of the Raccoon Creek coals (this being normally a disadvantage), but due to greater thicknesses, widespread distribution, and closer proximity to surface, Carbondale coals are more attractive for mining than other coals in the state. The upper interval, McLeansboro Group, lies on top of the Carbondale Group and, in terms of mining, is considered a barren sequence because of the absence of thick and continuous coal layers (Mastalerz and Harper, 1998).

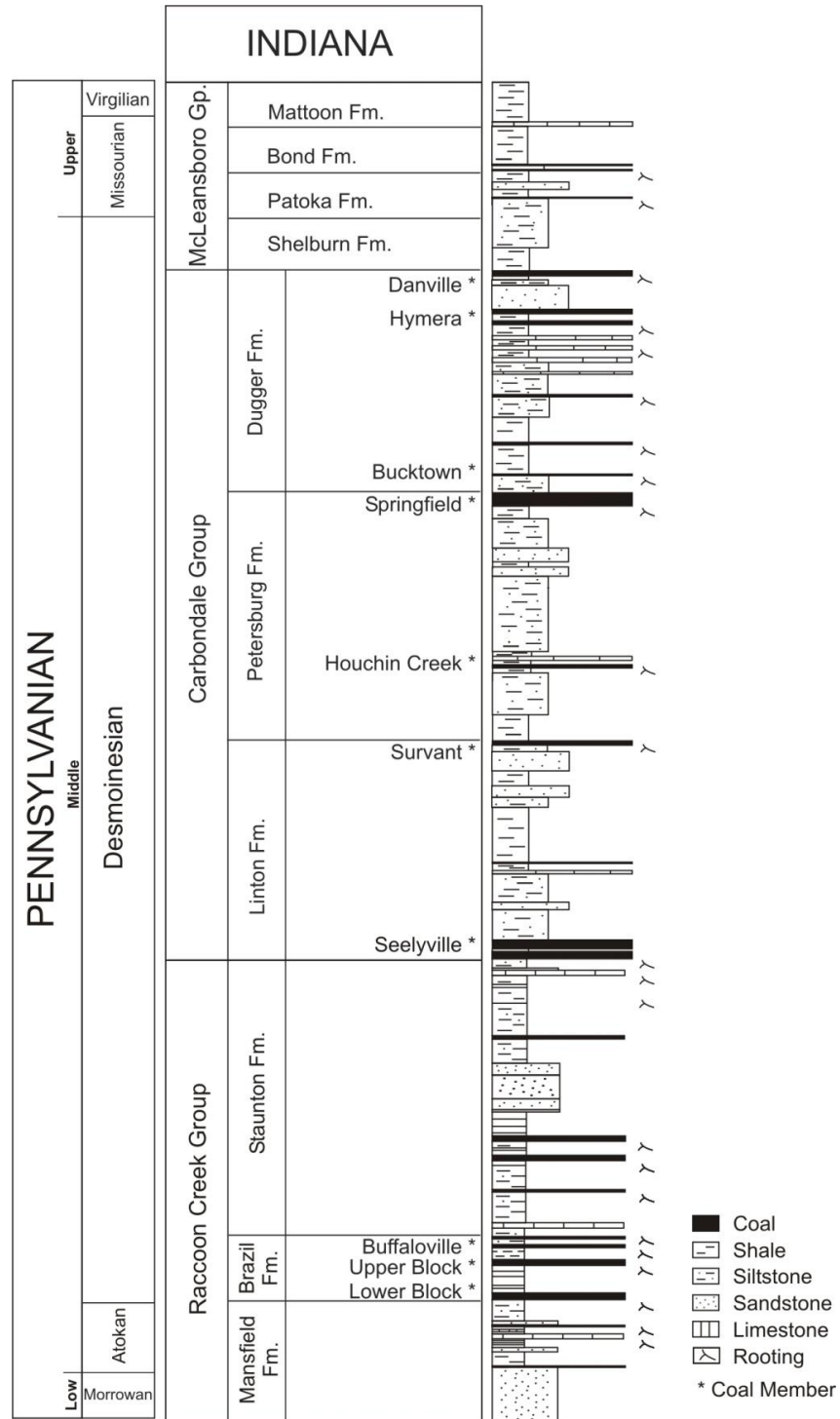


Figure 2. Generalized stratigraphic sequence of the coal-bearing units in the Pennsylvanian System of Indiana.

3.1.2. Coalbed methane potential of the Illinois Basin

The Illinois Basin contains a large coal resource that has been extensively mined since the early 19th century. According to Archer and Kirr (1984), the total coal resource of the Illinois Basin is equivalent to approximately $194 \cdot 10^9$ tons ($\sim 213.8 \cdot 10^9$ short tons). However, the vast majorities of these coals are discontinuous and are characterized by their variable thicknesses. Many units are considered not mineable owing to economical reasons. Yet, the widespread distribution of Pennsylvanian coal-bearing strata in the Illinois Basin represents an important resource for the study of potential gas accumulations.

Coal thickness, depth, overlying lithology, and structure are key factors in controlling gas content in the basin. Other factors such as rank and hydrodynamic setting also play an important role, especially with regard to the mechanisms of gas occurrence in coals. The rank of Illinois Basin coals ranges from high-volatile B to high-volatile A bituminous rank with increasing maturity with depth. In general, Illinois Basin coals exhibit a low maturity, which puts them in a low category for thermogenic gas generation. With the exception of Kentucky coals and perhaps some deep-seated coals near the center of the basin, most Illinois Basin coal gas generation can be attributed to microbial activity.

The relatively recent development of low-rank” gassy” coals from the Powder River Basin (Wyoming) and the Black Warrior Basin (Alabama) prompted additional exploration for coalbed gas in areas otherwise neglected because of the low gas contents observed from canister desorption measurements (i.e. in the Illinois Basin). Gas contents

measured from canister desorption in Illinois Basin coals generally range between ~0.94 to ~4.69 cm³/g (30 and 150 ft³/ short ton, respectively). Archer and Kirr (1984) estimated a potential gas in place of 0.07·10⁶ m³ (2.7·10¹² cubic feet) for two selected areas near the center of the basin. These authors also present a table with an estimated in-place coalbed gas resource of 0.57·10⁶ m³ (21·10¹² cubic feet) for the most widespread coal seams in the basin (i.e. Danville, Herrin, and Springfield coal seams and their equivalents). An assessment of this resource was reviewed by the USGS (1995), where gas potential was estimated as poor to fair, with technically recoverable amounts between 0.02·10⁶ m³ and 0.075·10⁶ m³ (0.84·10¹² and 2.77·10¹² cubic feet) for the basin. A reassessment of the gas potential and recoverable resource is currently under way by the USGS.

3.1.3. Coalbed methane potential of Indiana

The Seelyville Coal Member is considered the major target for CBM in the state because of its extension, continuity, thickness, and depth. Available canister desorption gas data from Indiana coals indicate that gas contents range between 0.5 and 5.7 cm³/g (15.4 and 182.2 ft³/short ton; Drobniak *et al.*, 2004) for the Seelyville Coal Member. Drobniak *et al.* (2004) estimated the CBM potential of the Seelyville Coal Member as 0.03·10⁶ m³ (1.1·10¹² cubic feet).

Other coal seams, such as the Springfield Coal Member indicate gas contents generally lower than 3.12 cm³/g (100 ft³/short ton), but with a large number of data between ~2.2 and 2.8 cm³/g (70 and 90 ft³/short ton; Mastalerz *et al.*, 2004). The net CBM potential of the state is still unknown and requires more data.

References

- Archer, P.L., Kirr, J.N., 1984. Pennsylvanian geology, coal, and coalbed methane resources of the Illinois Basin - Illinois, Indiana, and Kentucky. In: Rightmire, C.T., Eddy, G.E., Kirr, J.N. (Eds.), Coalbed Methane Resources of the United States. American Association of Petroleum Geologists, Studies in Geology 17, 105-134.
- Collinson, C., Sargent, M.L., Jennings, J.R., 1988. Illinois Basin region, Chapter 14. In: Sloss, L.L. (Ed.), Sedimentary Cover – North American Craton, U.S. Geological Society of America D-2, 383-426.
- Drobniak, A., Mastalerz, M., Rupp, J.A., Eaton, N., 2004. Evaluation of coalbed gas potential of the Seelyville Coal Member, Indiana, USA. International Journal of Coal Geology 57, 265-282.
- Gray, H.H., 1979. The Mississippian and Pennsylvanian (Carboniferous) Systems in the United States – Indiana. U.S. Geological Survey, Professional Paper 1110-K, K1-K20.
- Kvale, E.P., Archer, A.W., 1990. Tidal deposits associated with low-sulfur coals, Brazil Fm. (Lower Pennsylvanian), Indiana. Journal of Sedimentary Petrology 60, 563-574.
- Kvale, E.P., Mastalerz, M., 1998. Evidence of ancient freshwater tidal deposits. In: Davis, A.C., Davis, R., Henry, V. (Eds.), Tidalites: Processes and Products. SEPM (Society for Sedimentary Geology) Special Publications 61, 95–107.
- Kvale, E.P., Mastalerz, M., Furer, L.C., Engelhardt, D.W., Rexroad, C.B., Eble, C.F., 2004. Atokan and early Desmoinesian coal-bearing parasequences in Indiana,

- U.S.A. In: Pashin, J.C., Gastaldo, R.A. (Eds.), *Sequence Stratigraphy, Paleoclimate, and Tectonics of Coal-Bearing Strata*. American Association of Petroleum Geologists, *Studies in Geology* 51, 71–88.
- Mastalerz, M., Harper, D., 1998. *Coal in Indiana: A Geologic Overview*. Indiana Geological Survey, Special Report 60, 45 pp.
- Mastalerz, M., Drobniak, A., Rupp, J.A., Shaffer, N., 2004. Characterization of Indiana's coal resource: Availability of the reserves, physical and chemical properties of the coal, and the present and potential uses. Indiana Geological Survey, Open-file Study 04-02, 245 pp.
- McBride, J.H., Kolata, D.R., Hildebrand, T.G., 2003. Geophysical constraints on understanding of the origin of the Illinois basin and its underlying crust. *Tectonophysics* 363, 45-78.
- Potter, P.E., 1963. *Late Paleozoic sandstones of the Illinois basin*. Illinois State Geological Survey, Report of Investigations 217, 92 pp.
- Wanless, H.R., 1975. *Illinois Basin Region - Paleotectonic investigations of the Pennsylvanian System in the United States, Part 1: Introduction and regional analyses of the Pennsylvanian System*. U.S. Geological Survey, Professional Paper 853-E, 71-95.

CHAPTER 4

Coal-bed gas potential in Pennsylvanian coal beds of Indiana

Solano-Acosta, Wilfrido^{1,2}, Mastalerz, Maria¹, Rupp, John A.¹, Strapoć, Dariusz², and Schimmelmann, Arndt²

¹ Indiana Geological Survey, Indiana University, 611 N. Walnut Grove, Bloomington, IN 47405-2208, U.S.A.

² Department of Geological Sciences, Indiana University, 1001 E Tenth St., Bloomington, IN 47405-1405, U.S.A.

NOTICE: This is the author's version of a work that was accepted for publication in the Proceedings of the 2005 International Coalbed Methane Symposium, May 17-19, Bryant Conference Center, The University of Alabama, Tuscaloosa, AL. Paper 0526. Changes may have been made to this work since it was submitted for publication.

Abstract

The content of coal-bed methane (CBM) gas within the Pennsylvanian coal beds of the Illinois Basin varies widely depending on a series of factors including depth and thickness of the coal bed and lithologies of adjoining strata. Along the eastern margin of the Illinois Basin in Indiana, such a variable distribution is evident both laterally and vertically. In Daviess, Gibson, and Sullivan Counties, gas saturation can be generally related to the depth of coal beds, with higher gas volumes occurring at greater depths, although variations from this trend are common. In other areas, for example, western Posey County, gas volumes show erratic changes with depth, partly related to the lithologic composition of the strata overlying the coals, and specifically the proximity of porous and permeable sandstone-dominated sequences. The carbon and hydrogen stable isotopic compositions of coal-bed gases, $\delta^{13}\text{C}$ (-54 to -60 ‰) and δD (-180 to -210 ‰), from the Springfield and the Seelyville Coal Members from Gibson, Knox, and Sullivan Counties indicate that gas is of mixed thermogenic and biogenic origin, and that the contribution of biogenic gas ranges from 60 to more than 90 percent of the total CBM. The combination of variable origins and different degrees of gas saturation necessitates multiple exploration strategies for CBM in the Illinois Basin.

4.1. Introduction

Original coal reserves in Indiana have been recently estimated as $\sim 54 \cdot 10^9$ tons ($59.5 \cdot 10^9$ short tons) out of which, $51.4 \cdot 10^9$ tons ($56.7 \cdot 10^9$ short tons) remain unmined (Mastalerz *et al.*, 2004). Approximately $15.9 \cdot 10^9$ tons ($17.5 \cdot 10^9$ short tons) of coal remain available for either surface or underground mining, and $35.5 \cdot 10^9$ tons ($39.1 \cdot 10^9$ short tons) are unminable because of either technological limitations or due to land-use restrictions. Given this large volume of coal resources, the most continuous, thick, and widespread coal seams in the state of Indiana are currently under investigation for their potential as coal-bed methane sources.

A net CBM resource for the Illinois Basin has been estimated at $\sim 0.57 \cdot 10^{12} \text{ m}^3$ ($20 \cdot 10^{12}$ cubic feet of gas) by Archer and Kirr (1984) and at $0.59 \cdot 10^{12} \text{ m}^3$ ($21 \cdot 10^{12}$ cubic feet) by the Gas Research Institute (GRI, 1999). The gas potential of the Seelyville Coal Member, Linton Formation (Pennsylvanian) in Indiana was estimated to be $\sim 0.03 \cdot 10^{12} \text{ m}^3$ ($1.1 \cdot 10^{12}$ cubic feet; i.e., 1.1 Tcf, Drobniak *et al.*, 2004). Not being mined because of high ash yield and high sulfur content (Mastalerz and Harper, 1998), the Seelyville coal is one of the major CBM targets in Indiana because of its depth and thickness. Gas has been commercially produced from the Seelyville coal in Sullivan County, Indiana, for several years.

Other coal beds have not yet been evaluated for their gas potentials. The Danville and Springfield coals have been the primary targets for mining in Indiana, because of their thickness and quality, but neither of them have yet been prospected and economically exploited for coalbed methane. Other thinner coal beds, such as the

Houchin Creek, Survant, Colchester, or those in the Brazil Formation, complementing the thicker coal beds, might add significant CBM potential.

In order to understand coalbed gas distribution in Indiana, we are evaluating existing data from the perspective of coalbed methane exploration. This paper combines measured canister desorption CBM data from drilling operations, archived data sets, and laboratory analyses as tools to quantify the occurrence of CBM in this portion of the Illinois Basin.

4.2. Pennsylvanian coal stratigraphy

At the end of the Mississippian Period, major erosion and uplift rendered an unconformable surface upon which Pennsylvanian sediments were laid down onto an inclined surface that received sediments from the Canadian Shield and the Appalachian mountains (Archer and Kirr, 1984). The predominantly siliciclastic sequence that characterizes the Pennsylvanian System shows evidence of various sea level fluctuations that, in addition to coal intervals, ended with the deposition of alternating sands and shales, with minor interpositions of limestone and black shales indicating open marine conditions. Subaerial exposure is also evident in areas that exhibit good paleosol development.

Pennsylvanian coal-bearing strata in Indiana are subdivided into three main intervals that span from the Morrowan to the Desmoinesian Epochs (Raccoon Creek, Carbondale, and McLeansboro Groups). In the lower interval (Raccoon Creek Group), there are six coal seams, some of which are considered of economic importance due to their low sulfur

contents. However, none of them are thick and their extent is somewhat limited (Mastalerz and Harper, 1998).

The Carbondale Group (Figure 1) contains coals that account for most of the mining operations in Indiana (Mastalerz and Harper, 1998). This group is divided into three Formations (Linton, Petersburg, and Dugger). The sulfur content of Carbondale coals is greater than that of the Raccoon Creek coals. However, greater thickness, widespread distribution, and closer proximity to the surface make them more attractive for mining. The McLeansboro Group overlies the Carbondale Group and is considered a barren sequence because of the absence of thick and continuous layers of coal (Mastalerz and Harper, 1998).

The formations comprising the lower, middle, and upper Desmoinesian groups have been defined based on the intervals between mappable units such as limestone, coal beds, and shales. However, there are still some correlation problems among units because of the discontinuous nature of most strata, or alternatively, due to other problems such as coal seams that split into various benches. Correlations across Pennsylvanian age strata in the Illinois Basin are a difficult task that requires detailed subsurface information in addition to palynological data. Estimating the continuity of coal-bearing strata in Indiana has been traditionally done by correlating marker beds from both limestones and shales.

Upper and middle Pennsylvanian strata can be consistently identified on traditional oil and gas geophysical well logs due to their repetitive patterns and therefore predictable facies succession. Lower Pennsylvanian strata are not as consistent as in the Desmoinesian and younger units and they lack thick and widespread marker beds. The identification of parasequences, as well as the use of paleosols recognized from

continuous core data proved to be excellent tools in correlating intervals within the lower Pennsylvanian (Kvale *et al.*, 2004).

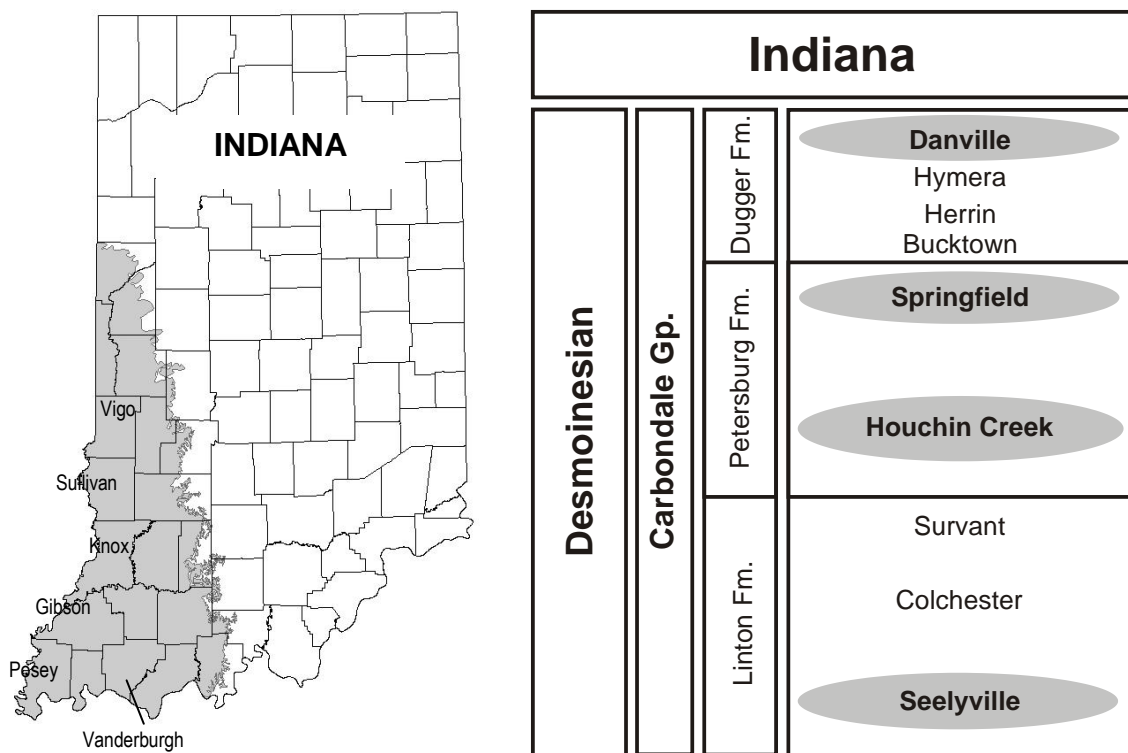


Figure 1. Geographic and stratigraphic distribution of Pennsylvanian coals of Desmoinesian age (Carbondale Group) in Indiana. Circled in gray and highlighted are the coal seams evaluated in this study.

4.3. Previous studies

Investigations on coal distribution and occurrence in western Indiana are available elsewhere (Harper, 1985, 1988a, 1988b, 1994; Eggert 1994; Harper and Eggert 1995; Mastalerz, *et al.*, 2003; Mastalerz *et al.*, 2004; Drobniak *et al.*, 2004). These works include data from surface and underground coal mining, geophysical logs from oil and gas drillings, and stratigraphic test holes. Although abundant information is available on geometry and structure of coal beds, the information on the gas content and gas distribution trends is limited.

Coalbed gas determinations have been carried out by some investigators (Harper, 1991; Mastalerz and Kvale, 1998; Mastalerz and Kvale, 2000; Mastalerz *et al.*, 2004). The gas content shows a direct correlation with depth in Daviess and Gibson Counties (Mastalerz and Kvale, 1998). However, such correlation is not so evident in Posey County, where an erratic distribution of gas content is observed (Mastalerz and Kvale, 2000). Gas contents measured with canister desorption techniques in Indiana vary anywhere from as little as 0.41 g/cm^3 (13 standard cubic feet per ton, raw basis) to as much as 4.66 g/cm^3 (149 scf/ton).

4.4. Coal distribution

Depth and thickness maps were created for the Danville, Springfield, Houchin Creek, and Seelyville Coal Members of the Pennsylvanian Carbondale Group. Figures 2 to 5 show the depths at which the coal could be expected, and the average thickness

values for each seam. The thickness of a coal seam is necessary information to determine the suitability of a coal seam for CBM well completions.

The depth to the Danville coal below the surface is charted geographically in meters by contour lines in Figure 2a. Most Danville coals at depths shallower than ~60.6 m (200 ft) are discarded for analysis from the CBM exploration point of view. The Danville Coal Member is generally very shallow, and it is one of the most extensively mined intervals due to its proximity to the surface. The thickness map for the Danville Coal Member (Figure 2b) shows very little areas where this coal is thicker than ~1.7 m (66 inches) and relatively small areas where the coal is between ~1.1 m and 1.7 m (44 and 66 inches), particularly where this coal occurs at depths greater than 60.6m (200 ft). Coal thickness distribution in this coal seam is very patchy, particularly in Gibson and Sullivan Counties, where this resource has been extensively mined and abundant information is available (Figure 2b). Its fairly constant distribution in Knox, Posey, and Vanderburgh Counties is more an artifact of the sample distribution, which is significantly more sparse than in the rest of the mapped area. Assessing the suitability of this seam for CBM in Indiana requires additional information including gas collection for determining its origin. Although gas contents for the Danville Coal Member have been measured from canister desorption techniques, there are no data about the isotopic composition of the gases associated with this coal seam. This isotopic information is critical in defining the exploration strategy for coalbed methane. Additional information is required to properly estimate the gas potential from this seam.

Similarly to the Danville Coal Member, the depth to the Springfield Coal Member was mapped (Figure 3a) showing in detail the occurrence of the Galatia channel in

Gibson County, Indiana. The geographic thickness distribution of this seam (Figure 3b) indicates an extensive and continuous coal deposit characterized by an overall thickness greater than ~1.06 m (42 inches), with few areas in Knox and Sullivan counties where its thickness is characteristically below 0.71 m (28 inches). Canister desorption data as well as isotopic gas compositions have been recently collected making this seam ideal for understanding the occurrence of CBM and therefore, allowing better predictions during exploratory phases.

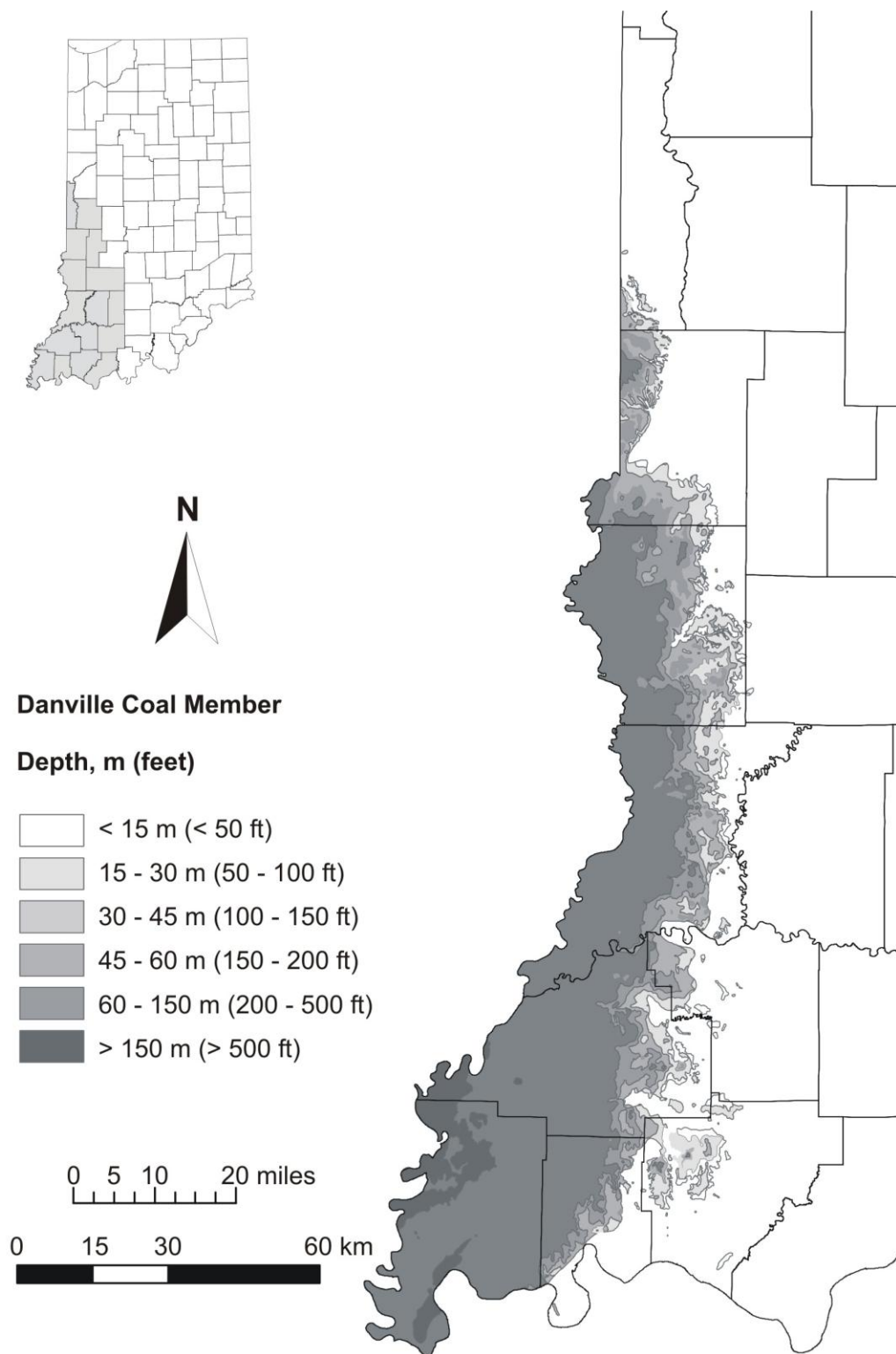


Figure 2a. Map showing depth of the Danville Coal Member in southwestern Indiana.

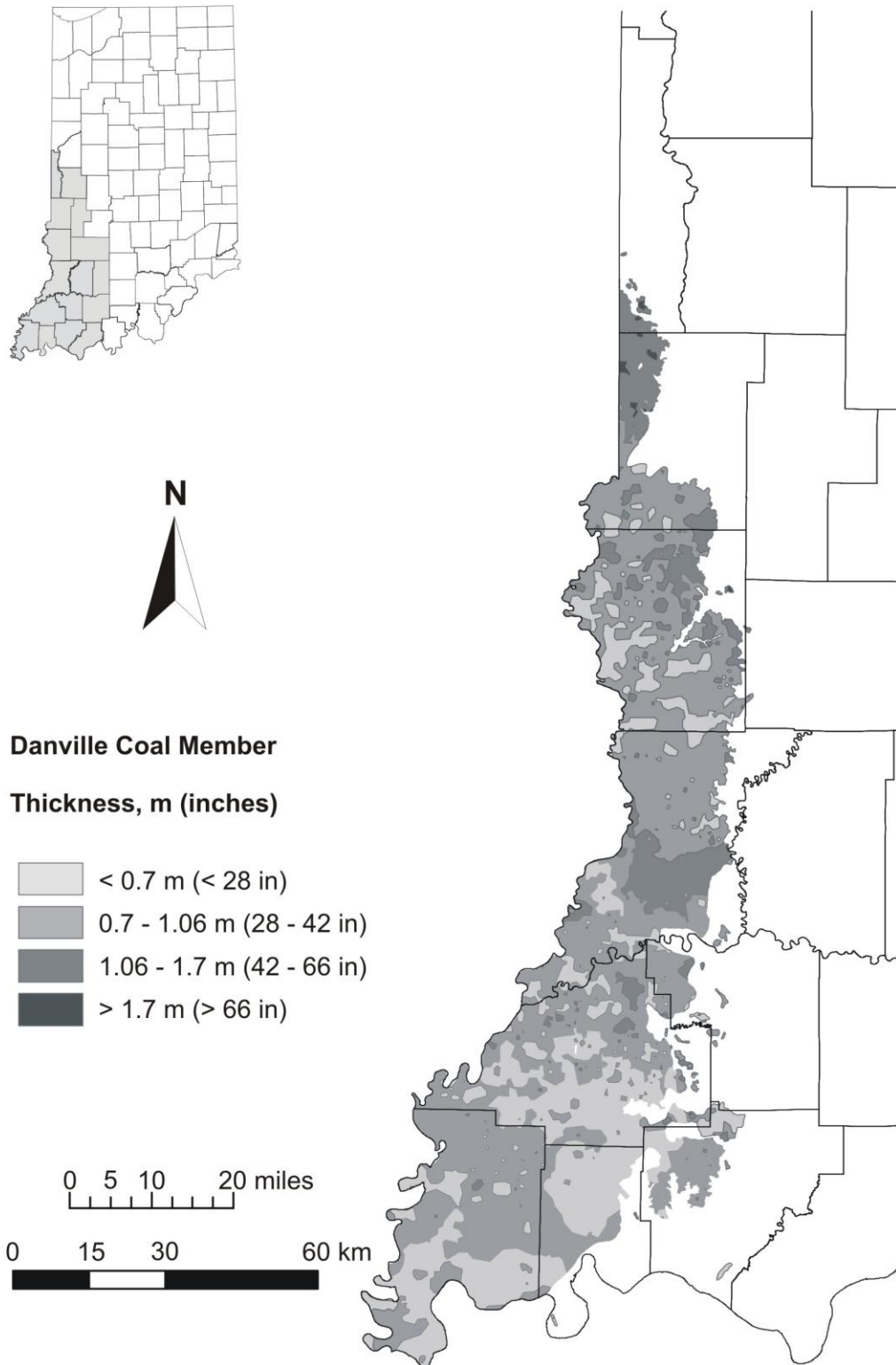


Figure 2b. Thickness map of the Danville Coal Member in southwestern Indiana.

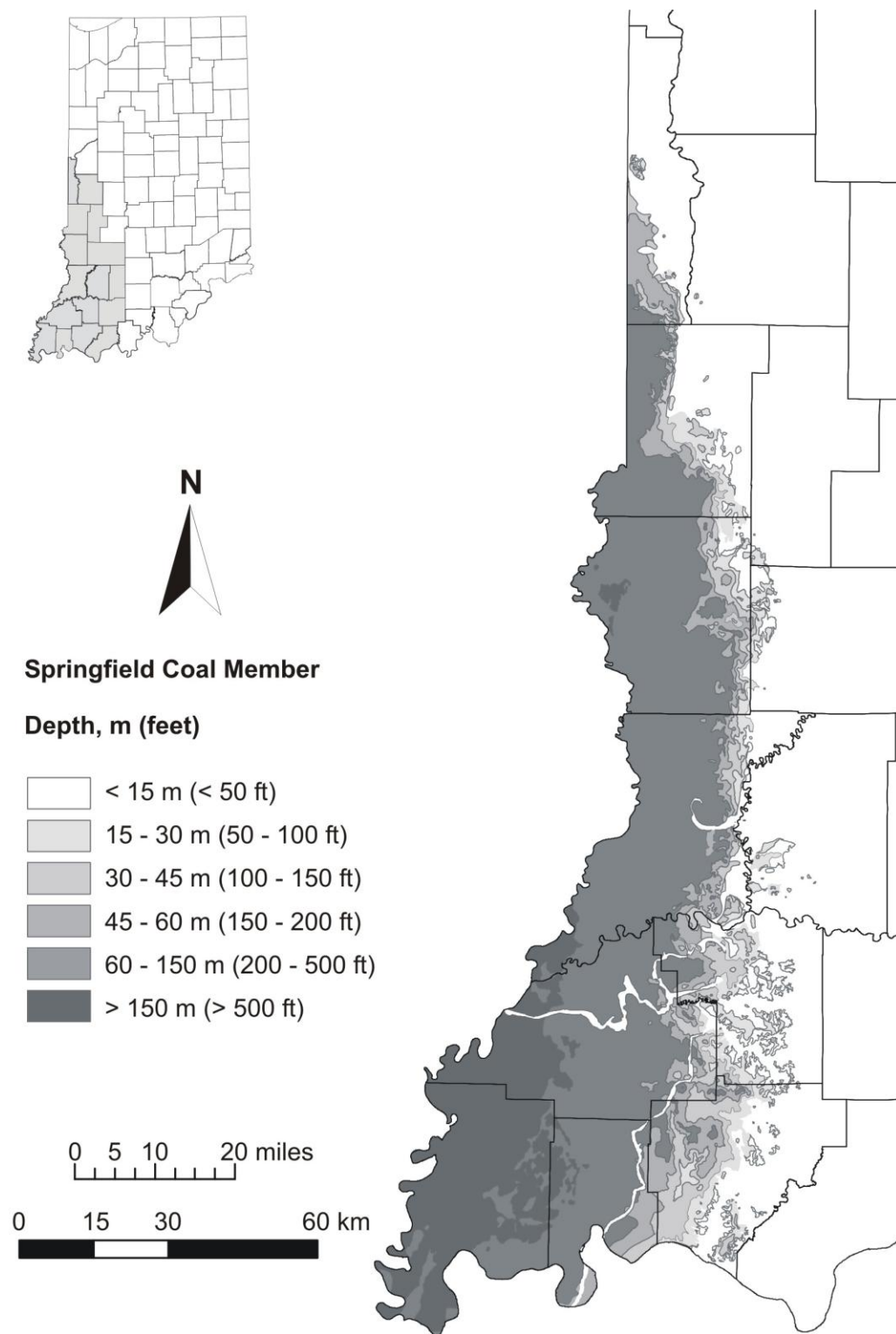


Figure 3a. Map showing depth of the Springfield Coal Member in southwestern Indiana.

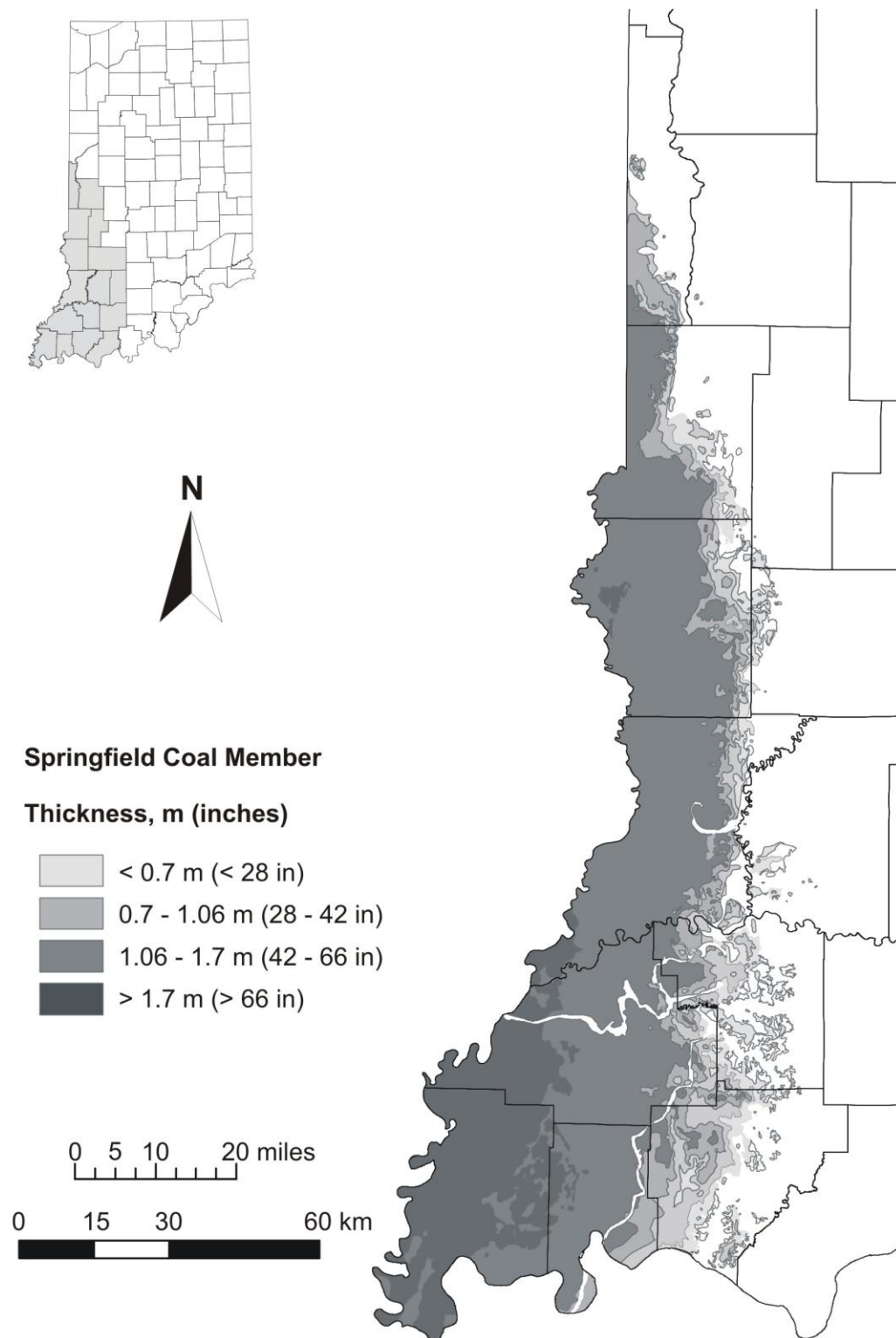


Figure 3b. Thickness map of the Springfield Coal Member in southwestern Indiana.

The Houchin Creek Coal Member was mapped for depth (Figure 4a) and thickness (Figure 4b) following the same methodology as for Danville and Springfield coals. Available information is significantly less detailed than that for the two overlying seams, but correlations made from geophysical logs from petroleum exploration indicate that this unit is one of the most continuous throughout southwestern Indiana, making this unit an ideal marker bed for regional correlations. Thickness of this unit is very variable, with significant contrasts in Gibson, Knox, and Sullivan Counties. Very little is known regarding the gas content and origin of this gas.

The Seelyville Coal Member was represented for depth and thickness based on available information (Figures 5a and 5b). This unit is considered as the primary target under investigation for CBM in Indiana because it features relatively large depth, thickness, and a wide regional distribution. Mapped thicknesses show great variability, particularly in Knox and Posey Counties (Figure 5b), where the adjacent lithologies are also characterized by the presence of discontinuous lenses of sandstone. The associated changes in adjacent lithology seem to play an important role in the occurrence of gas associated with this coal seam, and more detailed studies are required to understand the relationship between gas content and lithologic distribution.

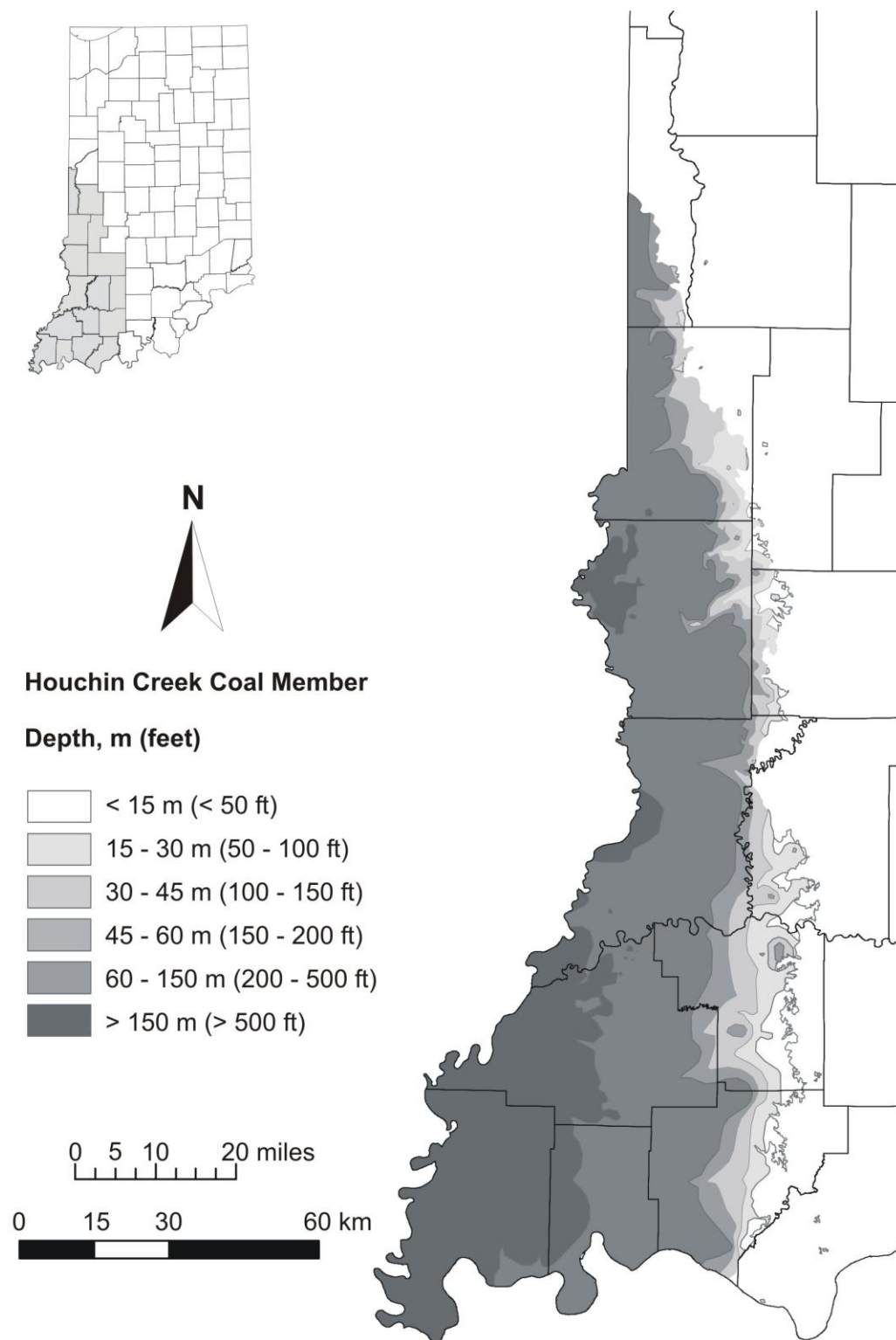


Figure 4a. Map showing depth of Houchin Creek Coal Member in southwestern Indiana.

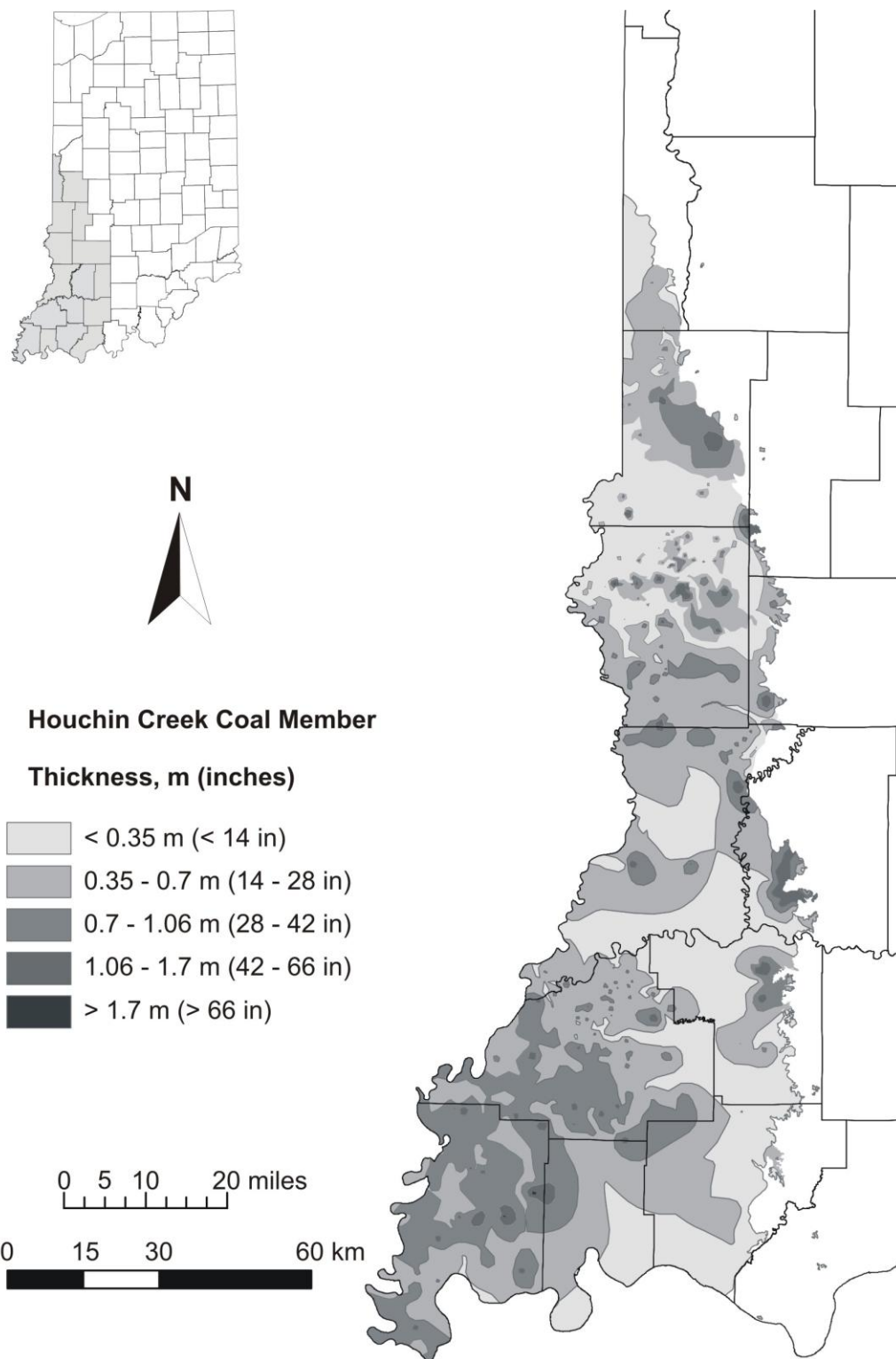


Figure 4b. Thickness map of the Houchin Creek Coal Member in southwestern Indiana.

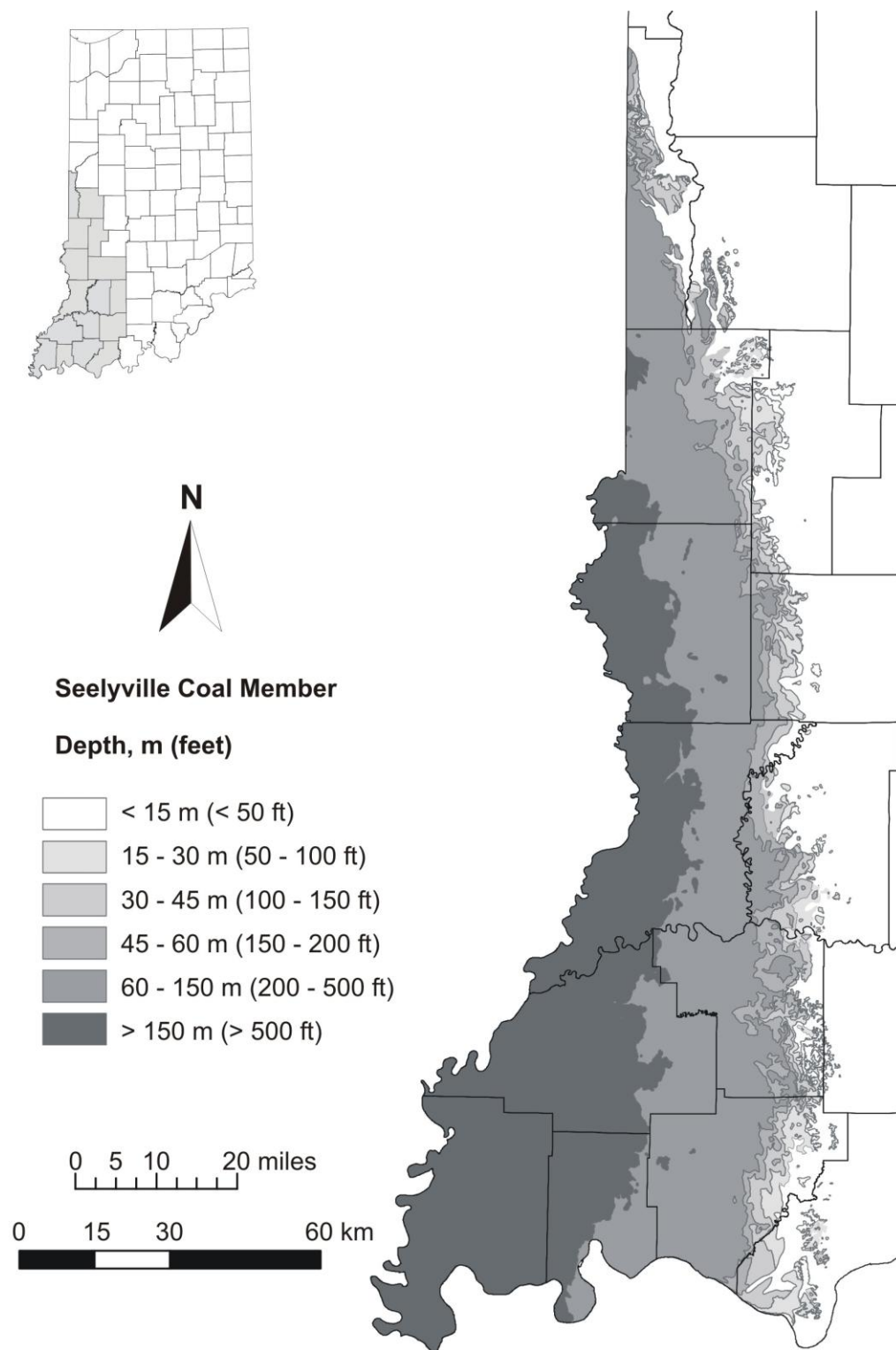


Figure 5a. Map showing depth of the Seelyville Coal Member in southwestern Indiana.

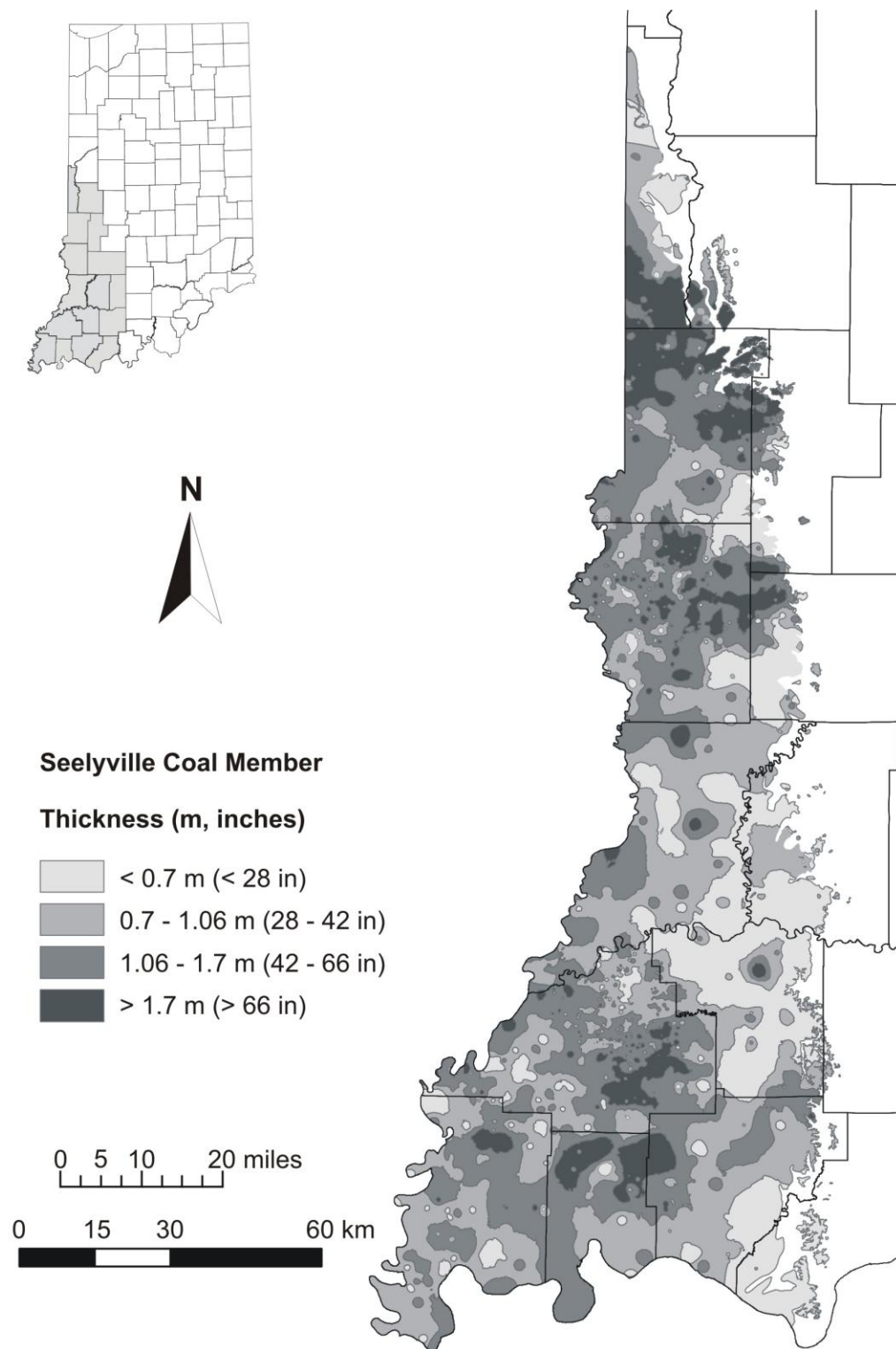


Figure 5b. Thickness map of the Seelyville Coal Member in southwestern Indiana.

4.5. Gas content

Direct gas measurements using canister desorption data have been used in Indiana to estimate the potential of Indiana's CBM resource as an alternative energy source.

Available canister desorption data from 58 wells drilled in Gibson, Knox, Posey, Sullivan, Vanderburgh, and Warrick Counties in southwestern Indiana were used to determine the maximum and minimum values for depth and gas contents of the studied coal seams. Table 1 shows the minimum and maximum depth and measured gas content for the Danville, Springfield, Houchin Creek, and Seelyville Coal Members.

The canister desorption data were plotted in terms of 'depth vs. gas content' to evaluate any correlation between these two parameters. The plot of all available data (Figure 6) indicates no significant correlation, probably due to the heterogeneity of facies above coals in some areas and the wide geographic distribution of data. The data for Sullivan and Gibson Counties were plotted on a new diagram (Figure 7) and indicate an overall increase in gas content with increasing depth. The facies distribution above the coals in these two counties is more homogeneous.

Table 1. Minimum and maximum depths and gas contents measured from canister desorption on Indiana coal samples ($1 \text{ cm}^3/\text{g} \approx 32 \text{ scf/ton}$).

Coal Seam	Depth, m (ft)		Gas Content, cm^3/g (scf/ton, raw basis)	
	Min	Max	Min	Max
Danville	50 (~145)	153 (~504)	0.9 (~29)	2.19 (~70)
Springfield	66 (~217)	203 (~669)	0.78 (~25)	3.0 (~96)
Houchin Creek	176 (~582)	234 (~772)	1.19 (~38)	2.28 (~73)
Seelyville	130 (~429)	286 (~943)	0.41 (~13)	4.66 (~149)

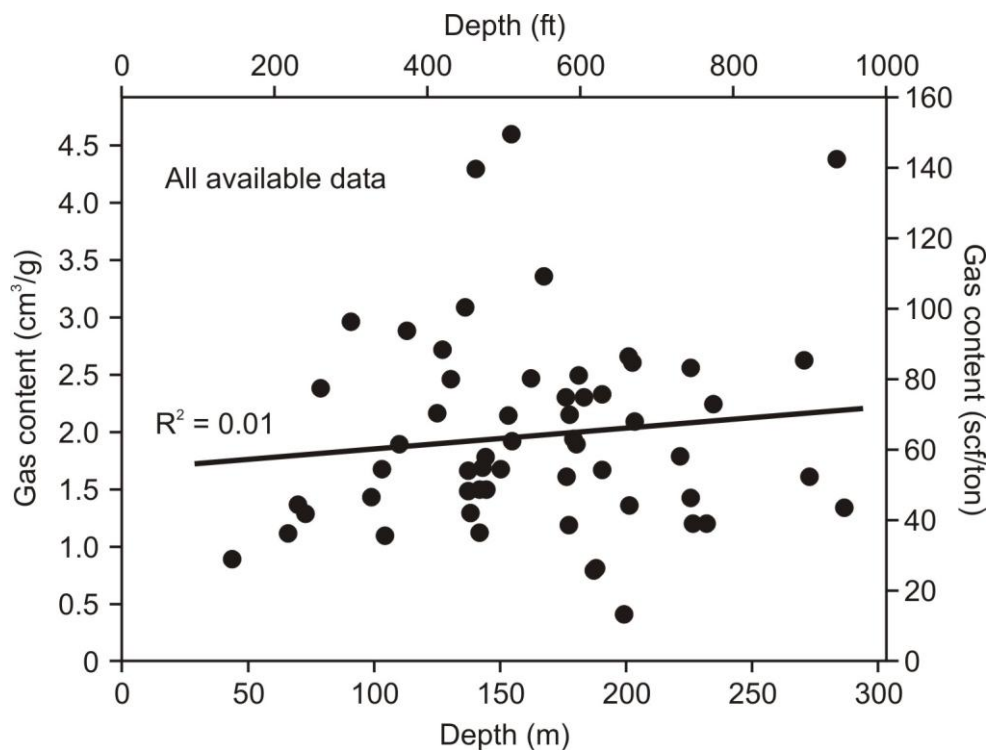


Figure 6. Depth vs. gas content data from canister desorption. No significant correlation observed for all available data.

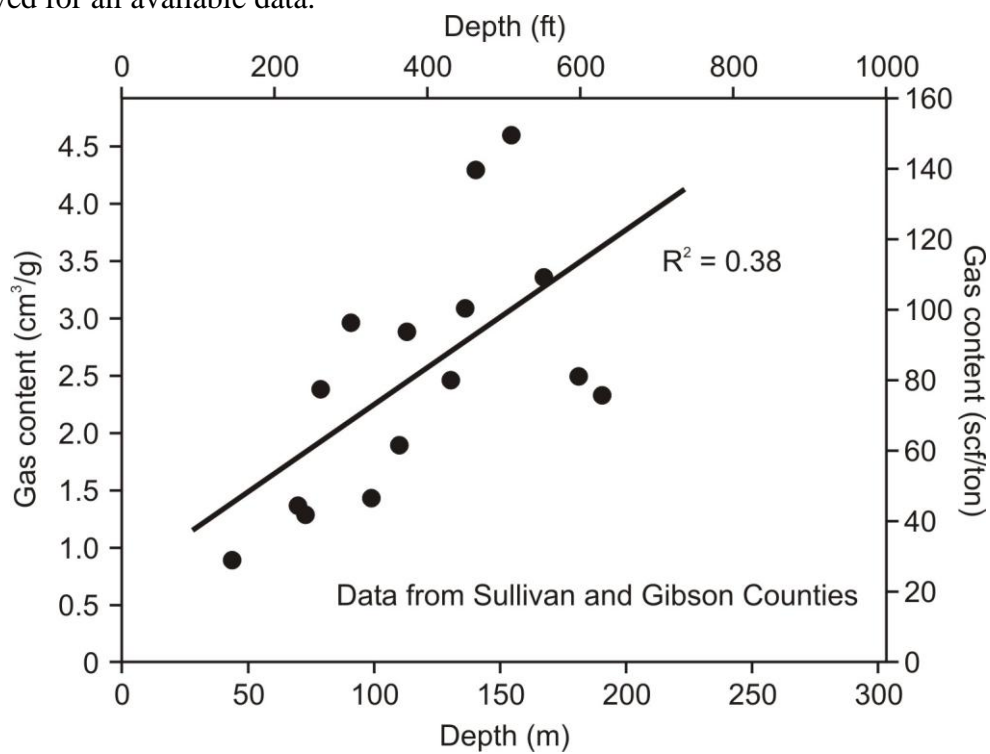


Figure 7. Data from Sullivan and Gibson Counties suggest a general increase in gas content with depth.

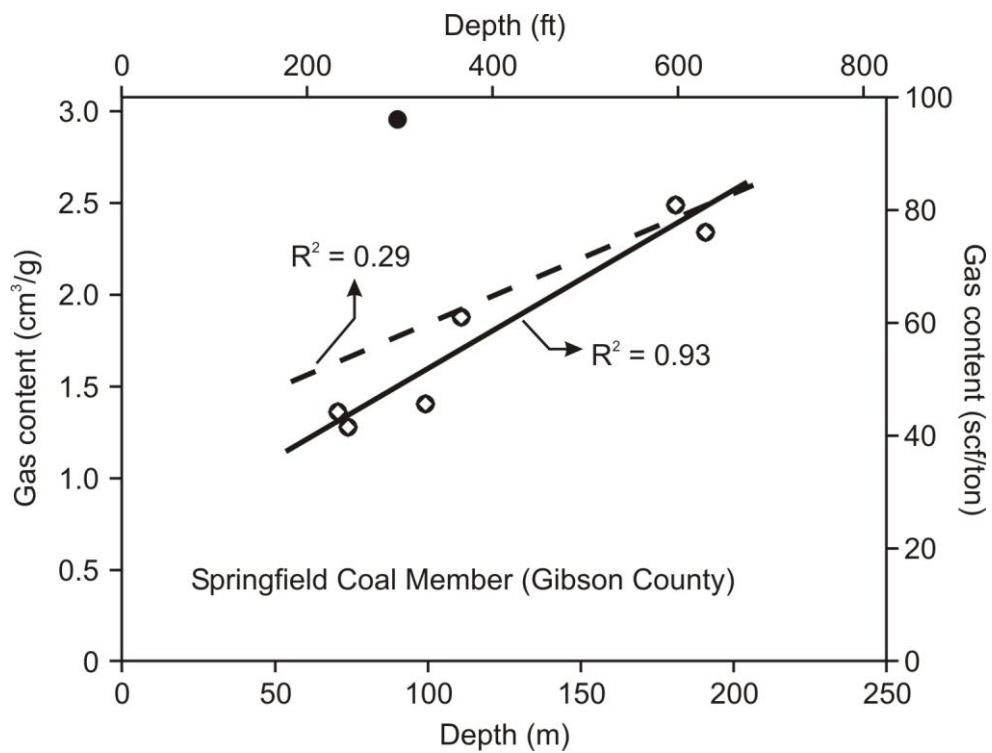


Figure 8. Data for Springfield coal in Gibson County suggest a very good correlation between gas content and depth ($R^2 = 0.93$). Only one value plotted outside the observed trend. When all data is included, the correlation drops ($R^2 = 0.29$).

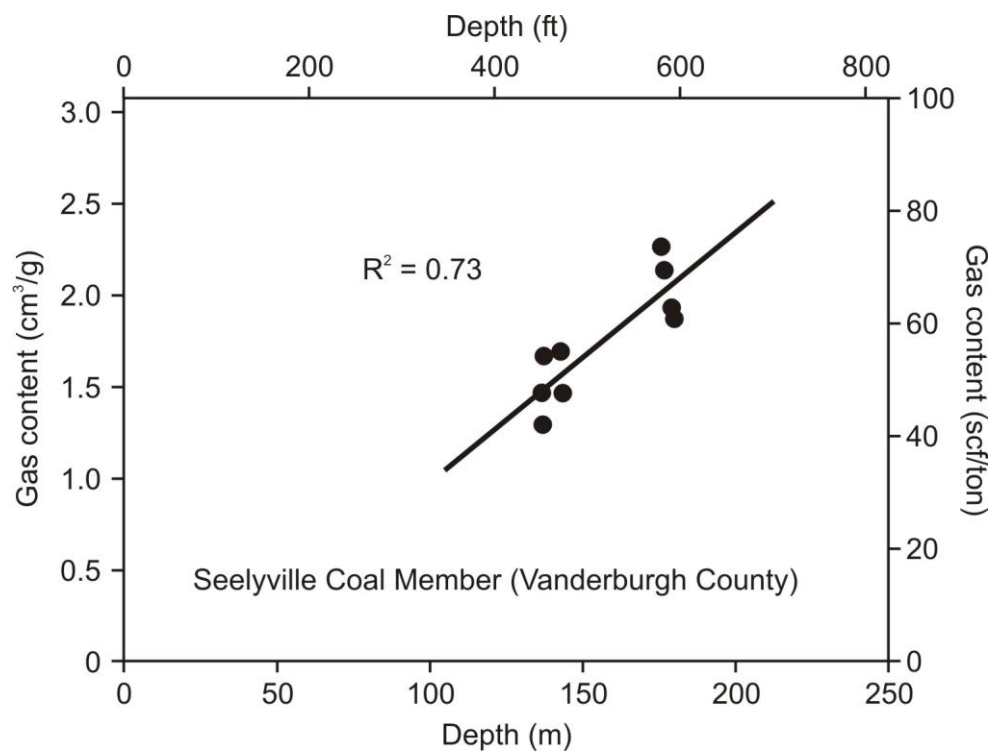


Figure 9. Data for Seelyville coals in Vanderburgh County showing a good correlation between gas content and depth ($R^2 = 0.73$).

To corroborate preliminary findings about the observed increase in gas content with increasing depth, Figure 8 shows the distribution of available data for the Springfield Coal Member in Gibson County. This diagram shows a consistent increase in gas content with increasing depth with the exception of a data point near ~90.9 m (300 ft) showing an anomalously high gas content value of 3 g/cm³ (96 scf/ton). A linear regression of all data indicates a poor correlation with $R^2 = 0.29$. However, eliminating the anomalous data point improves the correlation to $R^2 = 0.93$. The anomalously high CBM content of 3 g/cm³ (96 scf/ton) may be due to bacterially generated methane at shallow depths. Figure 9 shows a similar diagram as Figure 8 but the available data are from the Seelyville Coal Member in Vanderburgh County. The Seelyville coal in Vanderburgh County is slightly more mature (higher vitrinite reflectance values R_o) than the Springfield Coal Member in Gibson County and it occurs at greater depths. The data show a fairly good correlation between depth and gas contents (Figure 9). The relatively low gas contents are attributed to mainly thermogenic gas generation with minor contributions of biogenically generated methane in this portion of the basin.

4.6. Gas origin

Coal-bed gases in the Illinois Basin are generally of mixed thermogenic and biogenic origin. The biogenic end-member is generated via the microbial CO₂-reduction pathway, while thermogenic gas is a result of thermal cracking of organic compounds during burial. Most of the Illinois Basin coal-bed gases plot either within the isotopic field for microbial CO₂-reduction or the field for mixed-origin on the isotopic methane

classification graph shown in Figure 10 (Whiticar, 1999). Only the most mature gas sample from the Springfield coal of Kentucky indicates a well-defined thermogenic origin (Figure 10).

The contribution of the thermogenic end-member to the bulk gas varies depending on the coal maturity (R_o), which ranges from 0.52 to 0.75% (Table 2). Within this range of maturity, the microbial methane end member may range from 0 to almost 100% of the coalbed gas (Table 2), as roughly estimated following Katz *et al.*'s method (Katz *et al.*, 2002). Such a wide range of mixtures of microbial and thermogenic gas in Illinois Basin coals is expected because these coals are at or above the threshold for thermogenic gas generation. This threshold, usually considered at $R_o = 0.5$ to 0.6%, may be shifted up or down due to differences in maceral composition.

Table 2. Carbon and hydrogen isotope ratios of CBM from the Illinois Basin.

Coal Seam	Number of CBM samples	Depth, m (ft)	R_o (%)	δ¹³C (‰ vs. VPDB)	δD (‰ vs. VSMOW)	Biogenic contribution (% of total)
Springfield (IL)	1	161 (533)	0.52	-63.3	-200	100
Springfield (KY)	4	333 (1100)	0.75	-49.5	-180	0
Springfield (IN)	5	97 (321)	0.58	-69.9	-196	60
Houchin Creek (IN)	2	122 (366)	0.54	-58.6	-196	22
Seelyville (IN)	11	146 (483)	0.62	-58.2	-195	54

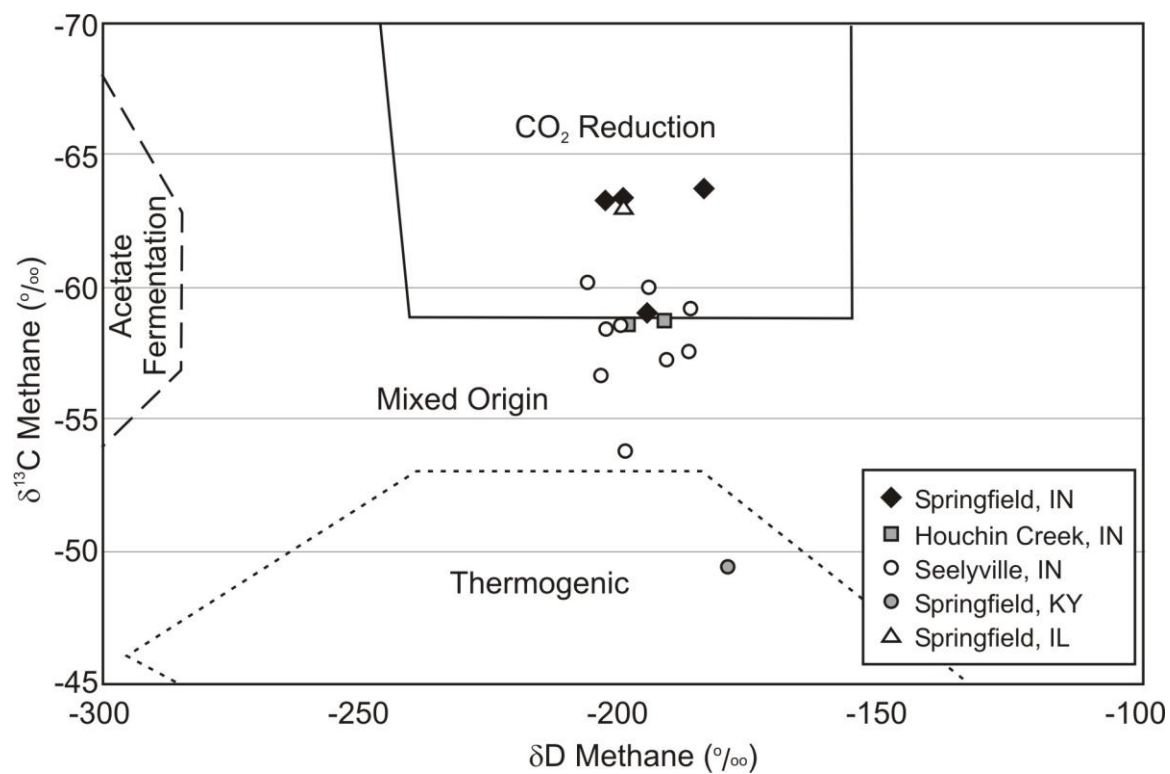


Figure 10. Carbon and hydrogen isotopes for available gas samples from coals in Indiana, Illinois, and Kentucky (isotopic ranges after Whiticar, 1999).

4.7. Conclusions

Indiana could potentially be attractive for CBM development because of abundant coal resources, and shallow depth of the coal (low pressure, high permeability) provided significant gas volumes are identified in the coal. Indiana coals, being of high volatile C bituminous rank, are not expected to generate much thermogenic gas, and the areas that have a mixture of thermogenic and biogenic gas may be the best target for economic CBM development.

Our CBM isotopic and compositional data from the Illinois Basin indeed indicate a whole spectrum for the origin of methane from almost purely thermogenic to purely biogenic.

Because of the mixed thermogenic and biogenic origin of coalbed gas in Indiana, exploration strategies must include elements of thermogenic and biogenic play to successfully predict and identify areas of highest gas contents.

References

- Archer, P.L., Kirr, J.N., 1984. Pennsylvanian geology, coal, and coalbed methane resources of the Illinois Basin — Illinois, Indiana, and Kentucky. In: Rightmire, C.T., Eddy, G.E., Kirr, J.N. (Eds.), Coalbed Methane Resources of the United States. American Association of Petroleum Geologists, Studies in Geology 17, 105–134.
- Drobniak, A., Mastalerz, M., Rupp, J.A., Eaton, N., 2004. Evaluation of coalbed gas potential of the Seelyville Coal Member, Indiana, USA. *International Journal of Coal Geology* 57, 265–282.
- Eggert, D.L., 1994. Coal Resources of Gibson County, Indiana. Indiana Geological Survey, Special Report 50, 36 pp.
- G.R.I., 1999. North American Coalbed Methane Resource Map. Gas Research Institute, Chicago, IL.
- Harper, D., 1985. Coal Mining in Vigo County, Indiana. Indiana Geological Survey, Special Report 34, 67 pp.
- Harper, D., 1988a. Coal Mining in Sullivan County, Indiana. Indiana Geological Survey, Special Report 43, 47 pp.
- Harper, D., 1988b. Underground mines in the Survant Coal Member (Pennsylvanian) of Indiana. Indiana Geological Survey, Special report 41, 19 pp.
- Harper, D., 1991. Coalbed Methane in Indiana. Indiana Geological Survey, Occasional Paper 56, 18 pp.

- Harper, D., 1994. Underground mines in the Hymera coal member (Pennsylvanian) of Indiana. Indiana Geological Survey, Occasional Paper 62, 12 pp.
- Harper, D., Eggert D.L., 1995. Coal Mining in Knox County, Indiana. Indiana Geological Survey, Special Report 54, 23 pp.
- Katz, B.J., Narimanov, A., Huseinzadeh, R., 2002. Significance of microbial processes in gases of the South Caspian Basin. *Marine and Petroleum Geology* 19, 783-796.
- Kvale, E.P., Mastalerz, M., Furer, L.C., Engelhardt, D.W., Rexroad, C.B., Eble, C.F., 2004. Atokan and early Desmoinesian coal-bearing parasequences in Indiana, U.S.A. In: Pashin, J.C., Gastaldo, R.A. (Eds.), *Sequence Stratigraphy, Paleoclimate, and Tectonics of Coal-Bearing Strata*. American Association of Petroleum Geologists, *Studies in Geology* 51, 71–88.
- Mastalerz, M., Ames, P.R., Padgett, P.L., 2003. Coals of the Brazil Formation (Pennsylvanian) in Indiana: observations of correlation inconsistencies and their implications. *International Journal of Coal Geology* 54, 209-222.
- Mastalerz, M., Drobnik, A., Rupp, J.A., Shaffer, N., 2004. Characterization of Indiana's coal resource: Availability of the reserves, physical and chemical properties of the coal, and the present and potential uses. Indiana Geological Survey, Open-file Study 04-02, 245 pp.
- Mastalerz, M., Harper, D., 1998. Coal in Indiana: A Geologic Overview. Indiana Geological Survey, Special Report 60, 45 pp.
- Mastalerz, M., Kvale, E.P., 1998. Coal-bed gas potential in Daviess County, Indiana. Indiana Geological Survey, Open-File Report 98-7, 53 pp.

Mastalerz, M., Kvale, E.P., 1998. Coal-bed gas potential in Gibson County, Indiana.

Indiana Geological Survey, Open-File Report 99-17, 39 pp.

Mastalerz, M., Kvale, E.P., 2000. Coal quality variation and coalbed gas content in

boreholes SDH-383 and SDH-384 in Posey County, Indiana. Indiana Geological

Survey, Open-File Study 00-5, 30 pp.

Whiticar, M.J., 1999. Carbon and hydrogen isotope systematics of bacterial formation

and oxidation of methane. *Chemical Geology* 161, 291-314.

CHAPTER 5

Cleats and their relation to geologic lineaments and coalbed methane potential in Pennsylvanian coals in Indiana

Wilfrido Solano-Acosta^{1,2}, Maria Mastalerz¹, and Arndt Schimmelmann²

¹ Indiana Geological Survey, Indiana University, 611 N. Walnut Grove, Bloomington,
IN 47405-2208, U.S.A.

² Department of Geological Sciences, Indiana University, 1001 E Tenth St.,
Bloomington, IN 47405-1405, U.S.A.

NOTICE: This is the author's version of a work that was accepted for publication in the International Journal of Coal Geology. Changes resulting from the publishing process, such as peer review, editing, corrections, structural formatting, and other quality control mechanisms may not be reflected in this document. Changes may have been made to this work since it was submitted for publication. A definitive version was subsequently published in <http://dx.doi.org/10.1016/j.coal.2007.02.004>

Abstract

Cleats and fractures in Pennsylvanian coals in southwestern Indiana were described, statistically analyzed, and subsequently interpreted in terms of their origin, relation to geologic lineaments, and significance for coal permeability and coalbed gas generation and storage. These cleats can be interpreted as the result of superimposed endogenic and exogenic processes. Endogenic processes are associated with coalification (*i.e.*, matrix dehydration and shrinkage), while exogenic processes are mainly associated with larger-scale phenomena, such as tectonic stress.

At least two distinct generations of cleats were identified on the basis of field reconnaissance and microscopic study: a first generation of cleats that developed early on during coalification and a second generation that cuts through the previous one at an angle that mimics the orientation of the present-day stress field. The observed parallelism between early-formed cleats and mapped lineaments suggests a well-established tectonic control during early cleat formation. Authigenic minerals filling early cleats represent the vestiges of once open hydrologic regimes. The second generation of cleats is characterized by less prominent features (*i.e.*, smaller apertures) with a much less pronounced occurrence of authigenic mineralization. Our findings suggest a multistage development of cleats that resulted from tectonic stress regimes that changed orientation during coalification and basin evolution.

The coals studied are characterized by a macrocleat distribution similar to that of well-developed coalbed methane basins (*e.g.*, Black Warrior Basin, Alabama). Scatter plots and regression analyses of meso- and microcleats reveal a power-law distribution between spacing and cleat aperture. The same distribution was observed

for fractures at microscopic scale. Our observations suggest that microcleats enhance permeability by providing additional paths for migration of gas out of the coal matrix, in addition to providing access for methanogenic bacteria.

The abundance, distribution, and orientation of cleats control coal fabric and are crucial features in all stages of coalbed gas operations (*i.e.*, exploration and production). Understanding coal fabric is important for coal gas exploration as it may be related to groundwater migration and the occurrence of methanogenic bacteria, prerequisite to biogenic gas accumulations. Likewise, the distribution of cleats in coal also determines pathways for migration and accumulation of thermogenic gas generated during coalification.

Keywords: cleats, lineaments, coalbed methane, permeability, Indiana, USA

5.1. Introduction

Cleats can be broadly defined as linear discontinuities forming a structural fabric that develops in coals as a result of physical and chemical changes during coalification. Two main types of cleats (face and butt) are generally present in coal beds (Ammosov and Eremin, 1963; Close, 1993; Laubach *et al.*, 1998; Ting, 1977). Face cleats represent the more prominent group and are developed perpendicular to bedding. Butt cleats are less conspicuous, perpendicular to bedding, and are oriented at nearly 90° to face cleats. In contrast, fractures are characterized by irregular discontinuities that do not follow a defined pattern. Their seemingly random distribution distinguishes fractures from face and butt cleats.

Cleats and fractures in coal are intimately related to stress conditions of the basin during and after coalification. Occurrence and development of cleats and fractures in coal have been interpreted as the result of endogenic stress in coal owing to devolatilization during thermal maturation, along with the concurrent exogenic (*i.e.*, not deriving from coal beds) tectonic stress that imposes preferred orientations to developing fractures (Close, 1993; Condon, 2003; Laubach *et al.*, 1998; Laubach *et al.*, 1991; Pashin, 1998; Pashin *et al.*, 1999; Pitman *et al.*, 2003).

Characterization of cleats and fractures is important both for coalbed methane (CBM) exploratory strategies as well as for successful recovery of coalbed gases, and this has been emphasized in numerous studies (Bustin, 1997; Pashin *et al.*, 1999; Pitman *et al.*, 2003; Scott, 1999, 2002; Su *et al.*, 2001). However, the link between cleat characteristics and CBM has remained elusive because of the lack of objective and quantitative measurements of cleats, and the presence of multiple populations of

cleats. These populations are difficult to discriminate and it is even more difficult to obtain statistically important number of measurements in the subsurface. Also, we lack an understanding of the contribution of microcleats to coal permeability.

To our knowledge, the relationship between coalbed gas occurrence and cleat directions in relation to geologic lineaments has not been investigated in Indiana. Although Bassett *et al.* (1978) addressed the relationship between gas production and lineaments in the Devonian New Albany Shale in southern Indiana, the authors did not find any significant correlations between gas occurrence and production with structure orientation or strike.

The objective of this paper is to show how field and laboratory data can be used to infer the origin, distribution, occurrence, and orientation of cleats in Indiana coals. Our goal is to better understand the effect that cleats and fractures have on coalbed methane potential. To accomplish this, special attention is paid to the various generations of cleats, the relationships that exist between cleats, fractures and geologic lineaments, and the possible implications for permeability and producibility of coalbed methane.

5.2. Geologic framework

The Pennsylvanian System in the Illinois Basin across Illinois, Indiana, and Kentucky (Figure 1) is part of a broad, shallow elongated depression called the Eastern Interior Basin. Major uplift and erosion at the end of the Mississippian created an unconformable surface upon which Pennsylvanian sediments were

deposited mainly from the Canadian Shield and the Appalachian mountains (Archer and Kirr, 1984).

Pennsylvanian rocks in southwestern Indiana are represented by a clastic sequence of shale, siltstone, and sandstone, with intercalated coals and limestones (Gray, 1979). This sequence of interbedded terrigenous and marine facies resulted from fluctuations in sea level. Deposition occurred along paralic and deltaic environments and was influenced by tidal regimes (Kvale and Archer, 1990; Kvale and Mastalerz, 1998; Kvale *et al.*, 2004). As a result, extensive development of swamps, marshes, and the deposition of alternating open marine (black shales and limestones) and continental facies (sandstones, siltstones, and associated coal deposits) occurred.

Pennsylvanian coal-bearing strata dating from the Morrowan to the Desmoinesian are subdivided in Indiana into three main groups, namely the Raccoon Creek, Carbondale, and McLeansboro Groups (Figure 2). Some of the coal seams of the Raccoon Creek Group have economic importance because of their low sulfur contents, but most have limited thickness and lateral extent (Mastalerz and Harper, 1998, and references therein). The Carbondale Group is stratigraphically divided into the Linton, Petersburg, and Dugger Formations containing widespread coals that account for most of the mining operations in Indiana (Mastalerz and Harper, 1998). Though the sulfur content in Carbondale coals is generally higher than that of Raccoon Creek coals, Carbondale coals are Indiana's most attractive coals for mining because of their widespread distribution, thickness, and proximity to the surface. The

McLeansboro Group lies on top of the Carbondale Group and contains no thick or continuous coal layers (Mastalerz and Harper, 1998).

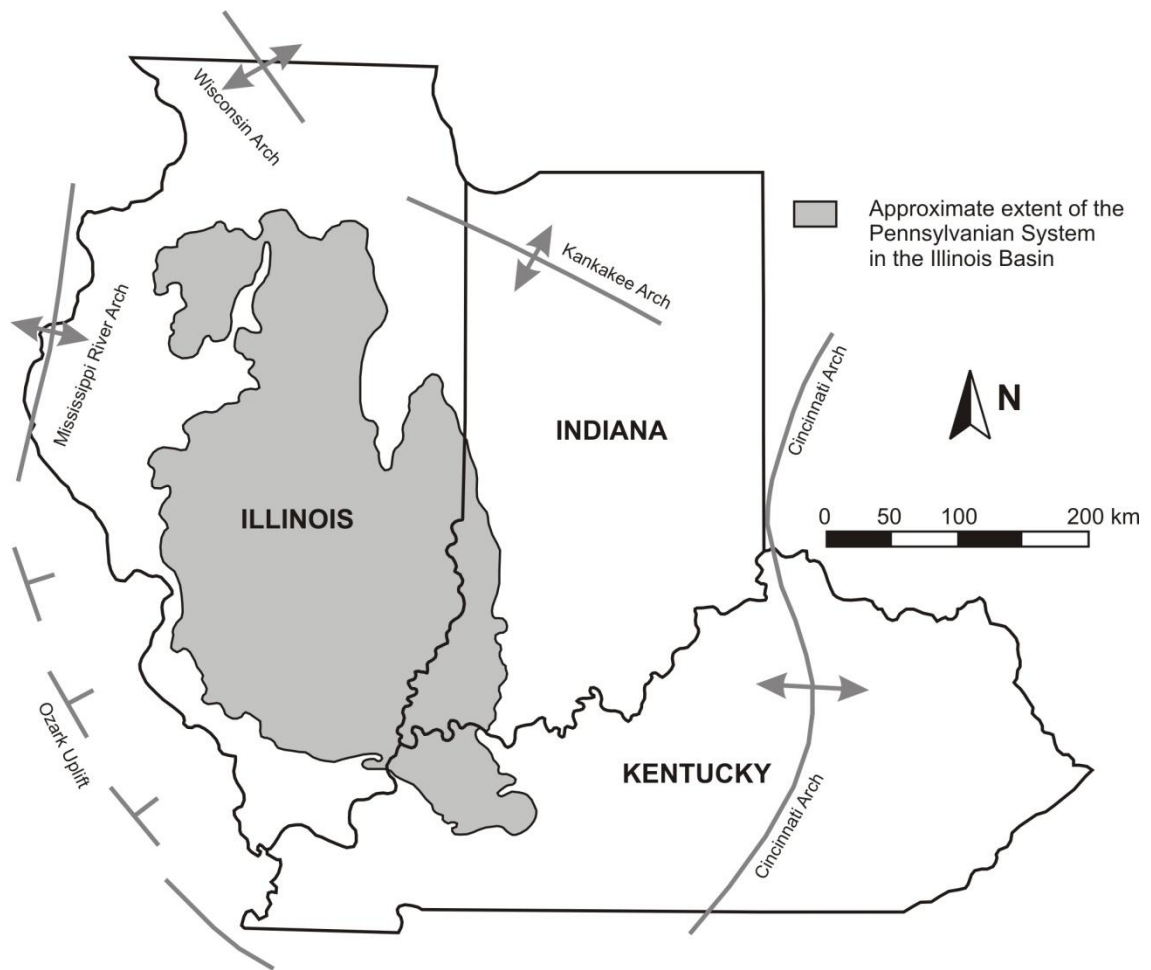


Figure 1. Structural configuration of the Illinois basin and extent of the Pennsylvanian System.

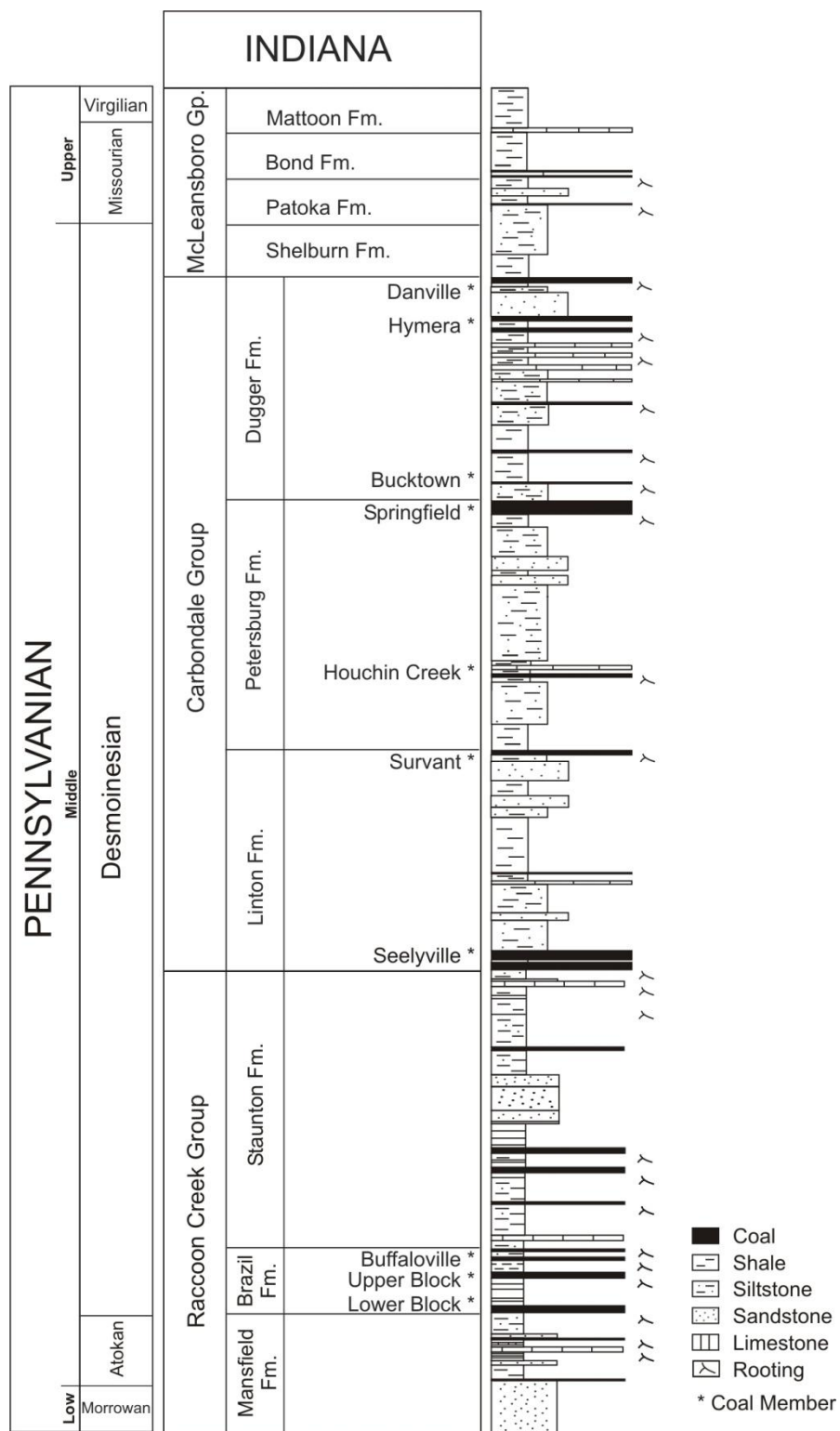


Figure 2. Generalized stratigraphic sequence of the coal-bearing units in the Pennsylvanian System of Indiana.

5.3. Methods

In this study, cleats and fractures in coal were identified at macro-, meso-, and microscales. On the largest scale, macrocleats can be readily identified in the field and measured directly. In contrast, mesocleats are characterized by more subtle features that, although visible with the naked eye, require collection of large samples that can be analyzed in the laboratory. On the smallest scale, microcleats correspond to those features that cannot be identified without a microscope. Identification of these three scales of cleats and fractures allows a better depiction of the pore network in coals, therefore, a better characterization of possible gas migration pathways.

To characterize coal fabric (*i.e.*, the geometric arrangement between cleat spacing and aperture width), a description of the cleat system can be made based on abundance of cleats per unit length in a perpendicular direction to face and butt cleats. Such description, together with measurements of cleat direction allows making inferences about the three-dimensional connectivity of the system available for fluid flow (Ortega *et al.*, 2006). Fracture intensity, also termed linear intensity, is defined as the number of fractures occurring in a linear segment (scanline) of known length (Mauldon *et al.*, 2001).

5.3.1. Measurements of macro- and mesocleats

Coal mines in southwestern Indiana were visited between 2004 and 2006 for collection of data on cleat spacing, distribution, and azimuth direction along various coal seams as they became accessible during mining operations. Table 1 shows the

group characterization of endogenic cleats proposed by Ammosov and Eremin (1963). A closely corresponding classification was adopted in this study. Field data presented in this paper most likely correspond to cleats of Groups 2 (macrocleats) and 3 (mesocleats), while laboratory data collected under the microscope refer to Group 4 (roughly corresponding to microcleats of this paper). Collected data also include the identification of relative fracture timing based on cross-cutting relationships. Macrocleat azimuth directions were measured with a hand-held compass corrected for magnetic declination.

Table 1. Populations of endogenic cleats.

This study's nomenclature	Relative cleat spacing	Ammosov and Eremin's (1963) classification of endogenic cleats^a
Macrocleats	Decimeters	Group 1: Traversing the entire thickness of a coalbed
	Centimeters	Group 2: Intersecting individual coal blocks
Mesocleats	Millimeters	Group 3: Intersecting individual petrographic varieties of coal
Microcleats	Micrometers	Group 4: Localized within interstratifications and lenses of vitrain and vitrinite coal

^a Ammosov and Eremin (1963) defined endogenic cleats as those developed because of coalification processes (i.e., matrix shrinkage, dehydration, etc). Cleats resulting from external processes (i.e., tectonism) are called exogenic.

Cleat and fracture data were collected from seven active surface mines in Daviess, Gibson, and Vigo Counties and from one underground mine in Greene County. Most data were collected on the top surface of the coals (plan-view measurements). Some measurements were taken from mine walls (side-view measurements).

Cleat data were collected for several coal seams in the Raccoon Creek Group (Lower Block, Upper Block, Buffaloville, and Staunton Coal Members) and in the Carbondale Group (Seelyville, Springfield, Hymera, and Danville Coal Members). Figure 3 shows the distribution and orientation of lineaments and the locations of cleat data from field measurements. At least ten measurements of face and butt cleats were collected in most outcrops. In locations where cleats were poorly developed, all available cleats were measured (Table 2).

For plan-view measurements, accessible areas were generally $<4 \text{ m}^2$. Azimuth, spacing, and length of cleats and fractures were collected, described, and occasionally photographed. Some intensely fractured coals prevented the identification of main cleat directions. In cases where fractures exhibited large variations in azimuth over relatively short distances, fracture patterns of adjacent lithologies were included in the observations to better evaluate possible associations with tectonism.

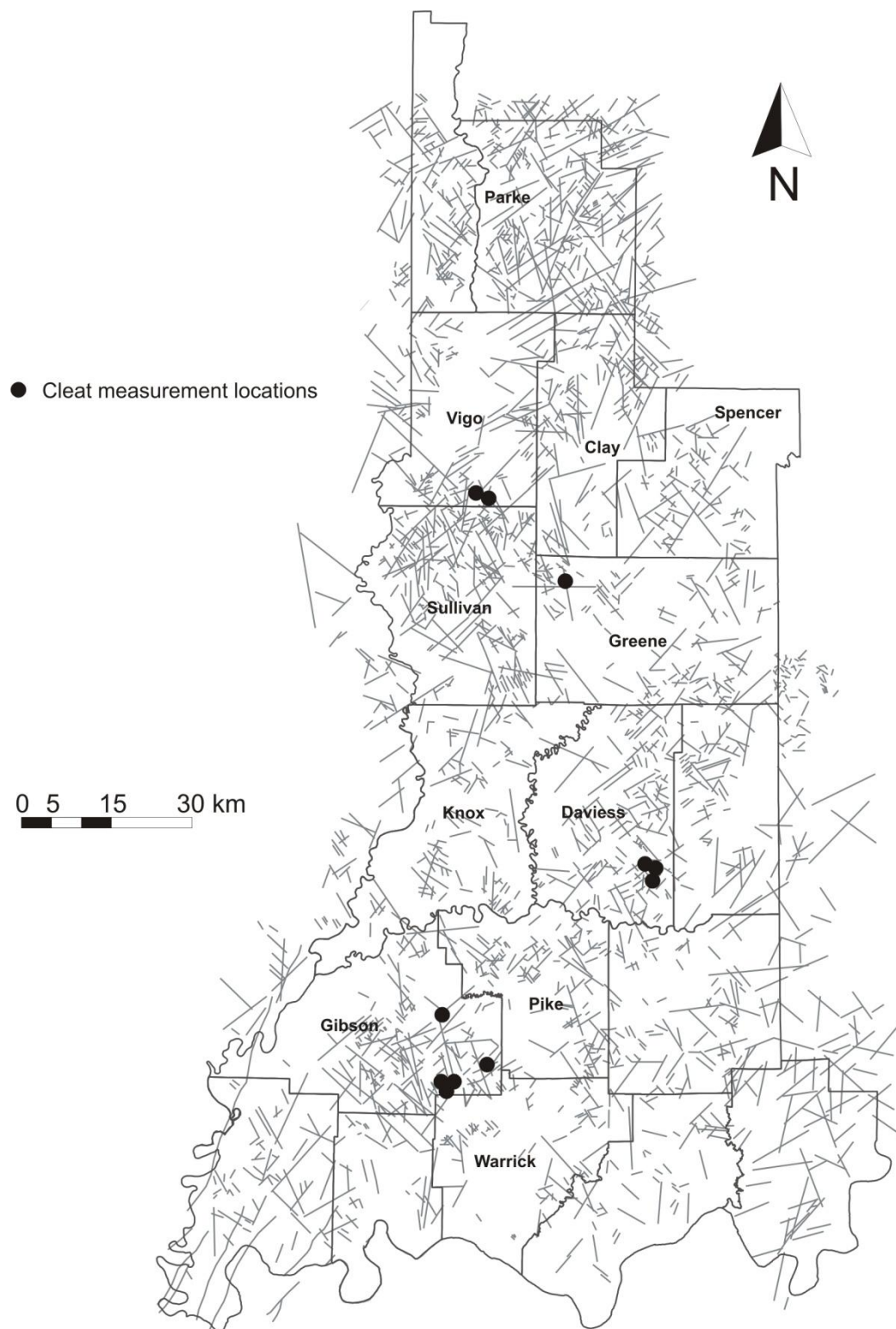


Figure 3. Photolinear interpretation of geological lineaments and faults in southwestern Indiana. Data compiled and modified from Wier *et al.*, (1974a, b).

Table 2. Measured macrocleat direction, spacing, and abundances in coals from various coal mines in southwestern Indiana. Macrocleats correspond to Group 2 of Ammosov and Eremin's (1963) classification.

County	Mine	Coal seam	Face cleats						Butt cleats					
			Abundance	Samples	Cleat spacing (cm)		Azimuth (°)		Abundance	Samples	Cleat spacing (cm)		Azimuth (°)	
			(cleat/cm)	(n)	Avg.	Std. Dev.	Avg.	Std. Dev.	(cleat/cm)	(n)	Avg.	Std. Dev.	Avg.	Std. Dev.
Davies	Billings	Lower Block	0.160	26	6.24	2.78	82.9	3.3	0.148	12	6.77	2.0	317.6	1.7
		Buffaloville	0.119	15	8.4	4.78	85.9	3.4	n.d.	7 ^b	n.d.	n.d.	n.d.	n.d.
	Corning	Lower Block	0.067	20	15	3.58	89.2	6.5	0.054	16	18.38	5.8	1.5	7.3
		Upper Block	0.081	21	12.38	2.8	87.3	6.0	0.054	14	18.36	5.0	356.9	6.7
	Midway	Staunton	0.141	22	7.09	2.66	104.6	3.4	n.d.	n.d.	n.d.	n.d.	n.d.	n.d.
		Buffaloville	0.061	17	16.3	8.36	112.4	8.5	n.d.	n.d.	n.d.	n.d.	n.d.	n.d.
		Upper Block	0.098	19	10.21	1.77	92.1	4.1	0.132	17	7.58	3.7	1.2	7.0
Gibson	Discovery	Hymera (VI)	0.146	10	6.84	2.56	72.3	12.3	n.d.	n.d.	n.d.	n.d.	n.d.	n.d.
		Springfield	0.152	6 ^b	6.58	2.91	103.3	9.0	n.d.	n.d.	n.d.	n.d.	n.d.	n.d.
		Danville	0.163	13	6.12	2.22	90.8	2.7	n.d.	n.d.	n.d.	n.d.	n.d.	n.d.
	Francisco	Upper VI	0.198	14	5.05	1.33	71.3	3.9	n.d.	n.d.	n.d.	n.d.	n.d.	n.d.
		Lower VI	0.179	20	5.59	1.95	74.8	4.6	n.d.	n.d.	n.d.	n.d.	n.d.	n.d.
			0.298	16	3.35	1.57	79.1	5.7	n.d.	n.d.	n.d.	n.d.	n.d.	n.d.
	Sommerville	Springfield	0.164	34	6.08	3.10	80.2	4.7	0.080	22	6.76	3.4	355.0	n.d.
		Hymera (VI)	0.141	51	4.33	2.25	87.5	4.6	0.084	4 ^b	11.9	1.9	n.d.	n.d.
		Danville	0.122	30	7.21	1.71	76.7	3.2	0.116	10	8.6	4.7	348.5	3.0
Greene	Howesville ^a	Lower Block	0.081	27	6.06	3.22	86.5	7.4	0.081	26	7.13	2.32	350	4.3
Vigo	Farmersburg	Danville	0.134	23	7.43	4.24	71.5	7.2	0.100	20	10	4.7	339.4	11.0
			0.094	21	10.62	5.16	80.3	6.3	0.081	21	12.38	7.5	347.2	2.4
		Hymera (VI)	0.115	21	6.21	3.25	72.0	5.2	0.084	27	6.02	3.0	335.9	5.3

n.d. - no data available for this location.

^a Underground mine

^b less than 10 measurements

Large coal blocks of various sizes (0.024 to 0.045 m³ on average) collected from freshly exposed outcrops in various surface mines were measured in-situ for macrocleats (Table 2), and carried to the laboratory for micro- and mesocleat measurements. The collected data set was complemented with previous measurements of cleat directions taken by Mastalerz from 1996 to 2002 from both surface and underground coal mines (Table 3), and from cleat data of Ambers (1993) and structural data of Ault *et al.* (1985). For comparison with field-collected data, mesocleats with a length of maximally 3 cm were measured from the same coal blocks in the laboratory (Table 4).

Table 3. Indiana macro- and mesocleat data collected prior to this study (Mastalerz, personal database).








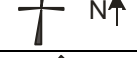




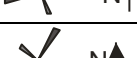


County	Mine	Coal seam	Type	Azimuth (°)	Rose
Clay	Salt City	Lower Block	face butt	70 165	 N↑
		Mansfield	face butt	85 165	 N↑
Daviess	Billings	Lower Block	face butt	0 85	 N↑
	Corning	Lower Block	face	94	 N↑
	Midway	Buffaloville	face butt	2 90	 N↑
Gibson	Sommerville	Lower Millersburg	face butt	175 90	 N↑
		Springfield	face butt	185 90	 N↑
	Gibson Co. Underground	Springfield	face butt	45 135	 N↑
Greene	Miller Creek	Lower Block	face butt	60 150	 N↑
		Mansfield	face butt	70 165	 N↑
Parke	Rainbow	Minshall / Buffaloville	face butt	80 145	 N↑
Spencer	Flint Hill	Lower Brazil	face butt	80 160	 N↑
		Mariah Hill	face butt	30 130	 N↑
Sullivan	Farmersburg	Danville	face butt	90 170	 N↑
Warrick	Cypress Creek	Springfield	face butt	71 170	 N↑

Table 4. Mesocleat measurements on hand specimens for selected coals. Mesocleats correspond to Group 3 of Ammosov and Eremin's (1963) classification.

County	Mine	Coal seam	Face cleats				Butt cleats			
			Abundance	Samples	Cleat spacing (mm)		Abundance	Samples	Cleat spacing (mm)	
			(cleat/cm)	(n)	Avg.	Std. Dev.	(cleat/cm)	(n)	Avg.	Std. Dev.
Daviess	Midway	Buffaloville	3.42	20	2.93	1.4	2.27	20	4.40	2.6
		Upper Block	2.63	20	3.80	2.1	2.52	20	3.98	2.0
		Lower Block	2.80	20	3.58	2.4	3.64	20	2.75	1.0
Gibson	Discovery	Hymera (VI)	4.65	20	2.15	0.9	2.63	10	3.80	2.0
		Danville	2.31	20	4.33	2.2	1.52	20	6.60	3.3
	Francisco	Upper VI	2.40	20	4.18	1.8	2.53	20	3.95	1.7
	Sommerville	Springfield	2.26	20	4.43	2.4	1.19	20	8.38	3.7
		Hymera (VI)	1.68	16	5.97	2.9	2.76	16	3.63	1.5
		Danville	2.52	20	3.98	1.5	2.27	20	4.40	1.3
Greene	Howesville ^a	Lower Block	1.86	16	5.38	2.5	2.29	20	4.38	2.0
Vigo	Farmersburg	Danville	1.85	16	5.41	2.7	2.94	20	3.40	1.4

^a Underground mine.

Table 5. Average microcleat apertures and spacing measured under the microscope. Microcleats correspond to Group 4 of Ammosov and Eremin's (1963) classification. Slit aperture and spacing measurements are also reported.

Face microcleats		Butt microcleats		Oblique face		Oblique butt		Microfractures	
Aperture	Spacing	Aperture	Spacing	Aperture	Spacing	Aperture	Spacing	Aperture	Spacing
1 - 6 μm	1.05 mm	1 - 3 μm	762 μm	<2 μm	202 μm	<2 μm	n.d.	1.18 μm	n.d.
Other linear discontinuities observed									
Parallel to face		Parallel to butt		Parallel to oblique face		Parallel to oblique butt		Irregular slits	
Aperture	Spacing	Aperture	Spacing	Aperture	Spacing	Aperture	Spacing	Aperture	Spacing
1.05 μm	82.2 μm	0.82 μm	73 μm	0.69 μm	62.5 μm	0.81 μm	n.d.	Irregular	n.d.
Slits: small, discontinuous linear features that resemble cleats and fractures are also present									

n.d. - no data available.

5.3.2. Microcleat analysis

Vitrinite-rich layers in coal were selected from coal seams because cleats tend to be developed more prominently along vitrinite intercalations. Five samples containing multiple vitrinite layers from Lower Block (1), Springfield (1), Hymera (1), and Danville (2) coals were prepared for petrographic analysis by cutting coal into small cubes (approximately 1 to 1.5 cm³) with a Leco[®] VC-50 high-precision saw. The samples were placed in Lucite powder and converted to Lucite-embedded pellets on a Leco[®] PR-15 mounting press via melting. The samples were polished with a semi-automated Leco[®] AP-60 polishing tool and mounted on glass plates for analysis under the microscope. Images (reflected light, in oil) were collected through a high-definition digital Spot Insight QE monochromatic camera attached to a reflected light Zeiss Photoscope II. Transects along vitrinite layers were photographed at 12-bit resolution (40X magnification). The analysis of collected images with MetaView[™] software allowed digital magnification of the images for measuring precise distances ($\pm 2 \mu\text{m}$) on the screen. The average aperture and spacing of microcleats and fractures along various transects were counted and presented in Table 5. Each discontinuity was identified either as face or butt cleat depending on their abutting relationships, or as irregular fractures based on their jagged appearance and their random relationships with main cleat directions. Because all microcleats and microfractures were measured in vitrinite-rich intervals from coals of the same rank, the data were combined into a single spreadsheet for statistical analysis.

5.3.3. Lineament analysis

Lineaments, in general, are defined as “regional linear features caused by the alignment of regional morphological features, such as streams, escarpments, and mountain ranges, and tonal features that in many areas are the surface expression of fractures or fault zones” (Lillesand and Kiefer, 1994). Analysis of lineaments, joints, and fractures provides a framework distribution of megascale features and also provides insight about coal fabric in unexplored areas (Diamond *et al.*, 1975, 1976).

Lineament data have previously been used to assess mining hazards, especially in relation to roof fall prediction (Wier *et al.*, 1974a, b). Photolinear analysis of satellite imagery and aerial photographs can also be used to predict trends in cleat direction and possible routes for groundwater migration. As with prediction of roof-rock failure zones via lineament data, such analysis may allow identifying groundwater conduits in coal, which may be associated with potential generation of coalbed methane.

Geologic lineament data from published maps of the Indiana Geological Survey (Powell, 1978; Wier *et al.*, 1974a, b) were georeferenced and digitized for geographic information system (GIS) analysis (ESRI® ArcMap™ 9.1). Figure 3 shows the distribution of lineaments from satellite imagery and aerial photographs. Preferential directions of lineaments were digitally analyzed using commercial software (Geoplus Petra®) to minimize interpreter bias. A grid of 20 km in radius was selected to perform the lineament analysis. The error in estimating a preferential orientation is mainly constrained by data density. Errors are greater near the edges of the grid, where data coverage is poor to nonexistent.

5.4. Results

5.4.1. Macro- and mesocleat data

Cleat data for Indiana coal seams that had been available prior to this study are listed in Table 3. Previously measured face-cleat directions indicate a preferential azimuth near 90° or at a low angle (<30°) due north from the east direction. However, two Gibson County mines (Sommerville and Gibson Co. Underground) depart from this trend by featuring ~45° face-cleat direction for the Gibson underground mine, and ~1° face-cleat direction for the Sommerville mine. Also, a discrepancy is observed in Daviess County for the Lower Block coal in two mines (Billings and Corning) where face-cleat directions differ by ~90° from one location to the other. The apparent discrepancy may have resulted from improper identification of face versus butt cleat data in the field, insufficient measurements, or presence of a secondary cleat system that complicates the interpretation. Our new cleat data reveal a more consistent orientation for both face and butt cleats. Table 2 shows a summary of macrocleat data (Group 2 of Ammosov and Eremin, 1963, Table 1) for seven surface mines in Daviess, Gibson, and Vigo Counties and one underground mine in Greene County. The average azimuth direction of face cleats is 85° and the average azimuth direction for butt cleats is 346°.

Figure 4 shows that the spacing of face macrocleats ranges between 3.3 cm and 12.3 cm (~8 cm on average for various coal beds). Butt cleats tend to be less well developed in many coal seams, are more difficult to measure, and exhibit a less regular spacing (~6 to 18.4 cm). Face and butt cleats are occasionally obliterated,

possibly as a result of annealing because of thermal maturation, while in other instances both face and butt cleats are preserved by authigenic mineralization. We identified various authigenic mineral phases forming quasi-continuous sheets of pyrite, kaolinite, or calcite along different cleat systems at macro-, meso-, and microscales.

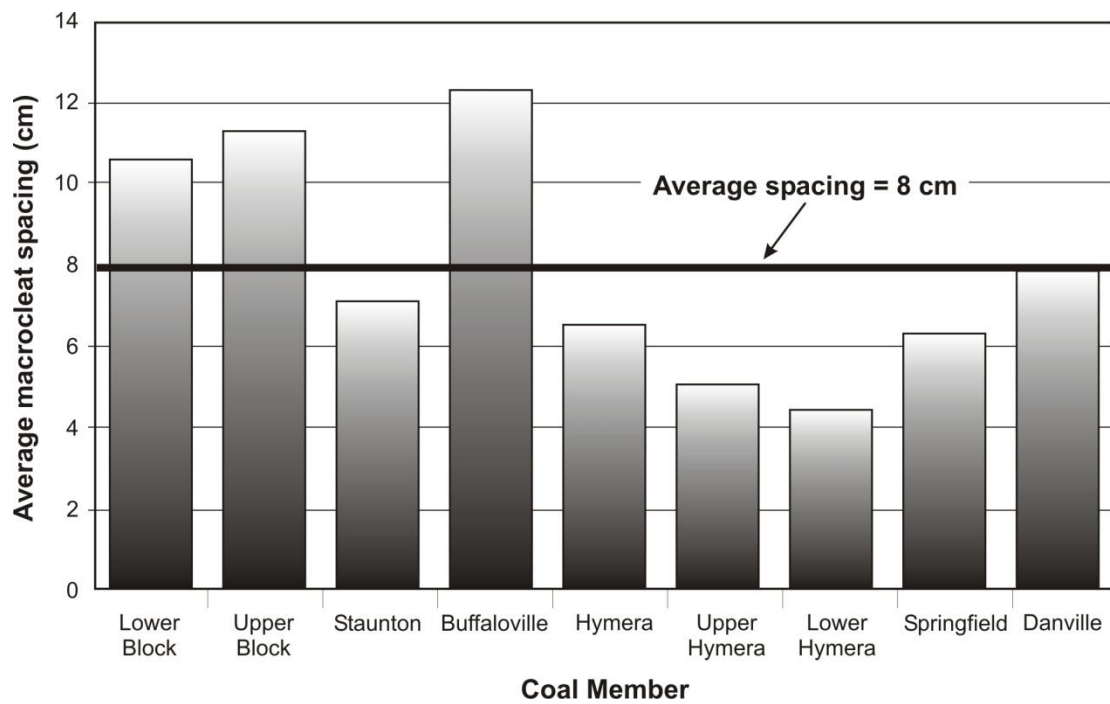


Figure 4. Distribution and average macrocleat spacing for all measurements collected from nine coal members in Indiana. Average value for all measurements is 8 ± 2.6 cm.

Figure 5 shows a power function relationship between kinematic aperture (*i.e.*, opening displacement or aperture, cf. Ortega *et al.*, 2006) and cumulative fracture intensity (abundance) for mesocleats. This observation is consistent with previously reported data for fracture patterns in other lithologies (Laubach *et al.*, 1998; Marrett *et al.*, 1999; Ortega *et al.*, 2006). Mesocleats were mainly observed in vitrain layers. Average and standard deviation of mesocleats are listed in Table 4.

The spacing between mesocleats (Group 3 of Ammosov and Eremin, 1963) was measured for 9 coal seams from 4 counties. More than 400 measurements indicate that the spacing of face mesocleats ranges between 2.15 and 5.97 mm, while the spacing of butt mesocleats ranges between 2.75 and 8.38 mm. Similarly to macrocleats, face mesocleats were more developed than butt mesocleats, and the apertures of face mesocleats were generally larger than those of butt counterparts (Table 4).

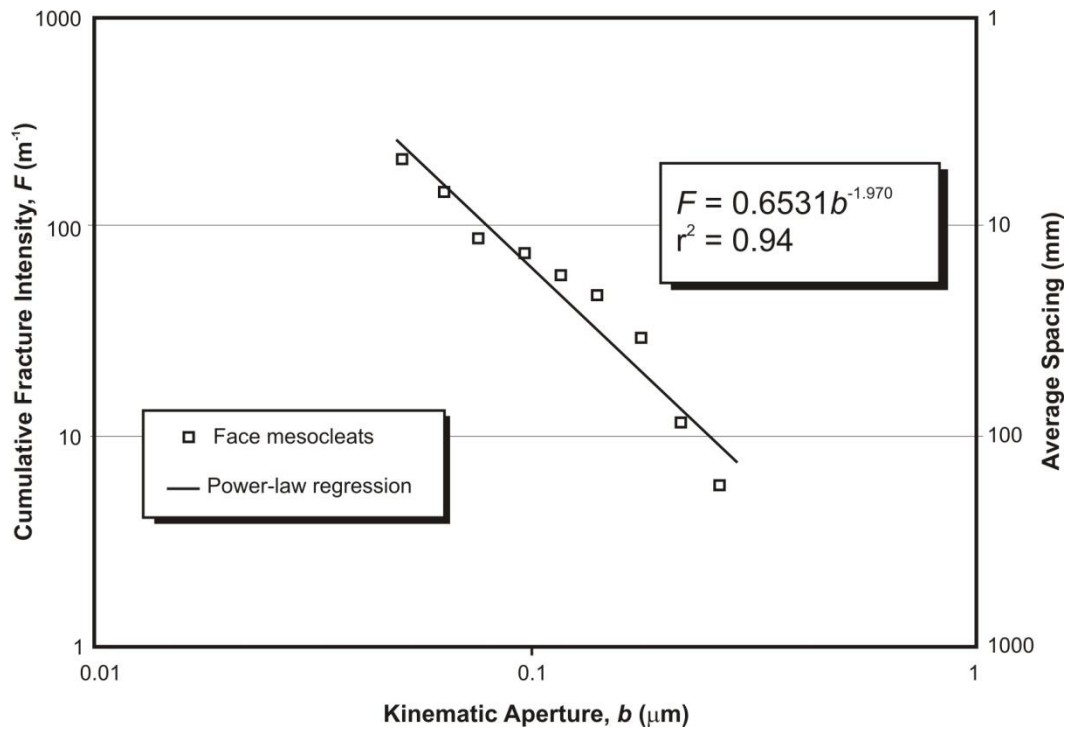


Figure 5. Power-law distribution of face mesocleats in relation with abundance (cumulative fracture intensity) and kinematic aperture.

5.4.2. Microcleat data

Microcleats are seldom filled or partially filled with authigenic minerals. Counting and classification of microcleats (face, butt, and oblique) and microfractures yielded >900 measurements from vitrinite-rich layers. Aperture measurements of coal microcleats in the laboratory range from 0.4 to 6 μm in the absence of confining stress. The most representative apertures of microcleats range between 0.8 and 1.2 μm . Laubach *et al.* (1998) observed features that most likely correspond to mesocleats and indicated that coal cleats have apertures of less than 0.1 mm at surface conditions. They also observed apertures between 0.01 to 0.2 mm in coal cores from the San Juan Basin of Colorado and New Mexico; however, smaller cleat apertures were not measured in their study.

Average values for apertures and spacing of different types of microcleats collected at the study sites are presented in Table 5. Note that face microcleats are better developed and show larger apertures than butt microcleats. Oblique-butt and oblique-face microcleats appear to be less abundant than face and butt microcleats. Microscopic analyses of irregular microfractures revealed a wide range of apertures having a mean value of $\sim 1.18 \mu\text{m}$. These microfractures are characteristically curved and contain jagged fracture segments with variable apertures (Figure 6). The occasional filling of microcleats with authigenic minerals attests to the natural occurrence of microfractures.

Regression analyses of meso-, microcleats, and microfractures indicate strong correlations ($r^2 \geq 0.94$) between kinematic aperture and cumulative fracture intensity (Figures 5 and 7). Note that plots of cumulative fracture intensity versus kinematic

aperture appear to follow a power law relationship of the form $f = ab^{-c}$, where f is the cumulative fracture intensity, a is the scaling factor, b is the kinematic fracture aperture, and c is the slope of the regression line (approximately equal to 2). Laubach *et al.* (1998) found a similar relation with measured volumetric sampling of cleat aperture data from the San Juan Basin ($c = 2.74 - 2.82$).

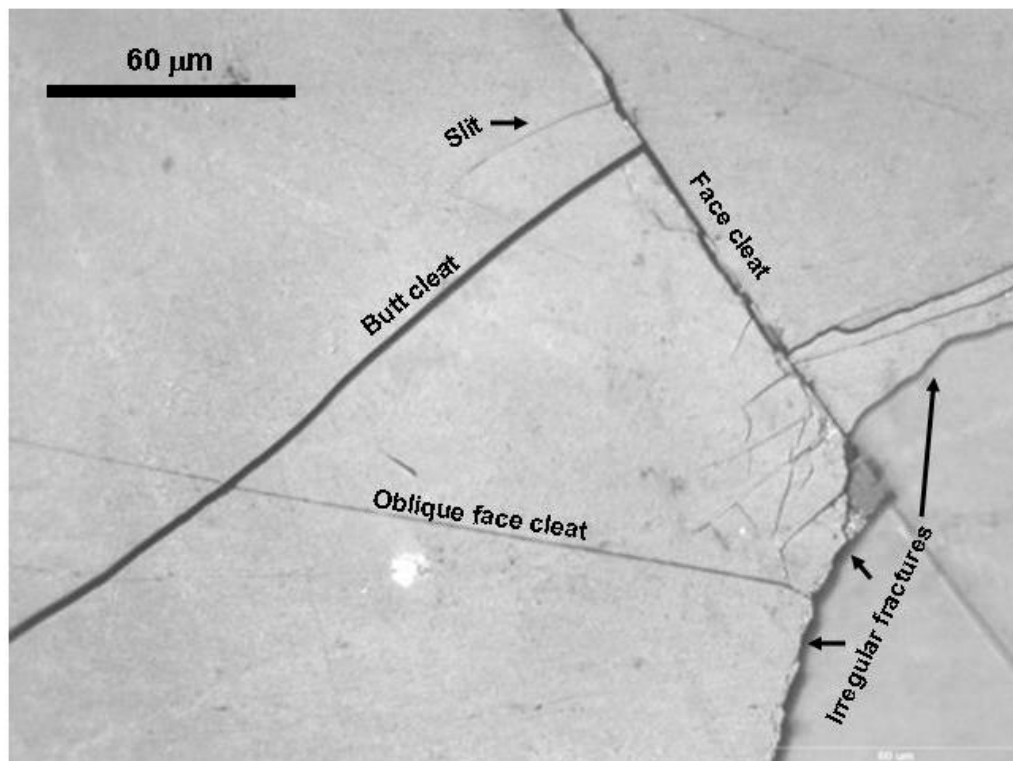


Figure 6. Photomicrograph showing microcleats and microfractures in a vitrinite-rich layer.

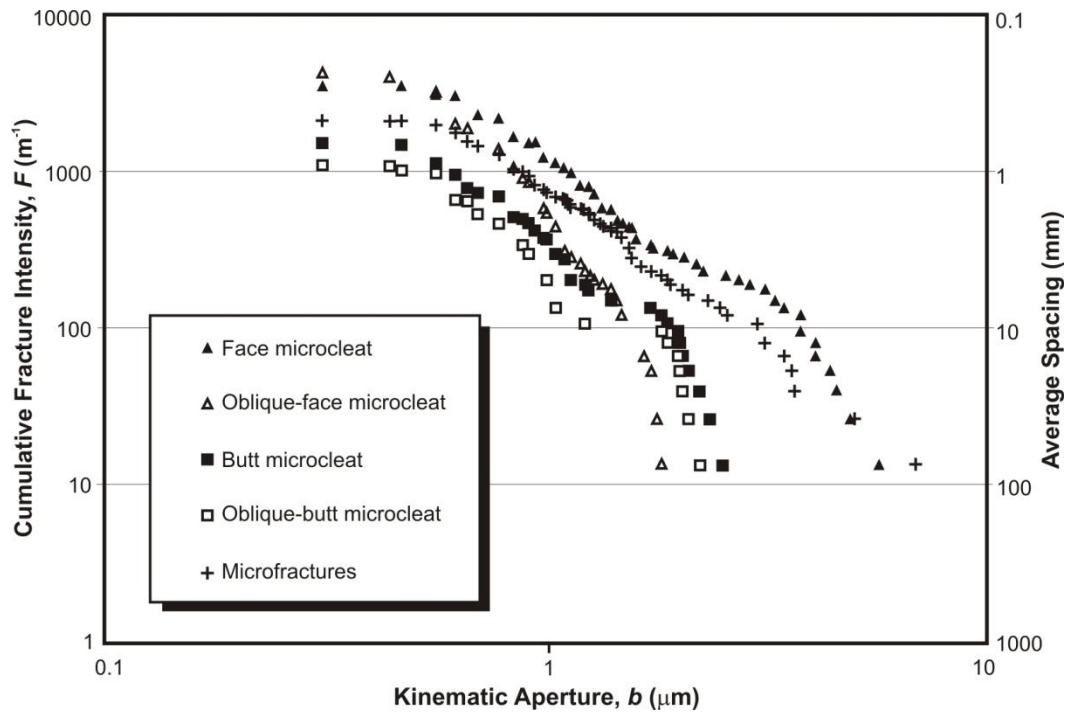


Figure 7a. Distribution of microcleats and microfractures in relation with abundance (cumulative fracture intensity) and kinematic aperture.

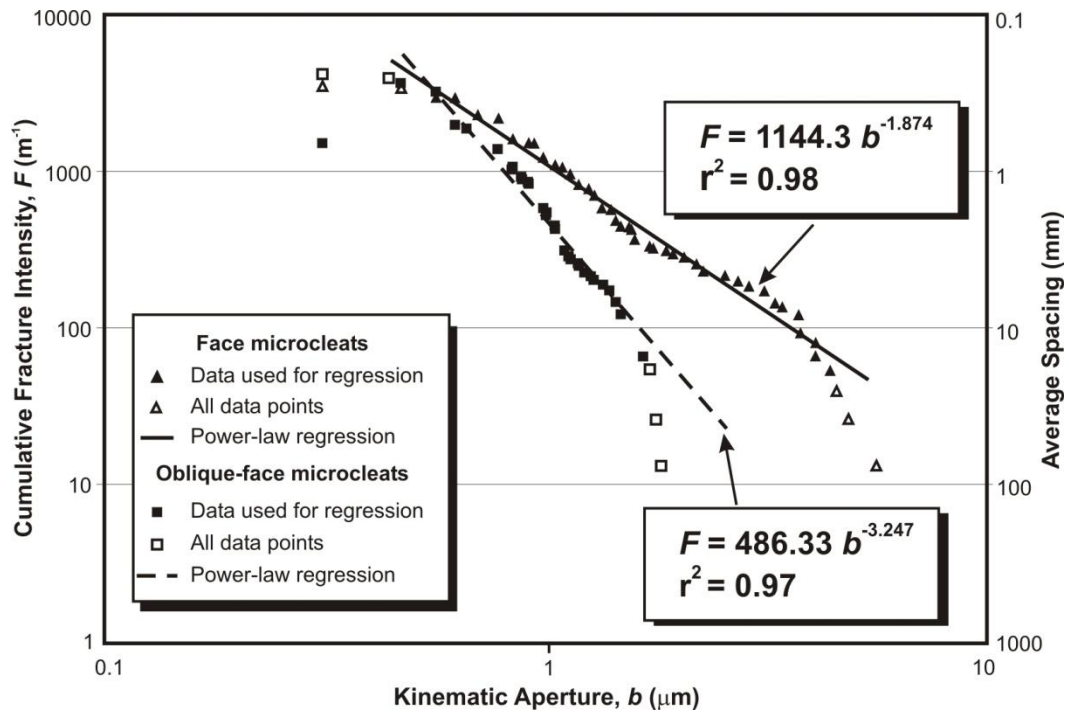


Figure 7b. Power-law distribution of face and oblique-face microcleats in relation with abundance (cumulative fracture intensity) and kinematic aperture.

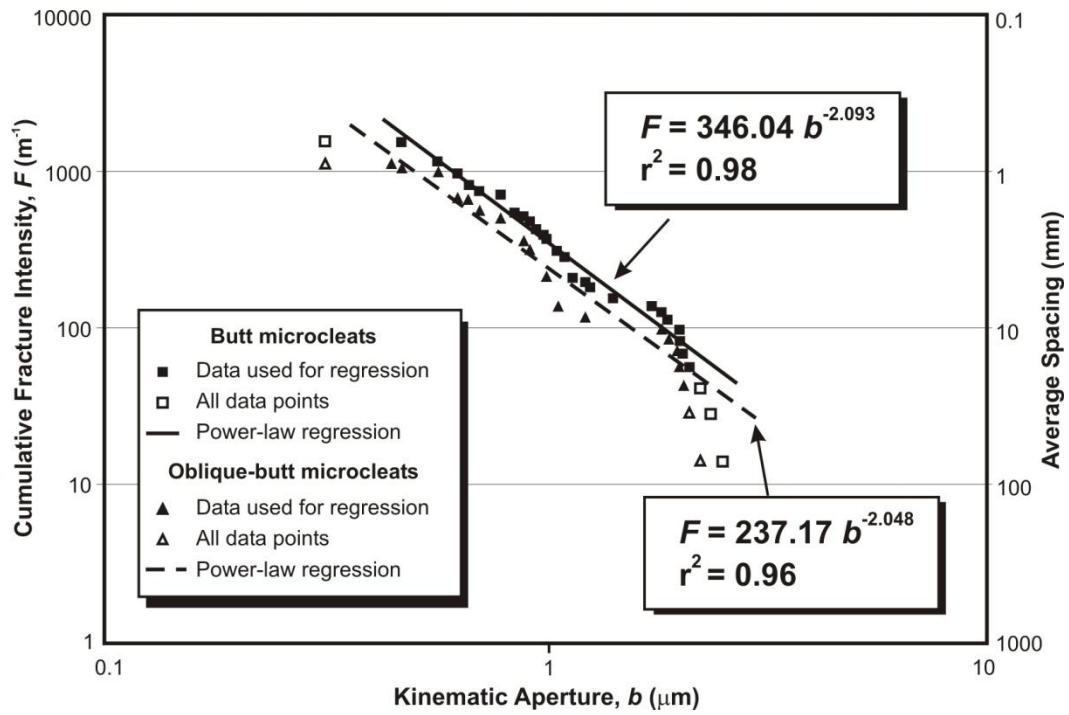


Figure 7c. Power-law distribution of butt and oblique-butt microcleats in relation with abundance (cumulative fracture intensity) and kinematic aperture.

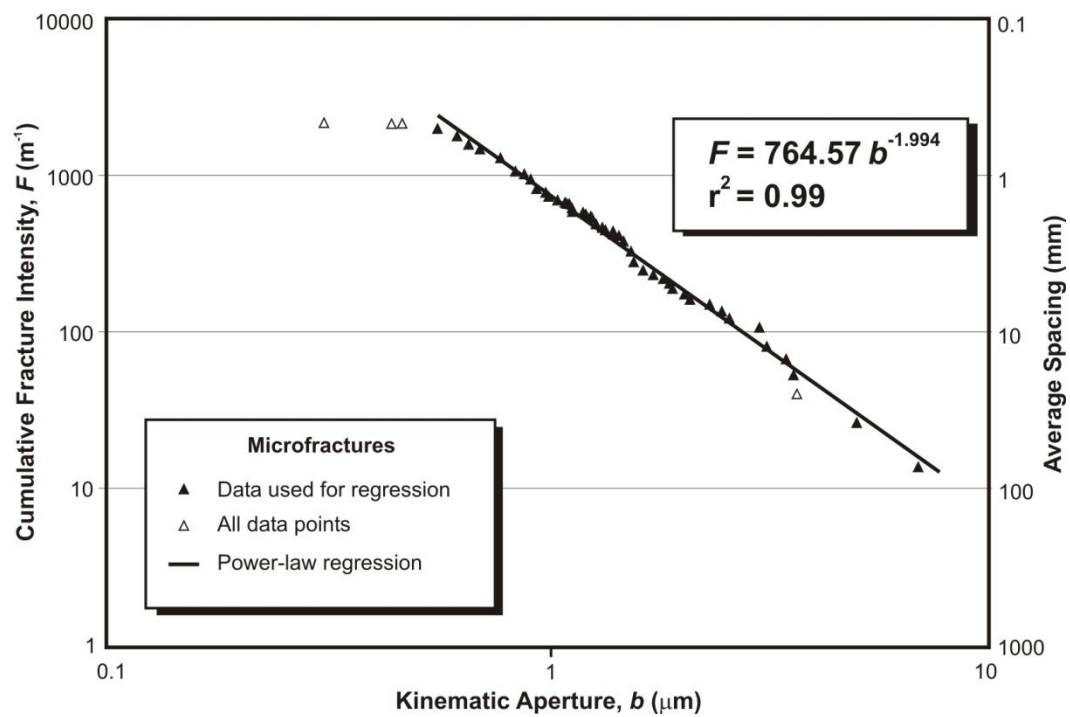


Figure 7d. Power-law distribution of microfractures in relation with abundance (cumulative fracture intensity) and kinematic aperture.

5.4.3. Lineament data

Figure 3 shows the orientation patterns of geologic lineaments in Indiana derived from satellite imagery and aerial photography (Powell, 1978; Wier *et al.*, 1974a, b). Computer analysis of lineament orientations indicates two dominant and orthogonal directions; a mean average azimuth value of 44° and a conjugate direction at nearly 315° (Figure 8). Average values for preferential lineament directions are shown next to rose diagrams in Figure 8. The conjugate set of lineaments is indicated graphically in the diagrams. The size of rose diagrams is proportional to the density of data analyzed on a grid of 20 km radius. Zones of sparse lineament coverage within the study area generally correspond to river floodplains, where lineaments are obscured by alluvial deposits.

The data in figure 8 indicate that lineaments tend to be aligned with the orientations of coal cleats and faults. However, there are some areas where the cleats and fractures are offset from the lineaments and these offsets may have resulted from changes in the tectonic regime and related stress vectors over time.

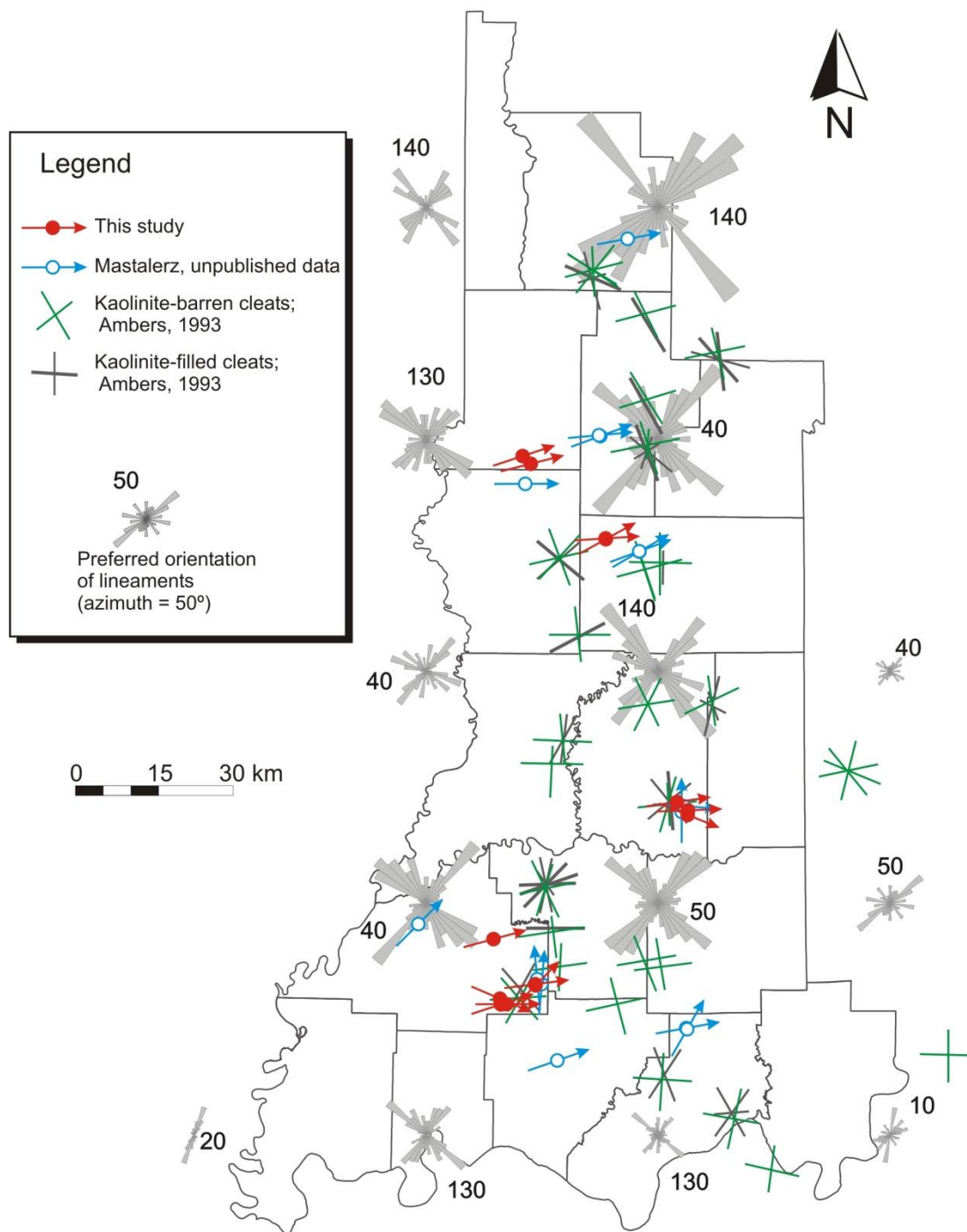


Figure 8. Rose diagrams depicting orientation patterns of cleats, fractures, and geologic lineaments. The size of the rose diagram is proportional to the density of data analyzed on a 20 km radius grid.

5.5. Discussion

5.5.1. Mechanisms of cleat formation

The most widespread notion is that coal cleats develop as a result of coalification processes (Ammosov and Eremin, 1963; Close, 1993; Condon, 2003; Laubach *et al.*, 1998; Laubach *et al.*, 1991; Pashin, 1998; Pashin *et al.*, 1999; Pitman *et al.*, 2003; Ryan, 2003; Ting, 1977). In addition, Ammosov and Eremin (1963) proposed that cleat development was caused in part by endogenic stress in coal deriving from mass loss during devolatilization and thermal maturation.

Coal cleats have also been identified as opening-mode (type I) fractures (Close, 1993; Kranz, 1983; Laubach *et al.*, 1998) that result from internal pressure working against remote compression (Olson and Pollard, 1989). It has been suggested that coal cleats as with other opening-mode fractures rarely exhibit shear offset (Laubach *et al.*, 1998). Different mechanisms have been proposed to explain the origin and evolution of opening-mode fractures, including compression, extension, and other manifestations of tectonism (Kulander *et al.*, 1990; Nelson, 1979; Pollard and Aydin, 1988; Stearns and Friedman, 1972). By analogy, the initiation and propagation of coal cleats can be ascribed to these mechanisms.

Cleat and fracture orientations are controlled by the tectonic stress regime present during their formation. Some studies have shown that fracture measurements allow determining the dominant tectonic stress direction present at the time of fracturing and the mode of fracture propagation (Condon, 2003; Kulander and Dean, 1993; Olson and Pollard, 1989). Likewise, measurements of cleat orientations in coal aid in deciphering past tectonic regimes.

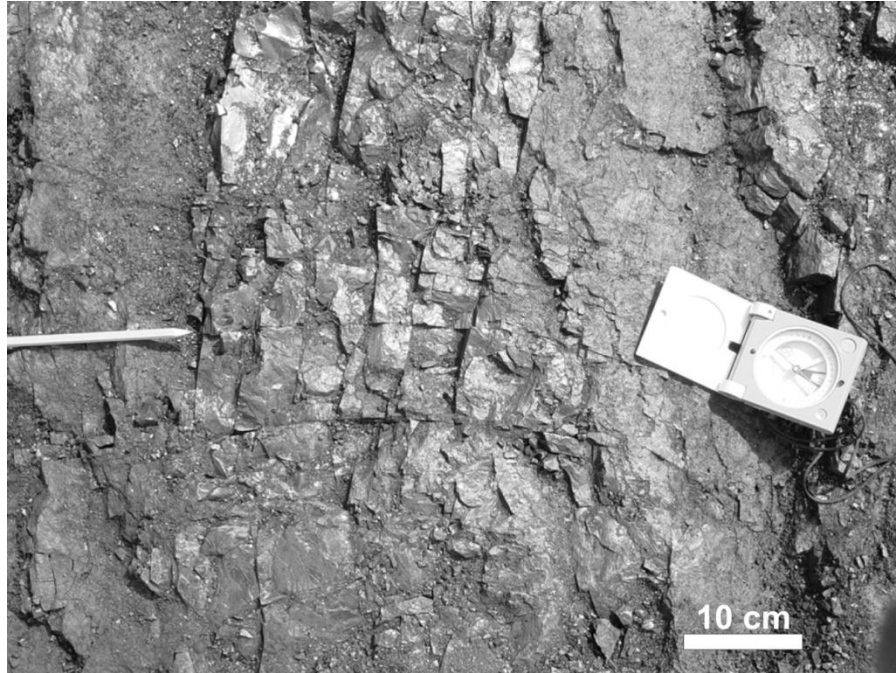


Figure 9. Changes in azimuth direction of face cleats near the axis of a small syncline. Photo from the Danville Coal Member in Vigo County, Indiana.

The presence of mineralized “early” cleats in Indiana coals with ~65° direction is in agreement with cleat directions observed in Demoinesian coals of Pennsylvania and Alabama, as well as in Morrowan coals from Kentucky and West Virginia (Nickelsen and Hough, 1967; Long, 1979; Kulander and Dean, 1993; Pitman *et al.*, 2003). The dominant stress field during this early cleat formation corresponds to the Appalachian-wide stress field proposed by Engelder and Whitaker (2006).

Postcoalification cleats and fractures may be related to cleat formation upon folding and faulting. The Danville Coal Member in Vigo County, for example, exhibits azimuth direction changes in its face cleats (Figure 9). Such changes in cleat orientation may reflect the stress concentration near the axis of the associated syncline (Figure 10). However, the overall azimuth direction of fractures in sandstones overlying the Danville Coal Member is 80° on average, which is parallel to the present-day stress field (Zoback and Zoback, 1981). The observed parallelism between cleats in nearby locations away from the syncline axis and fractures in adjacent lithologies may support the idea of an active tectonic control concurrent with cleat formation. Additional indications of tectonic control observed in Gibson County are the presence of slickensides and slickenlines on authigenic kaolinite-filled cleats (Figure 11), as well as stress-related faults in coal mines (Ault *et al.*, 1985).

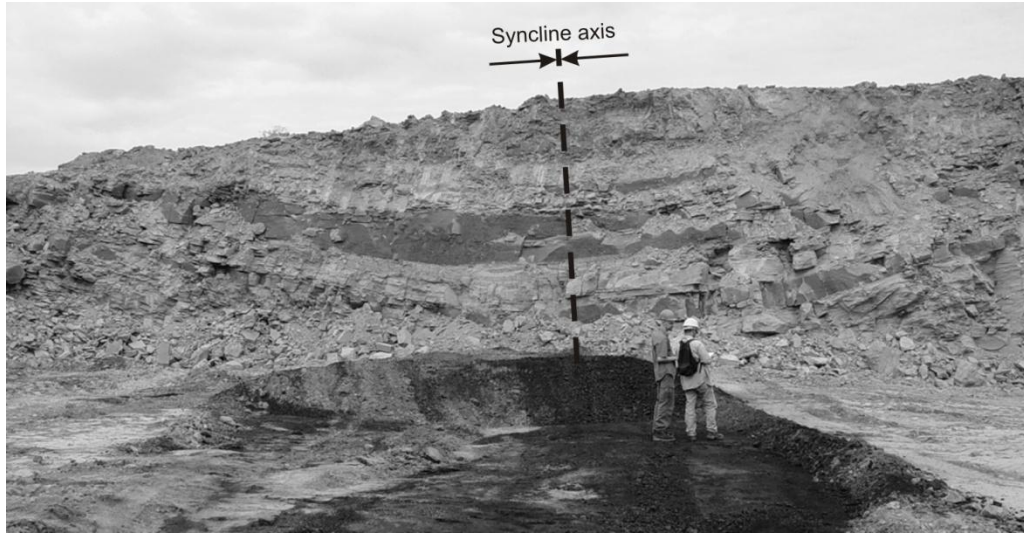


Figure 10. Small syncline depicted by sandstone facies overlying the Danville Coal Member in Vigo County, Indiana.

Development of a second generation of cleats in Indiana coals during the Permian, as proposed for Kentucky and West Virginia (Nickelsen and Hough, 1967; Long, 1979; Kulander and Dean, 1993; Pitman *et al.*, 2003), may owe its origin to the progressive counterclockwise rotation of the North American Plate in post-Paleozoic times, concurrent with coalification. Engelder and Whitaker (2006) suggested that continental collision during the assembly of Pangea caused rotation of Laurentia, resulting in the reorientation of Morrowan-Wolfcampian coal cleats and joints with the contemporary stress field.



Figure 11. Slickensides and slickenlines on a kaolinite-filled cleat from Gibson County, Indiana.

5.5.2. Cleat spacing

Understanding cleats in coal may help elucidate possible relationships between coalification and tectonism in relation to observed cleat abundance and distribution. A relationship between cleat abundance (*i.e.*, a measure of cleat spacing) and coal rank has been discussed in several studies (*e.g.*, Ammosov and Eremin, 1963; Pashin *et al.*, 1999). It was claimed that most cleats are formed in the bituminous rank, and the observed decrease in cleat abundance at high ranks has been attributed to annealing as thermal maturation increases with coalification. Yet, it has been suggested that annealing may occur at any stage during coal maturation (Levine, 1993; Su *et al.*, 2001).

We partially adopted Ammosov and Eremin's (1963) morphological classification of endogenic cleats (Table 1) to test the hypothesis of the relationship between rank and cleat abundance in Indiana coals. We modified Ammosov and Eremin's (1963) diagram by changing their metamorphic grade classification to the American Society for Testing and Materials (ASTM) coal rank classification scheme (ASTM, 2006) for improved clarity and data presentation (Figures 12 and 13).

All cleat data gathered were plotted in various diagrams to portray (qualitatively and quantitatively) cleat occurrence and distribution. The average abundance of macrocleats (Group 2 of endogenic fractures, according to Ammosov and Eremin, 1963) in Indiana coals is 13 macrocleats per meter, corresponding to an average spacing of approximately 8 cm between cleats (Figure 4).

Figure 12 shows the general distribution of mesocleats (Group 3 of endogenic fractures, according to Ammosov and Eremin, 1963) and their relation with coal

lithotype. Our data placed on this diagram show a widespread range of values varying from less than 10 to nearly 70 fractures per meter for mesocleats in the high volatile bituminous rank. This variation in fracture abundance is similar to that observed for the semi-lustrous and semi-dull groups of Ammosov and Eremin's study in the medium volatile bituminous rank (Figure 12).

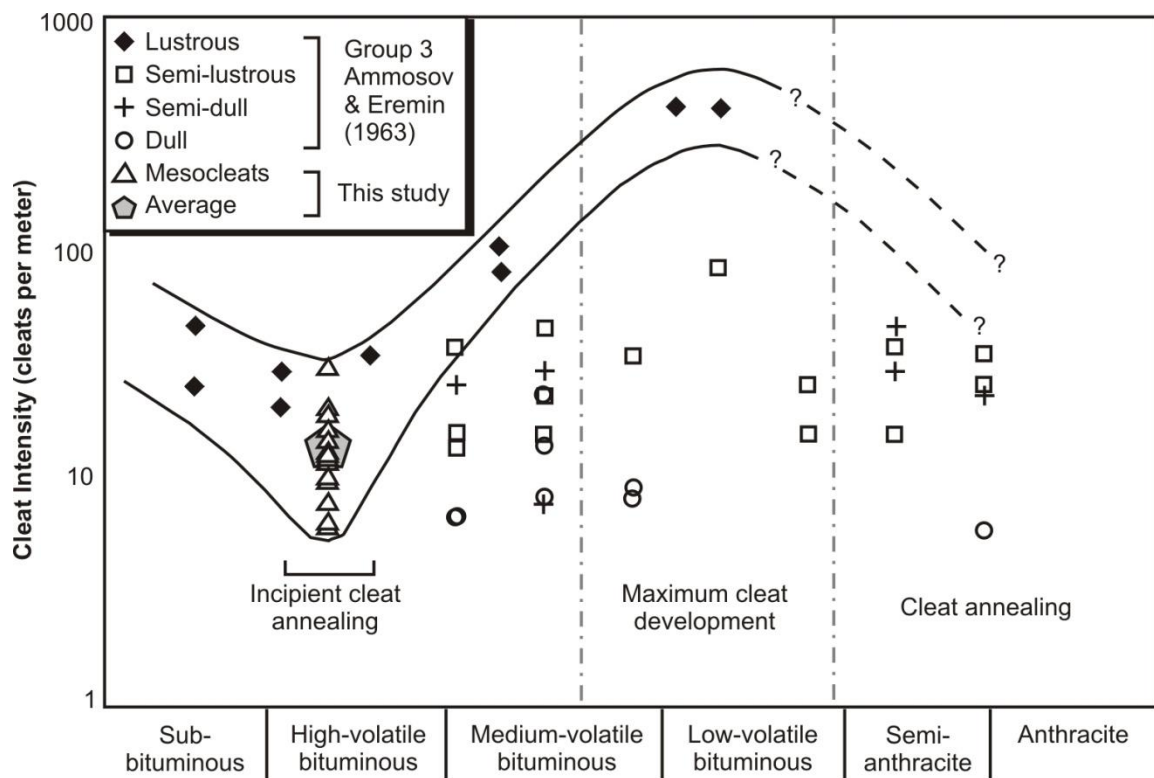


Figure 12. Ammosov and Eremin's (1963) original data are plotted with a modified grade classification. An envelope around all mesocleats in lustrous coals depicts the relation between coal rank and cleat abundance. The average value of all mesocleats abundance measurements from Indiana coals is represented by a gray-filled pentagon.

The observed decrease in mesocleat intensity for Indiana coals of high volatile bituminous rank in comparison with the data of Ammosov and Eremin (1963) may be associated with early stages of cleat annealing during coalification (described as incipient cleat annealing in Figure 12). The decrease in cleat abundance beyond the medium volatile bituminous rank has been attributed to cleat annealing, yet we have no data to compare with the proposed trend of Ammosov and Eremin (1963).

Figure 13 shows the rank distribution versus cleat intensity (cleat abundance) for microcleats (Group 4 of endogenic fractures, according to Ammosov and Eremin, 1963). The measured cleat intensity for face and butt microcleats shows a wide range (low 100's to upper 400's cleats/m) and indicates that, in general, there are more face than butt microcleats, at least in the lustrous coal type. Experimental data on coal fractures in the presence of confining stress at reservoir conditions suggest that microcleats may have width apertures between 0.1 μm and 0.1 mm (Close, 1993). Reported microcleat apertures vary between 0.5 μm and 20 μm (Gamson *et al.*, 1993), consistent with our observations. Karacan and Okandan (2000) reported an average microcleat aperture of 20.2 μm on polished coal surfaces from a Turkish basin, about three to ten times larger than our observed values for Indiana coals.

Despite large variations observed in the abundance of microcleats as a function of coal rank for high volatile bituminous coals, an envelope around the exponential relationship (dashed lines in Figure 13) suggests that an increase in fracture abundance with increasing rank may be modeled by this relationship, at least up to low volatile bituminous rank. Our average value of ~250 microcleats/m in the high

volatile bituminous rank is slightly less than expected by the exponential regression in Figure 13 ($r^2=0.83$), but well within the proposed envelope above and below.

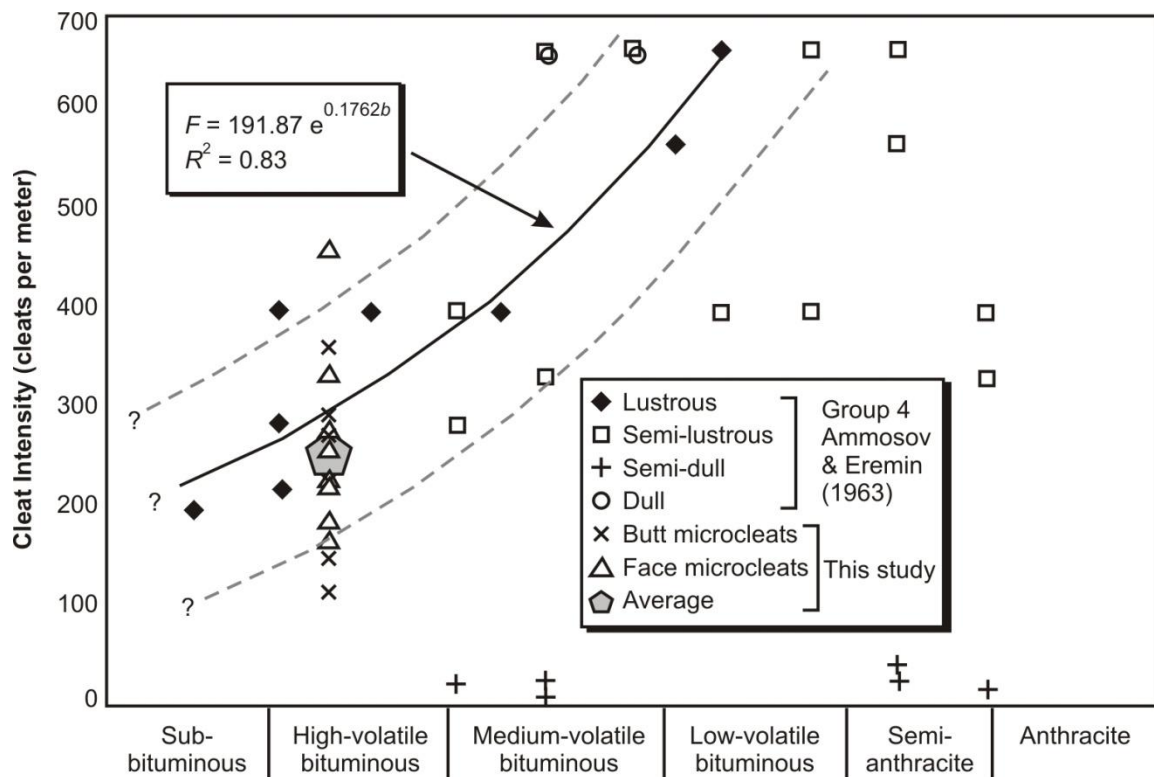


Figure 13. Ammosov and Eremin's (1963) original data are plotted with an ASTM rank classification. The average value of all microcleat abundance measurements from Indiana coals is represented by a gray-filled pentagon.

Figure 14 shows the proposed bell-shaped distribution for the abundance of microcleats vs. rank, reaching a maximum near medium volatile bituminous rank (Ammosov and Eremin, 1963). Despite the lack of cleat data beyond medium-to-low volatile rank, Ammosov and Eremin's study indicates that the proposed bell-shaped behavior has been observed in several other Russian studies. Laubach *et al.* (1998) and Su *et al.* (2001) also investigated the concept of cleat abundance as a function of rank and agreed with other authors that an initial increase of cleat development occurs up to vitrinite reflectance $R_o \sim 1.3\%$ (mediumvolatile bituminous rank), beyond which reduction or stabilization of cleat generation occurs.

Pashin *et al.* (1999) noted a similar relationship in high-volatile to low-volatile bituminous coals of the Black Warrior Basin (Figure 14). Their data are presented along with Ammosov and Eremin's data for Group 4. Although an apparent relation in relative cleat abundance is observed from both curves, it is important to note that those curves represent two different populations of cleats corresponding to macro- and microcleats (Groups 2 and 4 according to Ammosov and Eremin's classification). Because only relative cleat abundances were provided by Pashin *et al.* (1999), it was not possible to quantitatively contrast their values with our observations from meso- and microcleats.

Pashin *et al.* (1999) indicated that most high volatile B and C bituminous coals north and west of the outcropping Pottsville Formation in the Black Warrior Basin (Alabama) have primary face cleats (corresponding to our macrocleats) spaced as much as 10 cm apart. Our observations on average spacing of macrocleats indicate a slightly lower value of ~8 cm on average (~13 cleats/m, Figure 4). The relative

abundances of macro-, meso-, and microcleats (Groups 2, 3, and 4) from our study of Indiana coals are qualitatively indicated in Figure 14 by solid triangles. Our average value for macrocleat data agrees best with Pashin *et al.* (1999), while our average for microcleat data agrees better with Ammosov and Eremin's (1963) curve. Our mesocleat abundance data plot between macro- and microcleat abundances in Figure 14.

An exponential distribution among micro-, meso- and macrocleats in Indiana coals is depicted in Figure 15. The exponential increase in cleat abundance observed suggests that at smaller scales there may be a more intricate array of conduits favoring the migration of gases out of the coal matrix. Since it is expected that more gas will be produced from highly fractured reservoirs, Figure 15 reveals the importance of cleat scale and abundance from the point of view of coalbed methane exploration.

According to Pashin *et al.*'s (1999) curve in Figure 14, most cleats develop in the high volatile A bituminous rank, which seems to apply for macrocleats and perhaps to mesocleats. However, cleat data shown in Figure 14 indicate the presence of abundant microcleats in coal ranks as low as high volatile C bituminous. Thus, adding individual contributions of all cleats (at macro-, meso-, and microscopic scales) may render an adequate permeability regime for economic gas recovery in lower-rank coals, which have not reached the peak of maximum cleat development proposed by many studies.

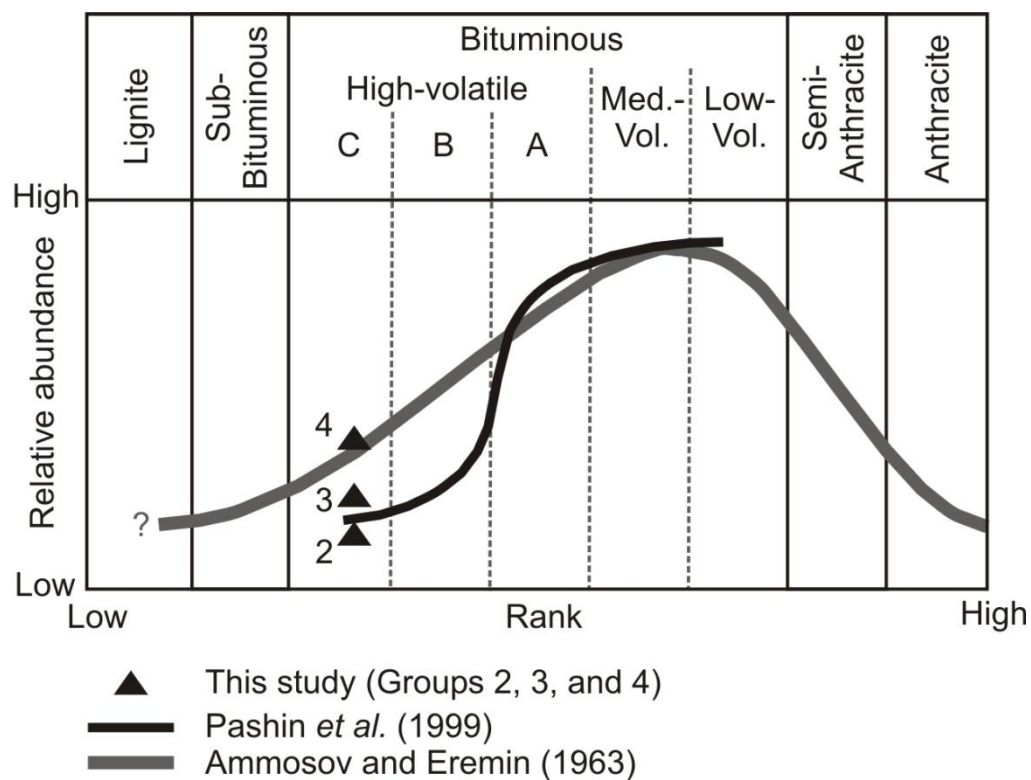


Figure 14. Cleat abundance in coals versus rank, adapted from Pashin *et al.* (1999). The average values of all cleat abundance measurements from Indiana coals from macro-, meso-, and microcleats (Groups 2, 3, and 4 of Ammosov and Eremin, 1963) are indicated by solid triangles.

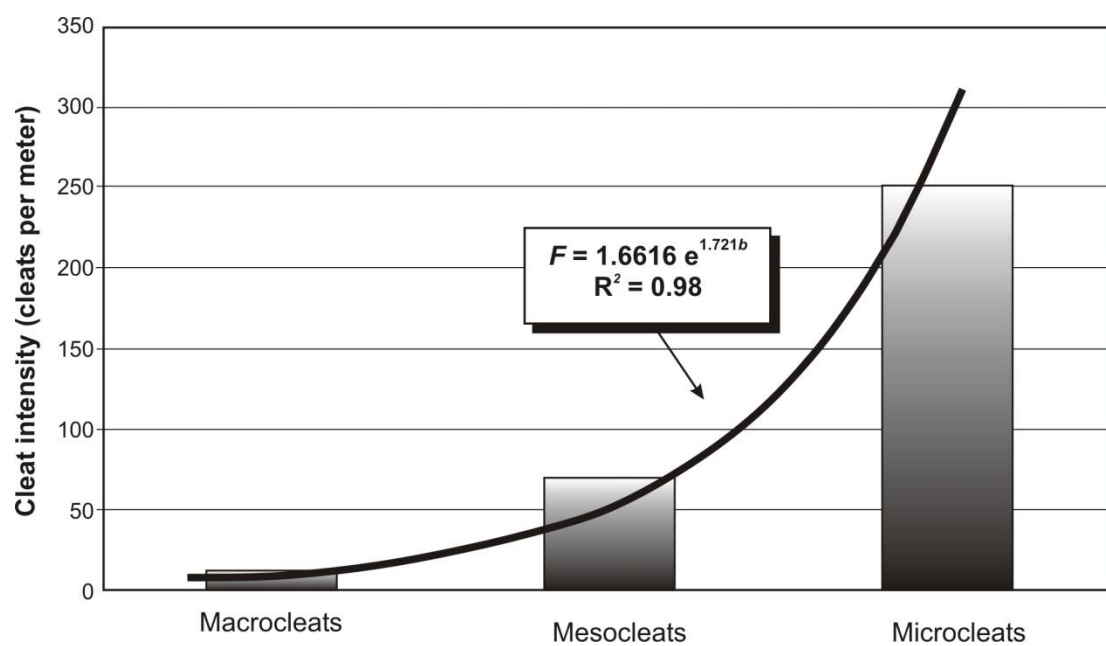


Figure 15. Distribution of cleat abundance versus cleat scale for Indiana coals. The average data for all measurements within each cleat category was used to calculate the exponential relationship presented.

The cleat distribution in Indiana coals is similar (at least in the macrocleat range) to cleat distributions in well-known coalbed methane provinces (*e.g.*, Black Warrior Basin). Additionally, in Indiana we observe large numbers of meso- and microcleats that enhance the available pore space in the coal matrix where gas adsorption/desorption takes place. The incorporation of small-scale cleat distributions in existing permeability models (currently based on macrocleats) would better predict coal reservoir behavior, resources, and coalbed gas extractability.

5.5.3. Cleats and geologic lineaments

The prediction of coal cleat occurrence and orientation based on lineaments can be applied to all coal settings, *i.e.*, to low-rank coals that have not yet generated large amounts of thermogenic gas, and also to higher-rank coals that have partially or completely lost associated gas owing to changes in reservoir conditions (*i.e.*, fracturing, stress regime, etc.). Previous studies have dealt with the occurrence of lineaments, joints, and fractures in southwestern Indiana (Amato *et al.*, 1974; Ault, 1989; Ault *et al.*, 1979, 1985, 1997; Ault and Haumesser, 1990; Ault and Sullivan, 1982; Powell, 1974, 1976, 1978; Wier *et al.*, 1974a, b). Some of these studies reveal that lineament data from satellite and aerial photographs in Indiana do not agree with present-day maximum stress directions. Wier *et al.* (1974a, b) identified two sets of lineaments (40° and 325°), but also indicated that substantial departures from these directions may be present locally.

In the Springfield Coal Member (Gibson County), there is an observable parallelism between authigenic-filled face cleats and the preferential orientation of

geologic lineaments (45° - 50°). The associated butt cleats are poorly developed having a direction of 325° . Lack of butt cleats in some locations suggests preferential annealing in the butt-cleat direction, or that these cleats were never formed. Measured open cleats from the same coal indicate an azimuth direction in agreement with the contemporary stress field, suggesting an active tectonic stress during cleat development.

In Daviess County, on the other hand, the dominant orientation ($\sim 40^{\circ}$) of geological lineaments suggests a connection with a calcite-filled cleat system. However, the evidence is less compelling because the correspondence between orientation of geologic lineaments and cleats is limited to the poorly developed butt-cleat direction. Nonetheless, mapped lineaments feature a nearly orthogonal conjugate set that agrees with the orientation of mineralized face cleats in Daviess County coals (50°). Mean orientations of mineral-filled cleats in different coal seams in Gibson (45°) and Daviess (50°) Counties are comparable to regional geologic lineament trends (40°), pointing towards a causal relationship.

Data from the Lower Block Coal Member in Daviess County indicate a dominant azimuth direction of 89° for face cleats and 1.5° for butt cleats. Abutting relationships indicate an early generation of cleats that was preserved by kaolinite mineralization and features a primary face-cleat direction of 20° - 25° (Figure 16). Poorly developed butt cleats indicate compass directions of 300° to 330° , but some of these cleats may have experienced partial annealing.

Collective evidence indicates that a tectonic mechanism influenced the orientation of coal cleats in southwestern Indiana through time. We extrapolate that

most cleat systems in the Illinois Basin coals are subject to important exogenic (tectonic) control, in addition to inherent endogenic controls during coalification.



Figure 16. Kaolinite-filled cleats in bright coal of the Lower Block Coal Member. Collected in Daviess County, Indiana.

5.5.4. Cleats and permeability

Stress-related coal cleats enhance reservoir porosity and permeability and have important implications in the development of coalbed methane (CBM) fields (Close, 1993; Diamond *et al.*, 1975; Ryan, 2003). The permeability of coalbed reservoirs has been proposed and modeled by several authors as a dual process involving Darcian flow through the cleat systems and gas diffusion in and out of the coal matrix (Bustin, 1997; Harpalani and Chen, 1997; Harpalani and Schraufnagel, 1990).

The occurrence and abundance of cleats in coal controls the geometry of the pore network and allows connectivity between possible flow paths. Therefore, it seems critical to understand the distribution of all cleat populations in coal to improve existing gas producibility models. Permeability models for coalbed methane recovery are traditionally based on the distribution of macrocleats. However, well-developed meso- and microcleat systems may play a significant role in the overall permeability of coal seams by reducing gas diffusion time through the coal matrix.

Cui and Bustin (2005) described the relevance of coal fabric in relation to cleat spacing and aperture. They stated that matrix size in coal is determined by cleat spacing, which, in turn, affects the gas matrix diffusion efficiency and cleat porosity. Matrix refers to the actual structure of the coal through which gas adsorption takes place at slow rates by diffusion. According to their theoretical permeability models, Cui and Bustin (2005) indicated that under same permeability regimes, higher gas production rates are expected where cleat spacing is closer. However, this scenario is dependent on several factors including the stress regime of the coal seam at the time of gas production, the required pressure drawdown via dewatering before the onset of

production, the saturation of the coal with respect to methane, and the coal fabric and gas permeability. Coal fabric and permeability are dependent on the magnitude of the effective stress (*i.e.*, overburden or lithostatic pressure minus pore pressure) (Bachu and Michael, 2003; Bustin, 1997). This concept has also been discussed in several studies (Bustin, 1997; Close, 1993; Cui and Bustin, 2005; Harpalani and Chen, 1997; Harpalani and Schraufnagel, 1990; Laubach and Tremain, 1991; Pitman *et al.*, 2003).

Development of fracture porosity/permeability in coals has been identified as one of the most important parameters for effective and economical coalbed methane production. Direct measurements of coal permeability are difficult or impossible to obtain. However, it has been observed that fracture permeability in coal ranges from microdarcys to darcys (Scott, 1999). Fracture and cleat abundances have been investigated in relation to coal permeability. In a study of three coal seams in northwestern Turkey, two coal seams were found more intensely fractured than the third (Karacan and Okandan, 2000). The authors suggested that coal fracturing may be favorable for gas production because of a reduction in diffusion time out of the coal matrix.

Because of the wide range in permeability observed in coals (microdarcys to darcys), increased permeability is expected in highly fractured reservoirs having abundant cleats. A study of carbonates yielded a relationship between permeability, abundance of fractures, and fracture aperture (Lucia, 1983). This relation indicates that permeability increases with the cube of the fracture aperture and varies with the inverse of the fracture spacing:

$$k = [84.4 \times 10^5] w^3/z \quad [1]$$

where k : permeability [darcys], w : fracture aperture [cm], and z : fracture spacing [cm]. The equation of Lucia (1983) is a modification of the standard definition of fracture permeability according to the cubic law (*i.e.*, Domenico and Schwartz, 1997, p.50), but simplified to account for only two variables (fracture aperture and spacing). Scott (1999) used the relation proposed by Lucia (1983) to model permeability behavior in coal. His rationale was that permeability occurs mainly through fractures because the matrix between fractures is considered impermeable in carbonates and coals, probably a reasonable assumption for coal owing to the slow gas diffusion out of the coal matrix. However, this assumption does not take into account the geometric distribution of microcleats and their possible contribution to permeability by facilitating gas transport within the coal matrix. Thus the question remains whether we can use cleat distribution in coal as a proxy for permeability. The very small spacing and apertures of microcleats in coals prompt us to hypothesize that microcleats may significantly enhance coal gas diffusion and permeability.

Figure 17 shows the relation between cleat aperture, cleat abundance, and calculated permeability using equation [1] above. We hypothesize the occurrence of three micro-, meso- and macrocleat-influenced permeability domains in coals: (1) the microcleat domain, where permeability is low and gas transport may be limited by diffusion; (2) the mesocleat domain with cleat apertures between 4 and 50 μm providing optimum permeability within the CBM production box according to Scott (2002); (3) the macrocleat domain, which is dominated by larger fractures and may be associated with extremely high permeability ranges; however, it may lead to excessive water production and is considered detrimental for CBM recovery (Scott,

2002). Coalbed gas studies often refer to the box in Scott's diagram (2002); as a cutoff for economic gas production (Figure 17). However, this diagram is valid for coals in the San Juan Basin, where Scott's (2002) study was conducted. Outside the box, the reduction in permeability and producibility of gas may depend on specific characteristics of individual basins.

A study of gas transport using X-ray computerized tomography (CT) by Karacan and Mitchell (2003) showed variations in gas adsorption behavior with coal lithotype. Similar techniques may prove useful in characterizing flow behavior in coal and the importance of cleat distributions for overall permeability upon cleat scaling.

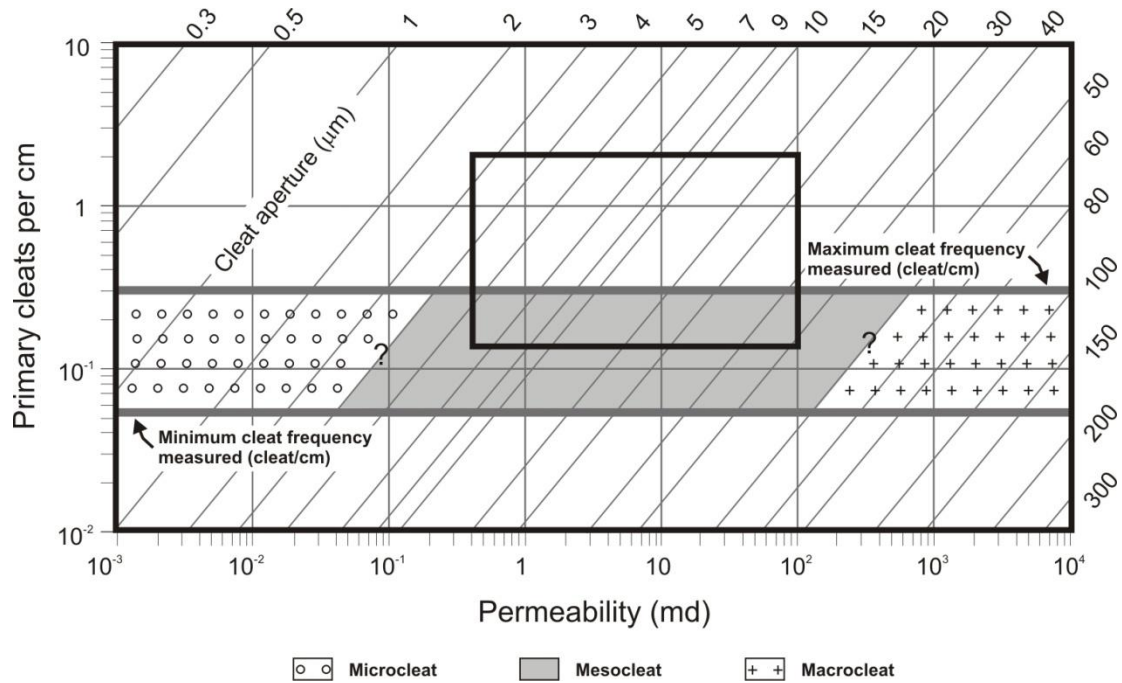


Figure 17. Relation between cleat abundance, cleat aperture, and resulting permeability in milidarcys (md). Bold horizontal grey lines correspond to maximum and minimum values measured for cleat abundance in Indiana coals. Microcleat aperture measurements were used to define the microcleat domain. The boundary between cleat domains is not very well constrained. Internal box corresponds to the permeability range of highly productive wells (0.5 – 100 md) and was used to delineate the mesocleats domain. Higher permeabilities are generally associated with macrocleats (adapted from Scott, 2002).

5.5.5. Cleats and coalbed methane potential

Pennsylvanian coal seams of Indiana may have reached a maximum burial depth of about 1.5 km sometime during the Permian (~270 Ma) (Rowan *et al.*, 2002). Observed vitrinite reflectance agrees with the expected R_o ~0.6 percent based on a normal geothermal gradient of 30°C/km. The R_o values indicate a maximum temperature during coalification of ~80 to 90°C (Barker and Pawlewicz, 1986). Thermal maturation in Indiana was insufficient to generate economic accumulations of thermogenic gas from coals. Nevertheless, economically important accumulations of biogenic coalbed gas are indeed present in SE Indiana coal beds (Drobniak *et al.*, 2004; Mastalerz *et al.*, 2004; Solano-Acosta *et al.*, 2005). According to Strapóć *et al.* (in press) these coalbed gases with ≥ 96 volume percent methane have been generated via bacterial CO₂-reduction.

Our observations suggest that although Indiana coals have not reached the appropriate maturity for maximum cleat development, a significant number of small-scale cleats have developed having important implications for gas diffusion, connectivity, and therefore, permeability. Strapóć *et al.* (in press) observed a close isotopic similarity of coalbed waters and modern regional meteoric precipitation, and hypothesized that erosional (postglacial) uplift may have caused fracturing that allowed hydrological infiltration of methanogenic bacteria into coal seams. Although the mechanisms and timing of CBM generation remain uncertain, the cleat system in coal may have facilitated access for microbial consortia that led to CBM generation. The observed apertures of microcleats are generally larger than the average microbe

size ($\sim 1 \mu\text{m}$), and much larger than ultramicrobacteria (cell volume $< 0.1 \mu\text{m}^3$) according to Scott (1999).

Indiana's Dugger Field CBM play in Sullivan County has been producing for a number of years from some of the coals described in this paper. Confidential production data from this field indicate permeability ranges significantly higher than those estimated with the aperture versus cleat abundance diagram (Figure 17). Therefore, our findings encourage further research in areas where potential CBM production has been discouraged because reservoir characteristics (cleat abundance, aperture, and permeability) seem to fall outside the presumed "optimum" range for economic production.

5.6. Conclusions

Cleat and fracture data from this study indicate that a power-law distribution exists between spacing and aperture of cleats and fractures at meso- and microscopic scales, as has been proposed for larger-scale fractures in other lithologies. r-square values greater than 0.94 from power-law distributions of meso- and microcleat populations allow making inferences about the distribution of cleats and fractures in coal seams. However, the net effect of all cleat domains (macro-, meso-, and microscopic) remains to be determined. A complete characterization of cleat distributions in space may provide a better tool for indirectly estimating porosity and permeability in coal reservoirs as critical parameters for coalbed methane extraction.

Measured azimuth directions of mineral-filled cleats from various locations show good agreement with observed directions of geologic lineaments from remote sensing imagery. Therefore, photolinear analysis of geologic lineaments may be used as a predictive tool for orientations of cleats in coal seams in southwestern Indiana and probably throughout the Illinois Basin. Additionally, photolinear orientation and size data of cleats and fractures may be used as proxy for estimating flow paths, and possibly, permeability, where actual data are not available. The data on Indiana coals suggest possible avenues for groundwater migration through the cleat system in coal. In turn, water migration can transport microbial consortia that are subsequently responsible for generating economic amounts of biogenic CBM. The distribution, abundance, and aperture of cleats in coal determine the network through which gases can migrate out of the coal matrix. Cleats and fractures provide necessary pathways for gas migration during CBM production.

Our observations suggest that a combination of endogenic and exogenic processes resulted in the distribution of cleats present in the high-volatile bituminous rank coals of Indiana. Based on the relationships observed among different generations of cleats from coal seams in Gibson and Daviess Counties in southwestern Indiana, we hypothesize that cleat orientations record the history of a changing regional stress field through time. In addition, data from open cleats and their apparent correlation with the contemporary stress field, folding, and the occurrence of tectonic indicators (*i.e.*, slickensides, small-scale thrust faults) suggest that the tectonic stress regime exerted control during and after cleat formation. A possible connection between the timing of cleat formation and the rotation of the North American plate during post-Paleozoic time is also suggested from cleat data.

The most critical aspects of cleat occurrence with regard to coalbed methane generation and extraction may be summarized as follows. 1) Cleats represent the main avenues for water flow through the coal. Groundwater conduits may help inoculate coal seams with methanogenic bacteria and provide a continuous supply of nutrients for microbial consortia, whereby large quantities of biogenic gas may be generated and laterally distributed through the cleat system. 2) Cleats control permeability in coal and facilitate migration routes for gas to diffuse at faster rates out of the coal matrix, therefore improving gas extractability. 3) Cleat orientation develops in response to changing tectonic regimes that ultimately control the distribution and occurrence of coalbed methane. From a practical perspective, the orientation, abundance, and distribution of cleats in coal constitute critical parameters in the design of horizontal drilling to maximize CBM extraction.

Acknowledgements

This work was supported by the Indiana Geological Survey (IGS) through a *John B. Patton Award* granted to W. Solano-Acosta. We thank P. Ames (Black Beauty Co.), M. Atkinson (Solar Sources), and C. Hutchison provided generous and invaluable access to coal mines and CBM drilling sites as well as Dr. Grzegorz Lis and Dr. Agnieszka Drobniaak for field assistance. We extend our gratitude to Dr. Greg Olyphant and two anonymous reviewers for their thoughtful reviews of this manuscript, and Dr. Jim Hower for editorial comments.

References

- Amato, R.V., Russell, O.R., Wier, C.E., Wobber, F.J., 1974. Application of ERTS-A imagery to fracture related mine safety hazards in the coal mining industry. Earth Resources Technology Satellite Program Office, ESC-355-12, 136 pp.
- Ambers, C.P., 1993. The nature and origin of very well crystallized kaolinite. Ph.D. dissertation, Indiana University, Bloomington, IN, 493 pp.
- Ammosov, I.I., Eremin, I.V., 1963. Fracturing in Coal, version translated from Russian. Office of Technical Services, U.S. Department of Commerce, Washington, D.C., 112 pp.
- Archer, P.L., Kirr, J.N., 1984. Pennsylvanian geology, coal, and coalbed methane resources of the Illinois Basin — Illinois, Indiana, and Kentucky. In: Rightmire, C.T., Eddy, G.E., Kirr, J.N. (Eds.), Coalbed Methane Resources of the United States. American Association of Petroleum Geologists, Studies in Geology 17, 105–134.
- ASTM, 2006. Annual book of ASTM standards. Section five. Petroleum products, lubricants, and fossil fuels. Gaseous fuels; coal and coke, 05.06, 705 pp.
- Ault, C.H., 1989. Directions and characteristics of jointing in the New Albany Shale (Devonian–Mississippian) of southeastern Indiana. Eastern Oil Shale Symposium, pp. 239–251.
- Ault, C.H., Haumesser, A.F., 1990. A central Indiana model for predicting jointing characteristics in underground limestone mines. 24th Forum on the Geology of Industrial Minerals, pp. 1–8.
- Ault, C.H., Sullivan, D.M., 1982. Faulting in southwestern Indiana. Prepared by the Indiana Geol. Survey for the Nuclear Regulatory Commission, NUREG/CR-2908, 50 pp.

- Ault, C.H., Sullivan, D.M., Tanner, G.F., 1979. Faulting in Posey and Gibson Counties, Indiana. *Proceedings of Indiana Academy of Sciences* 89-1980, 275–289.
- Ault, C.H., Harper, D., Smith, C.R., Wright, M.A., 1985. Faulting and jointing in and near surface mines of southwestern Indiana. Prepared by the Indiana Geological Survey for the Nuclear Regulatory Commission, NUREG/CR-4117, 27 pp.
- Ault, C.H., Kersey, R.W., Purcell, R.L., 1997. Map of Posey County, Indiana, showing structure on the Springfield coal member of the Petersburg formation - Pennsylvanian (ca. 1:66,000). Indiana Geological Survey, Bloomington, IN.
- Bachu, S., Michael, K., 2003. Possible controls of hydrogeological and stress regimes on the producibility of coalbed methane in Upper Cretaceous–Tertiary strata of the Alberta basin, Canada. *American Association of Petroleum Geologists, Bulletin* 87, 1729–1754.
- Barker, C.E., Pawlewicz, M.J., 1986. The correlation of vitrinite reflectance with maximum temperature in humic organic matter. In: Buntbarth, G., Stegena, L. (Eds.), *Paleogeothermics, Lecture Notes in Earth Science* 5, 79–93.
- Bassett, J.L., Blakely, R.F., Carr, D.D., Hasenmueller, N.R., Powell, R.L., 1978. Relationship of lineaments to gas production in the New Albany Shale in Indiana. *Second Eastern Gas Shale Symposium*, pp. 251–263.
- Bustin, R.M., 1997. Importance of fabric and composition on the stress sensitivity of permeability in some coals, Northern Sydney Basin, Australia: relevance to coalbed methane exploration. *American Association of Petroleum Geologists, Bulletin* 81, 1894–1908.
- Close, J.C., 1993. Natural fractures in coal. In: Law, B.E., Rice, D.D. (Eds.), *Hydrocarbons from Coal*, *American Association of Petroleum Geologists, Studies in Geology* 38, 119–132.

- Condon, S., 2003. Fracture network of the Ferron Sandstone Member of the Mancos Shale, east-central Utah, USA. *International Journal of Coal Geology* 56, 111–139.
- Cui, X., Bustin, R.M., 2005. Volumetric strain associated with methane desorption and its impact on coalbed gas production from deep coal seams. *American Association of Petroleum Geologists, Bulletin* 89, 1181–1202.
- Diamond, W.P., McCulloch, C.M., Bench, B.M., 1975. Estimation of coal-cleat orientation using surface-joint and photolinear analysis. *Geology* 3, 687–690.
- Diamond, W.P., McCulloch, C.M., Bench, B.M., 1976. Use of surface joint and photolinear data for predicting subsurface coal cleat orientation. *Bureau of Mines Report of Investigations* 8120, 13 pp.
- Drobniak, A., Mastalerz, M., Rupp, J.A., Eaton, N., 2004. Evaluation of coalbed gas potential of the Seelyville coal member, Indiana, USA. *International Journal of Coal Geology* 57, 265–282.
- Domenico, P.A., Schwartz, F.W., 1997. *Physical and Chemical Hydrogeology*, second ed. John Wiley & Sons, New York.
- Engelder, T., Whitaker, A., 2006. Early jointing in coal and black shale: evidence for an Appalachian-wide stress field as a prelude to the Alleghenian orogeny. *Geology* 34, 581–584.
- Gamson, P.D., Beamish, B.B., Johnson, D.P., 1993. Coal microstructure and micropermeability and their effects on natural gas recovery. *Fuel* 72, 87–99.
- Gray, H.H., 1979. The Mississippian and Pennsylvanian (Carboniferous) Systems in the United States - Indiana. *U.S. Geological Survey Professional Paper* 1110-K, K1–K20.

- Harpalani, S., Chen, G., 1997. Influence on gas production induced volumetric strain on permeability of coal. *Geotechnical & Geological Engineering* 15, 303–325.
- Harpalani, S., Schraufnagel, R.A., 1990. Shrinkage of coal matrix with release of gas and its impacts on permeability of coal. *Fuel* 69, 551–556.
- Karacan, C.O., Mitchell, G.D., 2003. Behavior and effect of different coal microlithotypes during gas transport for carbon dioxide sequestration into coal seams. *International Journal of Coal Geology* 53, 201–217.
- Karacan, C.O., Okandan, E., 2000. Fracture/cleat analysis of coals from Zonguldak basin (northwestern Turkey) relative to the potential of coalbed methane production. *International Journal of Coal Geology* 44, 109–125.
- Kranz, R.L., 1983. Microcracks in rocks; a review. *Tectonophysics* 100, 449–480.
- Kulander, B.R., Dean, S.L., 1993. Coal-cleat domains and domain boundaries in the Allegheny Plateau of West Virginia. *American Association of Petroleum Geologists, Bulletin* 77, 1374–1388.
- Kulander, B.R., Dean, S.L., Ward, B.J.J., 1990. Fractured Core Analysis — interpretation, logging, and use of natural and induced fractures in core. *American Association of Petroleum Geologists, Methods in Exploration Series* 8, 88 pp. Tulsa, OK, U.S.A.
- Kvale, E.P., Archer, A.W., 1990. Tidal deposits associated with low sulfur coals, Brazil Fm. (Lower Pennsylvanian), Indiana. *Journal of Sedimentary Petrology* 60, 563–574.
- Kvale, E.P., Mastalerz, M., 1998. Evidence of ancient freshwater tidal deposits. In: Davis, A.C., Davis, R., Henry, V. (Eds.), *Tidalites: Processes and Products*. SEPM (Society for Sedimentary Geology) Special Publications 61, 95–107.

- Kvale, E.P., Mastalerz, M., Furer, L.C., Engelhardt, D.W., Rexroad, C.B., Eble, C.F., 2004. Atokan and early Desmoinesian coal-bearing parasequences in Indiana, U.S.A. In: Pashin, J.C., Gastaldo, R.A. (Eds.), *Sequence Stratigraphy, Paleoclimate, and Tectonics of Coal-Bearing Strata*. American Association of Petroleum Geologists, *Studies in Geology* 51, 71–88.
- Laubach, S.E., Tremain, C.M., 1991. Distribution and origin of regional coal fracture (cleat) domains in Upper Cretaceous Fruitland Formation coal: possible effects on coalbed stimulation and methane production. *American Association of Petroleum Geologists, Bulletin* 75, 618 (Abs.).
- Laubach, S.E., Tremain, C.M., Ayers, W.B.J., 1991. Coal fracture studies: guides for coalbed methane exploration and development. *Journal of Coal Quality* 10, 81–88.
- Laubach, S.E., Marrett, R.A., Olson, J.E., Scott, A.R., 1998. Characteristics and origins of coal cleat: a review. *International Journal of Coal Geology* 35, 175–207.
- Levine, J.R., 1993. Coalification. In: Law, B.E., Rice, D.D. (Eds.), *The evolution of coal as source rock and reservoir rock for oil and gas*. *Hydrocarbons from Coal*, American Association of Petroleum Geologists, *Studies in Geology* 38, 39–77.
- Lillesand, T.M., Kiefer, R.W., 1994. *Remote sensing and image interpretation*, 3rd Ed. John Wiley & Sons, New York. 750 pp.
- Long, B.R., 1979. Regional survey of surface joints in eastern Kentucky: M.S. thesis, West Virginia University, 68 pp.
- Lucia, F.J., 1983. Petrophysical parameters estimated from visual descriptions of carbonate rocks: a field classification of carbonate pore space. *Journal of Petroleum Technology*, March, 629–637.

- Marrett, R.A., Ortega, O.J., Kelsey, C.M., 1999. Extent of power-law scaling for natural fractures in rock. *Geology* 27, 799–802.
- Mastalerz, M., Harper, D., 1998. Coal in Indiana: A Geologic Overview. Indiana Geological Survey, Special Report 60, 45 pp.
- Mastalerz, M., Gluskoter, H., Rupp, J.A., 2004. Carbon dioxide and methane sorption in high volatile bituminous coals from Indiana, USA. *International Journal of Coal Geology* 60, 43–55.
- Mauldon, M., Dunne, W.M., Rohrbaugh, M.B.J., 2001. Circular scanlines and circular windows: new tools for characterizing the geometry of fracture traces. *Journal of Structural Geology* 23, 247–258.
- Nelson, R.A., 1979. Natural fracture systems: description and classification. American Association of Petroleum Geologists, Bulletin 63, 2214–2221.
- Nickelsen, R.P., Hough, V.D., 1967. Jointing in the Appalachian Plateau of Pennsylvania. *Geological Society of America Bulletin* 78, 609–630.
- Olson, J.E., Pollard, D.D., 1989. Inferring paleostresses from natural fracture patterns: a new method. *Geology* 17, 345–348.
- Ortega, O.J., Marrett, R.A., Laubach, S.E., 2006. A scale-independent approach to fracture intensity and average spacing measurement. *American Association of Petroleum Geologists, Bulletin* 90, 193–208.
- Pashin, J.C., 1998. Stratigraphy and structure of coalbed methane reservoirs in the United States: an overview. *International Journal of Coal Geology* 35, 209–240.
- Pashin, J.C., Carroll, R.E., Hatch, J.R., Goldhaber, M.B., 1999. Mechanical and thermal control of cleating and shearing in coal: examples from the Alabama coalbed methane fields,

- USA. In: Mastalerz, M., Glikson, M., Golding, S.D. (Eds.), Coalbed Methane: Scientific, Environmental, and Economic Evaluation. Dordrecht, The Netherlands, Kluwer Academic Publishers, pp. 305–327.
- Pitman, J.K., Pashin, J.C., Hatch, J.R., Goldhaber, M.B., 2003. Origin of minerals in joint and cleat systems of the Pottsville Formation, Black Warrior basin, Alabama: implications for coalbed methane generation and production. American Association of Petroleum Geologists, Bulletin 87, 713–731.
- Pollard, D.D., Aydin, A., 1988. Progress in understanding jointing over the past century. Geological Society of America, Bulletin 100, 1181–1204.
- Powell, R.L., 1974. Joints in carbonate rocks in south-central Indiana. Proceedings of the Indiana Academy of Sciences 84-1975, 343–354.
- Powell, R.L., 1976. Some geomorphic and hydrologic implications of jointing in carbonate strata of Mississippian age in south-central Indiana: Ph.D. Dissertation, Purdue University, 168 pp.
- Powell, R.L., 1978. Preparation of lineament maps of southwestern Indiana: prepared by the Indiana Geological Survey for the U.S. Department of Energy — Eastern Gas Shales Project (EGSP), Morgantown, WV, 10 pp.
- Rowan, E.L., Goldhaber, M.B., Hatch, J.R., 2002. Regional fluid flow as a factor in the thermal history of the Illinois basin: constraints from fluid inclusions and the maturity of Pennsylvanian coals. American Association of Petroleum Geologists, Bulletin 86, 257–277.
- Ryan, B., 2003. Cleat development in some British Columbia coals, Geological fieldwork 2002; a summary of field activities and current research, Victoria, BC, Canada, British

- Columbia Ministry of Energy and Mines, New Ventures Branch, Victoria, BC, Canada (CAN), pp. 237–255.
- Scott, A.R., 1999. Improving coal gas recovery with microbially enhanced coalbed methane. In: Mastalerz, M., Glikson, M., Golding, S.D. (Eds.), *Coalbed Methane: Scientific, Environmental, and Economic Evaluation*. Kluwer Academic Publishers, Dordrecht, The Netherlands, pp. 89–110.
- Scott, A.R., 2002. Hydrogeologic factors affecting gas content distribution in coal beds. *International Journal of Coal Geology* 50, 363–387.
- Solano-Acosta, W., Mastalerz, M., Rupp, J.A., Strapoć, D., Schimmelmann, A., 2005. Coal-bed gas potential in Pennsylvanian coal beds of Indiana. 2005 International Coalbed Methane Symposium, Paper 0526. University of Alabama, Tuscaloosa, AL.
- Stearns, D.W., Friedman, M., 1972. Reservoirs in fractured rock. In: King, R.E. (Ed.), *Stratigraphic oil and gas fields. Classification exploration methods, and case histories*. American Association of Petroleum Geologists, Memoir 16, 82–106.
- Strapoć, D., Mastalerz, M., Eble, C., Schimmelmann, A., 2007. Characterization of the origin of coalbed gases in southeastern Illinois basin by compound-specific carbon and hydrogen stable isotope ratios. *Organic Geochemistry* 38, 267–287.
- Su, X., Feng, Y., Chen, J., Pan, J., 2001. The characteristics and origins of cleat in coal from Western North China. *International Journal of Coal Geology* 47, 51–62.
- Ting, F.T.C., 1977. Origin and spacing of cleats in coal beds. *Journal of Pressure Vessel Technology* 99, 624–626.
- Wier, C.E., Wobber, F.J., Russell, O.R., Amato, R.V., Leshendok, T.V., 1974a. Geological lineament map of the 1 degree×2 degrees Indianapolis Quadrangle, Indiana and Illinois.

Prepared by the Indiana Geological Survey for the U.S. Department of Energy — Eastern Gas Shales Project (EGSP).

Wier, C.E., Wobber, F.J., Russell, O.R., Amato, R.V., Leshendok, T.V., 1974b. Geological lineament map of the 1 degree×2 degrees Vincennes Quadrangle, Indiana and Illinois.

Prepared by the Indiana Geological Survey for the U.S. Department of Energy — Eastern Gas Shales Project (EGSP).

Zoback, M.D., Zoback, M.L., 1981. State of stress and intraplate earthquakes in the United States. *Science* 213, 96–104.

CHAPTER 6

Diagenetic mineralization in Pennsylvanian coals from Indiana, USA:

$^{13}\text{C}/^{12}\text{C}$ and $^{18}\text{O}/^{16}\text{O}$ implications for cleat origin and coalbed methane generation

Wilfrido Solano-Acosta^{1,2}, Arndt Schimmelmann², Maria Mastalerz¹, and Irene Arango^{2,3}

¹ Indiana Geological Survey, Indiana University, 611 N. Walnut Grove, Bloomington, IN 47405-2208, U.S.A.

² Department of Geological Sciences, Indiana University, 1001 E Tenth St., Bloomington, IN 47405-1405, U.S.A.

³ Current address: Chevron Energy Technology Company, 1500 Louisiana St. Houston, TX, 77002, USA

NOTICE: This is the author's version of a work that was accepted for publication in the International Journal of Coal Geology. Changes resulting from the publishing process, such as peer review, editing, corrections, structural formatting, and other quality control mechanisms may not be reflected in this document. Changes may have been made to this work since it was submitted for publication. A definitive version was subsequently published in <http://dx.doi.org/10.1016/j.coal.2007.06.002>

Abstract

Cleats and fractures in southwestern Indiana coal seams are often filled with authigenic kaolinite and/or calcite. Carbon- and oxygen-stable isotope ratios of kaolinite, calcite, and coalbed CO₂ were evaluated in combination with measured values and published estimates of $\delta^{18}\text{O}$ of coalbed paleowaters that had been present at the time of mineralization. $\delta^{18}\text{O}_{\text{mineral}}$ and $\delta^{18}\text{O}_{\text{water}}$ values jointly constrain the paleotemperature of mineralization. The isotopic evidence and the thermal and tectonic history of this part of the Illinois Basin led to the conclusion that maximum burial and heat-sterilization of coal seams approximately 272 Ma ago was followed by advective heat redistribution and concurrent precipitation of kaolinite in cleats at a burial depth of <1600 m at $\sim 78 \pm 5^\circ\text{C}$. Post-Paleozoic uplift, the development of a second generation of cleats, and subsequent precipitation of calcite occurred at shallower burial depth between ~500 to ~1300 m at a lower temperature of $43 \pm 6^\circ\text{C}$. The available paleowater in coalbeds was likely ocean water and/or tropical meteoric water with a $\delta^{18}\text{O}_{\text{water}} \sim -1.25\text{‰}$ vs. VSMOW. Inoculation of coalbeds with methanogenic CO₂-reducing microbes occurred at an even later time, because modern microbially influenced ¹³C-enriched coalbed CO₂ (*i.e.*, the isotopically fractionated residue of microbial CO₂ reduction) is out of isotopic equilibrium with ¹³C-depleted calcite in cleats.

Keywords: cleats, calcite, kaolinite, oxygen isotopes, carbon isotopes, mineralization, coal, Illinois Basin

6.1. Introduction

Diagenetically precipitated, authigenic minerals are common in coal as pore fillings and as thin sheets along cleats and fractures. Cleats are linear discontinuities that form a generally well-defined geometric pattern and develop in coal as a result of physical and chemical changes and in response to anisotropic tectonic stresses (Solano-Acosta *et al.*, in press, and references therein). Cleat- and fracture-filling minerals typically form thin sheets with a thickness in the μm to mm range. The most common diagenetic minerals occurring in coals are sulfides (*e.g.*, pyrite, sphalerite, chalcopyrite), carbonates (*e.g.*, calcite, ankerite, siderite), clay minerals (*e.g.*, kaolinite), and quartz (Ambers, 1993; Anderson *et al.*, 1980; Budai *et al.*, 2002; Daniels and Altaner, 1990; Daniels *et al.*, 1996; Hatch *et al.*, 1976; Pitman *et al.*, 2003; Price and Shieh, 1979; Shieh and Suter, 1979; Spears and Caswell, 1986 among others).

In the absence of mineralization, cleat annealing during coalification may obliterate the original cleat network and preclude the assessment of paleo-stress directions. Authigenic mineralization not only ‘preserves’ cleats, but may allow the recognition of successive mineralization events in intersecting fracture and cleat systems. Authigenic minerals can be used to estimate the relative timing of mineralization and to record changes in stress patterns resulting from multiple tectonic events (Engelder and Whitaker, 2006; Solano-Acosta *et al.*, in press). The spatial distribution of diagenetic minerals along cleats and fractures results from preferential migrations of ground-water flow and the associated transport of solutes. In some instances, diagenetic mineralization reflects tortuous or variable local flow patterns (Daniels *et al.*, 1996). A directionally

biased distribution of mineral phases provides a geometric framework of fluid permeability in areas where mineralization is not pervasive, and where cleats and fractures are ubiquitous. Therefore, diagenetic mineralization in coal can have diagnostic value for identifying paleohydrologic conditions.

Previous studies in Indiana present contradictory hypotheses regarding the timing and temperature of diagenetic mineralization. Shieh and Suter (1979) reported $\delta^{18}\text{O}$ values for kaolinite and calcite samples from Indiana and Illinois coals, in addition to a $\delta^{18}\text{O}_{\text{water}}$ value of -6.3‰ for seepage water from a coal mine in Indiana. The authors observed little variation in $\delta^{18}\text{O}_{\text{kaolinite}}$ values (16.5 to 17.6‰) and a moderate variation in $\delta^{18}\text{O}_{\text{calcite}}$ values (21.4 to 24.5‰). They did not report technical details of their analyses, but their $\delta^{18}\text{O}$ calibration relative to Standard Mean Ocean Water (SMOW) should be compatible with our calibration versus Vienna Standard Mean Ocean Water (VSMOW) using VSMOW and SLAP international water stable isotope standards according to Coplen's (1996) guidelines. Shieh and Suter (1979) proposed that kaolinite and calcite in coals formed in 'fairly recent geologic time' at shallow burial in isotopic equilibrium from a common parent solution having relatively uniform isotopic composition and temperature. An empirical relationship between $\delta^{18}\text{O}_{\text{kaolinite}}$ and $\delta^{18}\text{O}_{\text{water}}$ was developed by Kulla and Anderson (1978) based on measurements in a temperature range between 172° and 319°C. Shieh and Suter (1979) used this relationship to calculate kaolinite crystallization temperatures of -1 to 5°C in coal, but they dismissed this estimate as unreasonably low because of the uncertainties involved in their extrapolation. Instead, they adopted an alternative empirical relationship (Taylor, 1974) to propose a temperature range from 24 to 30°C for the formation of kaolinite. Furthermore, they

proposed a temperature range of 13 to 28°C for the precipitation of calcite in the studied coals (Figure 1), according to the calibration by O'Neil *et al.* (1969).

Coals from the Illinois Basin and the Forest City Basin (Iowa, Missouri, and Kansas) were used by Whelan *et al.* (1988) to determine $\delta^{18}\text{O}_{\text{kaolinite}}$ and $\delta^{18}\text{O}_{\text{calcite}}$ values (as well as sulfur isotope ratios in sphalerite and pyrite). Based on their $\delta^{18}\text{O}_{\text{kaolinite}}$ values between 19.2 and 20.2‰ and $\delta^{18}\text{O}_{\text{calcite}}$ values from 21.1 to 25.8‰ (all relative to SMOW) and the paragenetic sequence of cleat-filling minerals described by Cobb (1981), Whelan *et al.* (1988) proposed the following sequence of events: (i) cleat formation in coal beds; (ii) kaolinite crystallization at ~40°C; (iii) deposition of pyrite and sphalerite at ~100°C; (iv) uplift and erosion returning coals to shallower depths; and (v) formation of calcite at 15 to 75°C.

In sharp contrast, fluid-inclusion geothermometry from cogenetic sphalerite in geographically equivalent coals from the Illinois Basin led Ambers (1993) to the conclusion that coal cleats in Indiana formed at elevated temperatures during deep burial, with kaolinite precipitating as a result of thermal breakdown of organic matter at temperatures between 134 and 138°C. Based on fluid inclusion measurements from sphalerite and siderite coexisting with kaolinite in coals, Ambers (1993) applied a temperature correction to account for the salinity of fluid inclusions at 25 MPa under hydrostatic pressure conditions. The same study presented oxygen isotopic data to conclude that kaolinite predates calcite and that calcite must have formed at >70°C subsequent to the peaking of burial temperature.

This study aims to provide a consistent interpretation for the timing and temperature of diagenetic mineralization based on the integration of new and existing isotopic data.

This work focuses on oxygen and carbon stable isotope ratios (expressed as $\delta^{18}\text{O}$ and $\delta^{13}\text{C}$ values, respectively) of diagenetic calcite and kaolinite in Pennsylvanian coals from Indiana. $\delta^{18}\text{O}_{\text{calcite}}$ and $\delta^{18}\text{O}_{\text{kaolinite}}$ values are used to assess time of emplacement, paleotemperature, and the circumstances of mineralization and their relationships to cleat formation. For this assessment, newly obtained data are discussed in conjunction with previously published isotopic analyses from Indiana (Ambers, 1993; Shieh and Suter, 1979; Strapoc *et al.*, 2007).

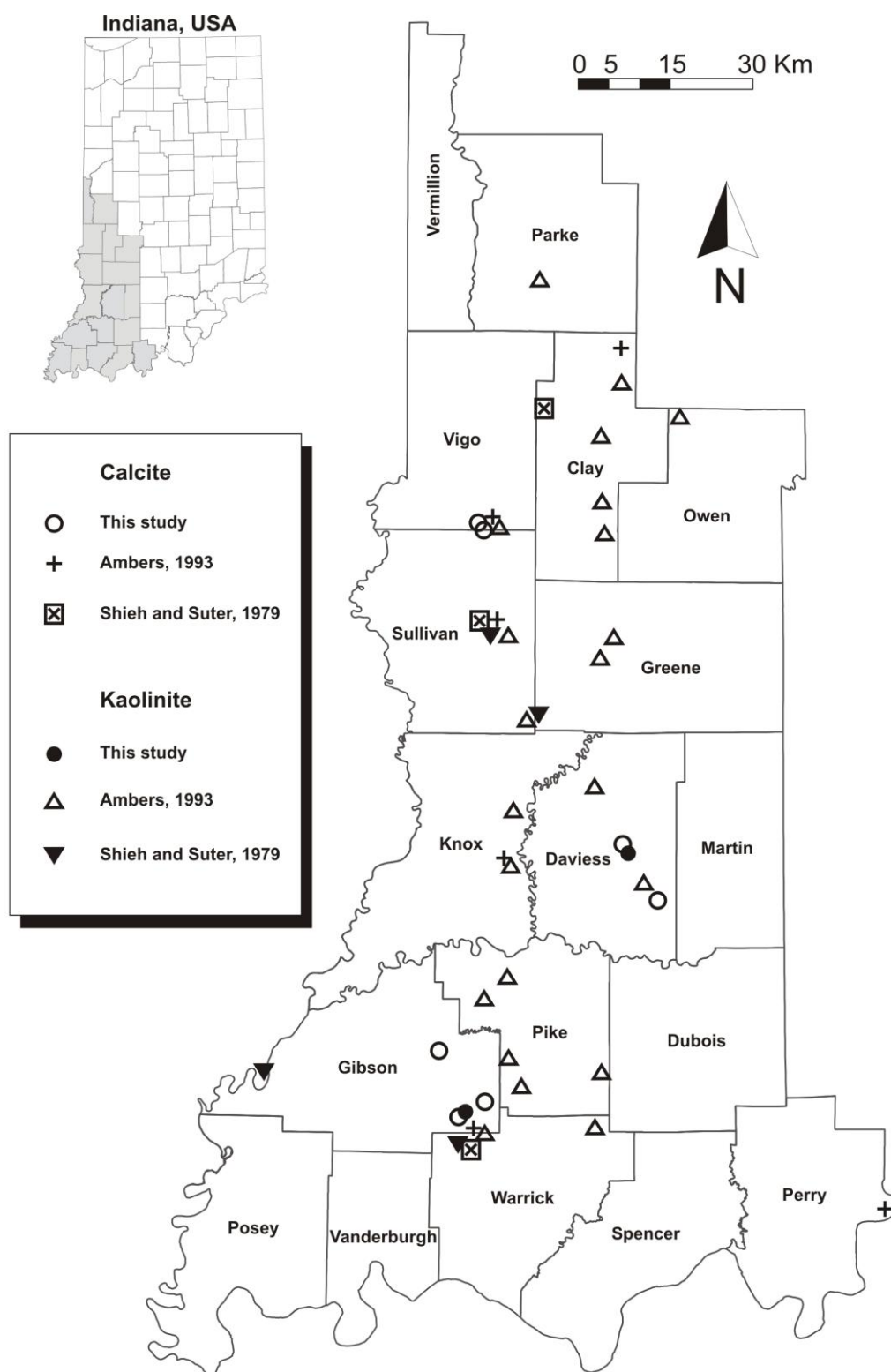


Figure 1. Map of southwestern Indiana showing the distribution of isotope data from calcite, kaolinite, and CO₂ from various sources. The expanded area corresponds to the gray-shaded counties in the index map of Indiana (top left).

6.2. Materials and methods

6.2.1. Sample origin

Mineral samples were collected from coal cleats and fractures in six active southwestern Indiana coal mines in Gibson County (Discovery, Sommerville, and Francisco mines), Daviess County (Midway and Corning Mines), and Sullivan County (Farmersburg Mine). Our sampling sites along with the locations of accessory data from Ambers (1993) and Shieh and Suter (1979) and CO₂ data of canister desorption gases from coalbed methane (CBM) production and exploratory wells in Indiana (Strapoć *et al.*, 2007) are shown in Figure 1. A generalized stratigraphic column with the distribution of coal members in the Pennsylvanian System of Indiana indicates the occurrence of diagenetic minerals analyzed in this study (Figure 2). Diagenetic calcite was collected from large, 5- to 20-kg coal blocks from five coals: namely, the Danville, Hymera, Springfield, Upper Block, and Lower Block Coal Members, throughout our sampling area. Kaolinite was obtained along cleats and fractures from the Hymera, Buffaloville, Upper Block, and Lower Block Coal Members in mines from Gibson and Daviess Counties.

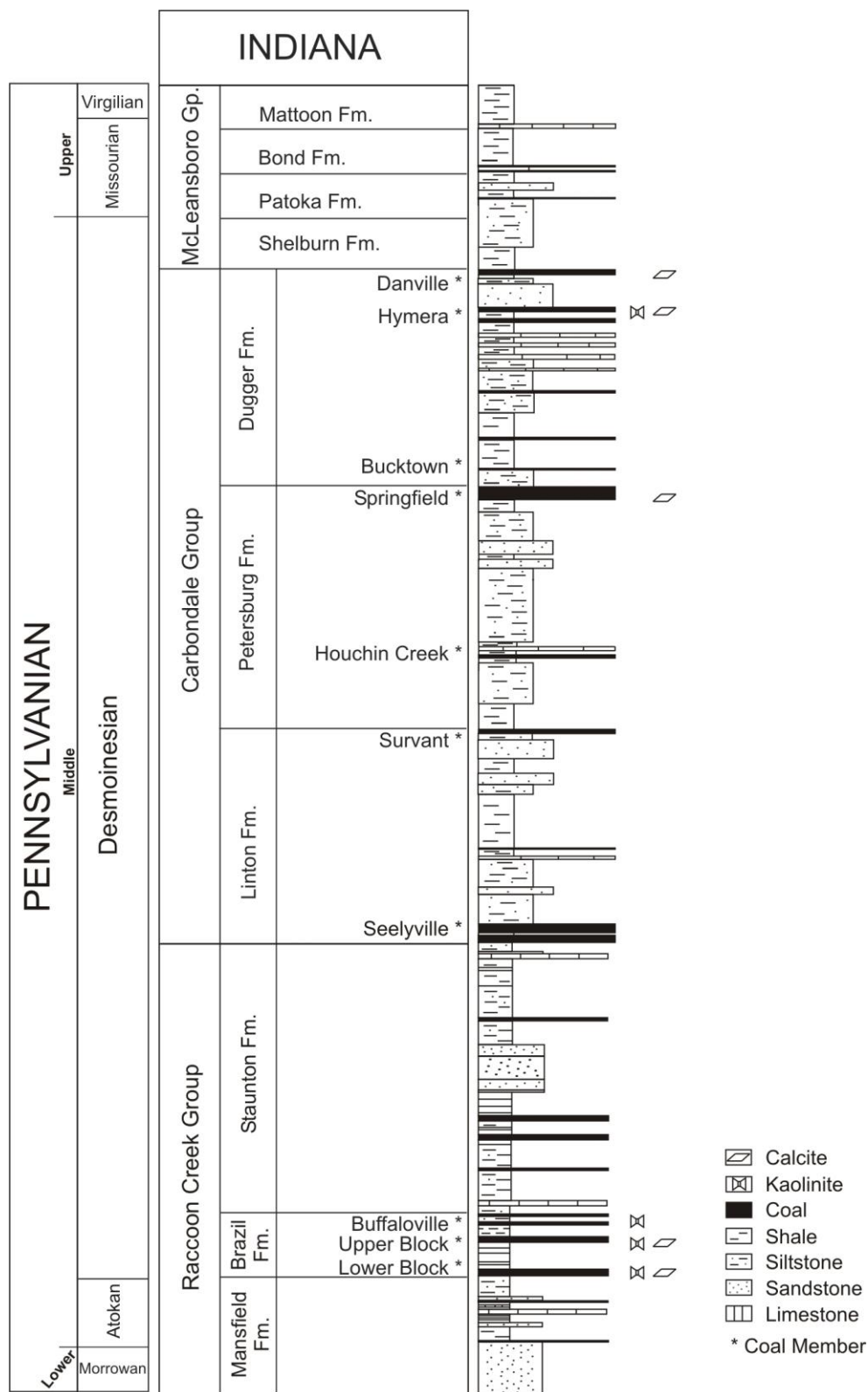


Figure 2. Generalized stratigraphic column of the Pennsylvanian section in Indiana identifying the coals from which calcite and kaolinite samples were collected.

6.2.2. X-ray diffraction

The mineralogical composition of cleat fillings was analyzed using a Bruker D8 Advance Series-2 X-ray diffractometer with Cu radiation. Samples for X-ray diffraction (XRD) were detached from cleat walls with a stainless steel blade and pulverized dry with an agate mortar and pestle to <5- μ m grain size. Powdered samples were placed on titanium holders and XRD measurements were made at 45 kV with a beam current of 35 mA over a scattering angle range of 2 to 70°, scan speed of 0.2 to 4 steps per second, and step increments of 0.02°. After running each sample in continuous step-scan mode for 4 hours, complete diffraction patterns were analyzed using EVA Search/Match[®] software.

6.2.3. Oxygen and carbon stable isotope ratios

Calcite crystals were hand-picked from coal cleats, rinsed with water, dried, powdered in a mortar with a pestle, and kept overnight in a vacuum oven at 150°C. Sample aliquots of ~5 mg, including aliquots of international carbonate standards NBS-19 and NBS-20, were reacted with 2 mL of anhydrous phosphoric acid in evacuated and sealed 9-mm o.d. Pyrex[®] Y-shaped tubes at 50°C. Carbon dioxide gas was cryogenically purified on a vacuum line and sealed in 6-mm o.d. Pyrex[®] tubes for transfer to a Delta Plus XP mass-spectrometer for off-line determination of $\delta^{13}\text{C}_{\text{calcite}}$ and $\delta^{18}\text{O}_{\text{calcite}}$ values.

Kaolinite samples from coal cleats were hand-picked, powdered, and dried in a vacuum oven at 150°C. The subsequent analytical procedure followed Clayton and Mayeda's (1963) methodology. Samples measuring ~5-mg kaolinite, as well as aliquots of international quartz oxygen isotope standard NBS-28, were placed in nickel vessels and heated to 250°C in vacuum for approximately 2 hours to eliminate adsorbed water.

Samples were treated with bromine pentafluoride (BrF₅, a strong oxidant) at room temperature and reacted at 600°C for 14 hours to release structural oxygen from kaolinite as elemental oxygen (O₂) that was converted to CO₂ by reaction with graphite. CO₂ was purified cryogenically and sealed in 6-mm o.d. Pyrex[®] tubes for transfer to a Delta Plus XP mass-spectrometer for off-line determination of $\delta^{18}\text{O}_{\text{kaolinite}}$ values.

Stable isotope ratios of carbon and oxygen are reported in customary δ -notation in ‰ with respect to Vienna Pee Dee Belemnite (VPDB) and VSMOW, respectively (Coplen, 1996). The analytical precision for $\delta^{13}\text{C}_{\text{calcite}}$, $\delta^{18}\text{O}_{\text{calcite}}$, and $\delta^{18}\text{O}_{\text{kaolinite}}$ values of CO₂ analyte gases was <0.04‰, <0.05‰, and $\pm 0.5\%$, respectively. $\delta^{18}\text{O}_{\text{calcite}}$ values were calculated from measured $\delta^{18}\text{O}$ values of CO₂ according to:

$$\delta^{18}\text{O}_{\text{calcite}} (\text{‰}) = [(\delta^{18}\text{O}_{\text{CO}_2 (\text{VSMOW})} + 1000)/\alpha] - 1000,$$

where $\alpha = 1.00924$ expresses the oxygen isotope fractionation factor during reaction of calcite with phosphoric acid at 50°C (Swart *et al.*, 1991).

6.2.4. Temperature corrections

Estimations of trapping temperature of fluid inclusions require knowledge of the actual pressure conditions during inclusion trapping and fluid salinity. In this work, we used the estimated burial of ~1.5 km (Rowan *et al.*, 2002) to calculate the maximum overburden pressure (~14.7 MPa), assuming hydrostatic conditions using a value of 9.79 MPa/km (0.433 psi/ft; Bradley, 1987). Additionally, we used the salinities of fluid inclusions proposed by Ambers (1993) to infer the appropriate temperature corrections. Our calculations indicate that a correction of up to ~20°C may be required to account for the actual trapping temperature of fluid inclusions.

6.3. Results

XRD analyses were conducted on fracture-filling material from four coals for mineralogical identification, yielding almost identical XRD patterns of kaolinite, such as the one shown in Figure 3. The titanium peak derives from the mounting plate. A small calcite peak (<1%) was detected in one of the samples.

Our new $\delta^{13}\text{C}_{\text{calcite}}$ values averaging $-4.32 \pm 4.29\text{‰}$ (n=11) are similar to Ambers's (1993) values with a mean of $-7.30 \pm 5.03\text{‰}$ (n=11). Individual data are listed in Table 1. New measurements of $\delta^{18}\text{O}_{\text{calcite}}$ from eleven calcite samples and earlier data from Ambers (1993) and Shieh and Suter (1979) are compiled in Table 1. Our $\delta^{18}\text{O}_{\text{calcite}}$ values averaging $23.3 \pm 1.0\text{‰}$ (n=11) are similar to Ambers's (1993) values with a mean of $23.9 \pm 1.2\text{‰}$ (n=11). They also match $\delta^{18}\text{O}_{\text{calcite}}$ data of Shieh and Suter (1979) with an average of $22.8 \pm 1.1\text{‰}$ (n=16).

Measurements of $\delta^{18}\text{O}_{\text{kaolinite}}$ from five kaolinite samples averaging $16.1 \pm 1.0\text{‰}$ (n=5) are similar to kaolinite data of Shieh and Suter (1979; $17.0 \pm 0.3\text{‰}$, n=20) and Ambers (1993; $17.6 \pm 0.4\text{‰}$, n=29). Individual data are listed in Table 2. Sampling locations for calcite and kaolinite from this study are shown in Figure 1.

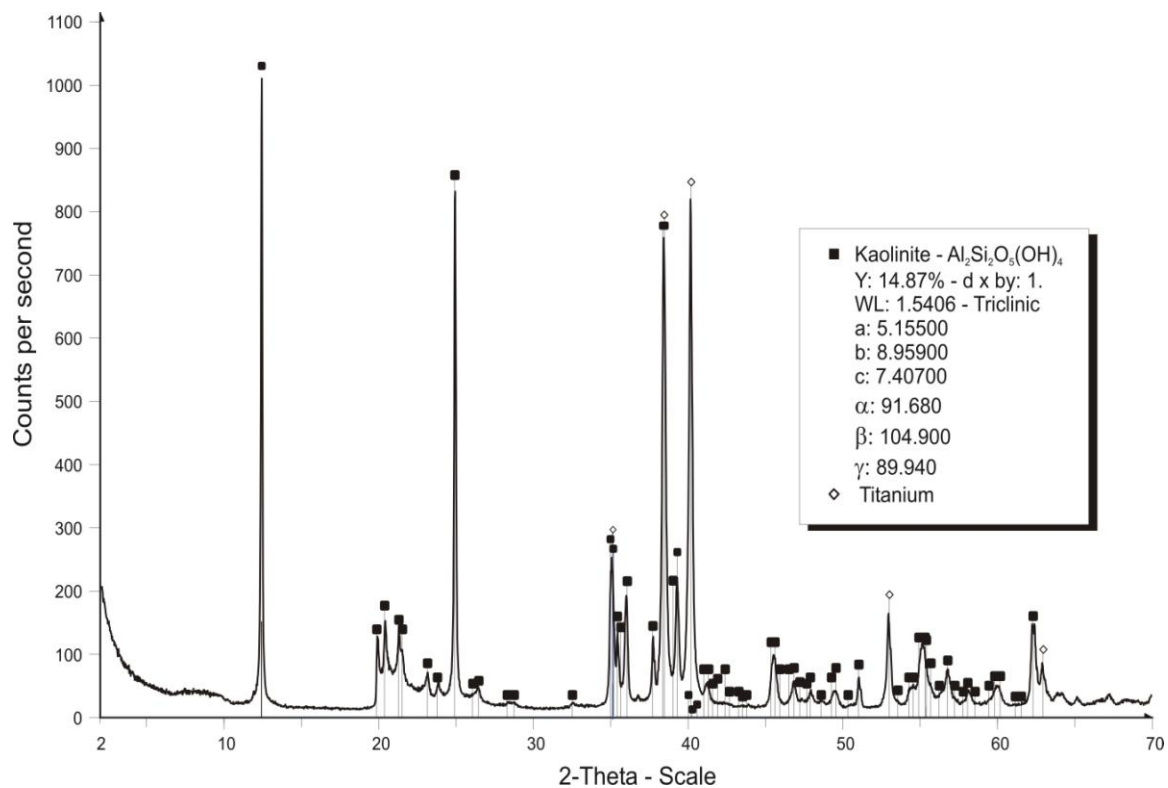


Figure 3. X-ray diffraction pattern of cleat-filling kaolinite from the Lower Block Coal Member in Danville, Indiana. The titanium signal derives from the mounting media.

Table 1. Carbon- and oxygen-stable isotope ratios of diagenetic calcites from coal cleats, and carbon-stable isotope ratios of carbon dioxide (CO₂) from coalbed gases. $\delta^{13}\text{C}$ and $\delta^{18}\text{O}$ values are expressed in ‰ relative to Vienna Pee Dee Belemnite (VPDB) and Vienna Standard Mean Ocean Water (VSMOW), respectively. The sequence of data entries within each data set is relative to stratigraphic position, from top to bottom.

	County	Coal Member	$\delta^{18}\text{O}_{\text{calcite}}$	$\delta^{13}\text{C}_{\text{calcite}}$	$\delta^{13}\text{C}_{\text{CO}_2}$
This Study	Gibson	Danville	24.49	-3.60	n.d.
	Gibson	Danville	24.35	-3.69	n.d.
	Gibson	Danville	23.92	-5.24	n.d.
	Gibson	Danville	24.28	-2.56	n.d.
	Gibson	Danville	22.87	-1.01	n.d.
	Gibson	Danville	23.19	-3.75	n.d.
	Gibson	Springfield	22.96	-5.88	n.d.
	Daviess	Upper Block	21.33	-11.05	n.d.
	Daviess	Upper Block	21.55	-11.13	n.d.
	Daviess	Upper Block	21.65	-11.07	n.d.
	Sullivan	Danville	23.63	-6.16	n.d.
	Sullivan	Danville	23.93	-4.96	n.d.
	Sullivan	Danville	23.86	-5.01	n.d.
	Gibson	Hymera	23.06	-0.06	n.d.
	Daviess	Lower Block	23.27	1.57	n.d.
	Daviess	Lower Block	23.28	1.51	n.d.
Ambers (1993)	n.i.	n.i.	22.60*	-16.06	n.d.
	n.i.	n.i.	22.98*	-13.55	n.d.
	n.i.	Danville	23.99*	-9.17	n.d.
	Gibson	Danville	24.31*	0.30	n.d.
	Knox	Danville	22.87*	-3.56	n.d.
	Clay	Upper Block	25.77*	-10.15	n.d.
	Vigo	Danville	24.85*	-7.44	n.d.
	Greene	Lower Block	22.96*	-10.10	n.d.
	Crawford	Bethel Fm.***	25.65*	-2.00	n.d.
	Sullivan	Hymera	22.77*	-4.34	n.d.
	Sullivan	Danville	23.81*	-4.20	n.d.
Shieh and Suter (1979)	Clay	Seelyville	21.7	n.d.	n.d.
	Clay	Seelyville	22.3	n.d.	n.d.
	Clay	Seelyville	22.7	n.d.	n.d.
	Clay	Seelyville	23.5	n.d.	n.d.
	Clay	Seelyville	22.5	n.d.	n.d.
	Sullivan	Hymera	21.4	n.d.	n.d.
	Sullivan	Hymera	21.6	n.d.	n.d.
	Sullivan	Hymera	22.1	n.d.	n.d.
	Sullivan	Hymera	24.5	n.d.	n.d.
	Sullivan	Danville	21.9	n.d.	n.d.
	Sullivan	Danville	24.4	n.d.	n.d.
	Warrick	Springfield	22.0	n.d.	n.d.
	Warrick	Springfield	22.4	n.d.	n.d.
	Warrick	Springfield	23.6	n.d.	n.d.
	Warrick	Springfield	24.3	n.d.	n.d.
	Warrick	Springfield	24.5	n.d.	n.d.
Strapoć et al. (2007)	Sullivan	Springfield	n.d.	n.d.	-2.3
	Sullivan	Houchin Creek	n.d.	n.d.	8.2
	Sullivan	Survant	n.d.	n.d.	8.7**
	Sullivan	Seelyville	n.d.	n.d.	7.6**
	Gibson	Springfield	n.d.	n.d.	-0.8**
	Gibson	Seelyville	n.d.	n.d.	-0.3**
	Gibson	Danville	n.d.	n.d.	-1.8
	Knox	Seelyville	n.d.	n.d.	9.5
	Sullivan	Danville	n.d.	n.d.	11.4
	Sullivan	Buffaloville	n.d.	n.d.	2.5
	Sullivan	Upper Block	n.d.	n.d.	3.6
	Sullivan	Lower Block	n.d.	n.d.	2.9
	Sullivan	Shady lane	n.d.	n.d.	-1.0

n.i. not identified; n.d. not determined.

* Converted to VSMOW using $\delta^{18}\text{O}_{\text{VSMOW}} = 1.03091 \delta^{18}\text{O}_{\text{PDB}} + 30.91\text{‰}$ (Coplen *et al.*, 1983)

** Average of all available data

*** Not a coal member

Table 2. Oxygen-stable isotope ratios of diagenetic kaolinites from coal cleats. $\delta^{18}\text{O}$ values are expressed in ‰ relative to Vienna Standard Mean Ocean Water (VSMOW). The sequence of data entries within each data set is relative to stratigraphic position, from top to bottom. Three data of Shieh and Suter (1979) derive from Illinois (IL). Averages of isotope ratios are indicated by asterisks next to the county when more than one data point is available from Ambers (1993) and Shieh and Suter (1979).

	County	Coal Member	$\delta^{18}\text{O}_{\text{kaolinite}}$
This study	Gibson	Hymera	14.8
	Gibson	Hymera	16.4
	Daviess	Buffaloville	16.9
	Daviess	Upper Block	17.2
	Daviess	Lower Block	15.4
Ambers (1993)	Gibson	Danville	17.6
	Sullivan*	Danville	17.8
	Vigo	Danville	18.5
	Knox*	Danville	17.6
	Sullivan	Hymera	17.6
	Pike*	Hymera	17.3
	Pike	Springfield	17.4
	Warrick	Survant	16.6
	Daviess	Colchester	17.9
	Pike	Colchester	17.5
	Clay	Minshall	17.8
	Daviess	Buffaloville	17.9
	Clay*	Upper Block	17.4
	Greene	Upper Block	17.5
	Parke	Upper Block	18.2
	Clay	Lower Block	17.9
	Greene	Lower Block	17.4
	Greene	Upper Mansfield Fm.**	17.2
	Owen*	Lower Mansfield Fm.**	18.3
Shieh and Suter (1979)	Sullivan	Hymera	16.6
	Sullivan	Hymera	17.6
	Sullivan*	Danville	16.9
	Greene*	Danville	16.9
	Warrick*	Springfield	17.2
	Gibson*	Springfield	17.0
	Saline* (IL)	Springfield	17.0

** Not a coal member

6.4. Discussion

6.4.1. Thermal history of the Illinois Basin

Burial and thermal histories of the Illinois Basin were reconstructed by Rowan *et al.* (2002) based on a multidisciplinary approach that included simulations of the effects of advective heat flow to explain coal maturity (*i.e.*, vitrinite reflectance), paleotemperature reconstructions from fluid inclusions, and biomarker data from previous studies. Their ‘hybrid model’ indicates that regional fluid flow initiated at the time of uplifting of the Ouachita fold belt during the Late Pennsylvanian and ended with the uplift of the Pascola Arch during the Mesozoic. High-temperature fluid inclusions and high vitrinite reflectance values in the northern Illinois Basin in the upper Mississippi valley district were explained by brief regional heating that lasted ~200,000 years and was caused by deep Permian magmatic intrusions approximately 272 Ma ago. This ‘hybrid model’ of Rowan *et al.* (2002) offers a reasonable mechanism to explain the maturity of coals and fluid inclusion data throughout the Illinois Basin. We adopt this model as a guide to interpret mineral isotopic data from cleats.

6.4.2. Isotopic equilibrium between oxygen in minerals and water during mineralization

The isotopic fractionation $\Delta^{18}\text{O} = \delta^{18}\text{O}_{\text{mineral}} - \delta^{18}\text{O}_{\text{water}} (\text{‰})$ during crystallization at thermodynamic equilibrium depends primarily on temperature and has been used extensively for isotopic paleothermometry (Valley and Cole, 2001). Pressure is not an important factor, as exemplified by Clayton *et al.*’s (1975) study of the fractionation factors of calcite-water system within a range of 100 to 2000 MPa. Curved lines in Figure

4 represent the relationships between oxygen isotopic fractionation of water and minerals as a function of temperature, according to equilibrium calibrations for kaolinite by Zheng (1993) and for calcite by Kim and O'Neil (1997):

$$10^3 \ln \alpha_{(\text{kaolinite} - \text{water})} = \delta^{18}\text{O}_{\text{kaolinite}} - \delta^{18}\text{O}_{\text{water}} = 4.29 \times 10^6 T^{-2} - 6.44 \times 10^3 T^{-1} + 2.03$$

$$10^3 \ln \alpha_{(\text{calcite} - \text{water})} = \delta^{18}\text{O}_{\text{calcite}} - \delta^{18}\text{O}_{\text{water}} = 18.03 \times 10^3 T^{-1} - 32.42,$$

where α is the isotopic fractionation factor (Criss, 1999) and T is the temperature in Kelvin.

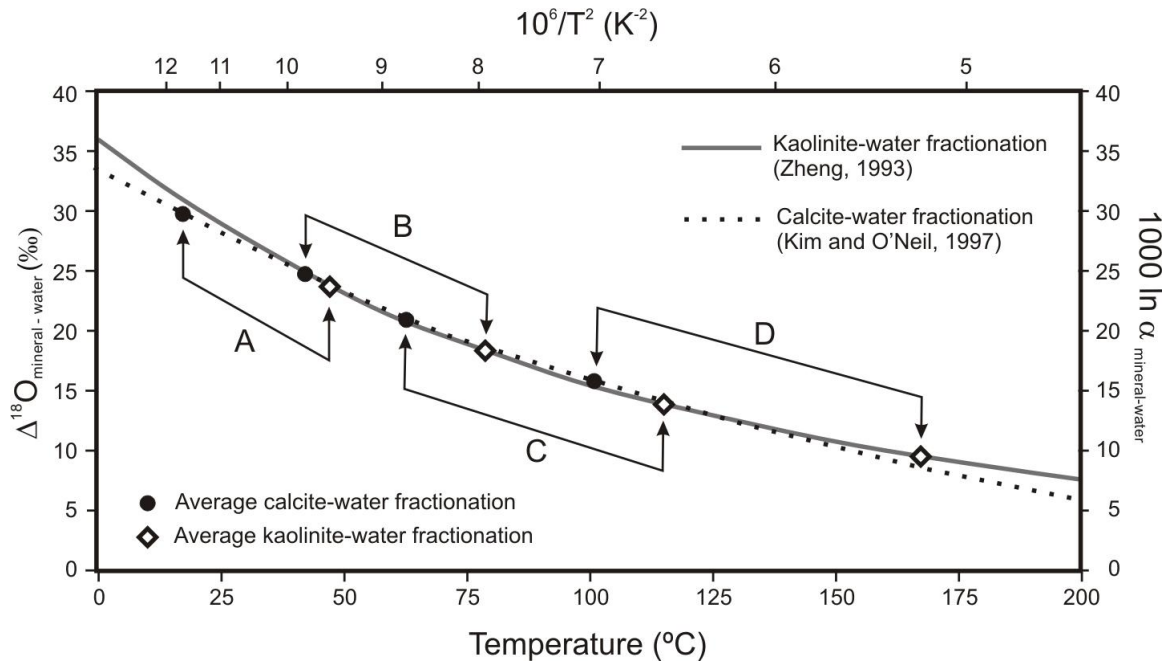


Figure 4. Empirical relationships of mineral-water fractionation factors for kaolinite (Zheng, 1993) and calcite (Kim and O'Neil, 1997). Averages of measured $\Delta^{18}O_{\text{mineral-water}}$ values are plotted for the proposed A, B, C, and D scenarios using estimated $\delta^{18}O_{\text{water}}$ values from Table 3; the isotopic standard deviation is smaller than the size of symbols.

6.4.3. Significance of the $^{18}\text{O}/^{16}\text{O}$ ratio of water for paleotemperature estimates

In the absence of direct information about $\delta^{18}\text{O}_{\text{water}}$ values of paleowaters in Illinois Basin coals during crystallization of cleat minerals, we consider four different scenarios (A, B, C, D; see Table 3) with increasing $\delta^{18}\text{O}_{\text{water}}$ values that are based on published data and estimates. The scenarios also differ with regard to burial conditions and the timing of emplacement of authigenic minerals. For each scenario, we calculated the temperatures for kaolinite and calcite precipitation in coal based on the equilibrium equations of Zheng (1993) and Kim and O'Neil (1997). Our calculations utilize all available and relevant $\delta^{18}\text{O}_{\text{mineral}}$ data jointly because previously published isotopic data (*i.e.*, Ambers, 1993; Shieh and Suter, 1979) are quantitatively comparable with our new data (Tables 1, 2).

The following sections will discuss individual scenarios and their paleotemperature estimates for the formation of authigenic minerals in Indiana coals. Scenario B with an intermediate $\delta^{18}\text{O}_{\text{water}}$ value and a moderate temperature regime will ultimately be our preferred choice as the most suitable candidate to explain the formation and distribution of authigenic kaolinite and calcite in coal cleats.

Table 3. Four scenarios of paleotemperatures in coals during mineralization based on published data and estimates of the oxygen isotopic signature of coalbed waters in equilibrium with precipitated authigenic minerals in coal cleats.

Scenario	$\delta^{18}\text{O}_{\text{water}}$ (‰ VSMOW)	Assumed origin of water in coal seams	References
A	-6.2	Average $\delta^{18}\text{O}_{\text{water}}$ value of -6.2‰ for Holocene meteoric water in coals, as constrained by the following data: (i) Modern meteoric water -6.3‰ sampled as seepage water from a surface mine by Shieh and Suter (1979). (ii) Holocene meteoric waters -6.29‰ co-produced with coalbed methane from the Seelyville Coal Member; assumed to represent all waters in deeper coal members located stratigraphically below the Springfield Coal Member. (iii) Holocene meteoric waters -6.12‰ co-produced with coalbed methane from the Springfield Coal Member; assumed to represent all waters in more shallow coal members above the Springfield Coal Member.	Shieh and Suter (1979); Strapoc <i>et al.</i> (2007)
B (preferred)	-1.25	Pre-glacial water , possibly of Cretaceous age, that derived from tropical seas and/or associated meteoric water; reconstructions of $\delta^{18}\text{O}_{\text{paleowater}}$ are based on $^{18}\text{O}/^{16}\text{O}$ ratios of fossil fish teeth and planktonic foraminifera.	Pucéat <i>et al.</i> (2007); Shackleton and Kennett (1975)
C	~3	Average of two fluids: (i) Basinal brine mixed with seawater or low-latitude meteoric water resulting in ~2.0‰, and (ii) 1:1 mixing of ^{18}O -enriched pristine basinal brine waters (7.5‰; Ambers, 1993) with ^{18}O -depleted pre-glacial tropical meteoric or ocean water (-1.25‰) resulting in ~4.4‰. The weighted average of all components is ~3‰.	Ambers (1993); Pucéat <i>et al.</i> (2007)
D	7.5	Basinal brine ; $\delta^{18}\text{O}_{\text{water}}$ modified by rock-water interaction during maximum burial of the Illinois Basin.	Ambers (1993)

6.4.3.1. Mineralization scenario A: low temperature and $\delta^{18}\text{O}_{\text{water}} \sim -6.2\text{‰}$

Scenario A follows Shieh and Suter's (1979) suggestion that kaolinite and calcite in coals formed in 'fairly recent geologic time' at shallow burial in contact with meteoric-derived water. Scenario A adopts a $\delta^{18}\text{O}_{\text{water}}$ value of -6.2‰ reflecting the strongest ^{18}O -depletion of all scenarios. The available $\delta^{18}\text{O}_{\text{kaolinite}}$ values range from 14.8 to 18.6‰ (Table 2) and indicate a mean temperature of kaolinite precipitation of $48.4 \pm 3.3^\circ\text{C}$ (range from 42.5 to 62.5°C; n=54; Table 4; Figure 5a). The observed range of all measured $\delta^{18}\text{O}_{\text{calcite}}$ values of 21.4 to 25.7‰ (Table 1) translates into a mean calculated equilibrium paleotemperature of $17.2 \pm 5.2^\circ\text{C}$ of calcite precipitation (range from 7.2 to 26.7°C; n=38; Table 5 and Figure 5b). $\delta^{18}\text{O}_{\text{water}}$ values and corresponding mineral $\delta^{18}\text{O}$ values constrain the paleotemperature of mineral precipitation (Figure 5) when crystal growth occurs close to thermodynamic equilibrium.

The similar positioning of the curved equilibrium lines in Figure 4, especially where they intersect (42.1 and 122.2°C), mandates that $\delta^{18}\text{O}_{\text{kaolinite}}$ and $\delta^{18}\text{O}_{\text{calcite}}$ values must be similar if both minerals were growing at the same temperature from the same fluid simultaneously. In contrast, large and systematic differences between our measured $\delta^{18}\text{O}_{\text{kaolinite}}$ and $\delta^{18}\text{O}_{\text{calcite}}$ values provide unambiguous evidence that these two mineral phases must have grown at different temperatures and/or from different fluids. Figure 4 demonstrates this fact by pairs of incongruent data points for calcite and kaolinite for each scenario.

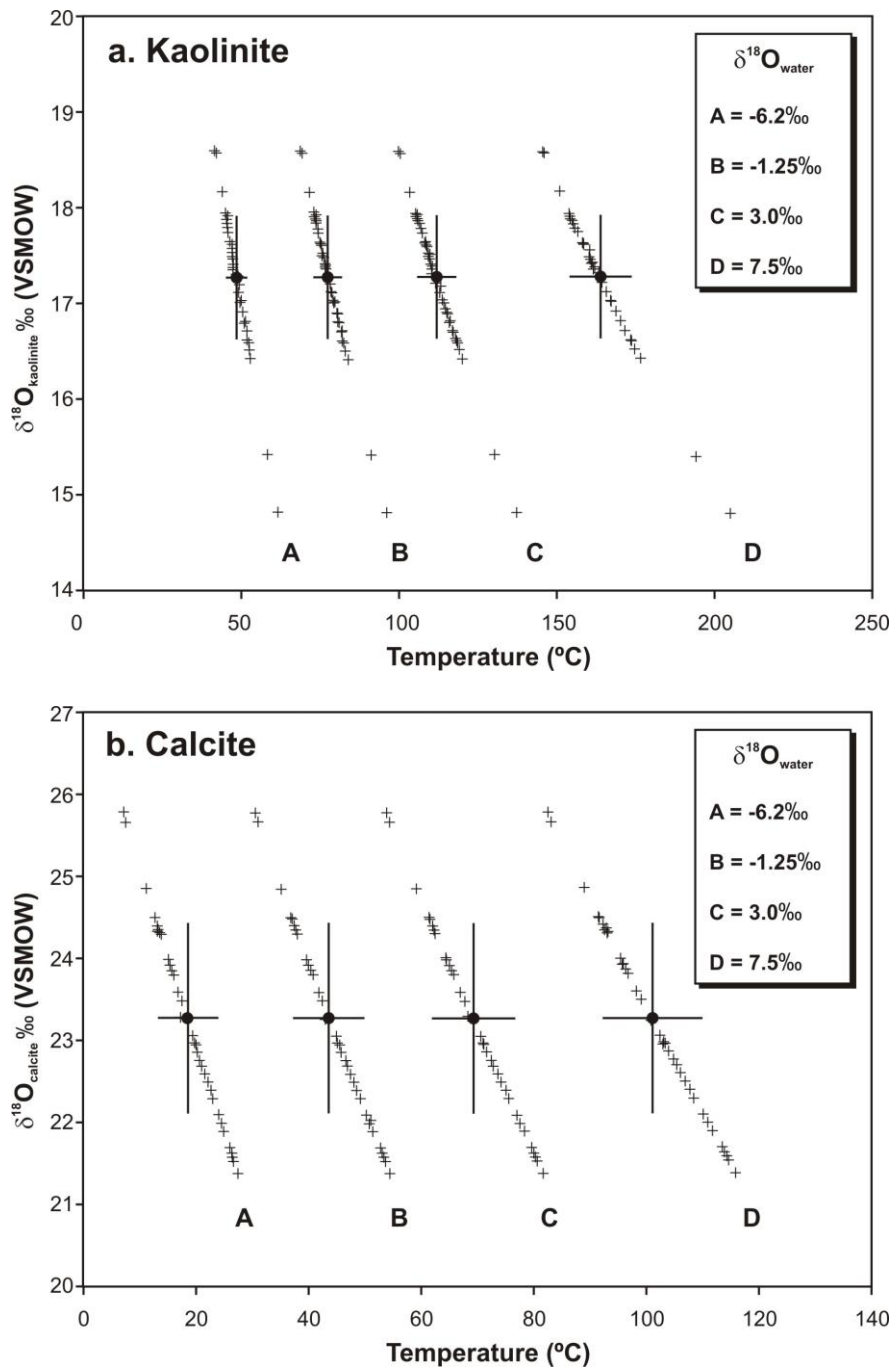


Figure 5. Measured $\delta^{18}\text{O}_{\text{calcite}}$ and $\delta^{18}\text{O}_{\text{kaolinite}}$ values and hypothetical $\delta^{18}\text{O}_{\text{water}}$ values from scenarios A, B, C, and D define temperatures of crystallization for (a) kaolinite and (b) calcite. Filled circles with error bars represent mean values and standard deviations from each data set.

Table 4. Measured $\delta^{18}\text{O}_{\text{kaolinite}}$ values and calculated formation temperatures of diagenetic kaolinites, according to four scenarios A, B, C, and D where isotopically different waters are in isotopic equilibrium with growing kaolinite. $\delta^{18}\text{O}_{\text{kaolinite}}$ values are reported in ‰ relative to Vienna Standard Mean Ocean Water (VSMOW). The equilibrium equation of Zheng (1993) was used for temperature calculations. The sequence of data entries within each data set is relative to stratigraphic position, from top to bottom. Averages of isotope ratios and of calculated temperatures are indicated by asterisks next to the county when more than one data point is available from Ambers (1993) and Shieh and Suter (1979).

	County	Coal Member	$\delta^{18}\text{O}_{\text{kaolinite}}$ (‰)	Paleotemperature Scenarios (°C)			
				A	B	C	D
This study	Gibson	Hymera	14.80	62.0	96.1	137.3	205.5
	Gibson	Hymera	16.40	53.1	83.9	120.0	176.9
	Daviess	Buffaloville	16.90	50.4	80.3	115.1	169.1
	Daviess	Upper Block	17.20	48.9	78.2	112.3	164.7
	Daviess	Lower Block	15.40	58.6	91.4	130.6	194.0
Ambers (1993)	Gibson	Danville	17.60	46.9	75.5	108.6	159.0
	Knox*	Danville	17.62	46.8	75.4	108.4	158.7
	Sullivan*	Danville	17.81	45.8	74.1	106.7	156.1
	Vigo	Danville	18.56	42.1	69.3	100.2	146.3
	Pike*	Hymera	17.35	48.1	77.2	110.9	162.8
	Sullivan	Hymera	17.63	46.7	75.3	108.3	158.6
	Pike	Springfield	17.39	47.9	76.9	110.5	162.0
	Warrick	Survant	16.58	52.1	82.6	118.2	174.0
	Daviess	Colchester	17.86	45.5	73.7	106.2	155.4
	Pike	Colchester	17.47	47.5	76.4	109.8	160.6
	Clay	Minshall	17.82	45.7	74.0	106.5	155.9
	Daviess	Buffaloville	17.93	45.2	73.3	105.6	154.5
	Clay*	U. Block	17.42	47.8	76.8	110.2	161.6
	Greene	U. Block	17.52	47.2	76.0	109.3	160.1
	Parke	U. Block	18.16	44.1	71.8	103.6	151.4
	Clay	L. Block	17.86	45.6	73.8	106.3	155.5
	Greene	L. Block	17.40	47.8	76.8	110.4	161.8
	Greene	U. Mansfield Fm.**	17.20	48.9	78.2	112.3	164.7
	Owen*	L. Mansfield Fm.**	18.23	43.8	71.4	103.1	150.7
Shieh and Suter (1979)	Sullivan*	Danville	16.89	50.5	80.4	115.3	169.4
	Greene*	Danville	16.93	50.3	80.1	114.8	168.6
	Sullivan*	Hymera	17.10	49.4	79.0	113.3	166.4
	Warrick*	Springfield	17.20	48.9	78.2	113.2	164.7
	Gibson*	Springfield	17.00	49.9	79.6	114.2	167.6
	Saline (IL)*	Springfield	17.03	49.8	79.4	113.9	167.2

** Not a coal member

One can estimate the approximate depth of mineralization by applying an equation that relates calculated mineralization temperature, average shallow ground-water temperature, and geothermal gradient. Geothermal gradients for the Illinois Basin have been estimated to 23.5°C/km by Kaegi (1976) and to 36°C/km by Zimmermann (1986). Using the average geothermal gradient (30°C/km), the mean value of calcite precipitation (17.2°C), the maximum value of calcite precipitation (26.7°C) (Table 5), and assuming a Holocene average shallow ground-water temperature of 15°C (Ambers, 1993), we estimate the depth of calcite mineralization within ~73 m to ~390 m. The present occurrence of coals at this depth range in southwestern Indiana would be consistent with Shieh and Suter's (1979) suggestion that calcite 'formed at or near the surface, perhaps in fairly recent geologic time.' Using the same geothermal gradient of 30°C/km, a depth interval for kaolinite mineralization is calculated between ~900 and ~1600 m, close to the suggested maximum burial depth of ~1300 m for the Herrin Coal Member (Rowan *et al.*, 2002). Calculated temperatures and their correspondence to burial depth suggest that kaolinite formed earlier than calcite, in agreement with cross-cutting relationships from mineral-filled cleats in Indiana coals (Solano-Acosta *et al.*, in press). These authors proposed that the angularity between two different sets of cleats observed in the field, consistent with lineament data, developed as a result of tectonic stress regimes that changed orientation during coalification and basin evolution. Solano-Acosta *et al.*, (in press) also suggested that the earliest mineralization event occurred early on during coalification, which allowed preservation of the original cleat system.

Previous studies have quantified the carbon isotope equilibrium fractionation between calcite and CO₂ at various temperatures (Bottinga, 1968; Chacko *et al.*, 1991;

Deines *et al.*, 1974; Emrich *et al.*, 1970; Halas *et al.*, 1997; Lesniak and Sakai, 1989; Turner, 1982). As a consequence of scenario A's low temperature and relatively recent crystallization of calcite in coal seams, it is expected that $\delta^{13}\text{C}_{\text{calcite}}$ values are in isotopic equilibrium with experimentally determined $\delta^{13}\text{C}_{\text{CO}_2}$ values from carbon dioxide in modern coalbed gases. Published $\delta^{13}\text{C}_{\text{CO}_2}$ values presented in Table 1, (Strapoć *et al.*, 2007) from coalbed-methane-producing wells from the Danville Coal Member (Gibson and Sullivan Counties) and from the Springfield Coal Member (Gibson County) were isotopically compared with $\delta^{13}\text{C}_{\text{calcite}}$ values from coal cleats and with the known equilibrium carbon stable isotope fractionation between CO_2 and calcite from 0 to 350°C (Figure 6). Only carbon dioxide from the Danville Coal Member in Gibson County could possibly be in equilibrium with calcite, although at an unrealistic temperature of >300°C. We conclude that calcites in Indiana coal cleats must have crystallized at a time when carbon dioxide in coal seams was far more ^{13}C -depleted than it is today. Overall, scenario A is firmly rejected based on the aforementioned isotopic and morphological evidence.

Table 5. Measured $\delta^{18}\text{O}_{\text{calcite}}$ values and calculated formation temperatures of diagenetic calcites, according to four scenarios A, B, C, and D where isotopically different waters are in isotopic equilibrium with growing calcite. $\delta^{18}\text{O}_{\text{calcite}}$ values are reported in ‰ relative to Vienna Standard Mean Ocean Water (VSMOW). The equilibrium equation of Kim and O'Neil (1997) was used for temperature calculations. The sequence of data entries within each data set is relative to stratigraphic position, from top to bottom.

	County	Coal Member	$\delta^{18}\text{O}_{\text{calcite}}$ (‰)	Paleotemperature Scenarios (°C)			
				A	B	C	D
This study	Gibson	Danville	24.49	12.5	36.9	61.3	91.8
	Gibson	Danville	24.35	13.2	37.6	62.2	92.8
	Gibson	Danville	23.92	15.1	39.9	64.5	96.0
	Sullivan	Danville	23.93	15.1	39.9	64.8	95.9
	Sullivan	Danville	23.86	15.4	40.2	65.2	96.5
	Gibson	Hymera	23.06	19.2	44.7	70.4	102.6
	Gibson	Springfield	22.96	19.6	45.2	71.1	103.4
	Daviess	Upper Block	21.55	26.5	53.4	80.6	114.8
	Daviess	Upper Block	21.65	26.0	52.8	79.9	114.0
	Daviess	Lower Block	23.27	18.2	43.5	69.0	101.0
	Daviess	Lower Block	23.28	18.1	43.4	69.0	100.9
Ambers (1993)	n.d.	n.d.	22.55	21.4	47.3	73.4	106.3
	n.d.	n.d.	22.93	19.5	45.1	70.9	103.2
	n.d.	Danville	23.95	14.8	39.5	64.4	95.5
	Gibson	Danville	24.27	13.3	37.8	62.4	93.1
	Knox	Danville	22.82	20.1	45.7	71.7	104.1
	Sullivan	Danville	23.76	15.7	40.5	65.6	96.9
	Vigo	Danville	24.80	10.9	35.0	59.1	89.1
	Sullivan	Hymera	22.72	20.6	46.3	72.3	104.9
	Clay	Upper Block	25.72	6.9	30.2	53.6	82.6
	Greene	Lower Block	22.92	19.6	45.2	71.0	103.4
	Crawford	Bethel Fm*	25.60	7.4	30.8	54.2	83.4
Suter and Shieh (1979)	Sullivan	Hymera	21.40	27.2	54.2	81.6	116.1
	Sullivan	Hymera	21.60	26.2	53.1	80.2	114.4
	Sullivan	Hymera	22.10	23.4	50.1	76.8	110.3
	Sullivan	Hymera	24.50	12.5	36.8	61.2	91.7
	Sullivan	Hymera	21.90	24.5	51.3	78.2	111.9
	Sullivan	Hymera	24.40	12.9	37.3	61.9	92.4
	Warrick	Springfield	22.00	24.3	50.7	77.5	111.1
	Warrick	Springfield	22.40	22.3	48.4	74.8	107.9
	Warrick	Springfield	23.60	16.6	41.7	66.9	98.4
	Warrick	Springfield	24.30	13.4	37.9	62.5	93.2
	Warrick	Springfield	24.50	12.5	36.8	61.2	91.7
	Clay	Seelyville	21.70	25.8	52.5	79.5	113.6
	Clay	Seelyville	22.30	22.8	49.0	75.5	108.7
	Clay	Seelyville	22.70	20.9	46.7	72.8	105.5
	Clay	Seelyville	23.50	17.1	42.2	67.5	99.2
	Clay	Seelyville	22.50	21.8	47.8	74.1	107.1

* Not a coal member

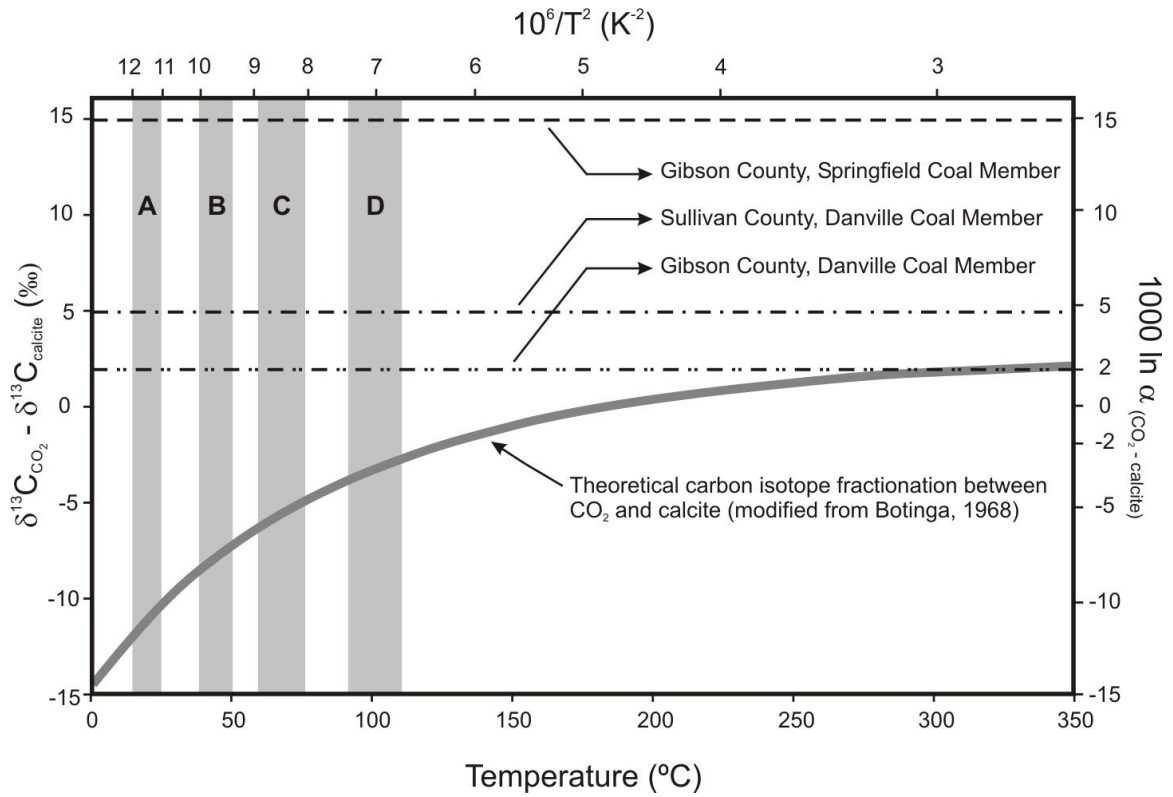


Figure 6. The observed carbon isotopic differences $\Delta^{13}\text{C}_{\text{CO}_2\text{-calcite}}$ (horizontal dashed lines) between calcites from cleats and carbon dioxide from coalbed gases from Gibson and Sullivan Counties in Indiana are not compatible with the equilibrium isotope fractionation of the CO_2 -calcite system (Bottinga, 1968) within the temperature range of scenarios A, B, C, and D (gray vertical bars). The widths of the gray bars correspond to the standard deviations around the mean values of each scenario.

6.4.3.2. Mineralization scenario B: intermediate temperature and $\delta^{18}\text{O}_{\text{water}} \sim -1.25\text{‰}$

Scenario B suggests that successive crystallization of kaolinite and calcite in Indiana coals occurred between the emplacement of igneous intrusions during the Permian and tectonic uplift during the Mesozoic, in the presence of pre-glacial meteoric or ocean waters that had infiltrated the coals. According to paleotectonic reconstructions of Scotese, the Illinois Basin occupied a near-equatorial paleolatitude between Carboniferous and Permian times¹. Meteoric tropical waters would have derived from a well-mixed ocean with $\delta^{18}\text{O}_{\text{ocean water}} = -1.25\text{‰}$ (Puc  at *et al.*, 2007) and entered the coal without significant isotope fractionation because tropical rainfall is isotopically similar to its marine source water (Criss, 1999).

The initial mineralization of kaolinite may have been promoted by a combination of factors including (i) an increased geothermal gradient owing to advective heat transport after the emplacement of magmatic intrusions in the basin, (ii) changes in stress conditions owing to continental collisions, (iii) cleat development during coalification, and (iv) presence of seawater-derived fluids (Whelan *et al.*, 1988). Calcite, on the other hand, seems to have formed at lower temperatures and probably during the development of a secondary cleat system resulting from the post-Paleozoic counterclockwise rotation of North America (Solano-Acosta *et al.*, in press). Such cleat formation is indicated by the presence of calcite-filled cleats that postdate kaolinite mineralization as demonstrated by cross-cutting relationships.

Scenario B advocates elevated mineralization temperatures on the basis of ground-water flow and advective heat distribution, according to recent models of the thermal

¹ Scotese, C.R., 2002, <http://www.scotese.com> (PALEOMAP website)

history of the Illinois Basin (Rowan *et al.*, 2002). The emplacement of Permian intrusive rocks in southern Illinois (Collinson *et al.*, 1988, and references therein) may have provided the necessary short-term heat pulse for mineralization in the Illinois Basin (~272 Ma ago), as well as to the Fluorspar and upper Mississippi valley districts (Rowan *et al.*, 2002). Kaolinite mineralization would have occurred possibly during the middle Permian when magmatic activity was sufficient to provide enough heat through advective heat redistribution to locally increase coal maturity, cause devolatilization, and the development of cleats.

Kaolinite would have formed as the first mineral phase in cleats at $77.8 \pm 4.6^\circ\text{C}$ (range 69.3 to 96.1°C; n=54; Table 4; Figure 5a). Assuming the same geothermal gradient of 30°C/km used in scenario A, our calculated temperatures would correspond to burial depths of ~1800 to 2700 m. Although this burial depth is consistent with peak burial estimates for the Illinois Basin (Ambers, 1993, and references therein), it contrasts with more recent burial depth and temperature estimates (~1300 m and ~80 °C for the Herrin Coal Member in the north central portion of the basin; Rowan *et al.*, 2002) that we adopt in this study. To support burial depths between ~1800 and 2700 m, very high rates of post-Pennsylvanian sedimentation and subsequent erosion would be required (Rowan *et al.*, 2002), but are not necessary to explain the existing data. Our $\delta^{18}\text{O}_{\text{kaolinite}}$ data agree with (i) scenario B's proposed value of <100°C for authigenic kaolinite in the anthracite region of Pennsylvania (Daniels and Altaner, 1990), (ii) available regional vitrinite reflectance data (Drobniak *et al.*, 2004; Rowan *et al.*, 2002), (iii) fluid inclusion measurements in the Illinois Basin (Ambers, 1993; Coveney *et al.*, 1987; Rowan *et al.*, 2002, and references therein), and (iii) burial depth and temperature estimates for Illinois

Basin coals (Rowan *et al.*, 2002). The same authors suggested a brief heating event lasting ~200,000 years in order to explain observed high vitrinite reflectance (R_o) values. The resulting unusually high temperature at relatively shallow depth is responsible for the observed $\delta^{18}\text{O}_{\text{kaolinite}}$. In other words, kaolinite would have formed at a much shallower depth than that proposed by Ambers (1993).

Following the crystallization of kaolinite at a higher temperature, calcite precipitated later at a lower calculated mean paleotemperature of $43.2 \pm 6.4^\circ\text{C}$ (range 30.2 to 54.2°C ; $n=38$; Table 5; Figure 5b) corresponding to a burial depth of ~500 to ~1300 m assuming that the geothermal gradient returned to a normal $30^\circ\text{C}/\text{km}$ after the heat was evenly redistributed throughout the basin. The proposed temperature for calcite precipitation is within the range of temperatures estimated by Whelan *et al.* (1988; ~15 to 75°C), based on oxygen isotope data of cleat-filling calcites.

Intermittent deep burial and heating would have sterilized the coal and surrounding sediments and produced thermogenic, relatively ^{13}C -depleted carbon dioxide. In agreement with our finding of relatively ^{13}C -depleted calcite, the subsequent precipitation calcite reflects a carbon dioxide pool that had not yet been affected by microbial fractionation via CO_2 -reductive methanogenesis (Figure 6).

Overall, we favor scenario B because the available oxygen-stable isotope data from kaolinite and calcite yield reasonable paleotemperature estimates that are in broad agreement with multidisciplinary evidence about the thermal history of the Illinois Basin.

In this (B) and the following scenarios (C and D), we assume that oxygen in formation waters did not significantly exchange isotopically with oxygen in the surrounding minerals, based on the premise that isotopic exchange reactions are slow at

low temperatures, unless dissolution and recrystallization occurs (O'Neil, 1987). $\delta^{18}\text{O}_{\text{water}}$ values of Mississippian meteoric water around -2‰ (McIntosh *et al.*, 2002) and accessory data compiled by Strapoc *et al.* (2007) show a significant shift in $\delta^{18}\text{O}_{\text{water}}$ of Indiana coal waters that most likely resulted from dilution of the original basinal brines due to hydrologic connectivity with meteoric water in “recent time.” The low chlorinity observed in coalbed waters also support hydrologic connectivity (McIntosh *et al.*, 2002; McIntosh and Walter, 2005). Because isotopic data of meteoric waters from the Mississippian were isotopically similar to seawater, our assumption that isotopic exchange was negligible during the time of kaolinite and calcite mineralization allows us to use different scenarios of paleo-formation waters to decipher the timing of occurrence of these diagenetic minerals in our coals.

6.4.3.3. Mineralization scenario C: intermediate temperature and $\delta^{18}\text{O}_{\text{water}} \sim +3\text{‰}$

Scenario C is based on successive formation of kaolinite and calcite in contact with water that is derived from mixing of ^{18}O -enriched basinal brine with ^{18}O -depleted tropical meteoric or ocean water yielding a bulk $\delta^{18}\text{O}_{\text{water}}$ value of $\sim +3\text{‰}$. The calculated mean kaolinite precipitation temperature of $111.8 \pm 6.3^\circ\text{C}$ (range from 100.1 to 130.6°C ; $n=54$; Table 4) is in close agreement with homogenization temperatures of 71 to 113°C determined from fluid inclusions in sphalerite-filling cleats from several locations in the Illinois Basin (Rowan *et al.*, 2002). Ambers (1993) concluded that a temperature correction of $\sim 40^\circ\text{C}$ was needed to account for minimum trapping temperatures of fluid inclusions with sodium chloride concentrations of 10-20 weight %. He used an estimated minimum pressure during sphalerite growth and fluid inclusion entrapment of $\sim 25\text{ MPa}$

(corresponding to a burial depth of approximately 2.8 km). However, we adopted Rowan *et al.*'s (2002) suggestion that 2.8 km of burial are not necessary to explain the observed trend in vitrinite reflectance throughout the basin. Instead, our calculated corrections suggest adding ~20°C at most, which would account for kaolinite formation temperatures of ~130°C, similar to ~134 to ~138°C reported by Ambers (1993).

The considerations of scenario C suggest that the formation of kaolinite occurred long after mixing of basinal brines with more ¹⁸O-depleted waters and long after the basin attained its maximum burial. Cleats must have been passable for kaolinite-mineralizing fluids, before any cleat annealing and before the development of secondary cleats that were subsequently filled with calcite. Based on a quantitative study of cleats in coal, Solano-Acosta *et al.* (in press) noted that annealing also occurred at early stages of coal maturation in Indiana coals. Although Indiana coals did not reach the optimum degree of maturation for maximum cleat development, early annealing of cleats would have inhibited cleat mineralization. Therefore, it is hypothesized that kaolinite mineralization took place relatively early after cleat formation, but before annealing took place. The calculated mean paleotemperature of calcite formation of $68.8 \pm 7.4^{\circ}\text{C}$ (range from 53.6 to 81.6°C; n=38; Table 5) is consistent with Ambers (1993) suggestion that calcite in coal formed at >70°C.

6.4.3.4. Mineralization scenario D: high temperature and $\delta^{18}\text{O}_{\text{water}} \sim +7.5\text{‰}$

Scenario D follows Ambers's (1993) suggestion that an ¹⁸O-enriched undiluted deep basinal brine with $\delta^{18}\text{O}_{\text{water}} \sim 7.5\text{‰}$ was present during the time of kaolinite formation. The calculated mean temperature for kaolinite crystallization of $164 \pm 9.9^{\circ}\text{C}$ (range 146.2

to 205.5°C; n=54; Table 4) represents the upper limit of our estimates for kaolinite crystallization. In the case of calcite, the calculated mean paleotemperature is $100.8 \pm 8.9^\circ\text{C}$ (range 82.6 to 116.1°C; n=38; Table 5).

Ambers (1993) observed cogenetic sphalerite and supported his findings with petrographic evidence and measurements on fluid inclusions in sphalerite. This author concluded that during the time of maximum burial the geothermal gradient must have increased to 43.9°C/km and that effective heating of the coals lasted between ~0.5 and 3 million years.

The calculated high mean kaolinite mineralization temperatures of $164 \pm 9.9^\circ\text{C}$ (n=54) for scenario D can only be explained if mineralization occurred within the Fluorspar district where reported fluid inclusion temperatures are ~175°C (Rowan *et al.*, 2002). However, there is no evidence in our sampling area that such high temperatures have ever occurred (*e.g.*, consistent low vitrinite reflectance values and no evidence of the loss of fluorescent properties of liptinite macerals).

6.4.4. Implications for coalbed methane occurrence

The presence of minerals in coal cleats may have great significance for methane generation and extraction from coal beds because (i) mineral fillings affect fluid flow and permeability, and (ii) the isotopic composition of authigenic calcite is diagnostic for the onset of microbial methanogenesis relative to calcite mineralization.

Calcites in coal cleats in the Black Warrior Basin in Alabama feature strong ^{13}C -enrichment (Pitman *et al.*, 2003) because microbes partially utilized the carbon dioxide pool for microbial methanogenic CO_2 -reduction before or during the time of calcite

formation. Preferential utilization of $^{12}\text{CO}_2$ caused ^{13}C -enrichment in residual CO_2 and in precipitating calcite (Figure 7). Coalbed gas CO_2 in our study area in the Illinois Basin also features strong ^{13}C -enrichment (Table 1) in the presence of microbial CO_2 reduction (Strapoć *et al.*, 2007). However, the available Illinois Basin $\delta^{13}\text{C}_{\text{calcite}}$ values are not in thermodynamic equilibrium with modern coalbed CO_2 (Figure 6). For comparison, Figure 7 contrasts the distribution of $\delta^{13}\text{C}_{\text{calcite}}$ versus $\delta^{18}\text{O}_{\text{calcite}}$ values from Indiana coals from the Illinois Basin against values from coals from the Black Warrior Basin (Pitman *et al.*, 2003). Although calcite mineralization in cleats of Indiana coal beds developed relatively late after mineralization of kaolinite, the $\delta^{13}\text{C}_{\text{calcite}}$ values give no evidence for microbial methanogenesis via CO_2 -reduction during the time of calcite mineralization. This suggests that the previously heat-sterilized sedimentary environment had not yet been inoculated with methanogenic microbial consortia and that microbial methanogenesis may be a relatively recent development, as already suggested by Strapoć *et al.* (2007).

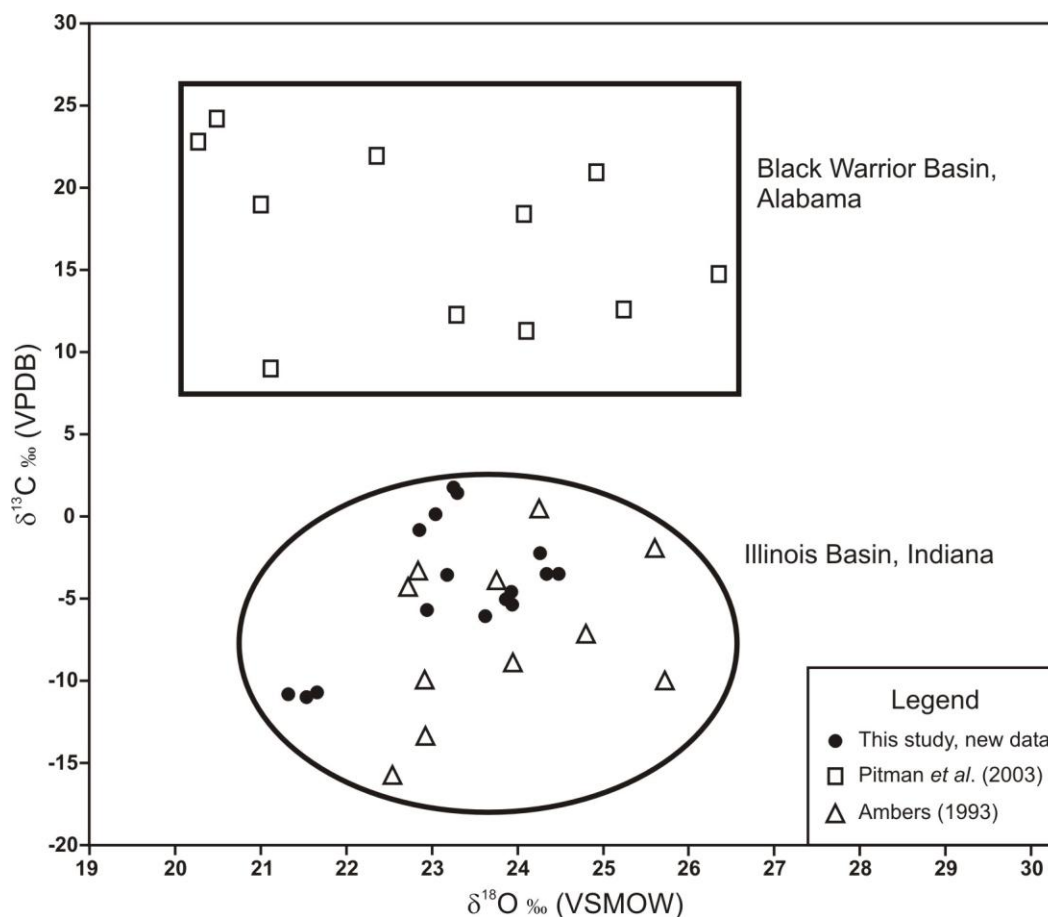


Figure 7. Distribution of $\delta^{13}\text{C}_{\text{calcite}}$ vs. $\delta^{18}\text{O}_{\text{calcite}}$ values from calcites recovered from coal cleats. Data from the Indiana section of the Illinois Basin (\bullet new data from this study; Δ Ambers, 1993) are distinctly different from the Black Warrior Basin, Alabama, where calcites reflect ^{13}C -enrichment of residual carbon dioxide as a result of preferential utilization of $^{12}\text{CO}_2$ during microbial methanogenesis via CO_2 -reduction (\square Pitman *et al.*, 2003).

Inoculation with CO₂-reducing methanogens must have occurred when microbes were migrating with fluids from cooler strata above the coal seams. Prior discontinuous mineralization along cleats may have preserved the cleat framework, kept pathways open for fluid migration, and thus facilitated access of methanogenic bacteria into coals. On the other hand, pervasive and continuous cleat mineralization is suited to inhibit the migration of fluids, including that of coalbed gases. In the case of Indiana coals, it is possible that the observed differences in gas content along various seams (Solano-Acosta *et al.*, 2005) partly result from anisotropic distribution of diagenetic minerals in cleats and limited distribution of microbes for biogenic gas generation. This hypothesis, however, requires further studies.

From the point of view of CBM production, cleat-filling minerals reduce the permeability of coal and inhibit gas extraction. They may also provide a large degree of anisotropy for gas migration in some areas, limiting the feasibility of economic extraction of CBM. For example, calcite cementation along cleats in the Black Warrior Basin in the vicinity of normal faults contributes to reservoir heterogeneity by effectively sealing the faults (Pashin and Groshong, 1998; Pitman *et al.*, 2003).

6.5. Conclusions

- Our new $\delta^{18}\text{O}_{\text{kaolinite}}$, $\delta^{18}\text{O}_{\text{calcite}}$ and $\delta^{13}\text{C}_{\text{calcite}}$ values from Indiana coal cleats are quantitatively compatible with earlier data sets from Ambers (1993) and Shieh and Suter (1979) from our study region.
- Authigenic mineralization along coal cleats not only prevents cleats from annealing, but offers diagnostic information about paleohydrologic conditions. $\delta^{18}\text{O}_{\text{calcite}}$ and $\delta^{18}\text{O}_{\text{kaolinite}}$ values constrain the time of emplacement and paleotemperatures, and assess the circumstances of mineralization and the relationship to cleat formation.
- Oxygen-stable isotope ratios of two or more authigenic minerals can be used to test the hypothesis that mineralization of different minerals occurred simultaneously from the same fluid at the same temperature. Large and systematic differences between our measured $\delta^{18}\text{O}_{\text{kaolinite}}$ and $\delta^{18}\text{O}_{\text{calcite}}$ values provide unambiguous evidence that these two mineral phases must have grown at different temperatures and/or from different fluids.
- Isotopic evidence and the thermal and tectonic history of the Illinois Basin suggest that initial precipitation of kaolinite in cleats occurred shortly after deep emplacement of igneous intrusives that promoted advective heat redistribution in the basin at $\sim 78 \pm 5^\circ\text{C}$ and a burial depth of < 1600 m. Following uplift and cooling, calcite precipitated possibly during a post-Paleozoic secondary cleat system that developed as continental collision changed the stress regime of the coals. Estimated temperatures of calcite mineralization are $\sim 43 \pm 6^\circ\text{C}$ at burial

depths between ~500 to ~1300 m. During mineralization, the available paleowater in coal beds was likely ocean water and/or tropical meteoric water, similar in isotopic composition to Mississippian age ocean water, with a $\delta^{18}\text{O}_{\text{water}} \sim -1.25\text{‰}$ vs. VSMOW.

- The isotopic composition of authigenic calcite constrains the onset of microbial methanogenesis via CO_2 reduction. Relatively negative $\delta^{18}\text{O}_{\text{calcite}}$ values indicate that calcites in Indiana coal cleats crystallized at a time when carbon dioxide in coal beds was far more ^{13}C -depleted than it is today. Apparently microbial fractionation of carbon dioxide via CO_2 -reductive methanogenesis did not occur at the time of calcite crystallization, possibly owing to prior sterilization of coal during deep burial and heating. This suggests that inoculation of uplifted coals with methanogenic microbial consortia and the onset of microbial methanogenesis were relatively late events.

Acknowledgments

Support for this project was partially provided by Indiana Geological Survey's *John Patton Award* to W.S.-A., and by the U.S. Department of Energy, Basic Energy Research Grant number DEFG02-00ER15032 awarded to A.S. and M.M. We thank P. Ames (Black Beauty Coal Co.) and M. Atkinson (Solar Sources, Inc.) for providing access to mines, T. Hite for providing a core sample from a CBM drilling site, A. Sarkar for analytical help with oxygen isotopes in kaolinite, and D. Strapóć, A. Drobniak, and G. Lis for field assistance.

References

- Ambers, C.P., 1993. The nature and origin of very well crystallized kaolinite. Indiana University, Bloomington, IN. Ph.D. dissertation, 493 pp.
- Anderson, T.F., Brownlee, M.E., Phillips, T.L., 1980. A stable isotope study on the origin of permineralized peat zones in the Herrin coal. *Journal of Geology* 88, 713-722.
- Botinga, Y., 1968. Calculation of fractionation factors for carbon and oxygen isotopic exchange in the system calcite-carbon dioxide- water. *Journal of Physical Chemistry* 72, 800-808.
- Bradley, H.B., 1987. *Petroleum Engineering Handbook*. The Society of Petroleum Engineers, third ed. Richardson, Texas.
- Budai, J.M., Martini, A.M., Walter, L.M., Ku, T.C.W., 2002. Fracture-fill calcite as a record of microbial methanogenesis and fluid migration: a case study from the Devonian Antrim Shale, Michigan Basin. *Geofluids* 2, 163-183.
- Chacko, T., Mayeda, T.K., Clayton, R.N., Goldsmith, J.R., 1991. Oxygen and carbon isotope fractionations between CO₂ and calcite. *Geochimica et Cosmochimica Acta* 55, 2867-2882.
- Clayton, R.N., Mayeda, T.K., 1963. The use of bromine pentafluoride in the extraction of oxygen from oxides and silicates for isotopic analysis. *Geochimica et Cosmochimica Acta* 22, 43-53.
- Clayton, R.N., Goldsmith, J.R., Karel, K.J., Mayeda, T.K., Newton, R.C., 1975. Limits on the effect of pressure on isotopic fractionation. *Geochimica et Cosmochimica Acta* 39, 1197-1201.

- Cobb, J.C., 1981. Geology and geochemistry of sphalerite in coal. University of Illinois, Urbana, IL. Ph.D. dissertation, 204 pp.
- Collinson, C., Sargent, M.L., Jennings, J.R., 1988. Illinois Basin Region, Chapter 14: The Geology of North America, Sedimentary Cover – North American Craton: U.S. Geological Society of America D-2, 383-426.
- Coplen, T.B., 1996. New guidelines for reporting stable hydrogen, carbon, and oxygen isotope-ratio data. *Geochimica et Cosmochimica Acta* 60, 3359-3360.
- Coplen, T.B., Kendall, C., Hopple, J., 1983. Comparison of stable isotope reference samples. *Nature* 302, 236-238.
- Coveney, R.M., Goebel, E.D., Ragan, V.M., 1987. Pressures and temperatures from aqueous fluid inclusions in sphalerite from midcontinent country rocks. *Economic Geology* 82, 740-751.
- Criss, R.E., 1999. Principles of Stable Isotope Distribution. Oxford University Press, New York.
- Daniels, E.J., Altaner, S.P., 1990. Clay mineral authigenesis in coal and shale from the anthracite region, Pennsylvania. *American Mineralogist* 75, 825-839.
- Daniels, E.J., Marshak, S., Altaner, S.P., 1996. Use of clay-mineral alteration patterns to define syntectonic permeability of joints (cleat) in Pennsylvania anthracite coal. *Tectonophysics* 263, 123-136.
- Deines, P., Langmuir, D., Harmon, R., 1974. Stable carbon isotope ratios and the existence of a gas phase in the evolution of carbonate ground waters. *Geochimica et Cosmochimica Acta* 38, 1147-1164.

- Drobniak, A., Mastalerz, M., Rupp, J., Eaton, N., 2004. Evaluation of coalbed gas potential of the Seelyville Coal Member, Indiana, USA. *International Journal of Coal Geology* 57, 265-282.
- Emrich, K., Ehhalt, D.H., Vogel, J.C., 1970. Carbon isotope fractionation during the precipitation of calcium carbonate. *Earth and Planetary Science Letters* 8, 363-371.
- Engelder, T., Whitaker, A., 2006. Early jointing in coal and black shale: Evidence for an Appalachian-wide stress field as a prelude to the Alleghenian orogeny. *Geology* 34, 581-584.
- Halas, S., Szaran, J., Niezgoda, H., 1997. Experimental determination of carbon isotope equilibrium fractionation between dissolved carbonate and carbon dioxide. *Geochimica et Cosmochimica Acta* 61, 2691-2695.
- Hatch, J.R., Gluskoter, H.J., Lindahl, P.C., 1976. Sphalerite in coals of the Illinois Basin. *Economic Geology* 71, 613-624.
- Kaegi, D.D., 1976. A coal rank profile of southeastern Illinois as determined by vitrinite reflectance. M.S. Thesis. Southern Illinois University. Carbondale, Illinois, 98p.
- Kim, S.T., O'Neil, J.R., 1997. Equilibrium and nonequilibrium oxygen isotope effects in synthetic carbonates. *Geochimica et Cosmochimica Acta* 61, 3461-3475.
- Kulla, J.B., Anderson, T.F., 1978. Experimental oxygen isotope fractionation between kaolinite and water. U.S. Geological Survey, Open File Report 78-101, 234-235.
- Lesniak, P.M., Sakai, H., 1989. Carbon isotope fractionation between dissolved carbonate ($\text{CO}_3^{=}$) and $\text{CO}_2(\text{g})$ at 25°C and 40°C. *Earth and Planetary Science Letters* 95, 297-301.

- McIntosh, J.C., Walter, L.M., Martini, A.M., 2002. Pleistocene recharge to midcontinent basins: Effects on salinity structure and microbial gas generation. *Geochimica et Cosmochimica Acta* 66, 1681-1700.
- McIntosh, J.C., Walter, L.M., 2005. Volumetrically significant recharge of Pleistocene glacial meltwaters into epicratonic basins: constraints imposed by solute mass balances. *Chemical Geology* 222, 292-309.
- O'Neil, J.R., Clayton, R.N., Mayeda, T., 1969. Oxygen isotope fractionation in divalent metal carbonates. *Journal of Chemistry and Physics* 51, 5447-5558.
- O'Neil, J.R., 1987. Preservation of H, C, and O isotopic ratios in the low temperature environment. In: Kyser, T.K. (Ed.), *Stable Isotope Geochemistry of Low Temperature Processes*. Mineralogical Association of Canada, Short course handbook, v. 13, Saskatoon, Saskatchewan, p. 85-128.
- Pashin, J.C., Groshong, R.H., 1998. Structural control of coalbed methane production in Alabama. *International Journal of Coal Geology* 38, 89-113.
- Pitman, J.K., Pashin, J.C., Hatch, J.R., Goldhaber, M.B., 2003. Origin of minerals in joint and cleat systems of the Pottsville Formation, Black Warrior basin, Alabama: Implications for coalbed methane generation and production. *American Association of Petroleum Geologists, Bulletin* 87, 713-731.
- Price, F.T., Shieh, Y.N., 1979. The distribution and isotopic composition of sulfur in coals from the Illinois Basin. *Economic Geology* 74, 1445-1461.
- Puc  at, E., L  cuyer, C., Donnadieu, Y., Naveau, P., Cappetta, H., Ramstein, G., Huber, B.T., Kriwet, J., 2007. Fish tooth $\delta^{18}\text{O}$ revising Late Cretaceous meridional upper ocean temperature gradients. *Geology* 35, 107-110.

- Rowan, E.L., Goldhaber, M.B., Hatch, J.R., 2002. Regional fluid flow as a factor in the thermal history of the Illinois basin: Constraints from fluid inclusions and the maturity of Pennsylvanian coals. *American Association of Petroleum Geologists, Bulletin* 86, 257-277.
- Shackleton, N.J., Kennett, J.P., 1975. Paleotemperature history of the Cenozoic and the initiation of Antarctic glaciations; oxygen and carbon isotope analyses in DSDP sites 277, 279, and 281. *Initial reports of the Deep Sea Drilling Project* 29, 743-755.
- Shieh, Y.N., Suter, T.G., 1979. Formation conditions of authigenic kaolinite and calcite in coals by stable isotope determinations. *Clay Mineralogy* 27, 154-156.
- Solano-Acosta, W., Mastalerz, M., Rupp, J.A., Strapóć, D., Schimmelmann, A., 2005. Coal-bed gas potential in Pennsylvanian coal beds of Indiana: Proceedings of the 2005 International Coalbed Methane Symposium, Univ. Alabama, Tuscaloosa, AL. Paper 0526.
- Solano-Acosta, W., Mastalerz, M., Schimmelmann, A., in press. Cleats and their relation to geologic lineaments, and coalbed methane potential in Pennsylvanian coals in Indiana. *International Journal of Coal Geology*, doi:10.1016/j.coal.2007.02.004
- Spears, D.A., Caswell, S.A., 1986. Mineral matter in coals: cleat minerals and their origin in some coals from the English midlands. *International Journal of Coal Geology* 6, 107-125.
- Strapóć, D., Mastalerz, M., Eble, C., Schimmelmann, A., 2007. Characterization of the origin of coalbed gases in southeastern Illinois Basin by compound-specific carbon and hydrogen stable isotope ratios. *Organic Geochemistry* 38, 267-287.

- Swart, P.K., Burns, S.J. Leder, J.J., 1991. Fractionation of the stable isotopes of oxygen and carbon dioxide during the reaction of calcite with phosphoric acid as a function of temperature and technique. *Chemical Geology* 86, 89-96.
- Taylor, H.P., Jr., 1974. The application of oxygen and hydrogen isotope studies to problems of hydrothermal alteration and ore deposition. *Economic Geology* 69, 843-883.
- Turner, J.V., 1982. Kinetic fractionation of carbon-13 during calcium carbonate precipitation. *Geochimica et Cosmochimica Acta* 46, 1183-1191.
- Valley, J.W., Cole, D.R., (Eds.), 2001. Stable isotope geochemistry. *Reviews in mineralogy and geochemistry* 43. The Mineralogical Society of America, Washington, D.C.
- Whelan, J.F., Cobb, J.C., Rye, R.O., 1988. Stable isotope geochemistry of sphalerite and other mineral matter in coal beds of the Illinois and Forest City Basins. *Economic Geology* 83, 990-1007.
- Zheng, Y.F., 1993. Calculation of oxygen isotope fractionation in hydroxyl-bearing silicates. *Earth and Planetary Science Letters* 120, 247-263.
- Zimmermann, R.A., 1986. Fission-track dating of samples of the Illinois basin drill-hole core: Shorter contributions to isotope research. U.S. Geological Survey, *Bulletin* 1622, 99-108.

CHAPTER 7

**Effects of coal storage in air on physical and chemical coal properties and on gas
adsorption at low pressure**

7.1. Introduction

Preservation and maturation of organic matter in coal seams occurs under anoxic conditions. The resulting organic geochemicals are in part chemically unstable in the presence of elemental oxygen. Storage of coal in oxidizing air can modify coal's physical and chemical properties due to oxidation and chemical weathering. The effects of low-temperature oxidation are significant for metallurgical coke production because by changing the elemental ratio of carbon to oxygen, fluidity, and other properties, they affect coke strength and reactivity (Crelling *et al.*, 1979; Gray *et al.*, 1976; Lowenhaupt and Gray, 1980; Marchioni, 1983; Rhoads *et al.*, 1983). Gray *et al.*, 1976 observed a slight decrease in calorific value, but no major changes in the coal's microscopic appearance as a result of oxidation. According to Marchioni (1983), weathering causes an increase in oxygen and volatile matter content, as well as a decrease in carbon content and calorific value. However, this author suggests that rheological properties of coal are more sensitive to weathering than chemical parameters derived from proximate and ultimate analyses.

Gentzis *et al.* (1992) distinguish between two modes of oxidation in coal. First, weathering (i.e., chemical weathering) encompasses slow oxidation of coal at temperatures below 30°C that may proceed over long time. Second, oxidation at >70°C results in rapid chemical changes over relatively short periods of time. Wu *et al.* (1988), on the other hand, defined coal weathering in terms of progressive changes in coal when exposed to temperatures below 80°C in humid air.

Coal oxidation studies have been conducted to understand and better predict self-heating and spontaneous combustion (Kaji *et al.*, 1983; Taraba *et al.*, 1988). Numerous studies have investigated the effects of low- and high-temperature oxidation of coal in the laboratory when applying various techniques to describe resulting changes in coal chemistry (Anderson and Johns, 1986; Calemme *et al.*, 1988; Fredericks *et al.*, 1983; Gentzis *et al.*, 1992; Jakab *et al.*, 1988; Kister *et al.*, 1988; Landais *et al.*, 1984; Landais and Rochdi, 1993; Mitchell *et al.*, 2005; Painter *et al.*, 1980, 1981; Pisupati and Scaroni, 1993; Pradier *et al.*, 1992; Rhoads *et al.*, 1983; Solomon and Carangelo, 1988; Wu *et al.*, 1988). These included changes in physical properties such as coal plasticity (Huffman *et al.*, 1985; Huggins *et al.*, 1987; Liotta *et al.*, 1983; Pis *et al.*, 1996), pore structure (Kaji *et al.*, 1985; Kaji *et al.*, 1986; Pis *et al.*, 1996), and vitrinite reflectance R_o (Bend and Kosloski, 1993; Calemme *et al.*, 1995; Chandra, 1962; Mastalerz and Bustin, 1993). It has also been demonstrated that oxidation of coal diminishes coking, caking capacity and calorific value (Cagigas *et al.*, 1987; Calemme *et al.*, 1988; Landais and Rochdi, 1993; Martínez and Escobar, 1995; Painter *et al.*, 1980).

Understanding the effects of oxidation on adsorptive characteristics during storage in air is critical for estimating gas saturation capacity in coal. Changes in the abundance of chemical functional groups during oxidation promote chemical structural changes that are expected to affect surface area and pore-size distribution. Ludvig *et al.* (1983) used high-temperature oxidation experiments to assess changes in surface area of coals of different rank. Samples were heated at a rate of 10°C/min until 400°C and maintained at 400°C for 4 hours. An intermittent increase in surface areas immediately after the experiments was followed by a reduction in surface areas after storage for up to 278 days in air at room

temperature. Ludvig *et al.* (1983) interpreted the observed reduction in surface area as being possibly the result of exposure to oxygen, water vapor, or other atmospheric gases and suggested that coal's pore structure changes with storage time.

Surface area and pore-size distribution are important controls of gas adsorption in coal (Busch *et al.*, 2004; Clarkson and Bustin, 1996). Low-pressure gas adsorption experiments allow estimating these two parameters and, therefore, making inferences about the expected changes in coal properties through time of air exposure. Low-pressure experiments with nitrogen provide information about the influence of mesopores (diameter 2 – 50 nm) on surface area, adsorbed gas volumes, and average mesopore width. Nitrogen is unable to enter micropores (<2 nm), but low-pressure adsorption experiments with carbon dioxide offer information about the microporous structure of coals including the saturation capacity of the monomolecular layer (monolayer capacity), the total surface area of coal, and the average size of micropores (Clarkson and Bustin, 1996; Webb and Orr, 1997).

Chemical effects of oxidation in coal appear to be related to the coal's moisture content. Schafer (1972) demonstrated relationships between equilibrium moisture content in coal and the carboxyl and hydroxyl contents. He concluded that the moisture content in low rank coals is more related to the abundance of carboxyl groups than to phenolic hydroxyl groups. It has been observed that oxidation increases the carboxyl group abundance (Liotta *et al.*, 1983). Kaji *et al.* (1986) studied the role of meso- and macropore structure and oxygen content in coals to elucidate factors controlling water-holding capacity. They observed a positive correlation between the abundances of oxygen-containing functional groups and hydrophilic sites in coal.

Understanding the extent of coal oxidation is critical to decipher the gas adsorption potential in coal, since water competes with gas for sorption sites. McCutcheon and Wilson (2003) investigated the influence of moisture on low-temperature oxidation of bituminous coals and identified two types of water associated with the coals, namely chemically bound absorbed water and physically adsorbed free water. They concluded from photo-electron spectroscopy that an increase in the abundance of C=O functional groups in coal that was oxidized in humid air occurred only after additional wetting. Their experimental study also revealed that water uptake was reduced following oxidation with dry oxygen, whereas water uptake remained constant following oxidation with humid air. A sample treated with hydrogen peroxide indicated a reduction in water uptake. McCutcheon and Wilson (2003) treated coal with aqueous hydrogen peroxide and concluded that adsorbed oxygen at the surface of coal blocked water access to pores during oxidation. They also suggested that atmospheric water vapor cannot become adsorbed on oxidized sites, unless liquid surface water is already present.

Monitoring of changes in chemical and physical properties of coal during storage under controlled laboratory conditions at low temperature, together with the evaluation of moisture loss in coals, is expected to improve our understanding of the gas adsorption capacity and coals' potential use for the sequestration and geologic storage of greenhouse gases such as CO₂. This work aims to investigate (1) chemical and petrographic changes in coal due to moisture availability and oxidation in air at ambient pressure and temperature over storage time, (2) changes in surface area and pore structure of coal due to changes in oxidation, moisture, and storage time, (3) the effects of oxidation and moisture on adsorption of N₂ and CO₂ through time and at elevated temperature up to

100°C, (4) changes in the abundance of selected chemical functional groups with increasing oxidation due to storage in air at room temperature and in comparison with the changes resulting from storage at elevated temperatures up to 75°C, and (5) possible implications for future CO₂ sequestration opportunities and the targeted reduction of anthropogenic greenhouse gas emissions to the atmosphere.

7.2. Methods

A large (~0.5 m³) sample of the Lower Block Coal Member from Billings Mine (Daviess County, Indiana) was collected and immediately transported to the laboratory at the Indiana Geological Survey in Bloomington, Indiana (USA). The sample was promptly crushed to particles to sizes smaller than 2 mm in diameter and stirred to produce a relatively homogeneous sample. A large aliquot of the coal was stored under nitrogen in a desorption canister. Fresh sample aliquots were used for chemical (proximate and ultimate) analyses, standard petrographic analysis, surface area and microporosimetry from low-pressure adsorption experiments, and functional group identification via Fourier Transform Infrared (FTIR) spectroscopy.

7.2.1. Sample preparation

A split of the coal sample was stored anoxically in a sealed desorption canister (Mavor and Nelson, 1997) under nitrogen to prevent oxidation with air. Several aliquots of ~2 cm³ were flame-sealed in glass ampoules under argon and kept refrigerated in the dark to minimize chemical changes. Other coal aliquots were split into various glass jars

that were left open to air in a dark room and were only covered with a thin layer of porous paper towels to prevent the settling of dust onto coal. Periodically, small aliquots of the exposed coal samples were sealed in glass ampoules under argon to stop chemical changes and were sent to the University of Kentucky for FTIR measurements. At the same time, larger splits were sent to a commercial laboratory for chemical (proximate and ultimate) analyses. Oxidation of these samples continued during 2 to 3 days of transport but subsequent analyses were performed promptly by the commercial laboratory.

Internal laboratory standards for quantification of coal oxidation were prepared from coal aliquots with distinct air exposure histories and from freshly mined coal with minimized contact with air (“zero exposure coal”). Coal aliquots were filled into glass ampoules and air was replaced by purging with argon gas for several minutes, followed by sealing with a torch. These sealed glass ampoules were refrigerated and kept in the dark to prevent further alteration. Multiple sealed ampoules with these standard coals were prepared as reference for future analyses. Splits of each exposed coal and the “zero exposure coal” were sent for FTIR analysis.

7.2.2. Proximate and ultimate coal chemical analyses

Splits of approximately 150 to 200 grams of coal samples exposed to oxidizing air in the laboratory were sealed in plastic containers and sent to Standard Laboratories, Inc. in Evansville via Express Mail for proximate and ultimate analyses. Proximate analyses included determination of moisture, mineral matter (ash), fixed carbon (i.e., all organic and inorganic carbon present in the analyzed coal, from which desorbed gases had been typically lost before analysis), and total sulfur contents, as well as the calorific value. The

elemental composition from ultimate analysis is determined by burning of an aliquot of coal in a combustion tube in a stream of oxygen. Carbon, hydrogen, and sulfur are oxidized and determined directly as oxides, whereas nitrogen is detected as N₂ and coal oxygen is determined by difference using the equation

$$\text{O}\% = 100 - (\text{C}\% + \text{H}\% + \text{S}\% + \text{N}\%) \text{ according to Kabe } et al. (2004).$$

Data from proximate and ultimate analyses were collected according to standard procedures (ASTM, 2006) and are presented in Table 1.

7.2.3. Petrographic analyses

Standard petrographic maceral and vitrinite reflectance analyses were performed on coal samples at all stages of the oxidation experiments to quantify changes with increasing exposure. Coal composition was determined by point counting (500 points) under reflected light on a Zeiss photoscope II. Random vitrinite reflectance (R_o) measurements were collected in 25 fragments of each coal sample. The reported R_o values represent averages of all 25 measurements.

7.2.4. Surface area and pore size distribution

Low-pressure gas adsorption measurements were conducted on a Micromeritics ASAP-2020 porosimeter and surface area analyzer (Figure 1). Coal samples weighing 1 to 2 grams were analyzed separately with nitrogen and carbon dioxide gases to obtain information about the mesopore (2 – 50 nm, accessible to both gases) and micropore characteristics (<2 nm, accessible only to carbon dioxide). Before analysis with either N₂

or CO₂, the samples were automatically degassed by heating at ~110°C in vacuum for about 14 hours to remove adsorbed moisture and atmospheric gases.

For quantification of nitrogen gas adsorption in coal, the temperature of the sample is reduced to the temperature of liquid nitrogen and incremental doses of nitrogen gas are admitted automatically by the computer-controlled instrument. For CO₂ adsorption, the temperature of the sample is reduced to 0°C and incremental doses of CO₂ gas are admitted to the sample. Because CO₂ can access both meso- and micropores, the adsorption data collected by the instrument are automatically corrected to account for the difference in gas accessibility.

The instrument's computer software automatically generates adsorption isotherms and allows estimating surface areas, pore volumes and pore distributions based on multiple adsorption theories, i.e. Langmuir, BET (Brunauer,-Emmett-Teller), BJH (Barrett-Joyner-Halenda), Dubinin-Radushkevich (D-R), and Dubinin-Astakhov (D-A), among others (Clarkson and Bustin, 1996; Webb and Orr, 1997). A brief description of the underlying equations and related terminology is as follows:

Adsorption: a physical process that corresponds to the uptake of gas by pore-filling or capillary condensation.

Absorption: refers to the chemical incorporation of gas molecules into the solid phase.

Adsorptive: any gas capable of being adsorbed.

Adsorbate: the material that is physically or chemically adsorbed to the surface of a solid phase.

Adsorbent: material upon which surface adsorption occurs.

The following parameters are used in the equations: P: equilibrium pressure; P_0 : saturation vapor pressure of adsorbate at temperature T; P/P_0 : relative pressure; V_0 : micropore capacity; V: volume adsorbed at equilibrium pressure; V_m : monolayer volume; V_L : molar volume of liquid adsorptive; B: structural constant related to the pore size distribution of the adsorbent; this parameter is expressed in energy units and corresponds to a Gaussian distribution of differential molar work of adsorption, which according to D-R theory is proportional to the pore size distribution; C: BET constant, related to the heat of adsorption; r_{pn} : radius of the largest pore filled at a given pressure; L(r): length of pores with radii between r and (r + dr); r_m : mean radius of curvature of meniscus between liquid adsorptive and its vapor; t: multilayer thickness at equilibrium pressure; R: molar gas constant; T: analysis bath temperature (K); γ : surface tension of the liquid adsorptive; β : affinity coefficient of the adsorbate; n: Astakhov exponent (usually ranging from 1 to 3); E_0 : characteristic energy describing the pore structure of the adsorbent.

The Langmuir equation is used to calculate adsorbed monolayer volumes.

$$\frac{P/P_0}{V} = \frac{1}{BV_m} + \frac{P/P_0}{V_m}$$

The BET (Brunnauer, Emmett, and Teller) equation is used to estimate mesopore surface areas. Linear BET plots are typically obtained between 0.05 and 0.35 relative pressure. In some instances this equation has been used to determine micropore surface areas, but with greater uncertainty at <0.30 relative pressure.

$$\frac{P}{V(P_0 - P)} = \frac{1}{CV_m} + \frac{C - 1}{V_m} \left(\frac{P}{P_0} \right)$$

The BJH (Barrett, Joyner, and Halenda) equation is used to calculate mesopore surface areas and pore-volume distributions of adsorbents with a hysteresis loop described by Type IV isotherms (Sing *et al.*, 1985). This equation is used in combination with the Kelvin equation to determine the radius of a cylindrically shaped pore core where capillary condensation occurs at a given relative pressure.

$$V_0 - V = \pi \int_{r_p}^{\infty} \int (r - t)^2 L(r) dr$$

The Kelvin equation states that at equilibrium pressures lower than the saturation pressure, the vapor may be in equilibrium with the condensed liquid adsorbate, depending on the radius of curvature of the meniscus. This equation was derived to account for the physical en chemical equilibrium established between a liquid and its vapor across a meniscus at a defined relative pressure. The Kelvin equation provides the radius of the core of a pore in which capillary condensation occurs at a given relative pressure P/P_0 .

$$\ln \frac{P}{P_0} = \frac{-2\gamma V_L}{RT r_m}$$

The D-R (Dubinin-Radushkevich) equation is used to obtain micropore capacity and surface areas for data collected at 0°C (273.15 K). This equation is thought to have a range of validity at relative pressures between 10^{-5} and 0.1. Therefore, the use of CO₂ seems adequate because adsorption data fall well within this range.

$$\log V = \log V_0 - \frac{BT^2}{\beta^2} \left[\log \frac{P_0}{P} \right]^2$$

The D-A (Dubinin-Astakhov) equation is a generalized version of the D-R equation used to obtain pore size distribution data.

$$\log V = \log V_0 - \left[\frac{RT}{\beta E_0} \log \frac{P_0}{P} \right]^n$$

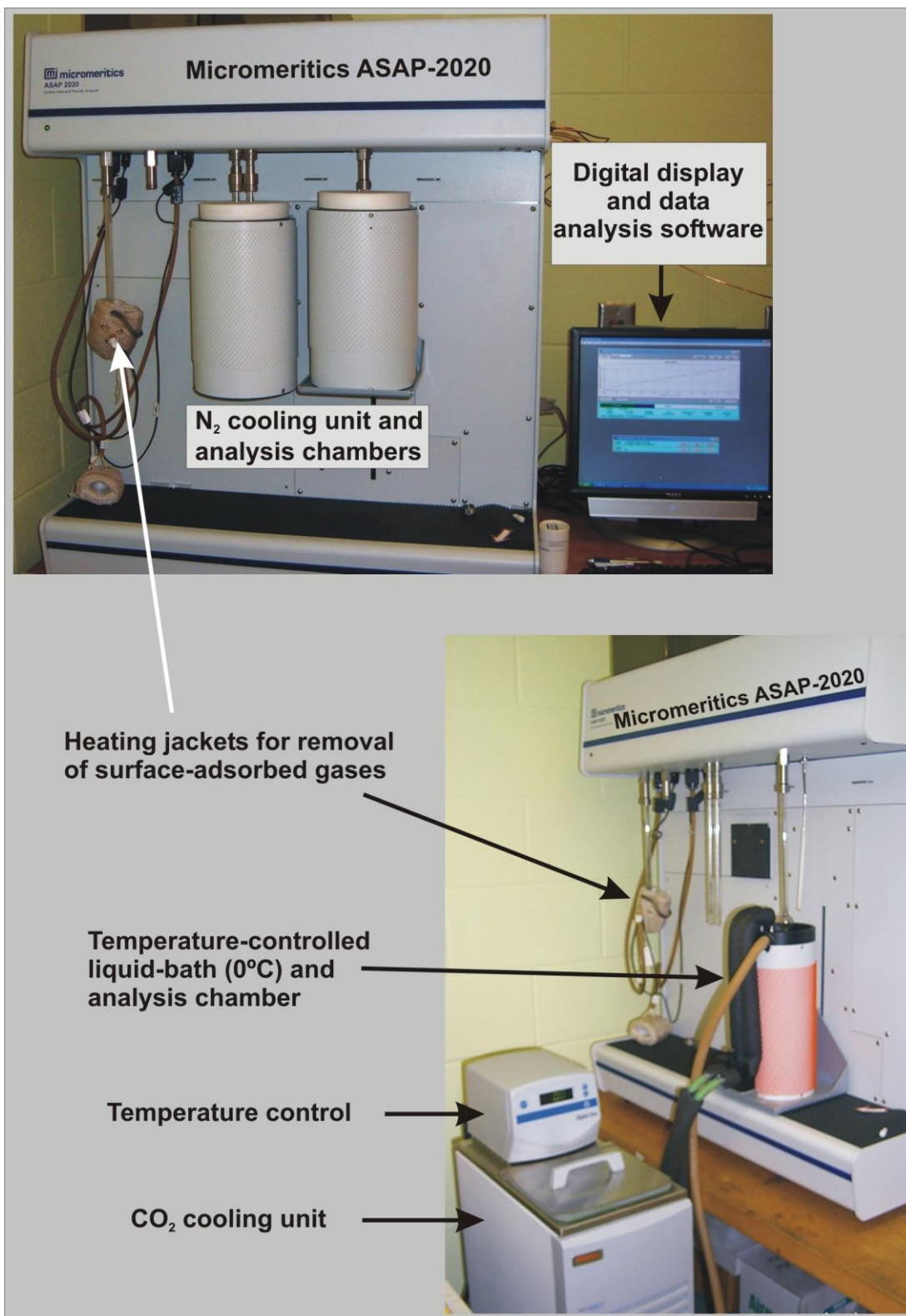


Figure 1. Low-pressure volumetric adsorption apparatus (Micromeritics ASAP-2020).

7.2.5. Fourier transform infrared (FTIR) spectroscopy

FTIR spectroscopy is considered one of the most versatile tools to study the chemistry of fossil fuels, such as coal (Solomon and Carangelo, 1988). Painter *et al.* (1981), among others, suggested that FTIR spectroscopy is sensitive to the small changes occurring at the initial stages of oxidation of macromolecular materials, such as coal. In this work, samples for FTIR measurements were prepared as potassium bromide (KBr) pellets and were analyzed at the University of Kentucky at Lexington. The FTIR instrument was a Nicolet 20SXC spectrometer equipped with a DTGS detector, collecting 1024 scans per sample at a resolution of 4 cm^{-1} . Bands of absorption were identified by comparison with published spectra (Painter *et al.*, 1981; Fredericks *et al.*, 1983; Walker and Mastalerz, 2004). A baseline correction was applied to all FTIR spectra to appropriately integrate the regions beneath each spectrum.

The integrated areas of the following absorption bands were determined: aromatic C-H stretching region ($3100\text{-}3000\text{ cm}^{-1}$; $\text{Ar}_{(3100-3000)}$), aliphatic C-H stretching region ($3000\text{-}2800\text{ cm}^{-1}$; $\text{Al}_{(3000-2800)}$), oxygenated ($\text{O}_{(1800-1700)}$) groups and aromatic/olefinic ($\text{C}_{(1700-1600)}$) region ($1600\text{-}1800\text{ cm}^{-1}$; $\text{O+C}_{(1800-1600)}$), CH_2 and CH_3 bending mode region ($\text{CH}_2_{(1450)}$ peak at 1450 cm^{-1} ; $\text{CH}_3_{(1375)}$ peak at 1375 cm^{-1}), and aromatic out-of-plane C-H deformation region ($700\text{-}900\text{ cm}^{-1}$; $\text{Ar}_{(900-700)}$). Corrections to absorption spectra and data manipulation utilized software provided with the instrument.

The ratios of FTIR absorption intensities from selected functional groups can be used as an indication of oxidation. For example, Wu *et al.* (1988) defined a parameter called oxidation index as the ratio of the integrated intensity of the carbonyl band ($1635\text{-}1850\text{ cm}^{-1}$) to that of the C-H stretching band ($2746\text{-}3194\text{ cm}^{-1}$). Several ratios have been

proposed in the literature to indicate changes in functional groups (Calemma et al., 1988; Lis et al., 2005; Mastalerz and Bustin, 1993; Painter et al., 1980, 1981; Wu et al., 1988, among others). The ratios included $\text{Ar}_{(3100-3000)} / \text{Al}_{(3000-2800)}$; $\text{Al}_{(3000-2800)} / \text{O+C}_{(1800-1600)}$; $\text{Ar}_{(900-700)} / \text{Al}_{(3000-2800)}$; $\text{Al}_{(3000-2800)} / \text{O}_{(1800-1700)}$; $\text{CH}_2(1450) / \text{CH}_3(1375)$ and a parameter defined as oxidation index, corresponding to the inverse of the $\text{Al}_{(3000-2800)} / \text{O+C}_{(1800-1600)}$ ratio. These or similar ratios of FTIR-identified functional groups were calculated in this study to observe trends in oxidation as a result of storage over 13 months at low-temperature conditions in the laboratory.

7.2.6. Outline of experimental strategy

Experiment 1 exposed coal for up to 13 months to laboratory air in order to constrain the effects of storage time and sample preservation on adsorption characteristics, and to quantify the changes in physical and chemical properties of coals resulting from oxidation and moisture loss through time. Additionally, small sample aliquots were exposed to elevated temperatures in Experiments 2 and 3 to artificially oxidize the coals for a period of 10 days. Figures 2A and 2B indicate the various types of analyses and timing of measurements in Experiments 1, 2, and 3.

Figure 2A. Analyses performed on samples from long-term experiments (up to 13 months).

Available data (analyses)	Experiment 1: Timing of analyses (months of coal exposure in air at room temperature)													
	0	1	2	3	4	5	6	7	8	9	10	11	12	13
Proximate and Ultimate														
FTIR														
Low-pressure N ₂ adsorption														
Low-pressure CO ₂ adsorption														
Petrography														

Figure 2B. Short-term experiments lasting for 10 days.

Experiment temperature (°C)	Experiment 2	Experiment 3
21		
35		
60		
75		
100		

	No data
	Zero exposure
	After 10 days

7.3. Results

7.3.1. Proximate and ultimate chemical coal analyses

Data from proximate analyses of 7 air-exposed coal samples in Experiment 1 indicate a substantial decrease in moisture content from 14.1 wt. % at the beginning of Experiment 1 in early February 2006 to 2.5 wt. % 13 months later in March 2007. A slight intermittent increase in moisture was observed in the 7th month from August to September, probably due to a temporary increase in summer air humidity in the laboratory (Figure 3). Drying of coal resumed over the remaining months (Table 1). Overall, the calorific value (MJ/kg) slightly decreased from ~33.8 MJ/kg (14,407 BTU/lb) to ~33.3 MJ/kg (14,183 BTU/lb). No significant long-term trends were observed for mineral matter (ash), volatile matter (VM), fixed carbon (Fix C), and sulfur (S) concentrations (Figure 3; data are numerically listed in Table 1 in weight % on a dry, ash-free basis, daf).

Ultimate analyses of the O, C, H, N, and S-elemental composition demonstrated subtle changes with no apparent long-term trends for hydrogen (H, wt. % daf), nitrogen (N, wt. % daf), and sulfur (S, wt. % daf). The oxygen content increased significantly from 8.64 to 10.18 wt. % daf after the first month of exposure to laboratory air in Experiment 1 (Figure 4), followed by minor long-term oxygen content fluctuations between 10.1 and 10.4 wt. % daf (Figure 4). The carbon content (C, wt. % daf) decreased after the first month of exposure to laboratory air, followed by an increase and stabilization with minor fluctuations between 81.8 and 82.2 wt. % daf (Figure 4).

Table 1. Proximate and ultimate analyses of coal samples exposed to laboratory air from zero to 13 months in Experiment 1. The first row of data describes the original “zero exposure coal”.

Exposure (months)	Proximate analyses (wt. % on dry, ash-free basis, daf)						Ultimate analyses (wt. % daf)				
	Moisture	Ash	MJ/kg*	VM	Fixed C	S	C	H	N	O	S
0	14.1	2.7	33.8	39.9	57.4	0.7	83.4	5.5	1.6	8.6	0.7
1	7.0	2.0	33.9	39.0	59.1	0.6	80.3	5.5	1.7	10.2	0.6
3	3.7	2.1	33.6	37.1	60.8	0.6	82.1	5.4	1.7	10.1	0.6
5	3.3	2.7	33.4	38.9	58.4	0.7	81.8	5.5	1.5	10.4	0.8
7	4.5	2.8	33.4	37.3	59.9	0.7	82.0	5.4	1.6	10.3	0.7
9	3.4	2.4	33.5	36.2	61.3	0.7	82.2	5.4	1.6	10.1	0.7
13	2.51	2.6	33.3	38.7	58.7	0.7	81.9	5.4	1.6	10.3	0.8

*Units for calorific value: 1 MJ/kg \approx 426 BTU/lb.

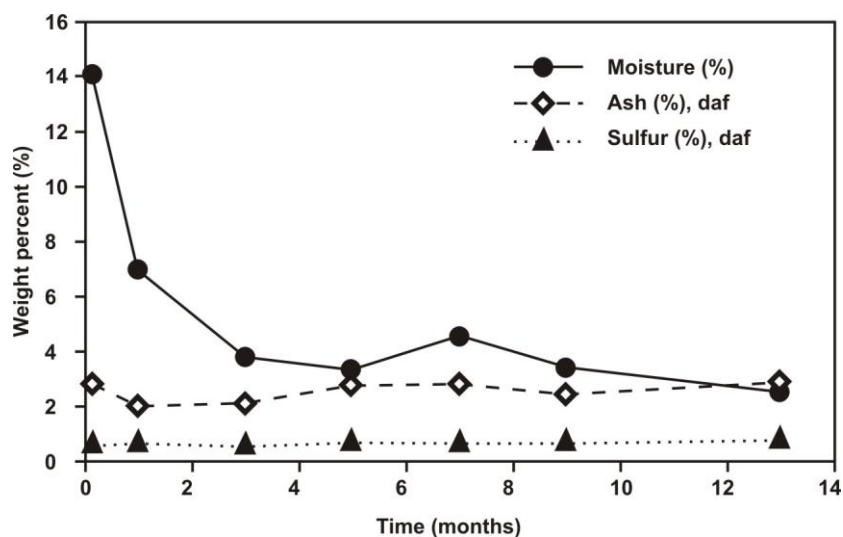


Figure 3. Proximate chemical analyses showing changes in moisture, ash, and sulfur contents in coal during the exposure to air over 13 months in Experiment 1. Observed variations in ash reflect heterogeneity within coal samples.

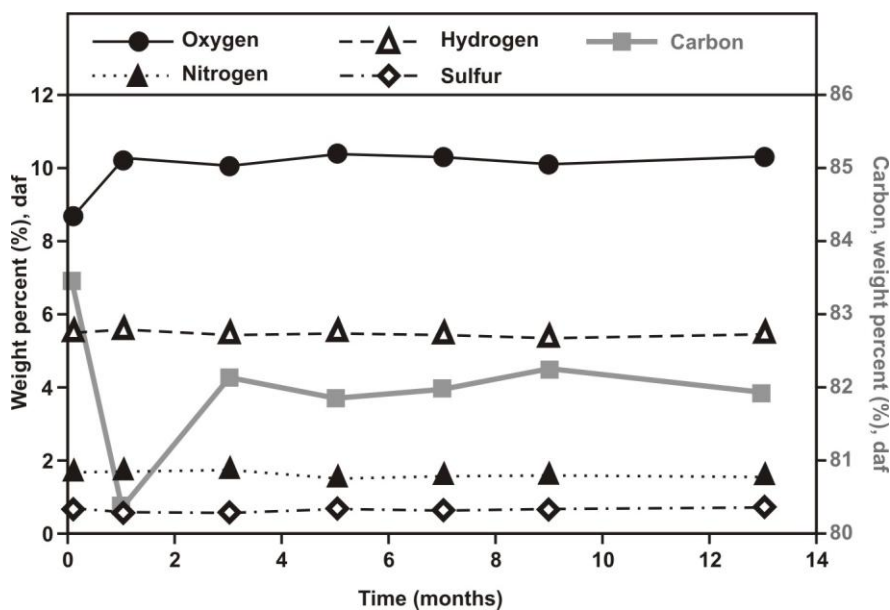


Figure 4. Ultimate chemical analyses showing changes in O, N, H, S, and C contents during the 13 months exposure of Experiment 1. Elemental data are reported in weight % on a dry, ash-free basis.

7.3.2. Petrographic analyses

Maceral composition, mineral-matter content, and vitrinite reflectance data from the beginning and the end of the 13th month in Experiment 1 are presented in Table 2.

7.3.3. Mesopore characteristics constrained by low-pressure N_2 adsorption

Analyses of surface areas and low-pressure adsorption characteristics were performed on coals from three oxidation experiments. Experiment 1 evaluated the effects of oxidation in air at room temperature over a period of 13 months. The most significant changes were observed in the mesopore characteristics (Table 3). N_2 adsorption revealed a marked decrease in mesopore surface area with increasing drying and oxidation over time as calculated by BET and BJH methods (from 44.4 to 40.1 m^2/g , and from 36.5 to 20.5 m^2/g , respectively; Figure 5). Good agreement was observed for N_2 adsorption data collected in duplicate for the first month (Figures 6 and 7).

Experiment 2 compared the original “zero exposure coal” with another aliquot of the same coal that had been exposed to laboratory air at 75°C for ten days. The resulting accelerated drying and oxidation affected the mesopore characteristics strongly (Table 3), causing significant decreases in BET mesopore surface area (from 36.4 to 27.9 m^2/g) and BJH mesopore surface area (from 31.8 to 24.6 m^2/g), along with an increase in the average mesopore width from 5.3 to 5.6 nm (Figure 5).

Experiment 3 gathered low-pressure N_2 adsorption data from coal aliquots that had been exposed for 10 days isothermally to laboratory air at various temperatures from 21 to 100°C. The observed changes in coal properties resulting from oxidation and drying in air at increasing temperatures corroborated observations from Experiments 1 and 2.

Nitrogen adsorption indicates a general decrease in BET surface area from 40.5 m²/g after 21°C exposure to 34.2 m²/g at 100°C. Similarly, the BJH surface area decreased from 33.3 at 21°C to 29.8 m²/g at 100°C. The average mesopore width increased slightly from 5.0 nm at 21°C to 5.4 nm at 100°C. No significant correlation was observed for BJH cumulative pore volumes with increasing temperature (Table 3; Figure 5).

Table 2. Petrographic analyses of samples exposed to oxidizing air in the laboratory for 13 months in Experiment 1. Data normalized to 100% by volume (vol. %). Experiment 1 resulted in no changes in vitrinite reflectance (R_o). The first row of data describes the original “zero exposure coal”.

Exposure (months)	Petrographic composition (vol. %) and vitrinite reflectance (R_o)				
	Vitrinite	Liptinite	Inertinite	Mineral matter (ash)	R_o (%)
0	69.6	16.0	13.6	0.8	0.62
13	68.9	15.7	13.4	2.0	0.62

Table 3. Low-pressure N_2 adsorption data. Note the changes in surface area and mesopore characteristics resulting from isothermal oxidation in air at increasing temperatures.

Experiment	Temperature (°C)	Low-pressure N_2 adsorption			
		BET surface area (m ² /g)	BJH adsorption in mesopores		Adsorption average mesopore width (nm)
			Surface area (m ² /g)	Cumulative mesopore volume (cm ³ /g)	
1*	21	44.4	36.5	n.d.	4.8
	21	40.1	20.5	0.0133	2.6
2	21	36.4	31.8	0.0417	5.3
	75	28.0	24.6	0.0344	5.6
3	21	40.5	33.3	0.0429	5.0
	35	38.1	32.9	0.0432	5.2
	60	38.8	32.5	0.0426	5.1
	100	34.2	29.8	0.0484	5.4

n.d. = no data available. * Experiment 1 was repeated within a few days to obtain cumulative pore volumes.

Low-pressure adsorption data from Experiments 1, 2 and 3 are represented graphically in Figures 5A, B, and C, where several trends can be observed with increasing temperature. Nitrogen adsorption data (Figures 5 through 9) reveal a consistent decrease in BET mesopore surface area (Figure 5A). The opposite trend is observed for average mesopore width (Figure 5C), but no consistent trend is evident for the cumulative mesopore volume (Figure 5B).

Low-pressure nitrogen adsorption isotherms from Experiment 1 display a consistent decrease in gas adsorption capacity of coal with increasing exposure to air (Figure 6). For example, at 0.5 relative pressure, the adsorption capacity of the original (i.e., “zero exposure”) coal is $\sim 18.8 \text{ cm}^3/\text{g}$, whereas the adsorption capacity after 13 months of exposure in Experiment 1 is diminished to $\sim 15.2 \text{ cm}^3/\text{g}$. This change is also reflected in the decrease of the BJH cumulative pore volume with increasing exposure (Figure 7).

Nitrogen adsorption isotherm data from Experiment 2 (Figure 8) reveal a slightly larger decrease in adsorption capacity ($4.1 \text{ cm}^3/\text{g}$), from 15.9 to $11.8 \text{ cm}^3/\text{g}$ at 0.5 relative pressure, as a result of increased exposure temperature compared to that observed for Experiment 1 ($3.6 \text{ cm}^3/\text{g}$). The adsorption capacity decreases from 18.8 to $15.2 \text{ cm}^3/\text{g}$ at 0.5 relative pressure after prolonged coal exposure at room temperature in Experiment 1.

Experiment 3 also indicates a decrease in nitrogen adsorption capacity with increasing coal exposure as revealed by isotherm plots in Figure 9. Low-pressure adsorption data for this experiment show that the amount of adsorbed nitrogen decreases with increasing temperature. The difference in adsorption capacity observed between the experiments at 21°C (room temperature) and after heating coal to 100°C for 10 days is about $2.8 \text{ cm}^3/\text{g}$ at 0.5 relative pressure.

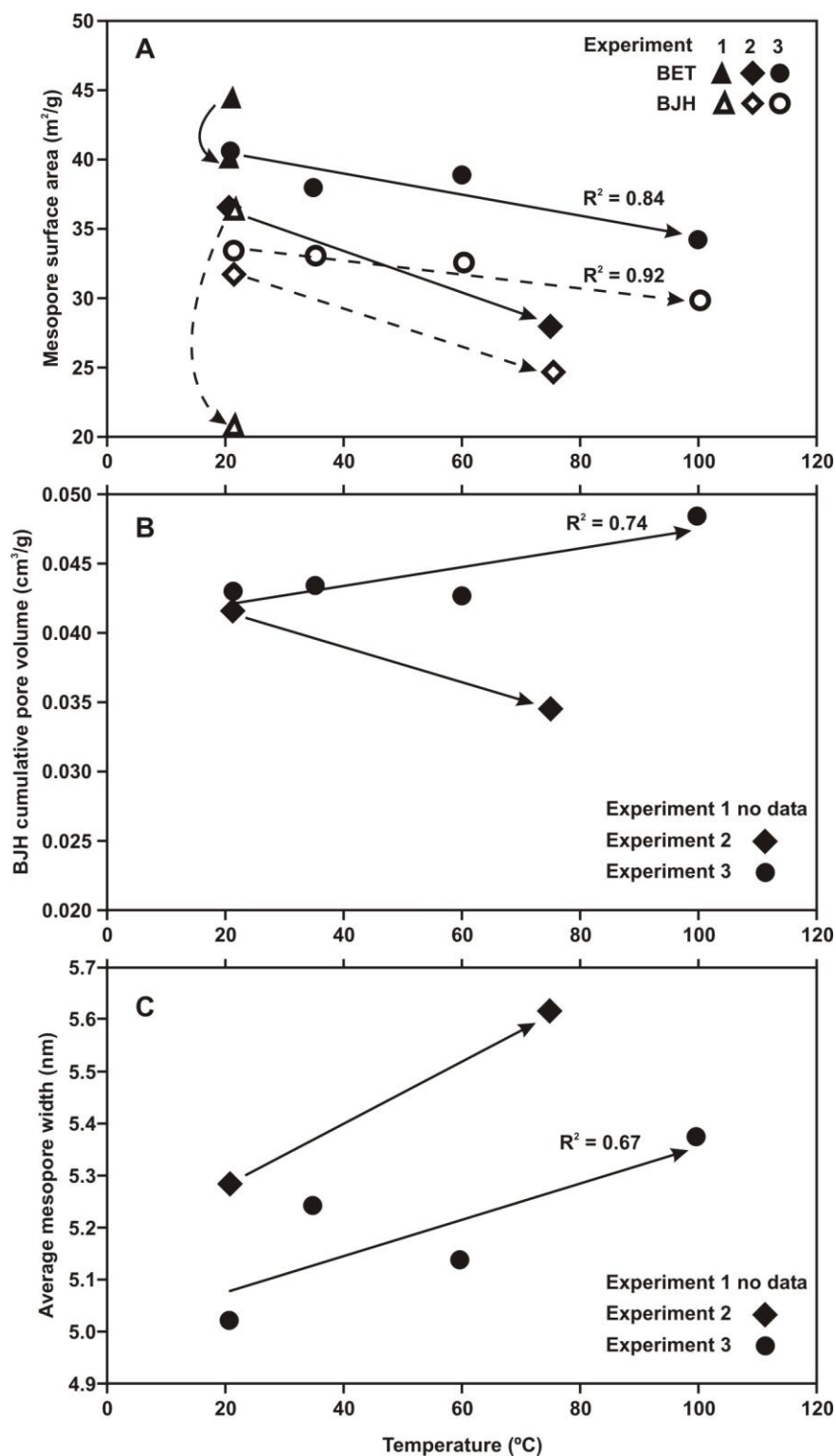


Figure 5. Low-pressure nitrogen adsorption data versus temperature. A: Consistent decrease in mesopore surface area with temperature increase. B: No clear trend in cumulative mesopore volume with temperature increase. C: Consistent increase in mesopore width with increasing temperature.

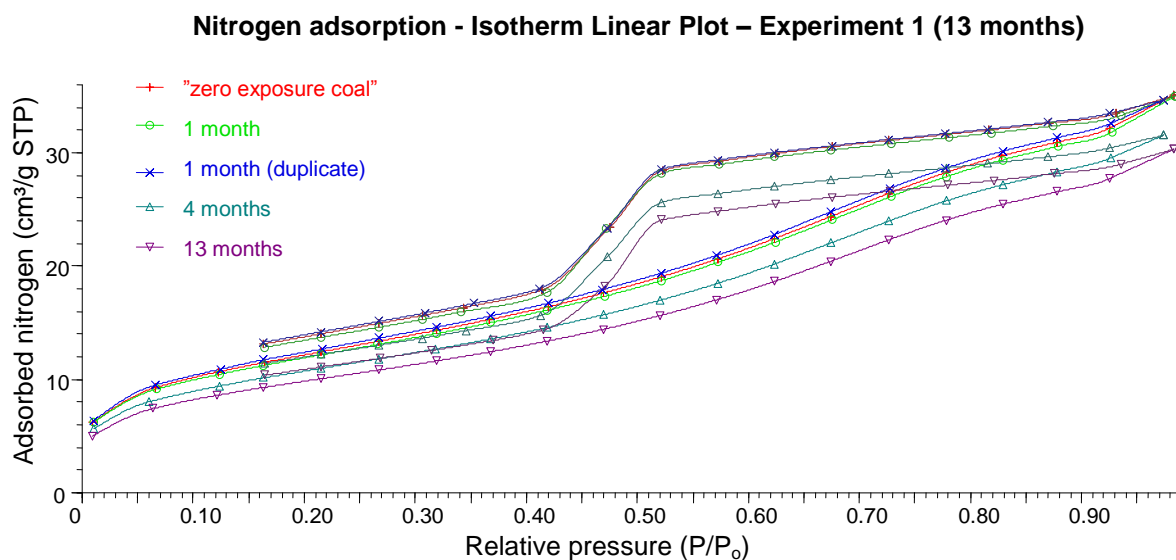


Figure 6. Low-pressure nitrogen isotherm adsorption data for Experiment 1. Note the decrease in adsorption capacity with exposure time. Data graphed at standard temperature and pressure (STP) conditions (0°C and 0.101 MPa).

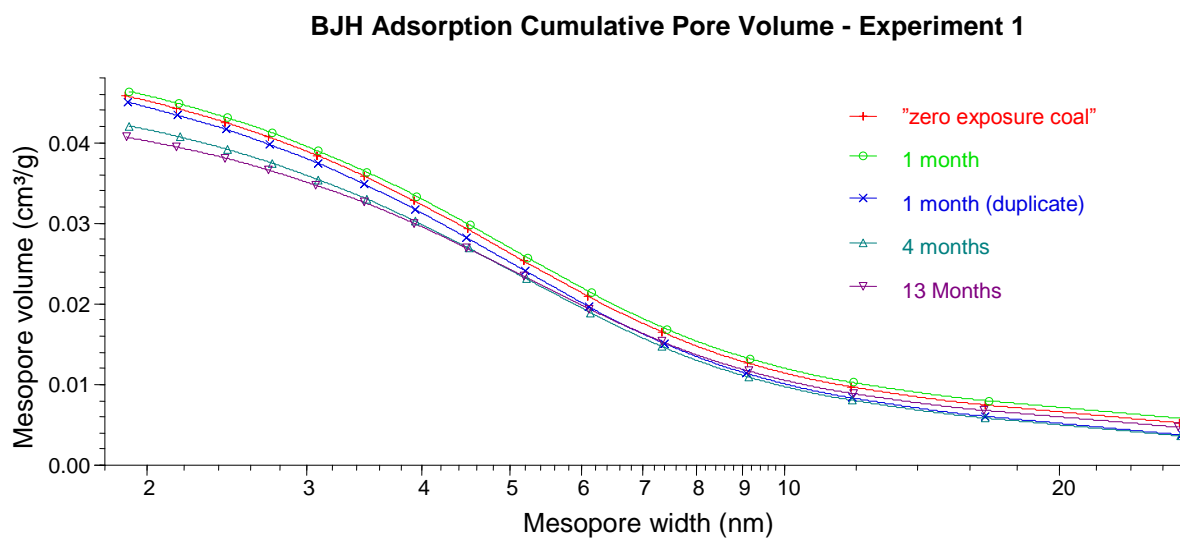


Figure 7. Decrease in cumulative mesopore volume with increasing exposure of coal in Experiment 1. The X-axis has a logarithmic scale.

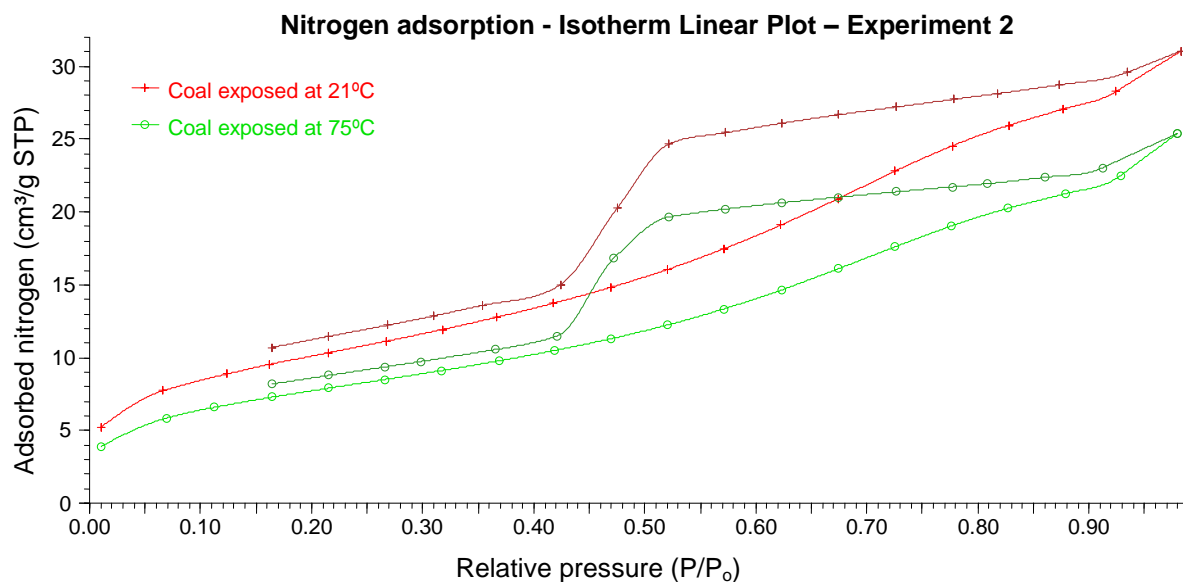


Figure 8. Low-pressure nitrogen isotherm adsorption data from Experiment 2. A significant decrease in adsorption capacity occurred when coal was heated in air to 75°C for 10 days. Data graphed at standard temperature and pressure (STP) conditions (0°C and 0.101 MPa).

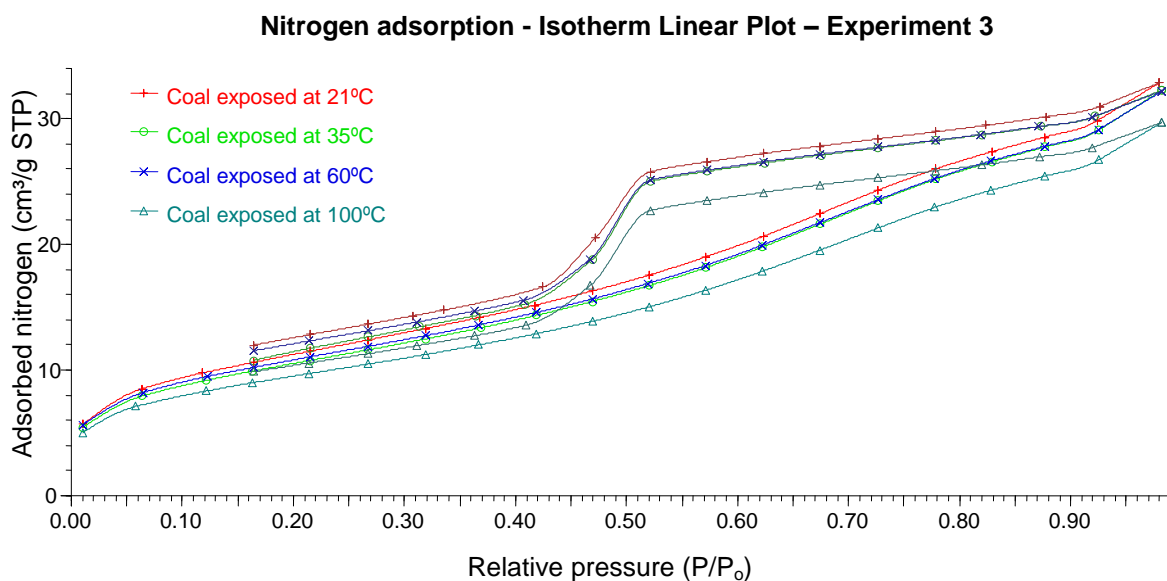


Figure 9. Low-pressure nitrogen isotherm adsorption data from Experiment 3. A decrease in adsorption capacity of coals resulted from isothermal heating at different temperatures for 10 days. Data graphed at standard temperature and pressure (STP) conditions (0°C and 0.101 MPa).

7.3.4. Micropore characteristics constrained by low-pressure CO₂ adsorption

Analyses of surface area and low-pressure adsorption characteristics were conducted with CO₂ on coals from Experiments 1, 2 and 3. Experiment 1 shows the effects of isothermal oxidation and drying at room temperature over 13 months. Only a slight increase in BET surface area from 81.2 to 81.7 m²/g was observed for low-pressure adsorption with CO₂ (Table 4).

Experiment 2 heated coal at 75°C in laboratory air for ten days and compared the resulting oxidized coal with the original “zero exposure” coal. The resulting effects on the micropore characteristics (Table 4) were stronger than in Experiment 1. Low-pressure CO₂ adsorption data show that the BET surface area increased from 81.8 to 104.8 m²/g in Experiment 2. The D-R micropore surface area and monolayer capacity calculations also indicated increases from 127.9 to 153.6 m²/g, and from 27.9 to 33.6 cm³/g, respectively. The D-A limiting micropore volume experienced a more subtle increase from 0.06 to 0.09 cm³/g.

Corroboration of results from Experiments 1 and 2 derives from Experiment 3 where low-pressure CO₂ adsorption data were collected from coal aliquots that had been heated isothermally for 10 days at distinct temperatures up to 100°C.

Table 4. Low-pressure CO₂ adsorption data. Note the changes in surface area and micropore characteristics resulting from isothermal oxidation in air at increasing temperatures.

Experiment	Temperature (°C)	Low-pressure CO ₂ adsorption				
		BET surface area (m ² /g)	Dubinin-Radushkevich		Dubinin-Astakhov	Average micropore size (nm)
			Micropore surface area (m ² /g)	Monolayer capacity (cm ³ /g)	Limiting micropore volume (cm ³ /g)	
1*	21	n.d.	127.6	27.94	0.0590	n.d.
	21	81.3	126.9	27.77	0.0581	1.36
	21	81.8	126.8	27.76	0.0609	1.37
2	21	81.8	127.9	27.99	0.0610	1.37
	75	104.8	153.6	33.63	0.0923	1.31
3	21	78.4	120.6	26.40	0.0592	1.38
	35	78.3	121.0	26.60	0.0578	1.37
	60	79.7	123.6	27.06	0.0580	1.38
	100	81.5	128.0	28.03	0.0579	1.38

n.d. = no data available. * Analyses pertaining to Experiment 1 were run three times as indicated in Figure 2A.

Low-pressure CO₂ adsorption data also revealed changes in the micropore characteristics of the exposed coals (Table 4). The BET micropore surface area increased from 78.4 at 21°C exposure to 81.5 m²/g following 100°C exposure, and the D-R micropore surface area increased from 120.6 at 21°C to 128.0 m²/g at 100°C. Monolayer capacity also increased from 26.4 at 21°C to 28 cm³/g at 100°C. No distinct changes were observed for the D-A limiting micropore volume. A slight increase in micropore size was observed from 1.37 cm³/g at 21°C to 1.38 cm³/g at 100°C.

Low-pressure carbon dioxide adsorption data from Experiments 1, 2 and 3 revealed consistent increases in calculated surface areas (BET and Dubinin-Radushkevich – D-R), as well as for D-R monolayer capacity calculations (Figures 10A, B, C). Experiment 2 indicated pronounced changes from the original “zero exposure” coal to exposed and oxidized coal. The higher temperatures of 10-day exposures in Experiment 3 resulted in weaker trends in Figures 5, 10, and 11. Nonetheless, good correlations were observed in most cases ($R^2 > 0.67$). Dubinin-Astakhov (D-A) calculations for micropore volumes and the average micropore sizes did not yield clear trends for Experiments 2 and 3 (Figures 11A, B). However, the correlations between these parameters and temperature improved for Experiment 3 (Figures 11A, B).

Carbon dioxide adsorption isotherms do not indicate a significant change in adsorption capacity (~12.5 cm³/g at 0.02 relative pressure), although a slight increase is apparent with increasing exposure of coal (Figure 12). Figure 13 expresses a subtle increase in cumulative surface area with increasing exposure for Experiment 1, but conveys a similar picture like Figure 12.

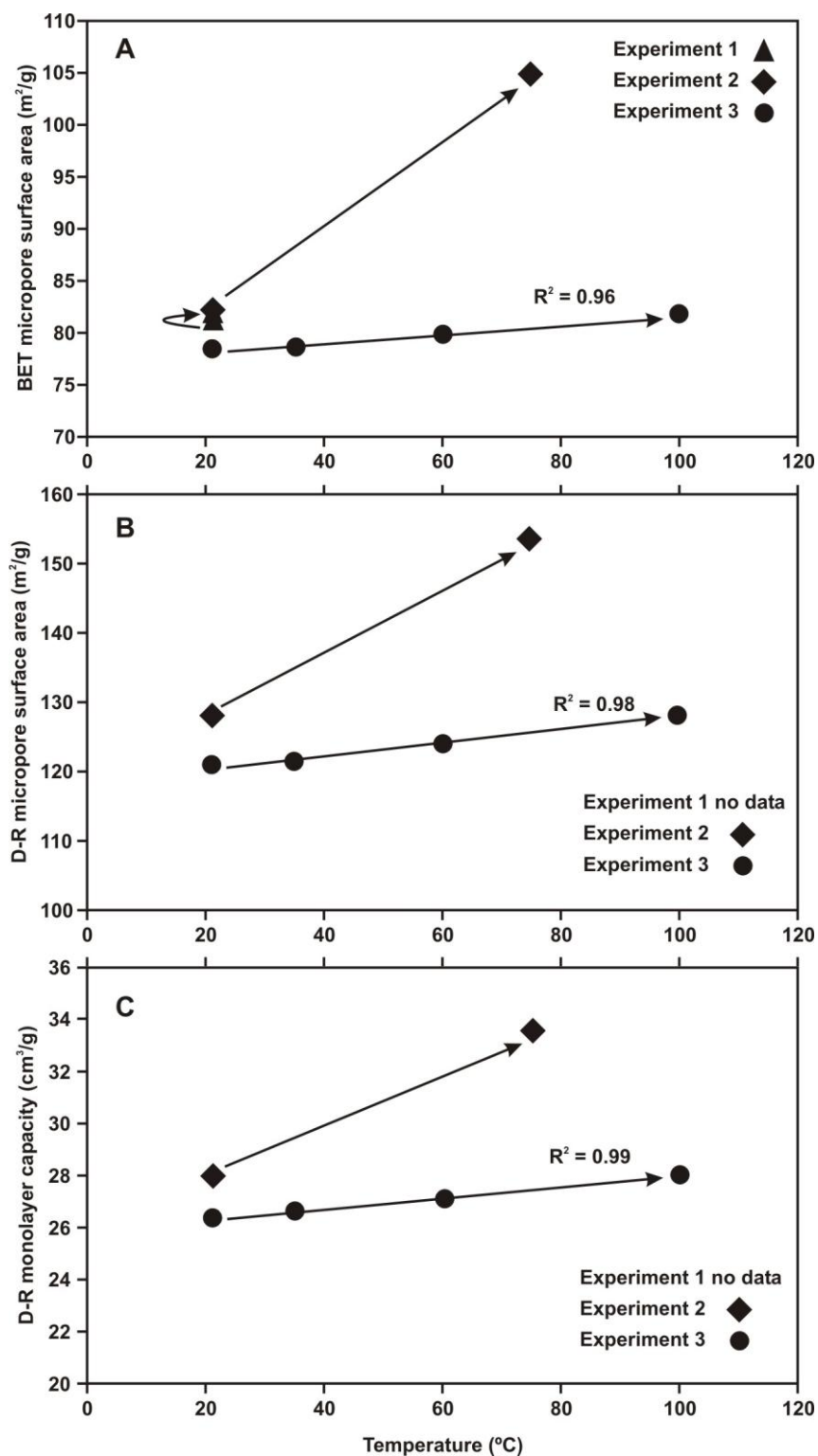


Figure 10. Low-pressure CO_2 adsorption data versus temperature. Diagrams A, B, and C show that micropore surface area and monolayer capacity increase with increasing temperature of exposure.

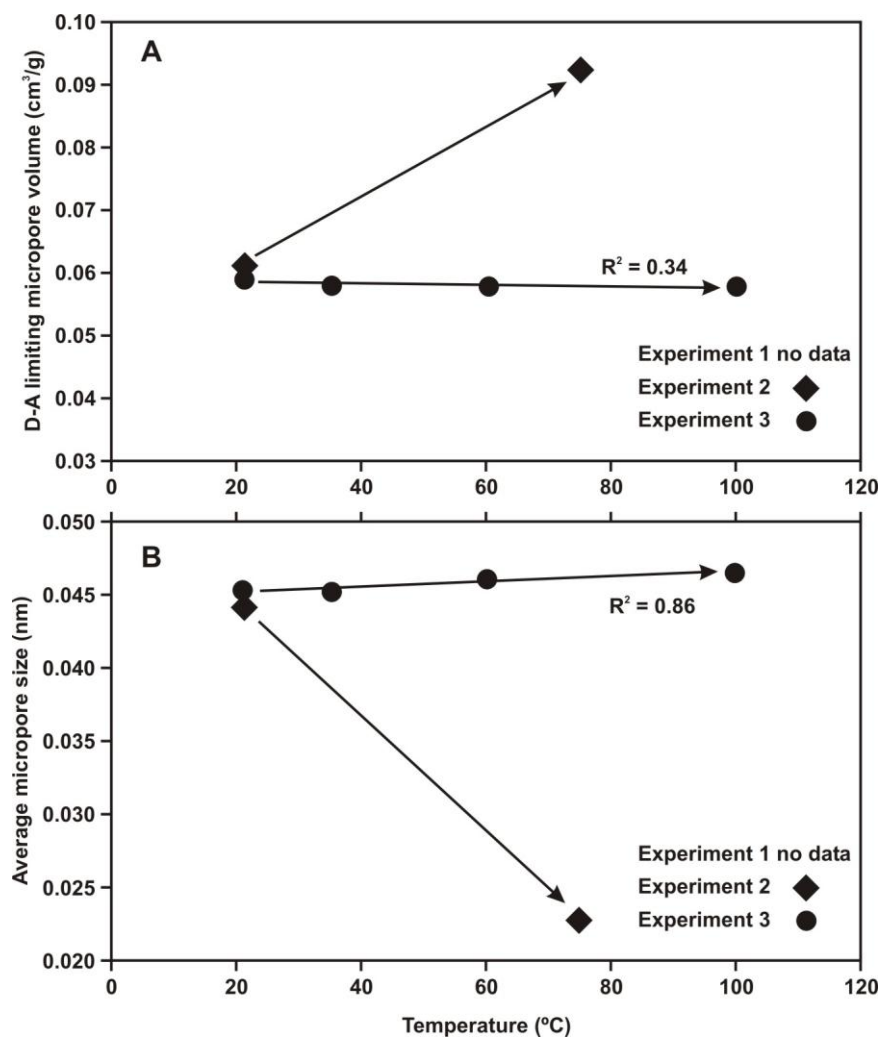


Figure 11. Low-pressure CO₂ adsorption data versus temperature of exposure to air. No consistent trends are observed for the limiting micropore volume (A) and the micropore size (B) with increasing temperature.

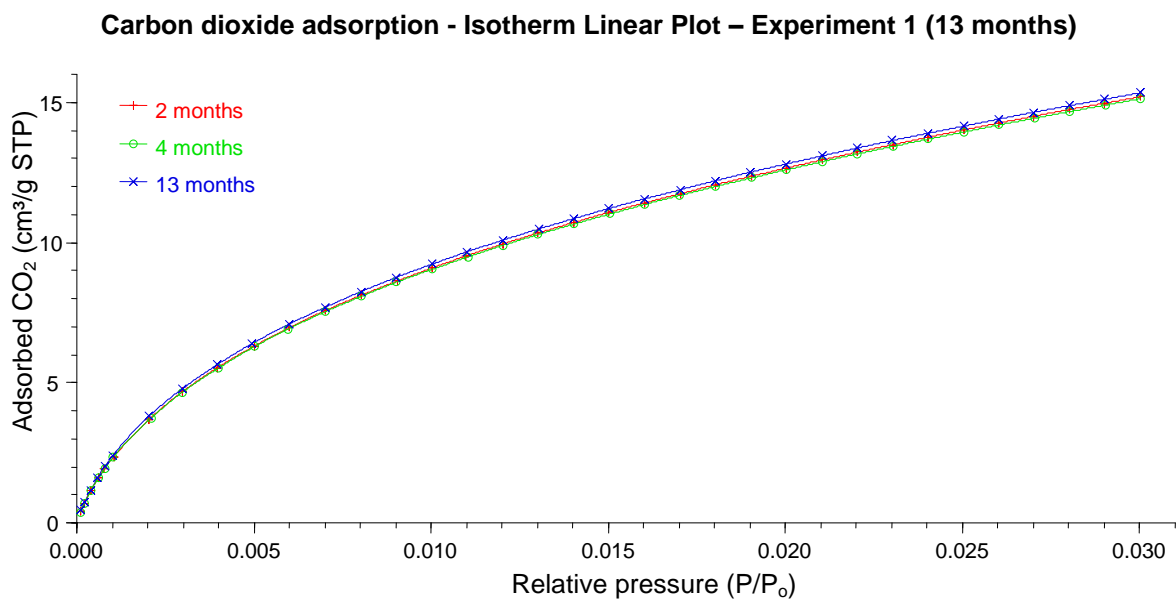


Figure 12. Low-pressure carbon dioxide adsorption isotherm for Experiment 1. No significant difference is observed with time of exposure of coal to laboratory air at room temperature. Data expressed at standard temperature and pressure (STP) conditions (0°C and 0.101 MPa).

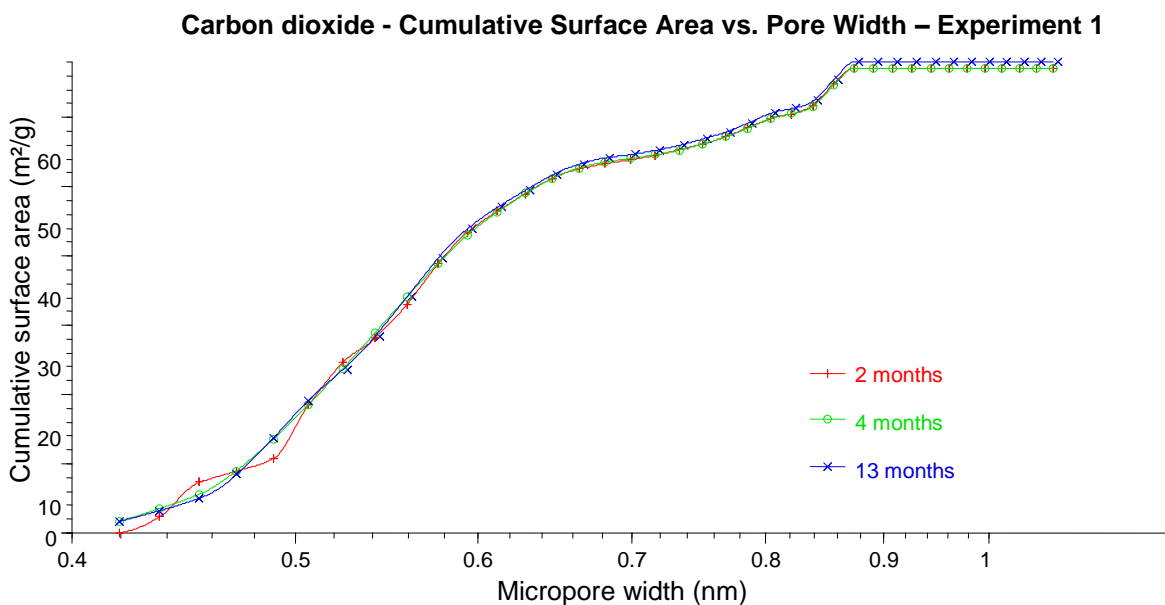


Figure 13. Minimal changes in micropore surface area are observed with increasing time of exposure of coal to laboratory air at room temperature in Experiment 1.

The carbon dioxide adsorption isotherms of thermally altered coals of Experiment 2 indicate an adsorption capacity increase of $\sim 2.3 \text{ cm}^3/\text{g}$ with increasing thermal exposure that is expressed by diverging isotherms in Figure 14. This stands in contrast to (i) “zero exposure” coal (Figure 15), as well as (ii) to exposed coals from Experiment 1 at room temperature where change was almost negligible (Figure 12).

In contrast to the behavior observed for nitrogen adsorption, the low-pressure CO_2 adsorption data reveal an increase of about $0.5 \text{ cm}^3/\text{g}$ at 0.02 relative pressure for coal heated to 100°C in Experiment 3 with respect to coal kept at 21°C (Figure 15). The calculated cumulative surface area from Experiment 3 (Figure 16) also increases with increasing thermal exposure.

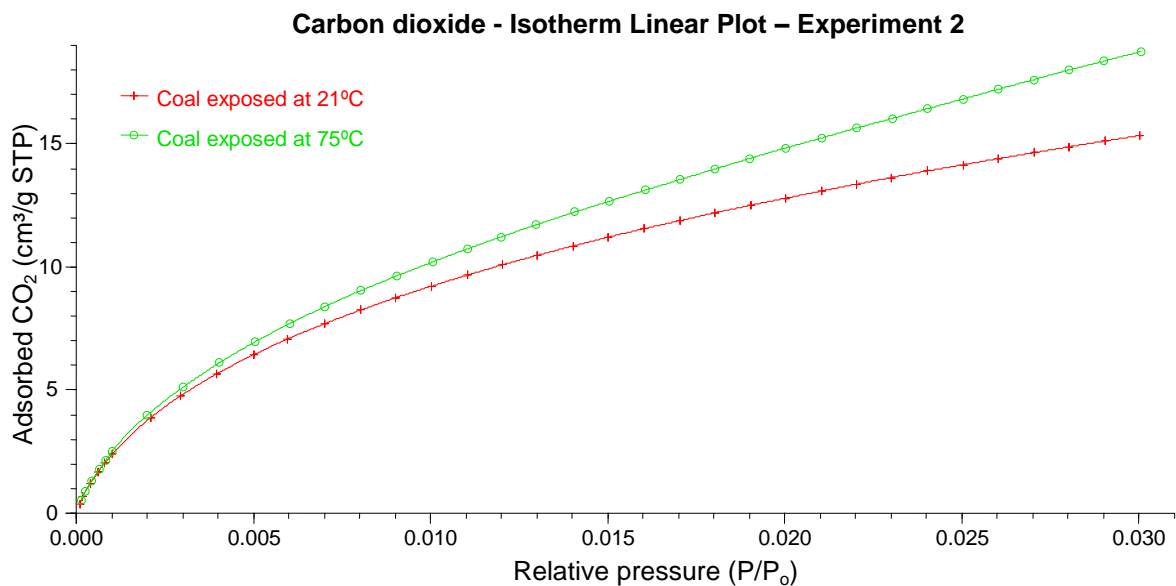


Figure 14. Low-pressure carbon dioxide adsorption isotherms for Experiment 2. A large increase in adsorption capacity occurred during heating in laboratory air at 75°C for 10 days.

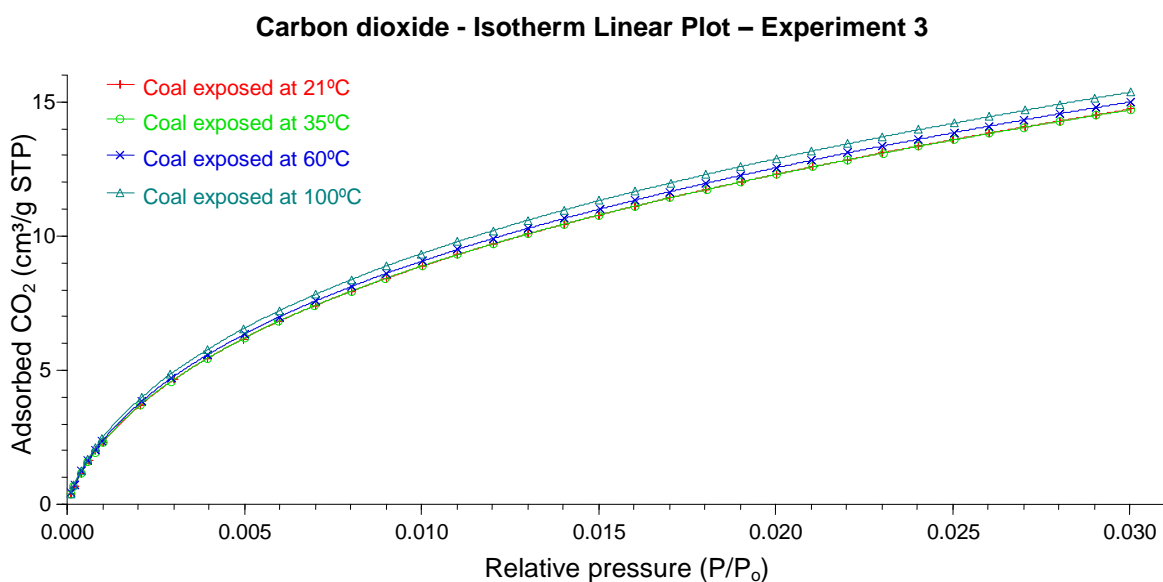


Figure 15. Small increases in adsorption capacity were observed for coals that were isothermally exposed to laboratory air at increasing temperatures for 10 days in Experiment 3.

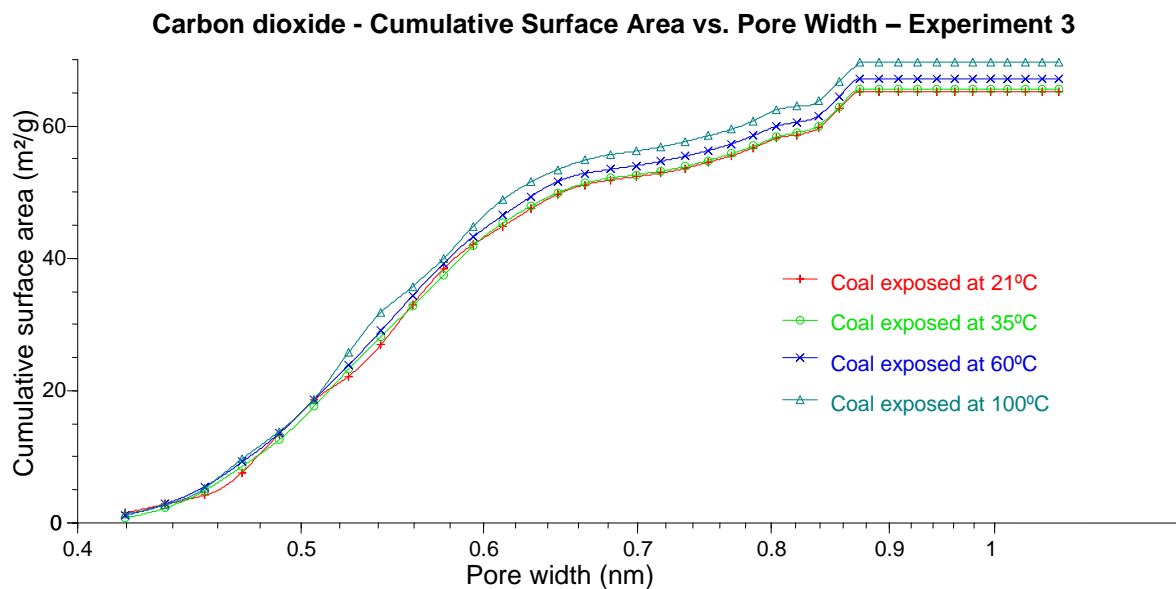


Figure 16. Small increases in cumulative micropore surface area were observed for coals that were isothermally exposed to laboratory air at increasing temperatures for 10 days in Experiment 3.

7.3.5. Fourier Transform Infra-red (FTIR) analyses

FTIR spectroscopy was used to quantify the distribution of chemical functional groups in 7 coals that had been exposed to oxidizing air at room temperature for a period of nine months in Experiment 1. A generalized FTIR spectrum defining the absorption bands of selected functional groups in terms of wavenumbers (cm^{-1}) is presented in Figure 17. All coal samples exhibit a wide hydroxyl absorption band between 3100 and 3700 cm^{-1} and well-defined aromatic and aliphatic stretching regions between 3000-3100 cm^{-1} and 2800-3000 cm^{-1} , respectively. The aliphatic stretching region is characterized by two peaks near 2850 and 2920 cm^{-1} . The carbonyl/carboxyl peak appears occasionally around 1701 cm^{-1} . A very distinct aromatic carbon peak at $\sim 1600 \text{ cm}^{-1}$ is ubiquitous in all samples (Figures 17 and 19). In all coal samples the aliphatic bending region is characterized by a well-defined CH_2 peak at 1442 cm^{-1} and a less conspicuous CH_3 peak around 1370 cm^{-1} . Mineral matter is possibly associated with kaolinite and appears at 1032 cm^{-1} . The aromatic out-of-plane region (700 and 900 cm^{-1}) is characterized by three peaks at approximately 750, 815, and 860 cm^{-1} . Sulfur compounds are common and appear at peaks around 540 and 470 cm^{-1} .

Fourier self-deconvolution (Thermo Nicolet's OMNIC v. 6.0 software) of the aliphatic stretching region (2800-3000 cm^{-1}) allowed resolving CH_2 (2920 and 2848 cm^{-1}) and CH_3 (2953 and 2866 cm^{-1}) stretching bands (Figure 18). It has been suggested that the ratio between CH_2 and CH_3 (i.e., 2920 cm^{-1} /2953 cm^{-1}) is sensitive to the length of aliphatic chains and to the degree of branching of the molecular carbon skeleton (Lis *et al.*, 2005). Selected ratios between functional groups (Table 5) show no distinct trend with increasing oxidation exposure (Figure 5).

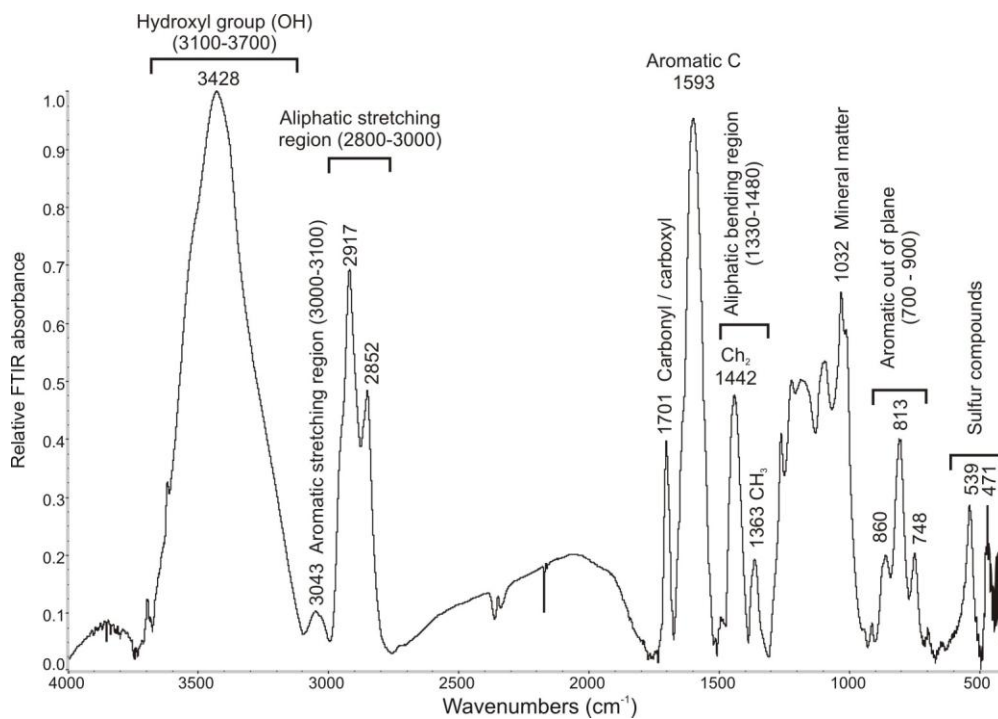


Figure 17. FTIR band assignments and approximate peak locations of functional groups of a high-volatile C bituminous coal from the Lower Block Coal Member, Billings Mine, Indiana, that was used in this study.

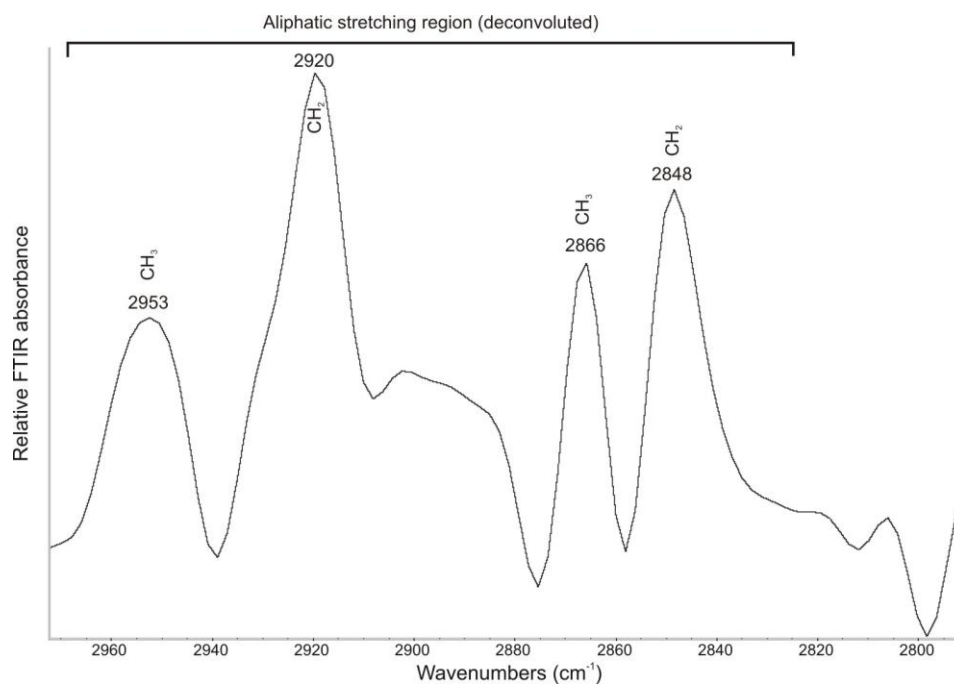


Figure 18. Fourier self-deconvolution of the aliphatic stretching region ($2800\text{--}3000\text{ cm}^{-1}$) in the sample illustrated above.

Table 5. Selected ratios of FTIR-identified functional groups in coals that were exposed to laboratory air at room temperature for up to 9 months in Experiment 1. No particular trends can be discerned from collected data and their ratios. Data from coal that was heated in air for 10 days at 75°C (Experiment 2) are presented in the last row for comparison.

Experiment	$\frac{Ar_{(3100-3000)}}{Al_{(3000-2800)}}$	$\frac{Al_{(3000-2800)}}{O+C_{(1800-1600)}}$	Oxidation index*	$\frac{Ar_{(900-700)}}{Al_{(3000-2800)}}$	$\frac{Al_{(3000-2800)}}{O_{(1800-1700)}}$	$\frac{CH_2_{(1450)}}{CH_3_{(1375)}}$
0 months	0.05	0.84	1.19	0.51	8.58	5.35
1 month	0.04	0.87	1.15	0.35	19.22	3.65
2 months	0.05	0.62	1.61	0.46	312.07	11.52
3 months	0.04	0.55	1.81	0.48	160.16	11.61
5 months	0.04	0.72	1.38	0.28	8.26	4.47
6 months	0.04	0.62	1.61	0.43	58.71	11.80
9 months	0.05	1.10	0.91	0.60	8.26	5.14
@75°C	0.04	0.79	1.27	0.41	6.66	3.76

* Oxidation index corresponds to the inverse of the $Al_{(3000-2800)} / O+C_{(1800-1600)}$ ratios.

FTIR spectra from Experiment 1 through a period of nine months of coal exposure to laboratory air at room temperature are shown in Figure 19. The most prominent change is the temporary decrease in absorbance in the hydroxyl group region 3700-3100 cm^{-1} after 5 and 6 months of exposure. This feature appears to be related to incorporation of oxygen or water vapor molecules from the atmosphere in response to changing air/humidity conditions in the laboratory.

Low-temperature oxidation during exposure of coal to laboratory air in Experiment 1 did not result in any significant FTIR changes affecting the aliphatic stretching region (2800-2600 cm^{-1}), the aromatic out-of-plane region (900-700 cm^{-1}), or the carbonyl/carboxyl groups' region (~1700 cm^{-1}). The random appearance of carboxyl/carbonyl peaks (~1700 cm^{-1} ; Figure 19) suggests external factors (e.g. incorporation of moisture from the laboratory air prior to FTIR analysis) rather than changes resulting from oxygen incorporation into the coal's structure.

For comparison, an FTIR spectrum was measured for coal that had been exposed at 75°C for 10 days to laboratory air (spectrum A in Fig. 20). This spectrum can be compared with the FTIR spectrum of the original "zero exposure" coal (spectrum B) and a differential spectrum (A - B) can be constructed (Fig. 20). The differential spectrum shows (i) a negative peak around 1600 cm^{-1} indicating consumption of aromatic carbon, and (ii) a well-defined peak around 1700 cm^{-1} that may represent the formation of carbonyl/carboxyl groups.

The ratios of selected functional groups that have been considered diagnostic of oxidation in previous studies are shown in Figure 21. Oxidation indices vary between 0.7 and 1.8 without expressing a clear trend with increasing oxidation or exposure of coal.

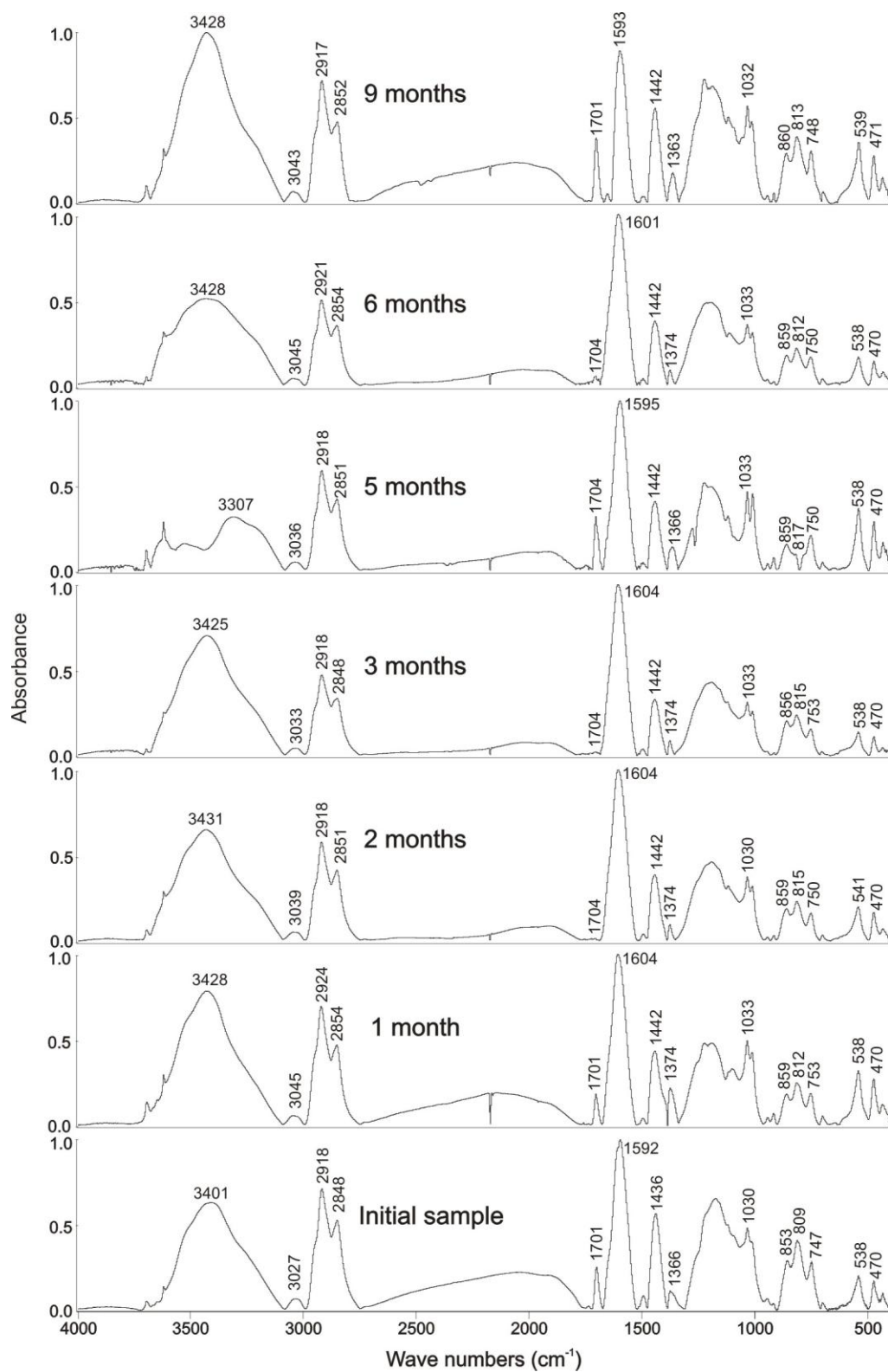


Figure 19. FTIR spectra of a coal sample exposed to laboratory air at room temperature for up to 9 months in Experiment 1. No long-term distinct changes are observed in functional group abundance through time.

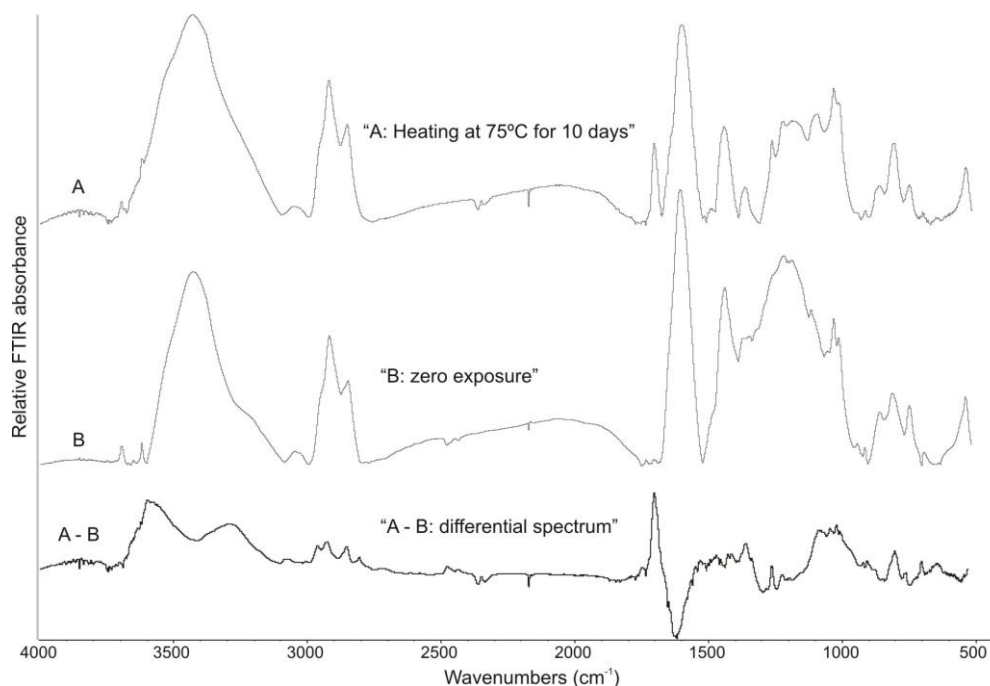


Figure 20. A differential spectrum (A - B, bottom) was obtained by subtracting the FTIR spectrum of coal that had been heated in air at 75°C for 10 days (Experiment 2, spectrum A, top) from the FTIR spectrum of the original “zero exposure” coal (spectrum B, middle). The negative peak near 1600 cm^{-1} in the differential spectrum suggests partial loss of aromatic carbon from coal during heat exposure in air, whereas a well-developed peak near 1700 cm^{-1} suggests the generation of carbonyl/carboxyl groups.

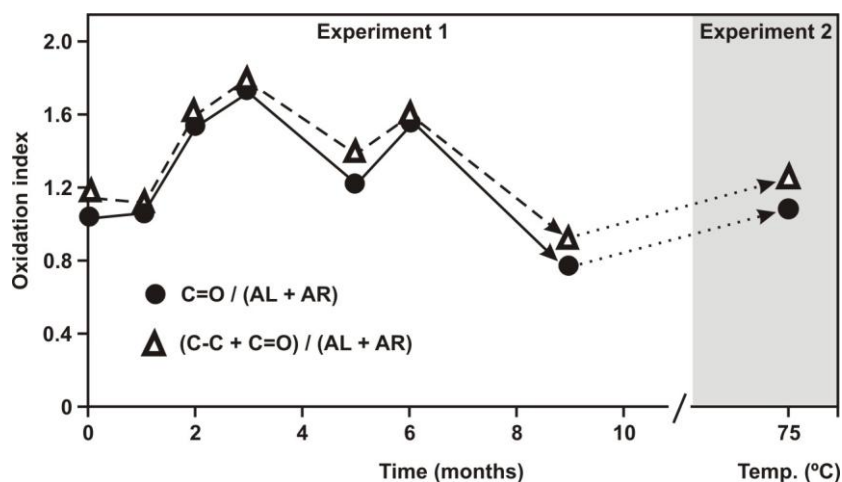


Figure 21. Oxidation indices from FTIR-derived ratios of functional groups for Experiments 1 and 2. No distinct long-term trends are observed with increasing exposure (Experiment 1). The shaded area represents the coal sample heated in air at 75°C (Experiment 2). No change is observed between the original “zero exposure coal” and coal that was exposed to 75°C.

7.4. Discussion

7.4.1. Elemental chemistry and petrographic changes

Proximate analyses of all coal samples demonstrated changes in moisture and calorific value as the most important consequences of coal storage in air. Fluctuations in coal's moisture content appear to be related to the humidity of ambient air. The intermittent increase in coal moisture content in Experiment 1 coincided with the warmest months of the year and peak humidity. Ultimate analyses revealed an initial increase in oxygen content that reached relatively stable values within the first month after the sample was exposed to air. These results agree with Martínez and Escobar's (1995) assessment that most geochemical parameters in air-exposed coal remain unchanged at low levels of chemical weathering, except the calorific value. Pis *et al.* (1996) studied the oxidation of coals at controlled laboratory conditions and concluded that oxidizing storage of coal at high temperatures for short periods of time and at lower temperatures for longer periods of time resulted in similar chemically altered compositions.

No significant changes were observed in petrographic characteristics of coals that had been exposed to air at room temperature over 13 months in Experiment 1. Vitrinite reflectance is only affected by oxidation at higher temperatures (Bend and Kosloski, 1993; Chandra, 1962) and by rank increase (Mastalerz and Bustin, 1993). The increase in temperature of exposure for Experiments 2 and 3 was not high enough to modify the vitrinite reflectance value. Vitrinite reflectance values of coals from Experiments 1, 2 and 3 range narrowly between 0.62 and 0.63%.

7.4.2. Changes in physical properties

Experiments 2 and 3 suggest that some changes in coal's physical properties occur as a result of oxidative storage at temperatures above 30°C. Most noticeably, BET surface areas calculated from nitrogen adsorption were reduced with increasing thermal exposure (Figure 5A) and mesopore widths increased (Figure 5C). These changes are directly related to micropore characteristics calculated from CO₂ adsorption data of Experiments 1, 2 and 3, where consistent increases were observed for BET surface areas (Figure 10A), D-R surface areas (Figure 10B), and D-R monolayer capacities (Figure 10C). These results agree with the conclusion of Pis *et al.* (1996) that oxidation enhances porosity and surface area, but the extent of enhancement depends on the degree of oxidation.

The differences in porosity and surface area between (1) coal in Experiment 1 that had been exposed to air at room temperature for up to 13 months and (2) coals that had been exposed to higher air temperatures in Experiments 2 and 3 suggest an origin due to increased reactivity of coal with atmospheric oxygen at increased temperatures (Figures 8, 14, and 20).

The changes in pore characteristics in Experiments 2 and 3 at elevated temperatures (up to 100°C) support the hypothesis that plasticity of coal is reduced as a result of oxidation. Similar results were obtained by Huffman *et al.* (1985), who investigated the effects of artificial oxidation and weathering during stockpiling of high- and low-volatile bituminous coals. Pis *et al.* (1996) concluded that the rate of oxidation decreases with increasing particle size because larger diameters slow the diffusional transport of oxygen

into the coal's interior. They also concluded that oxidation can eliminate plasticity from bituminous coals.

Martínez and Escobar (1995) studied Venezuelan coals ranging in rank from peat to high volatile C bituminous coal and observed that chemical weathering caused an increase in water absorption capacity. However, they did not find a correlation between moisture increase and the degree of weathering. Likewise, observations from this study suggest that moisture loss occurs as a result of drying during storage, but no correlation is apparent between the oxygen content in coal and the extent of oxidation or chemical weathering in the laboratory. In a similar study, Kaji *et al.* (1986) observed no correlation between water-holding capacity and pore volume in coal, and no correlation between the water-holding capacity and the ash content of various rank coals ranging from lignite to anthracite. However, they found that equilibrium moisture increased in proportion to the number of oxygen-containing functional groups on the coal surface.

McCutcheon and Wilson (2003) investigated the influence of moisture content on low-temperature oxidation of bituminous coals. They identified two types of water associated with the coals, namely (1) chemically bound water and (2) physically adsorbed free water. They also concluded that an increase in the abundance of carbonyl (CO) functional groups was apparent only after wetting the coal following oxidation in a humid atmosphere. Their experimental study revealed that exposure of coal to hydrogen peroxide reduced subsequent water uptake. Their experiments with dry oxygen showed reduced water uptake compared with that from oxidation with humid air.

7.4.3. Effects of air exposure on gas adsorption characteristics in coal

Mavor *et al.* (1990) reported that oxidation can reduce the sorption capacity of coal by as much as 11%. Our air exposure Experiments 2 and 3 suggest a reduction for nitrogen adsorption (Figures 8 and 9), but an opposite trend for CO₂ adsorption (Figures 14 and 15). Additional sorption of CO₂ occurs on the increased surface area of micropores (Figure 16).

Data from Experiment 1 at room temperature, however, only show a significant decrease in nitrogen adsorption capacity with prolonged exposure of coal to air (Figure 6), consistent with a decrease in cumulative mesopore volume (Figure 7). Our observations from low-pressure CO₂ adsorption in Experiment 1 over 13 months of exposure to oxidizing air in the laboratory do not reflect a significant gain in adsorption potential at the micropore scale.

The differences noted between the oxidation at temperatures above 21°C (Experiments 2 and 3) and at room temperature (Experiment 1) suggest that oxidation does not play a significant role in adsorption characteristics. Instead, it is hypothesized that moisture loss has a more important role and that exposure-related changes in adsorption characteristics result mostly from the drying of coal.

7.4.4. Changes in the abundance of chemical functional groups

The effects of low-temperature oxidation on the chemical distribution of functional groups in coal have been investigated with FTIR on numerous occasions (Anderson and Johns, 1986; Cagigas *et al.*, 1987; Fredericks *et al.*, 1983; Huffman *et al.*, 1985; Huggins *et al.*, 1987; Jakab *et al.*, 1988; Landais *et al.*, 1984; Painter *et al.*, 1980, 1981; Pisupati

and Scaroni, 1993; Rhoads *et al.*, 1983; Wu *et al.*, 1988). All these studies observed a decrease in absorbance related to aliphatic stretching and an increase in carbonyl and carboxylate groups. Investigations on the effects of coal oxidation at higher temperatures also observed the occurrence of esters, ketones and anhydrides in addition to carbonyl and carboxylate groups (Calemma *et al.*, 1988; Calemma *et al.*, 1995; Gentzis *et al.*, 1992; Kister *et al.*, 1988). Two studies used micro-FTIR to investigate the chemistry and influence of oxidation on maceral composition (Landais and Rochdi, 1993; Mastalerz and Bustin, 1993). The effects of photo-oxidation of coals under controlled laboratory conditions were studied by Michell *et al.* (1995) and Pradier *et al.* (1992). All these studies arrived at similar conclusions with regard to functional group abundance in coals and suggested that an increase in carbonyl/carboxylate groups results from oxidation.

Apparently the achieved degree of oxidation was insufficient in Experiments 1, 2 and 3 in this study to result in significant FTIR absorption changes that would mirror formation of oxygen-containing functional groups. Instead, the data suggest that changes in coal chemistry are mainly associated with the loss of moisture throughout exposure to air rather than via oxidation. Figure 21 displays the ratios of selected functional groups that have been considered diagnostic for oxidation in previous studies (i.e., Huggins *et al.*, 1987; Wu *et al.*, 1988). The observed non-systematic variations of these indices suggest that oxidation did not play a significant role during exposure to air for up to 13 months at room temperature (Experiment 1) or during exposure at 75°C for 10 days (Experiment 2). Experiment 3 indicated less pronounced changes than Experiment 2, therefore, oxidation did not affect these samples with increasing temperature of up to 100°C for 10 days.

7.4.5. Implications for CO₂ sequestration in coal

Sequestration of carbon dioxide in coal seams may serve as a geologic sink to reduce the emission of anthropogenic carbon dioxide into the atmosphere and to mitigate the impact of fossil fuel burning on global climate change. The experimental data gathered in this study have relevance from the perspective of CO₂ sequestration because gas adsorption mechanisms ultimately control the potential capacity of coal to sequester carbon dioxide.

Several experiments are being conducted in laboratories worldwide to quantify the CO₂ adsorption capacity of coals at subcritical and supercritical conditions. Although this study is limited to low-pressure gas adsorption characteristics, its results point to coal sample preservation as a critical aspect for adequate adsorption capacity testing in laboratories.

Our data suggest that oxidation is not detrimental for the physical and chemical properties of high volatile bituminous coal stored in air for prolonged periods of time at low to moderate temperatures. Moisture content, on the other hand, seems to exert an important control on the physical and chemical properties of coal that are critical for industrial processes and gas adsorption potential.

Changes in gas adsorption characteristics resulting from external factors rather than intrinsic coal properties, are still a matter of debate, for example the effects of crushing and grinding of coals to enhance diffusional transport during gas adsorption experiments. Additional experiments are needed to study gas adsorption characteristics in well-preserved coal samples under high-pressure conditions in the laboratory and *in situ* in

coal seams. Chapter 8 will address high-pressure testing of coals under different preservation conditions.

7.5. Conclusions

A correlation exists between moisture loss and the decrease of calorific value in coal during oxidative storage in air at low temperature in the laboratory. No correlation is evident between exposure to air at room temperature (21°C) and the oxygen content in coal. Drying of coal over the duration of coal storage reduces moisture content, adsorption capacity for nitrogen, and mesopore surface area available for gas adsorption. At the same time, drying increases the surface area of micropores and the CO₂ adsorption potential in coal.

Adequate preservation of freshly mined or cored coal samples is critical for accurate assessment of resource gas-in-place evaluations, and therefore, for estimating the adsorption potential for applications such as CO₂ sequestration.

References

- Anderson, K.B., Johns, R.B., 1986. Oxidation studies of Australian coals – I. Aliphatic and aromatic hydrocarbon centres of oxidative attack. *Organic Geochemistry* 9, 219-224.
- ASTM, 2006. Annual Book of ASTM Standards. Section Five: Petroleum Products, Lubricants, and Fossil Fuels. Gaseous Fuels; Coal and Coke. West Conshohocken, PA, 05.06, 705 pp.
- Bend, S.L., Kosloski, D.M., 1993. A petrographic examination of coal oxidation. *International Journal of Coal Geology* 24, 233-243.
- Busch, A., Gensterblum, Y., Krooss, B.M., Littke, R., 2004. Methane and carbon dioxide adsorption-diffusion experiments on coal: upscaling and modeling. *International Journal of Coal Geology* 60, 151-168.
- Cagigas, A., Escudero, J.B., Low, M.J.D., Pis, J.J., Tascon, J.M.D., 1987. A comparison of various characterization techniques for low-temperature oxidation of coal. *Fuel Processing Technology* 15, 245-256.
- Calemma, V., Rausa, R., Margarit, R., Girardi, E., 1988. FTIR study of coal oxidation at low temperature. *Fuel* 67, 765-769.
- Calemma, V., del Piero, G., Rausa, R., Girardi, E., 1995. Changes in optical properties of coal during air oxidation at moderate temperature. *Fuel* 74, 383-388.
- Chandra, D., 1962. Reflectance and microstructure of weathered coals. *Fuel* 41, 185-193.

- Clarkson, C.R., Bustin, R.M., 1996. Variation in micropore capacity and size distribution with composition in bituminous coal of the western Canadian sedimentary basin. *Fuel* 75, 1483-1498.
- Crelling, J.C., Schrader, R.H., Benedict, L.G., 1979. Effects of weathered coal on coking properties and coke quality. *Fuel* 58, 542-546.
- Fredericks, P.M., Warbrooke, P., Wilson, M.A., 1983. Chemical changes during natural oxidation of a high volatile bituminous coal. *Organic Geochemistry* 5, 89-97.
- Gentzis, T., Goodarzi, F., McFarlane, R.A., 1992. Molecular structure of reactive coals during oxidation, carbonization and hydrogenation – an infrared photoacoustic spectroscopic and optical microscopic study. *Organic Geochemistry* 18, 249-258.
- Gray, R.J., Rhoades, A.H., King, D.T., 1976. Detection of oxidized coal and the effect of oxidation on the technological properties. *Transactions of the Society of Mining Engineers* 260, 334-341.
- Huffman, G.P., Huggins, F.E., Dunmyre, G.R., Pignocco, A.J., Lin, M.-C., 1985. Comparative sensitivity of various analytical techniques to the low-temperature oxidation of coal. *Fuel* 64, 849-856.
- Huggins, F.E., Huffman, G.P., Dunmyre, G.R., Nardozi, M.J., Lin, M.C., 1987. Low-temperature oxidation of bituminous coal: Its detection and effect on coal conversion. *Fuel Processing Technology* 15, 233-244.
- Jaakab, E., Hoesterey, B., Windig, W., Hill, G.R., Meuzelaar, H.L.C., 1988. Effects of low temperature air oxidation (weathering) reactions on the pyrolysis mass spectra of US coals. *Fuel* 67, 73-79.

- Kabe, T., Ishihara, A., Quian, E.W., Sutrisna, I.P., Kabe, Y., 2004. Coal and Coal-Related Compounds. Structures, Reactivity, and Catalytic Reactions. In: Delmon, B., Yates, J.T., Centi, G. (Eds.). Studies in Surface Science and Catalysis 150, Kodansha Ltd., Tokyo, 341 p.
- Kaji, R., Hishinuma, Y., Nakamura, Y., 1985. Low temperature oxidation of coals. Effects of pore structure and coal composition. *Fuel* 64, 297-302.
- Kaji, R., Muranaka, Y., Otsuka, K., Hishinuma, Y., 1986. Water absorption by coals: effects of pore structure and surface oxygen. *Fuel* 65, 288-291.
- Kister, J., Guiliano, M., Mille, G., Dou, H., 1988. Changes in the chemical structure of low rank coal after low temperature oxidation or demineralization by acid treatment. *Fuel* 67, 1076-1081.
- Landais, P., Monthieux, M., Meunier, J.D., 1984. Importance of the oxidation/maturation pair in the evolution of humic coals. *Organic Geochemistry* 7, 249-260.
- Landais, P., Rochdi, A., 1993. In situ examination of coal macerals oxidation by micro-FT-ir spectroscopy. *Fuel* 72, 1393-1401.
- Liotta, R., Brons, G., Isaacs, J., 1983. Oxidative weathering of Illinois No. 6 coal. *Fuel* 62, 781-791.
- Lis, G.P., Mastalerz, M., Schimmelmann, A., Lewan, M.D., Stankiewicz, B.A., 2005. FTIR absorption indices for thermal maturity in comparison with vitrinite reflectance R_o in type-II kerogens from Devonian black shales. *Organic Geochemistry* 36, 1533-1552.

- Lowenhaupt, D.E., Gray, R.J., 1980. The alkali-extraction test as a reliable method of detecting oxidized metallurgical coal. *International Journal of Coal Geology* 1, 63-73.
- Ludvig, M.M., Gard, G.L., Emmett, P.H., 1983. Use of controlled oxidation to increase the surface area of coal. Applications to a bituminous and a semi-anthracite coal. *Fuel* 62, 1393-1396.
- McCutcheon, A.L., Wilson, M.A., 2003. Low-temperature oxidation of bituminous coal and the influence of moisture. *Energy & Fuels* 17, 929-933.
- Marchioni, D.L., 1983. The detection of weathering in coal by petrographic, rheologic and chemical methods. *International Journal of Coal Geology* 2, 231-259.
- Martínez, M., Escobar, M., 1995. Effect of coal weathering on some geochemical parameters. *Organic Geochemistry* 23, 253-261.
- Mastalerz, M., Bustin, R.M., 1993. Variation in maceral chemistry within and between coals of varying rank: an electron microprobe and micro-Fourier transform infrared investigation. *Journal of Microscopy* 171, 153-166.
- Mavor, M.J., Nelson, C.R., 1997. Coalbed Reservoir Gas-In-Place Analysis, Chapter 3. Gas Research Institute, Report No. GRI-97/0263, Chicago, Illinois.
- Mavor, M.J., Owen, L.B., Pratt, T.J., 1990. Measurement and evaluation of coal sorption isotherm data. *Society of Petroleum Engineers SPE* 20728, 157-170.
- Mitchell, G.D., Davis, A., Chander, S., 2005. Surface properties of photo-oxidized bituminous vitrains. *International Journal of Coal Geology* 62, 33-47.
- Painter, P.C., Snyder, R.W., Pearson, D.E., Kwong, J., 1980. Fourier transform infrared study of the variation in the oxidation of a coking coal. *Fuel* 59, 282-286.

- Painter, P.C., Coleman, M.M., Snyder, R.W., Mahajan, O., Komatsu, M., Walker, P.L. Jr., 1981. Low temperature air oxidation of caking coals: Fourier transform infrared studies. *Applied Spectroscopy* 35, 106-110.
- Pis, J.J., Centeno, T.A., Mahamud, M., Fuertes, A.B., Parra, J.B., Pajares, J.A., Bansal, R.C., 1996. Preparation of active carbons from coal. Part I. Oxidation of coal. *Fuel Processing Technology* 47, 119-138.
- Pisupati, S.V., Scaroni, A.W., 1993. Natural weathering and laboratory oxidation of bituminous coals: organic and inorganic structural changes. *Fuel* 72, 531-542.
- Pradier, B., Landais, P., Rochdi, A., Davis, A., 1992. Chemical basis of fluorescence alteration of crude oils and kerogens – II. Fluorescence and infrared micro-spectrometric analysis of vitrinite and liptinite. *Organic Geochemistry* 18, 241-248.
- Rhoads, C.A., Senftle, J.T., Coleman, M.M., Davis, A., Painter, P.C., 1983. Further studies of coal oxidation. *Fuel* 62, 1387-1392.
- Schafer, H.N.S., 1972. Factors affecting the equilibrium moisture contents of low-rank coals. *Fuel* 51, 4-9.
- Sing, K.S.W., Everett, D.H., Haul, R.A.W., Moscou, L., Pierotti, R.A., Rouquérol, J., Siemieniewska, T., 1985. Reporting physisorption data for gas/solid systems with special reference to the determination of surface area and porosity (IUPAC Recommendations 1984). *Pure & Applied Chemistry* 57, 603-619.
- Solomon, P.R., Carangelo, R.M., 1988. FT-ir analysis of coal. 2. Aliphatic and aromatic hydrogen concentration. *Fuel* 67, 949-959.

- Taraba, B., Dobal, V., Čáp, K., Harašta, M., 1988. Differentiation of thermal effects during low temperature oxidation of coal. *Fuel* 67, 758-763.
- Walker, R., Mastalerz, M., 2004. Functional group and individual maceral chemistry of high-volatile bituminous coals from southern Indiana: controls on coking. *International Journal of Coal Geology* 58, 181-191.
- Webb, P.A., Orr, C., 1997. *Analytical Methods in Fine Particle Technology*. Micromeritics Instrument Co., Norcross, GA, USA.
- Wu, M.M., Robbins, G.A., Winschel, R.A., Burke, F.P., 1988. Low-temperature coal weathering: its chemical nature and effects on coal properties. *Energy & Fuels* 2, 150-157.

CHAPTER 8

Effects of grain size, maceral composition, and moisture content on adsorption characteristics of bituminous coals

8.1. Introduction

The concept of using coal seams as geological receptacles to permanently sequester CO₂ underground, reduce anthropogenic atmospheric carbon dioxide emissions, and mitigate the greenhouse effect has spawned multiple recent studies about the selectivity of coal to adsorption of single gases and gas mixtures. An additional motivation to study gas-adsorption in coal is the economic advantage of extracting methane from coal (coalbed methane, CBM) and to inject carbon dioxide into CBM-containing coals for enhanced CBM recovery (CO₂-ECBM).

Most adsorption studies focused on establishing the maximum gas retention capacity of coals and *in situ* gas saturation at reservoir conditions. Knowing the maximum amount of gas that a coal can adsorptively store allows us to calculate the theoretical gas volumes available for CBM production and for CO₂ storage. Some studies have also modeled the displacement of methane by injection of CO₂, in a process called CO₂-ECBM enhanced recovery, where carbon dioxide is sequestered while methane is simultaneously being desorbed and produced (Busch *et al.*, 2007; Mazumder *et al.*, 2003; Mazumder *et al.*, 2006; van Bergen *et al.*, 2003). Adequate assessment of coal-gas resources requires that all experiments be performed under conditions that resemble *in situ* reservoir conditions.

The amount of gas that can be recovered from coal or adsorbed/captured in coal depends on the temperature and pressure of the reservoir (Mavor *et al.*, 1990; Pashin and McIntyre, 2003; Saunders *et al.*, 1985; Scott *et al.*, 1994). The presence of extractable gas from coal manifests itself in two ways. First, gas can be physically adsorbed on the coal surface which includes the walls of a widespread network of passageways and

interconnected pores within the coal's sieve-like macromolecular network. In this case, gases are held to the coal surface by van der Waals forces of attraction (Bachu and Michael, 2003; Clarkson and Bustin, 1996; Crosdale *et al.*, 1998; Dubinin, 1960; Goodman *et al.*, 2005; Levy *et al.*, 1997; White *et al.*, 2003; Yee *et al.*, 1993). Second, free gas can be present in fractures, pores, and dissolved in formation water, but not physically attached to the coal structure.

Complex sorption theories developed early in the twentieth century explain sorption mechanisms in coal (Brunauer *et al.*, 1938; Brunauer *et al.*, 1940; Dubinin, 1960; Langmuir, 1918; Low, 1960; Slater and Kirkwood, 1931). Graphical adsorption isotherms illustrate the theoretical relationship between relative amounts of gas adsorbed onto a surface at constant temperature and variable pressure (Figure 1).

Although the mechanisms of gas adsorption in coal have been extensively studied in the laboratory, significant differences in the saturation of measured gas from field operations suggest that our understanding of gas sorption in the subsurface is still fragmentary. For example, the influence of particle size, coal composition, moisture, lithology, fracturing, and tectonic regime on gas sorption in coal is still unclear.

This chapter explores the relationships between particle size, equilibrium moisture, coal composition, and gas adsorption with data from laboratory experiments. Adsorption data include low-pressure adsorption isotherms from an automatic device to quantify adsorption (Micromeritics ASAP-2020, as described in the methods section of Chapter 7) and high-pressure adsorption measurements derived from two volumetric adsorption apparatuses. One such apparatus (used for in-house measurements) was designed and custom-built with the technical advice of the mechanical instrument services section of

the Department of Chemistry at Indiana University. Additional measurements were obtained from a specialized commercial laboratory (RMB Earth Science Consultants Ltd.).

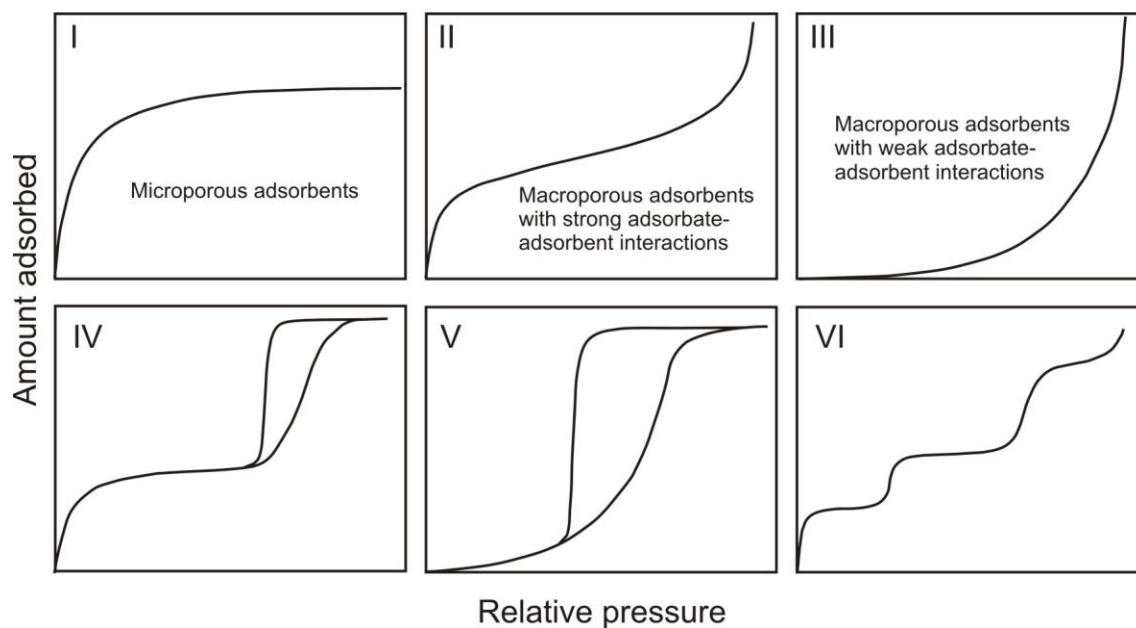


Figure 1. Experimental adsorption isotherm classification according to Sing *et al.* (1985). Type I isotherms are characteristic of microporous adsorbents for subcritical, near-critical, and supercritical conditions. Type II represents adsorption on non-porous or macroporous adsorbents with strong gas adsorption affinities. Type III (not common) represents the adsorption on macroporous adsorbents with weak gas adsorption affinities. Types IV and V represent adsorption on mesoporous adsorbents with strong (for mesoporous industrial adsorbents) and weak (uncommon) gas adsorption affinities. Both types exhibit adsorption hysteresis at low temperatures. Type VI is characteristic for multilayer adsorption on a uniform non-porous surface.

8.1.1. Influence of particle size on CO₂ and CH₄ sorption in coal

High-pressure gas adsorption analyses in coal are typically performed on crushed material (<60 mesh \approx 250 μ m diameter) in order to minimize the time of internal diffusion through the coal matrix (Mavor *et al.*, 1990). Mavor *et al.* (1990) suggested that crushing increases the surface area by 0.1 to 0.3%, but that this does not greatly affect the determination of gas storage capacity. Uncertainty remains about the net effect of particle size distribution on gas adsorption, and whether all pores in coal are accessible to gas in the reservoir. Results from adsorption experiments show that high-pressure adsorption isotherms in coal can be modeled using the Type-I Langmuir isotherm (Busch *et al.*, 2003a, b; Ceglarska-Stefanska, 2002; Clarkson and Bustin, 1999a; Clarkson and Bustin, 1999b; Clarkson and Bustin, 2000; Cui *et al.*, 2004; Krooss *et al.*, 2002; Levy *et al.*, 1997; Mavor *et al.*, 1990).

Few studies evaluated the effects of particle size in relation to adsorption and diffusion in coal (Busch *et al.*, 2004; Cloke *et al.*, 2002; Nandi and Walker, 1975; Siemons *et al.*, 2003). Nandi and Walker (1975) suggested that grinding creates additional macropores and cracks that affect diffusion characteristics in coal. In a study of kinetics and gas adsorption, Siemons *et al.* (2003) found that particle size cannot serve as a reliable predictor for adsorption capacity. They found that the adsorption capacity with regard to methane increased with increasing grain size of dry coal, but the adsorption capacity for carbon dioxide did not follow the same pattern. The study of Siemons *et al.* (2003) also observed that sorption rates remained approximately constant when coal particle diameters were larger than about 0.5 to 1.0 mm.

Busch *et al.* (2003a, b, 2004) experimented with a crushed coal of Pennsylvanian age from the Upper Silesian Basin in Poland ($R_o = 0.8 - 0.9\%$). Sieving of this coal produced six different grain size fractions that were measured separately in an adsorption apparatus. As expected, adsorption rates from their experiments indicated fastest equilibration for the smallest particle size. However, some variations in the shapes of adsorption isotherms were attributed to maceral fractionation during sieving (Busch *et al.*, 2004). Cloke *et al.* (2002) noticed the same fractionation effects in their study of size fractions from ten coals worldwide.

Although some studies investigated the effect of particle size on gas adsorption, the net effect of particle size with regard to surface area and its adsorptive characteristics remains poorly understood. This chapter aims to provide additional data to improve the understanding of high-pressure adsorption in relation to particle size distribution. Additional laboratory research will be needed to fully understand this physical process and to improve the quality of predictions for the occurrence and storage of gas in coal seams.

8.1.2. Influence of coal type on CO_2 and CH_4 sorption

Coal maceral composition influences grain-size distribution, pore structure of coal, and therefore coal's potential gas adsorption capacity (Clarkson and Bustin, 1996). Results from several investigations suggest a correlation between pore distribution and coal rank (Gamson *et al.*, 1993; Gan *et al.*, 1972; Medek, 1977; Olague and Smith, 1989; Toda *et al.*, 1971; Unsworth *et al.*, 1989; Walker *et al.*, 1988; Zwietering and van Krevelen, 1954).

Although there is no direct evidence for the influence of maceral composition on gas adsorption in coal, some authors observed a correlation between vitrinite content and the < 2 nm microporous structure (Clarkson and Bustin, 1996; Crosdale *et al.*, 1998; Karacan and Mitchell, 2002; Karacan and Mitchell, 2003; Lamberson and Bustin, 1993; Mastalerz *et al.*, 2004). Vitrinite-rich coals exhibit greater microporosity than other coals with different maceral composition (e.g., inertinite-, and liptinite-rich coals) leading to larger gas adsorption capacities in vitrinite-rich lithotypes (Clarkson and Bustin, 1996; Crosdale *et al.*, 1998; Lamberson and Bustin, 1993).

Analysis of the relationship between gas adsorption capacity and the fixed carbon content of coals (on a dry ash-free basis, daf, in weight %) suggests a graphically concave distribution with minimum values in the vicinity of 80 wt. % fixed carbon (Levy *et al.*, 1997). A similar trend was observed in Turkish coals of the Zonguldak basin (Gurdal and Yalcin, 2001) for relationships between micropore capacity (cm^3/g , daf) and rank (expressed in terms of vitrinite reflectance R_o in %), and also between Langmuir monolayer volumes (cm^3/g , daf) and rank (R_o %) where Langmuir monolayer volume minimum values occur at $R_o = 1.0\%$.

It has been noted that bright, vitrinite-rich coals adsorb greater amounts of gas than dull, inertinite-rich coals (Crosdale *et al.*, 1998), although the opposite adsorption behavior had been reported earlier by Ettinger *et al.* (1966). However, the latter study may have inadvertently introduced a bias by using hand-picked specimens of vitrinite- and fusinite-rich coals. In some coals, semifusinites express larger surface areas, enhanced microporosity, and larger adsorption capacity relative to other macerals (Lamberson and Bustin, 1993). Crossdale *et al.*, (1998) found that gas desorption rates

vary between bright and dull coals. Bright specimens usually have lower gas desorption rates in response to their highly microporous structure (Crosdale *et al.*, 1998).

A complete understanding of the gas-adsorptive differences between bright versus dull coal types remains elusive. In this study, high-pressure adsorption experiments were conducted on different coal lithotypes that had been characterized in terms of petrographic maceral composition and chemical proximate and ultimate analyses. A comparison of experimental data from this work provides insight into the adsorption behavior of different Indiana coals. This study also aims to help elucidate the variability in adsorption characteristics observed for high volatile bituminous coals (Gurdal and Yalcin, 2001; Levy *et al.*, 1997; Mastalerz *et al.*, 2004).

8.1.3. Effects of moisture content on gas sorption in coal

Some physical parameters such as temperature and pressure can be easily simulated in the laboratory, whereas it is difficult to simulate reservoir moisture conditions. The estimation of moisture content in coal is of particular importance because ‘in situ’ coals are usually saturated with water that competes with gases for adsorption sites. Some methodological procedures have been proposed (e.g., ASTM method D1412 and the improved method of Testa and Pratt, 2003) to account for the role of coal moisture in gas adsorption. Additional laboratory protocols have been recommended to obtain adequate adsorption data from moisture equilibrated samples (e.g., Hartman and Pratt, 2005; Pratt and Baez, 2003).

Taylor *et al.* (1998) showed a decrease in moisture content in coal with an increase in carbon content (wt. %), and with increasing coal depth. These observations confirm the

relation between moisture content and coal rank. Although a correlation between coal's maceral composition and moisture content is expected, Unsworth *et al.* (1989) reported that inertinite-rich and vitrinite-rich coals of the same rank contain approximately the same pore-held moisture. Variations in moisture content have a significant effect on gas adsorption capacity (Bustin and Clarkson, 1998; Krooss *et al.*, 2002; Levy *et al.*, 1997; Yee *et al.*, 1993). These studies also indicate that an increase in moisture content correlates with a decrease in methane adsorption capacity.

8.2. Methods

8.2.1. Experimental approach, coal selection, and sample preparation

High-pressure adsorption isotherm analyses were performed on multiple coal samples to evaluate the effects of storage in laboratory air on adsorption capacity. A sample from the Lower Block Coal Member (Billings Mine, Daviess County, Indiana) was crushed to <3 mm in diameter. The resulting mixture of grain sizes was stirred thoroughly to obtain a relatively homogenous batch of crushed coal. Aliquots of this coal mixture were tested repeatedly using two high-pressure volumetric adsorption instruments, one at Indiana University (small-volume high-pressure adsorption apparatus) and one from a commercial laboratory located at British Columbia, Canada (RMB Earth Science Consultants, Ltd.). High pressure adsorption isotherms were gathered to estimate the coal's adsorption capacity. The resulting data complement those discussed in Chapter 7, where the same coal samples were characterized in low-pressure adsorption experiments in order to measure the effects of oxidative storage on pore characteristics.

Table 1 shows the data from high-pressure adsorption analyses collected at Indiana University and through RMB Earth Science Consultants, Ltd. Two aliquots of the crushed coal from the Lower Block Coal Member had been exposed to laboratory air at room temperature for 10 months and 13 months (i.e., samples '10 months' and '13 months'). Sample 'zero months' corresponds to a split of the freshly mined coal that had been stored under nitrogen in a leak-proof desorption canister (Mavor and Nelson, 1997) and represented "zero exposure coal". These three coals were tested for high-pressure adsorption characteristics at RMB Earth Science Consultants, Ltd.

In addition to Lower Block coal from Billings Mine, other Indiana coal samples were tested under dry and moisture-equilibrated conditions to assess the effect of moisture content on the quality of adsorption data. Coal samples weighing >120 grams were divided into two aliquots, followed by high-pressure adsorption measurements of one air-dried aliquot, whereas the second aliquot was analyzed after moisture-equilibration with water vapor using the conventional ASTM D-1412 protocol (ASTM, 2006). This approach allowed comparing adsorption capacities for dry versus moisture-equilibrated coals.

To attain equilibrium-moisture, pre-wetted samples (using distilled water) were placed in a vacuum-type desiccator containing a saturated solution of potassium sulfate K_2SO_4 which allows maintaining a relative humidity of 96 to 97%. The desiccator was partially evacuated to a gas pressure of 30 mm Hg. Samples were kept for at least two weeks at room temperature before adsorption measurements. A fraction of each coal sample (0.2 g) was removed from the desiccator, weighed, placed in an oven at 105°C for

1½ hours and re-weighed. The equilibrium moisture in weight % was calculated using the following Equation 1

$$\text{Equilibrium moisture (\%)} = \frac{(B - C)}{(B - A)} \times 100 \quad \text{Equation 1}$$

where A = weight of empty dish, B = weight of dish and wet coal, and C = weight of dish and dried coal.

Additional samples corresponding to various coal seams from Indiana were selected for various analyses. These samples were collected and kept stored in closed plastic containers at the Indiana Geological Survey coal laboratory. These samples were previously crushed to less than 3 mm diameter and analyzed for proximate and ultimate chemical analyses at Standard Laboratories, Inc., in Evansville, Indiana. Twelve coal samples (including the Billings Mine sample described above) were selected for analyses of grain size, petrography, and low-pressure adsorption analyses using the Micromeritics ASAP-2020 instrument described in Chapter 7. Among these samples, a few were selected to investigate their relationship between maceral composition, grain size and adsorption capacity. Most coal samples used in this study were selected to reflect a wide compositional variability, ranging from bright to dull coals. One additional sample was gathered from a drilling core from Sullivan County, Indiana, but its petrographic composition was not determined in this study (sample 13. 20052770-T31). Table 2 includes all experimental and laboratory data from analyses.

Table 1. High-pressure adsorption analyses performed on coal samples to investigate the effects of moisture content and exposure to air at room temperature on adsorption capacity.

Experimental apparatus	Sample condition	High-pressure experiments: Timing of analyses (consecutive months)													
		0	1	2	3	4	5	6	7	8	9	10	11	12	13
Analyses at Indiana University	Dry														
	Moisture-equilibrated														
Analyses by RMB Earth Science Consultants, Ltd.	Moisture-equilibrated														

 Data available

 No data

Table 2. Inventory of laboratory analyses that were performed on selected Indiana coal samples. The sequence of samples is arranged by coal member in stratigraphic order.

Sample No.	Coal Member	County	Petrography	Grain size data	Low-pressure adsorption		High-pressure adsorption			
					Nitrogen	CO ₂	CH ₄		CO ₂	
							Dry	Moisture-equilibrated	Dry	Moisture-equilibrated
1. 20011113-A2	Springfield	Warrick								
2. 20011113-A6	Springfield	Warrick								
3. 20031009-1	Springfield	Gibson								
4. 20031009-2	Springfield	Gibson								
5. 20031009-3	Springfield	Gibson								
13. 20052770-T31	Seelyville	Sullivan								
6. 20040428-C1	Buffaloville	Daviess								
7. 20040428-C3	Buffaloville	Daviess								
8. 20040428-B1	Upper Block	Daviess								
9. 20040428-B2	Upper Block	Daviess								
10. Billings	Lower Block	Daviess								
11. 20040428-A2	Lower Block	Daviess								
12. 20040428-A3	Lower Block	Daviess								

 Data available

 No data

8.2.2. Preparation of grain size fractions and petrographic characterization

Twelve coal samples were selected that had been crushed to diameters of < 3 mm (samples 1-12 in Table 2). Sieving produced five grain size fractions, namely > 1.19 mm, 1189-840 μm , 839-595 μm , 594-250 μm , and < 250 μm . Each fraction was homogenized and split in two aliquots for high-pressure adsorption analyses, one for dry conditions, and one for moisture-equilibrated conditions. The individual grain size aliquots were normalized to 100 percent by weight for comparison purposes. Petrographic data on the 12 bulk crushed coals were gathered using the methodology described in Chapter 7 (Section 7.2.3).

8.2.3. High-pressure adsorption analysis

8.2.3.1. Instrumentation

There are only few laboratories worldwide generating high-pressure adsorption coal isotherm data from custom-built instrumentation. Generally these laboratories are supplying contract services for industry that can afford expensive analyses. The high costs involved in sample preparation and data acquisition make it financially challenging for academic laboratories to engage in coal adsorption research. Therefore, a high-pressure instrument for volumetric measurement of gas adsorption characteristics in crushed coal was designed and custom-built in the Department of Geological Sciences at Indiana University.

Our small-volume high-pressure volumetric adsorption apparatus is a modification of the isotherm experimental apparatus of Mavor *et al.* (1990) and consists of four identical stainless steel pressure test cells of ~ 200 mL that are connected through the main gas-

feed line to a buffer volume in the form of a 75 mL stainless steel pressure flask (Figure 2). All test cells and the buffer volume are housed in a temperature-controlled water bath with heating and cooling units (Figure 3a) to keep the system isothermal at subambient to elevated temperatures for mimicking coal seam temperatures in the subsurface. Three gas cylinders with compressed helium (He), CO₂, and CH₄ are connected in parallel to the main feeder valve. Helium is used to leak-check the system by running tests at higher pressures than required for experiments with CO₂ and CH₄.

This study used only pure methane or pure carbon dioxide to characterize the adsorption behavior of coals, but the instrument can utilize any other gas or a combination of gases. The purpose of the buffer volume is to allow compressed gas to attain thermal equilibrium with the water bath before the gas is expanded into individual test cells. The individual internal volumes of all test cells were measured multiple times for calibration. Two test cells serving as reference cells do not receive coals. Instead, their internal volumes are reduced by containing steel billets with known non-compressible volume, zero porosity, and a negligible surface adsorption capacity. The smaller volumes of reference cells allow precise calibration of sample and void volumes that are needed to calculate adsorption characteristics in test cells containing coal.

Components of the small-volume high-pressure volumetric adsorption apparatus were constructed by the mechanical instrument services in the Department of Chemistry at Indiana University. Tubing, pressure fittings, and high-pressure gauges were selected to safely exceed the requirements for maintaining experimental pressures and to guarantee the integrity of the system at high pressures. Pressure integrity of the system was a priority because accidental venting of flammable methane poses a fire and

explosion hazard, and vented carbon dioxide can cause asphyxiation. This instrument is housed within a vented fume hood in compliance with standard safety regulations for handling flammable gases at Indiana University.

The small-volume high-pressure volumetric adsorption apparatus can simultaneously measure gas adsorption characteristics of two coal samples. All test cells are fitted with electronic pressure transducer sensors that are connected to a National InstrumentsTM data acquisition board. Calibrated pressure readings are sent in real time to a computer where all data are processed using Labview 8.0TM software. A user-defined program interface was adapted for data acquisition and display purposes. Labview 8.0TM software also allows parallel collection of data from a second instrument in the laboratory that is designed to characterize high-pressure gas adsorption in segments of uncrushed coal cores (Figure 3b).

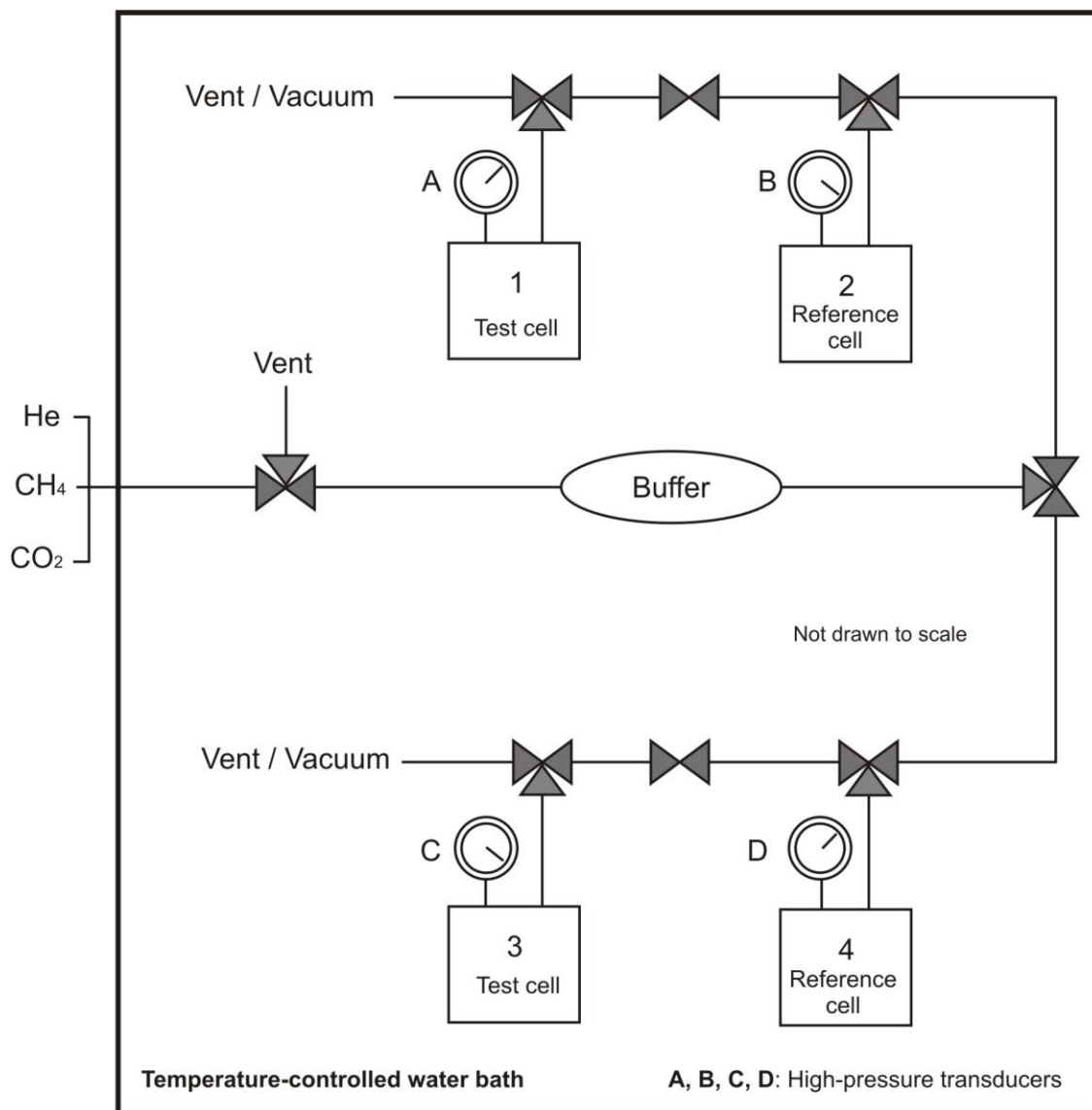


Figure 2. Experimental design of the small-volume high-pressure volumetric adsorption apparatus that uses crushed coal in two test cells (1, 3) in comparison with two calibrated reference cells (2, 4).

The small-volume high-pressure volumetric adsorption apparatus was designed to characterize the isothermal gas adsorption characteristics of crushed coal at high-pressure conditions. Data gathered from this apparatus are typically represented as adsorption isotherms. Adsorption isotherms are conventionally used to quantify the gas adsorption capacity of coal relative to the hydrostatic gas pressure (e.g., reservoir pressure).

A large-volume high-pressure volumetric adsorption apparatus with a single 2.55 L (2,545.8 mL) stainless steel pressure vessel was designed and constructed to test adsorption in both crushed coal and uncrushed coal core segments. Adsorption characteristics of uncrushed coal should approach *in situ* natural reservoir conditions even more than adsorption characteristics of crushed coal. Technical difficulties of hardware and software limited the collection of data, but preliminary results suggest that differences in grain size affect the amount of gas that can be adsorbed in coal. Five adsorption isotherms were produced from crushed coal with carbon dioxide as adsorbed gas and were compared with high-pressure adsorption data from coals using the small-volume high-pressure volumetric adsorption apparatus described above.

8.2.3.2. Data acquisition

An adsorption isotherm relates to equilibrium conditions between an adsorbate (gas) and an adsorbent (in this case, coal) at a constant temperature across a range of pressures. Many measurements at incremental pressure increases (and decreases, to test for hysteresis) are necessary to define the shape of an adsorption isotherm that characterizes the interaction between gas adsorbate and coal adsorbent according to one out of six basic adsorption types (Figure 1). The experimentally determined adsorption isotherms

collected in this study correspond to Type I and are modeled by the Langmuir theory of adsorption. The underlying assumption in Langmuir's theory is that the surface of the adsorbent is covered by a single homogenous monolayer of adsorbed gas molecules when adsorption capacity has been reached. The layer of adsorbed gas molecules loses density with increasing temperature and decreasing pressure. Reproducibility of measurements and subsequent calculations of adsorption characteristics require that the system is in thermodynamic equilibrium.

Adsorption calculations are based on the real gas law, which is an extension of the ideal gas law in order to account for variations in gas compressibility. Two versions of a custom-designed spreadsheet with macros and embedded formulas were used for calculations involving methane and carbon dioxide. Spreadsheets utilized physical constants from the National Institute of Standards and Technology (NIST standard reference database 12) and equations for gas compressibility that were empirically derived to calibrate our apparatus. The graph of 'compressibility factor over pressure' for different gases in Figure 4 highlights the basis for calibration. Langmuir's theory still satisfactorily explains adsorption data from experiments and the field for practical purposes, although alternative adsorption theories have been proposed to describe multimolecular layer adsorption in porous materials (Sing *et al.*, 1985).

The small-volume high-pressure volumetric adsorption apparatus described above allows calculating the moles of gas adsorbed per unit mass of coal during each incremental pressure increase (also called the Gibbs excess adsorption) via application of the real gas law (Goodman *et al.*, 2004; Mavor *et al.*, 1990) according to Equation 2

$$\Delta n^{ex} = \left(\frac{1}{RT_{iso} m_c} \right) \left[V_R \left(\frac{P_{ri}}{Z_{ri}} - \frac{P_{rf}}{Z_{rf}} \right) - V_v \left(\frac{P_{sf}}{Z_{sf}} - \frac{P_{si}}{Z_{si}} \right) \right] \quad \text{Equation 2}$$

where Δn^{ex} = Gibbs excess adsorption, R = molar gas constant, T_{iso} = isothermal temperature (i.e. temperature of water thermostat bath in Kelvin), m_c = mass of coal, V_R = volume of the reference cell, P_{ri} = initial pressure of the reference cell, Z_{ri} = gas compressibility factor at the initial pressure of the reference cell, P_{rf} = final pressure of the reference cell, Z_{rf} = gas compressibility factor at the final pressure of the reference cell, V_v = void volume, P_{sf} = final pressure of the sample cell, Z_{sf} = gas compressibility factor at the final pressure of the sample cell, P_{si} = initial pressure of the sample cell, and Z_{si} = gas compressibility factor at the initial pressure of the sample cell. An Excel spreadsheet was designed to include all parameters that are required to calculate the monolayer adsorption characteristics for each pressure test.

Equation 2 does not apply to engineering calculations for estimating gas potentials in coal reservoirs because it fails to account for the decrease in void volume with increasing gas adsorption. Measures for the true (absolute) adsorption require inclusion of a density correction factor to account for the volume change due to adsorbed gas. The corrected adsorption is calculated using Equation 3

$$n^{abs} = n^{ex} \left(\frac{\rho_a}{\rho_a - \rho_g} \right) \quad \text{Equation 3}$$

where n^{abs} = absolute adsorbed amount at a defined pressure step, n^{ex} = total Gibbs excess sorption (equal to the sum of incremental adsorptions Δn^{ex}), ρ_a = density of the adsorbed gas phase, and ρ_g = density of the free gas phase.

8.2.4. Low-pressure gas adsorption measurements

Low-pressure adsorption data were collected using a Micromeritics ASAP-2020 porosimeter and surface area analyzer. The data collected with this instrument result from the application of adsorption theoretical equations that allow calculating mesopore surface areas (Brunnauer, Emmett and Teller equation – BET), mesopore-volume distribution (Barrett, Joyner and Halenda equation – BJH), micropore capacity and surface areas (Dubinin-Radushkevich equation – D-R), and micropore-size distribution (Dubinin-Astakhov equation – D-A). Descriptions of these equations and their significance are presented in Chapter 7 (Section 7.2.4).

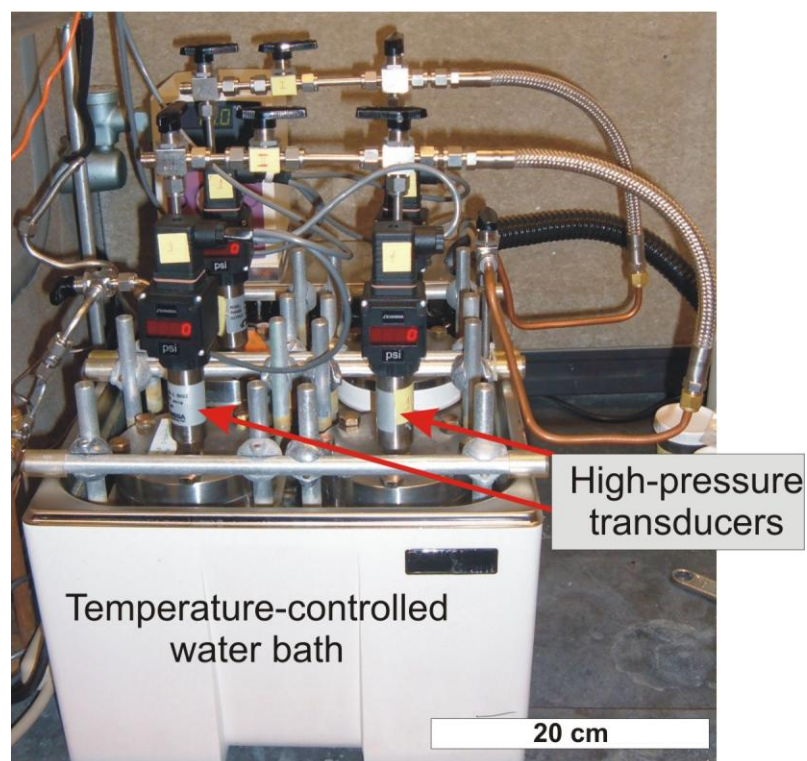


Figure 3a. Photograph of the small-volume high-pressure volumetric adsorption apparatus. The illustration shows four pressure cells inside a temperature-controlled water bath. Each pressure cell is connected to a high-pressure transducer.

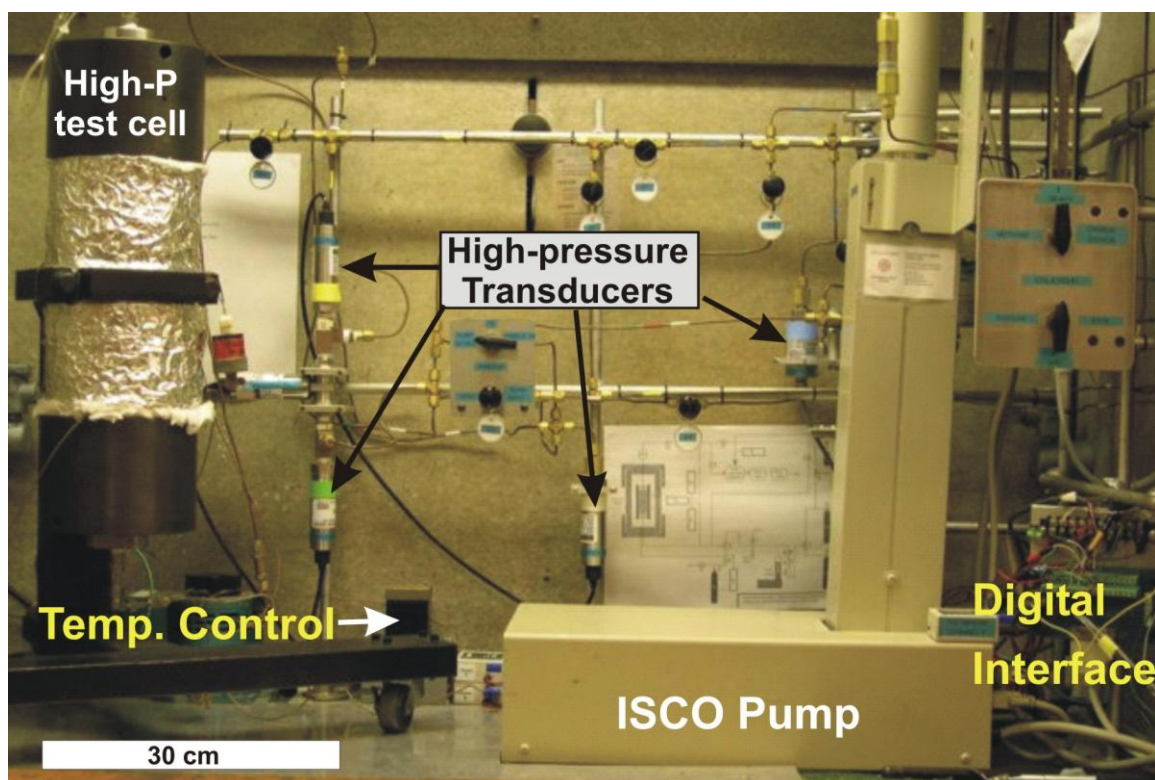


Figure 3b. Photograph of the large-volume high-pressure volumetric adsorption apparatus. The instrument is housed in a fume hood for safety compliance with Indiana University. A high-pressure ISCO pump capable of injecting pressures up to 70 MPa (10,000 psi) is connected to the instrument. The high-pressure test cell was built to potentially reach a maximum pressure of 31.5 MPa (4,500 psi).

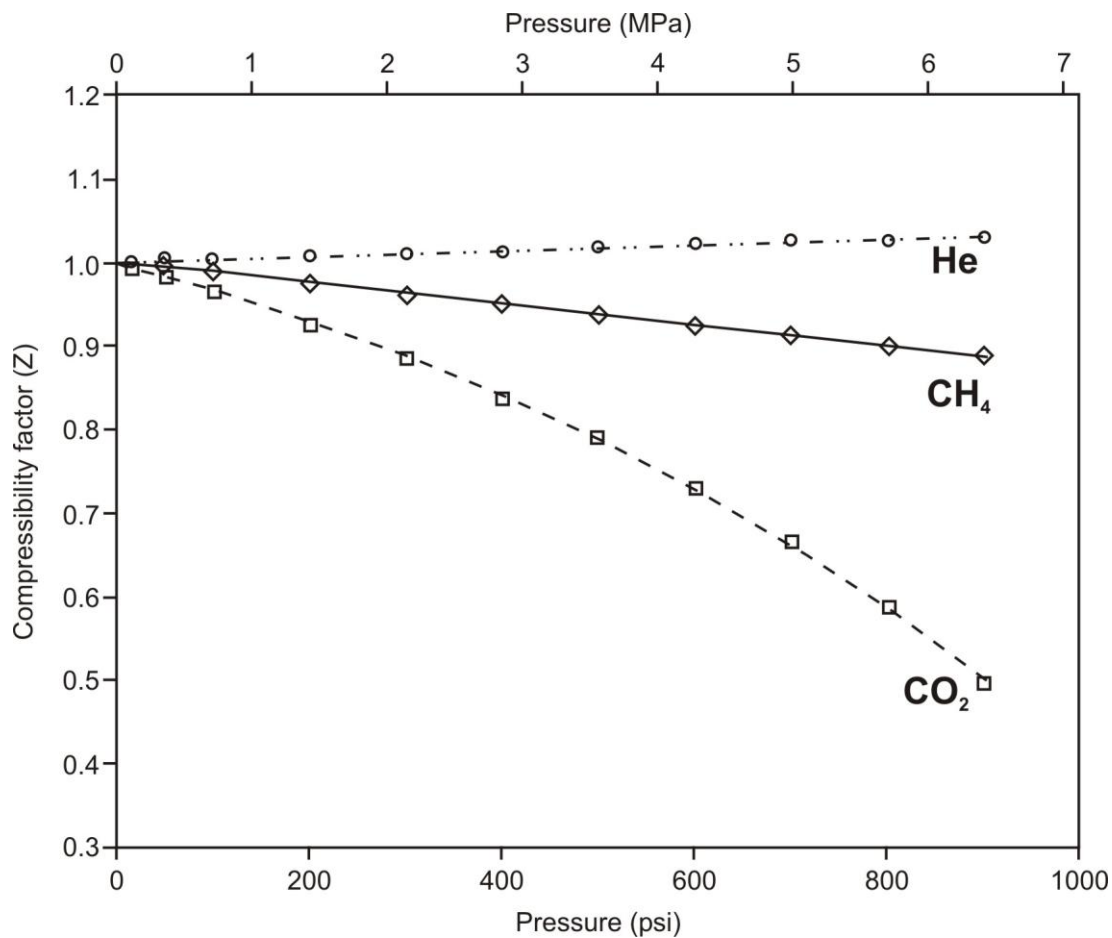


Figure 4. Compressibility factors derived experimentally using our small-volume high-pressure volumetric adsorption apparatus. The data are compatible with theoretical compressibility factors from the National Institute for Standards (NIST) database.

8.3. Results and Discussion

8.3.1. High-pressure adsorption of CH_4 on coal

8.3.1.1. CH_4 adsorption capacity of dry versus moisture-equilibrated coals

High-pressure adsorption isotherms were determined using our small-volume high-pressure volumetric adsorption apparatus for air-dried (Table 1) and moisture-equilibrated (Table 3) bulk crushed coal samples of the Lower Block coal from Billings Mine (Daviess County, Indiana).

Figure 5 illustrates the variability in methane adsorption capacity among coal samples from several Indiana coal seams. Data labeled with the date format correspond to several measurements using Lower Block Coal from Billings Mine. A significant difference in CH_4 adsorption capacity is observed between dry coal samples (gray dashed lines) and the same dried coals that were subsequently moisture-equilibrated (black solid lines). Table 4 shows data for dry samples. Tables 4 and 5 list all data collected for high-pressure methane adsorption isotherms.

Table 5 presents calculated ratios between methane adsorption capacities of dry and moisture-equilibrated samples. Methane-related adsorption ratios were calculated for pairs of dry and moisture-equilibrated coal samples of the same origin. The observed ratios vary depending on gas pressure. The ratios of CH_4 adsorption capacities in dry versus moisture-equilibrated coals are consistently lower at 2.8 MPa (400 psi) than those at 2.07 MPa (300 psi).

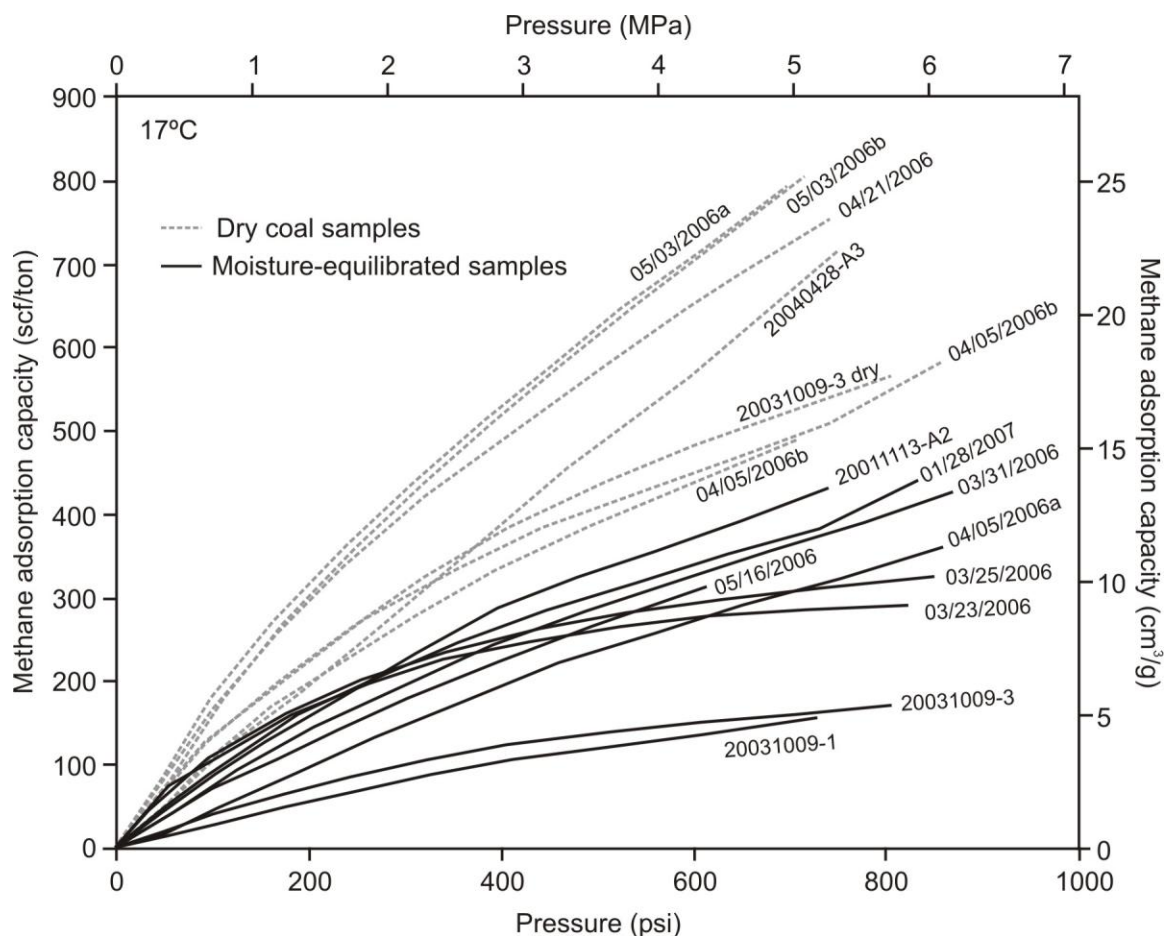


Figure 5. Methane adsorption isotherms determined at 17°C from selected Indiana coals using our small-volume high-pressure volumetric adsorption apparatus. Dry coal samples express significantly larger adsorption capacities for CH₄ than the same coals after moisture-equilibration. Data presented in scientific (SI) and U.S. industry standard units.

8.3.1.2. Changes in CH₄ adsorption capacity with increasing time of exposure to air

Lower Block coal samples were measured during the third and fourth month of exposure to laboratory air at room temperature of 21°C. One sample was measured at the beginning of April 2006. (Tables 4a, b; sample 04/05/06b) and duplicate samples were measured at the beginning of the fourth month (Tables 4a, b; samples 05/03/2006a, b). The adsorption isotherms from these tests confirm the reproducibility of data from duplicate analyses. One sample was also run between the measurements described above (Tables 4a, b; sample 04/21/2006). The decrease in sample moisture over time with increasing exposure to air resulted in a significant increase of 3.9 cm³/g in adsorption potential for methane at 2.07 MPa (i.e., from 9.4 to 13.3 cm³/g, corresponding to 300 to 424 scf/ton at 300 psi) and an increase of 2.1 cm³/g in CH₄ adsorption potential at 2.8 MPa (i.e., from 11.2 to 13.3 cm³/g; 359 to 424 scf/ton at 400 psi; all reported on a dry, ash-free basis). The observed change represents a ~30% increase in adsorption capacity for methane resulting from moisture loss during the first few months of coal exposure in laboratory air.

Figure 6 plots high-pressure CH₄ adsorption capacities of three aliquots of Billings Mine coal that had been exposed to air during storage in the laboratory. Moisture equilibration and adsorption capacities of methane in these coal samples were determined at RMB Earth Science Consultants, Ltd. Coal samples had been moisture-equilibrated using the same standard procedure described in the methods section for coal samples measured at Indiana University. Adsorption isotherm data collected at RMB Earth Science Consultants, Ltd., are consistent with the observed decrease in equilibrium-moisture values (wt. %) from 12.61% in the original “zero exposure coal” to 9.99% after

13 months of exposure. A 40% increase in CH₄ adsorption capacity of moisture-equilibrated coal of 2.7 cm³/g is also observed after 13 months of exposure (i.e., from 3.9 to 6.6 cm³/g at 2.07 MPa; 125 to 211 scf/ton at 300 psi). A higher pressure of 2.8 MPa (400 psi) increases the CH₄ adsorption capacity by 3.3 cm³/g over 13 months, from 4.8 to 8.1 cm³/g (152 to 259 scf/ton). Table 3 shows that the moisture-equilibrated coals at RMB Earth Science Consultants, Ltd., did not reach the same equilibrium-moisture content of the original ‘zero exposure coal’. The drying of coal in laboratory air cannot be completely reversed by moisture-equilibration, resulting in dehydration/hydration hysteresis.

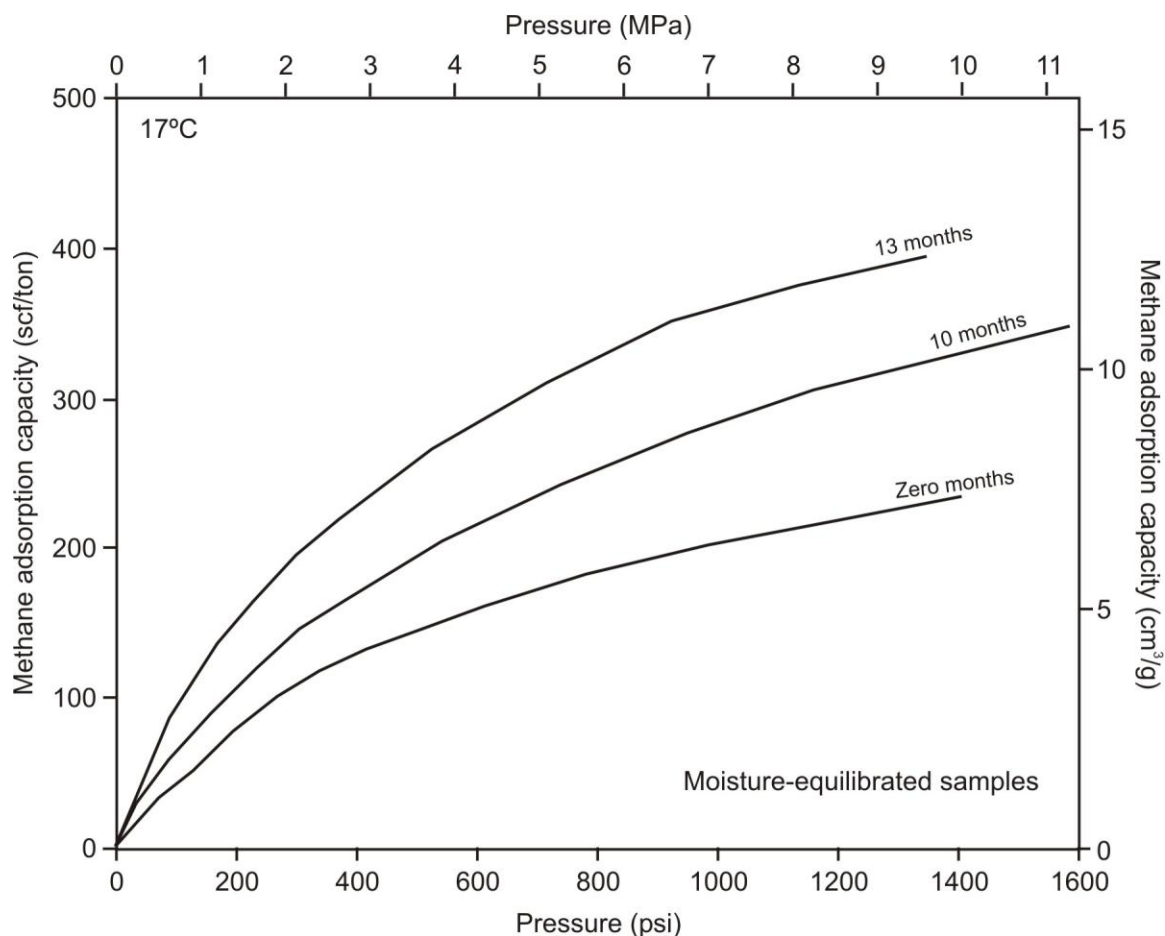


Figure 6. Methane adsorption isotherms collected at 17°C from moisture-equilibrated coal samples. The samples were exposed to air in the laboratory for up to ~13 months, followed by moisture-equilibration and measurement at RMB Earth Science Consultants, Ltd. Although all coals were moisture-equilibrated before measurements, coals exposed longer to air were less able to become re-hydrated. The observed decrease in equilibrium-moisture content translates into an increase in adsorption capacity.

8.3.2. High-pressure adsorption of CO₂ on coal

8.3.2.1. CO₂ adsorption capacity of dry versus moisture-equilibrated coals

CO₂ adsorption isotherms measured with our small-volume high-pressure volumetric adsorption apparatus show remarkable differences in adsorption capacity of dry versus moisture-equilibrated coal samples (Figure 7). As with methane, adsorption of carbon dioxide is significantly larger on dry coal samples compared to moisture-equilibrated samples.

Table 5 lists calculated CO₂ adsorption ratios between dry and moisture-equilibrated samples with decreasing pressure from 2.8 MPa (400 psi) to 2.07 MPa (300 psi). CO₂-related adsorption ratios were calculated for pairs of dry and moisture-equilibrated coal samples of the same origin. The observed ratios vary depending on gas pressure. On average, the ratios of CO₂ adsorption capacities in dry versus moisture-equilibrated coals are lower at 2.8 MPa (400 psi) than those at 2.07 MPa (300 psi).

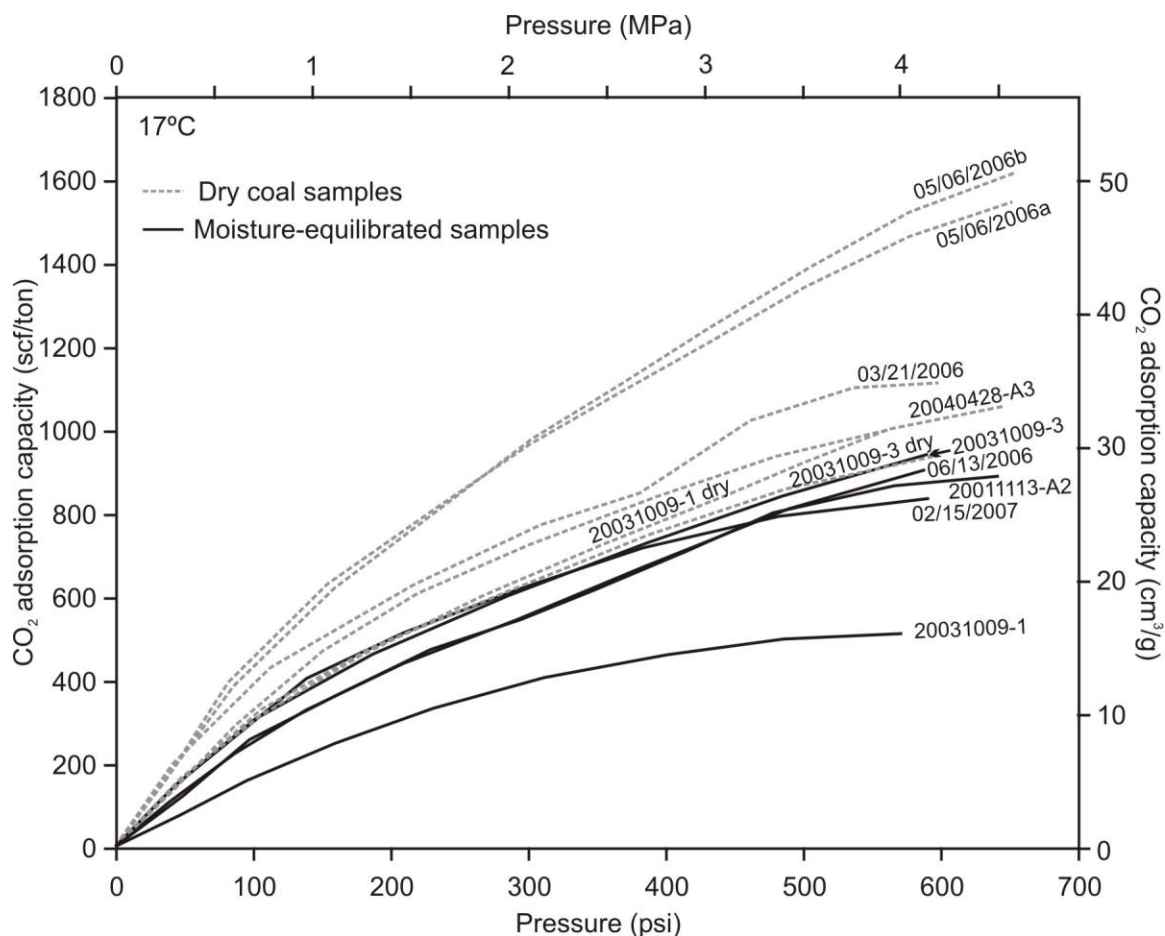


Figure 7. Carbon dioxide isotherms measured at 17°C from selected Indiana coals using our small-volume high-pressure volumetric adsorption apparatus. Dry samples show significantly larger adsorption capacities than moisture-equilibrated samples. Data are presented in scientific (SI) and U.S. industry standard units.

8.3.2.2. Changes in CO₂ adsorption capacity with increasing time of exposure to air

Coal samples from the Lower Block Coal Member from Billings Mine in Daviess County, Indiana, were measured on two occasions, including duplicate measurements in May 2006 (Tables 4a, b; samples 03/21/2006 and 05/06/2006a, b). Duplicate measurements show virtually the same CO₂ adsorption capacities at pressures below 2.8 MPa (400 psi). In comparison, the sample measured in March (03/21/2006) has a significantly lower CO₂ adsorption capacity of 22.9 cm³/g at 2.07 MPa (732 scf/ton at 300 psi) and 27.3 cm³/g at 2.8 MPa (875 scf/ton at 400 psi). The CO₂ adsorption capacities from samples 03/21/2006 and 05/06/2006b are 22.9 and 30.5 cm³/g at 2.07 MPa (732 to 975 scf/ton at 300 psi), respectively. These values increase at higher pressure of 2.8 MPa to 27.3 and 36.3 cm³/g (875 to 1160 scf/ton at 400 psi), respectively. It appears that the loss of moisture with increasing exposure to air in the laboratory is related to a 25% increase in CO₂ adsorption capacity.

The moisture-equilibrated coal samples that had been measured for their CH₄ adsorption capacity (section 8.3.1.2) were also tested for CO₂ adsorption capacity at RMB Earth Science Consultants, Ltd. (Figure 8). The ‘zero exposure coal’ has a significantly lower CO₂ adsorption capacity compared to the same coal that had been exposed to air for 13 months, similar to the results with regard to methane adsorption. The measured CO₂ adsorption capacities of ‘zero exposure’ and ‘13-month-exposed’ coals are 17.6 and 22 cm³/g at 2.07 MPa (563 to 702 scf/ton at 300 psi, reported on a dry, ash-free basis, daf), respectively. The equivalent data at 2.8 MPa (400 psi) are 21.1 and 25.7 cm³/g (675 to 822 scf/ton), representing an increase of 18% in CO₂ adsorption capacity after 13 months of exposure.

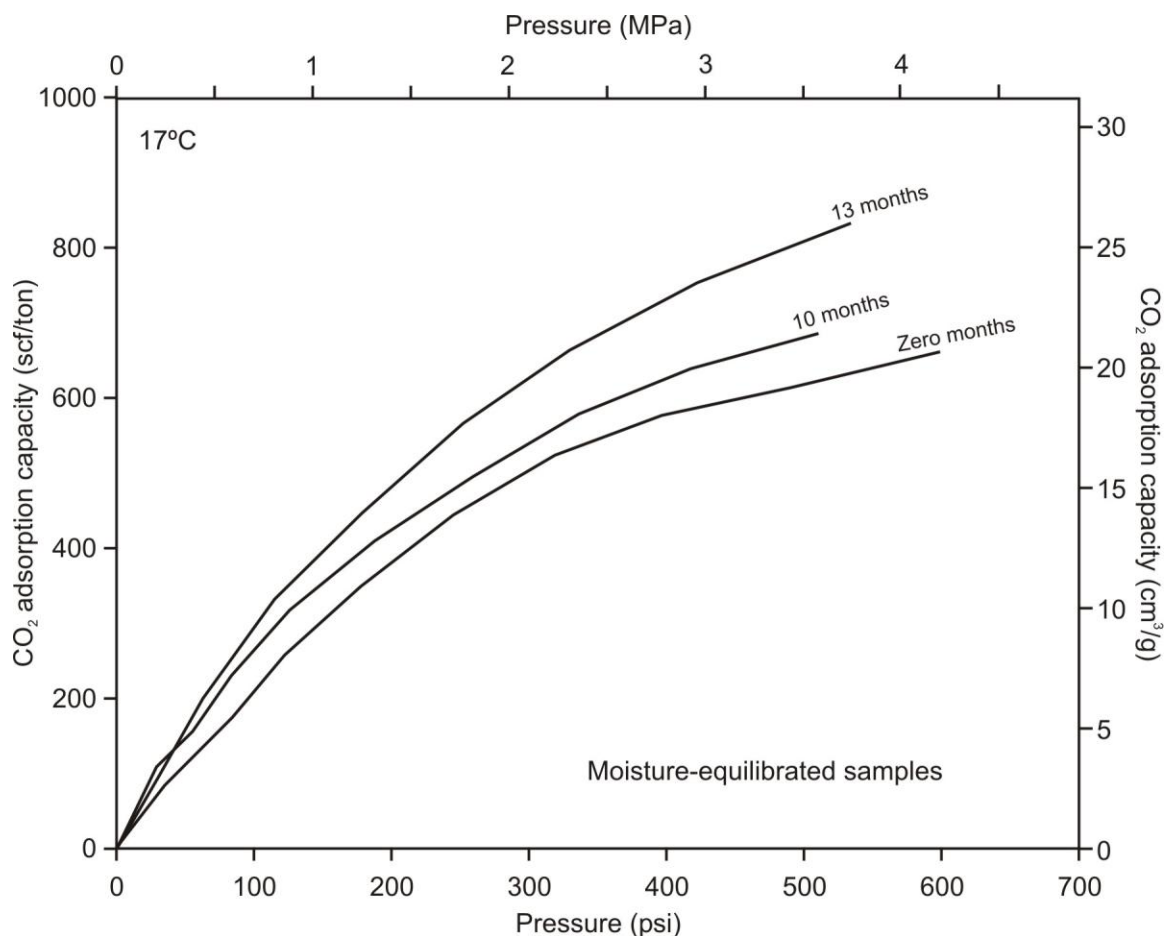


Figure 8. Carbon dioxide adsorption isotherms collected at 17°C from moisture-equilibrated coal samples that had been exposed to air in the laboratory for up to ~13 months, followed by moisture-equilibration and measurement at RMB Earth Science Consultants, Ltd. Although all coals were moisture-equilibrated before measurements, the more exposed coals were less able to become re-hydrated. The observed decrease in moisture content translates into an increase in adsorption capacity.

Table 3a. Gas adsorption data of moisture-equilibrated coal samples at gas pressures 2.07 MPa (300 psi) and 2.8 MPa (400 psi). Data are reported ‘as received’ and on a dry, ash-free basis (daf). CO₂/CH₄ volume ratios (daf) were calculated for both pressures. Equilibrium moisture and ash contents are expressed as weight %; n.d. = no data.

Moisture-equilibrated coal samples												
Coal sample	CH ₄ adsorption capacity (cm ³ /g)				CO ₂ adsorption capacity (cm ³ /g)				CO ₂ /CH ₄ volume ratio		Equilibrium moisture (wt. %)	Ash (wt. %)
	As received		Dry, ash-free basis		As received		Dry, ash-free basis					
	2.07 MPa	2.8 MPa	2.07 MPa	2.8 MPa	2.07 MPa	2.8 MPa	2.07 MPa	2.8 MPa	2.07 MPa	2.8 MPa		
zero exposure	3.3	4.1	3.9	4.8	15.0	18.0	17.6	21.1	4.5	4.4	12.61	2.17
10 months expos.	4.5	5.3	5.2	6.0	16.4	19.1	18.9	21.9	3.6	3.6	10.99	2.06
13 months expos.	5.8	7.1	6.6	8.1	19.2	22.5	22.0	25.7	3.3	3.2	9.99	2.47
3/23/2006	6.6	7.5	7.6	8.6	n.d.	n.d.	n.d.	n.d.	n.d.	n.d.	9.94	2.35
3/25/2006	6.8	7.9	7.7	9.0	19.7	23.4	22.4	26.7	2.9	3.0	9.9	2.35
3/31/2006	5.8	7.7	6.6	8.7	n.d.	n.d.	n.d.	n.d.	n.d.	n.d.	9.95	2.35
4/5/2006	4.4	6.1	5.0	6.9	n.d.	n.d.	n.d.	n.d.	n.d.	n.d.	10.26	2.35
5/16/2006	5.5	7.1	6.2	8.1	n.d.	n.d.	n.d.	n.d.	n.d.	n.d.	10.03	2.35
6/13/2006	n.d.	n.d.	n.d.	n.d.	19.8	23.8	22.5	27.1	n.d.	n.d.	10.03	2.35
1/28/2007	6.6	8.2	7.5	9.4	n.d.	n.d.	n.d.	n.d.	n.d.	n.d.	9.84	2.35
2/15/2007	n.d.	n.d.	n.d.	n.d.	19.2	22.5	21.9	25.7	n.d.	n.d.	9.84	2.35
3/4/2007	n.d.	n.d.	n.d.	n.d.	n.d.	n.d.	n.d.	n.d.	n.d.	n.d.	9.61	2.35
20011113-A2	6.9	9.0	8.5	11.1	17.2	20.9	21.2	25.8	2.5	2.3	7.86	11.09
20031009-1	2.4	3.3	2.8	3.9	11.7	14.1	13.8	16.6	4.9	4.3	8.38	6.69
20031009-3	3.1	3.8	3.6	4.4	17.2	21.3	19.6	24.2	5.5	5.5	8.79	3.31
20040428-C1	3.7	4.9	4.2	5.7	13.1	16.6	15.1	19.2	3.6	3.4	8.53	5.12

Table 3b. Gas adsorption data of moisture-equilibrated coal samples at gas pressures 300 psi (2.07 MPa) and 400 psi (2.8 MPa). Data are reported ‘as received’ and on a dry, ash-free basis (daf). CO₂/CH₄ volume ratios (daf) were calculated for both pressures. Equilibrium moisture and ash contents are expressed as weight %; n.d. = no data. Data are presented in U.S. industry standard units. The same data in SI units are listed in Table 3a. Unit conversion: 1 cm³/g \approx 32 scf/ton.

Moisture-equilibrated samples												
Coal sample	CH ₄ adsorption capacity (scf/ton)				CO ₂ adsorption capacity (scf/ton)				CO ₂ /CH ₄ volume ratio		Equilibrium moisture (wt. %)	Ash (wt. %)
	As received		Dry, ash-free basis		As received		Dry, ash-free basis					
	300 psi	400 psi	300 psi	400 psi	300 psi	400 psi	300 psi	400 psi	300 psi	400 psi		
zero exposure	106	130	124.4	152.5	480	575	563.2	674.7	4.5	4.4	12.61	2.17
10 months expos.	145	168	166.8	193.2	525	610	603.8	701.6	3.6	3.6	10.99	2.06
13 months expos.	185	227	211.3	259.3	615	720	702.5	822.5	3.3	3.2	9.99	2.47
3/23/2006	212	240	241.7	273.6	n.d.	n.d.	n.d.	n.d.	n.d.	n.d.	9.94	2.35
3/25/2006	216	254	246.2	289.5	630	750	717.9	854.7	2.9	3.0	9.9	2.35
3/31/2006	186	245	212.1	279.4	n.d.	n.d.	n.d.	n.d.	n.d.	n.d.	9.95	2.35
4/5/2006	140	194	160.2	222.0	n.d.	n.d.	n.d.	n.d.	n.d.	n.d.	10.26	2.35
5/16/2006	175	227	199.7	259.1	n.d.	n.d.	n.d.	n.d.	n.d.	n.d.	10.03	2.35
6/13/2006	n.d.	n.d.	n.d.	n.d.	632	760	721.3	867.4	n.d.	n.d.	10.03	2.35
1/28/2007	212	263	241.4	299.5	n.d.	n.d.	n.d.	n.d.	n.d.	n.d.	9.84	2.35
2/15/2007	n.d.	n.d.	n.d.	n.d.	615	721	700.4	821.1	n.d.	n.d.	9.84	2.35
3/4/2007	n.d.	n.d.	n.d.	n.d.	n.d.	n.d.	n.d.	n.d.	n.d.	n.d.	9.61	2.35
20011113-A2	220	287	271.4	354.1	550	670	678.6	826.7	2.5	2.3	7.86	11.09
20031009-1	77	105	90.7	123.6	375	450	441.5	529.8	4.9	4.3	8.38	6.69
20031009-3	100	123	113.8	139.9	550	682	625.7	775.9	5.5	5.5	8.79	3.31
20040428-C1	117	157	135.5	181.8	418	530	484.1	613.8	3.6	3.4	8.53	5.12

Table 4a. Gas adsorption data of dry coal samples at 2.07 and 2.8 MPa (300 and 400 psi). The same data in U.S. industry standard units are listed in Table 4b. Data reported on dry, ash-free basis (daf); n.d. = no data. CO₂/CH₄ volume ratios (daf) were calculated for both pressures.

Dry coal samples							
Coal sample	CH ₄ adsorption capacity, daf (cm ³ /g)		CO ₂ adsorption capacity, daf (cm ³ /g)		CO ₂ /CH ₄ volume ratio		Ash (wt. %)
	2.07 MPa	2.8 MPa	2.07 MPa	2.8 MPa	2.07 MPa	2.8 MPa	
3/21/2006	n.d.	n.d.	22.9	27.3	n.d.	n.d.	2.35
4/5/2006	9.4	11.2	n.d.	n.d.	n.d.	n.d.	2.35
4/21/2006	12.3	15.2	n.d.	n.d.	n.d.	n.d.	2.35
5/3/2006	13.3	16.4	n.d.	n.d.	n.d.	n.d.	2.35
5/3/2006	13.3	16.4	n.d.	n.d.	n.d.	n.d.	2.35
5/6/2006	n.d.	n.d.	29.7	35.3	n.d.	n.d.	2.35
5/6/2006	n.d.	n.d.	30.5	36.3	n.d.	n.d.	2.35
20031009-1	8.2	10.6	22.7	26.6	2.8	2.5	6.69
20031009-3	9.6	11.9	19.3	23.1	2.0	1.9	3.31
20040428-A3	9.1	12.0	20.2	24.2	2.2	2.0	10.13
20040428-C1	6.3	7.9	18.4	22.3	3.0	2.8	5.12

Table 4b. Gas adsorption data of dry coal samples at 300 and 400 psi (2.07 and 2.8 MPa). Data are presented in U.S. industry standard units. The same data in SI units are listed in Table 4a. Data reported on dry, ash-free basis (daf); n.d. = no data. CO₂/CH₄ volume ratios (daf) were calculated for both pressures.

Dry coal samples							
Coal sample	CH ₄ adsorption capacity, daf (scf/ton)		CO ₂ adsorption capacity, daf (scf/ton)		CO ₂ /CH ₄ volume ratio		Ash (wt. %)
	300 psi	400 psi	300 psi	400 psi	300 psi	400 psi	
3/21/2006	n.d.	n.d.	732	875	n.d.	n.d.	2.35
4/5/2006	300	359	n.d.	n.d.	n.d.	n.d.	2.35
4/21/2006	393	487	n.d.	n.d.	n.d.	n.d.	2.35
5/3/2006	427	526	n.d.	n.d.	n.d.	n.d.	2.35
5/3/2006	424	525	n.d.	n.d.	n.d.	n.d.	2.35
5/6/2006	n.d.	n.d.	950	1130	n.d.	n.d.	2.35
5/6/2006	n.d.	n.d.	975	1160	n.d.	n.d.	2.35
20031009-1	263	340	725	850	2.8	2.5	6.69
20031009-3	307	380	618	739	2.0	1.9	3.31
20040428-A3	290	383	645	775	2.2	2.0	10.13
20040428-C1	200	254	590	715	3.0	2.8	5.12

Table 5a. Calculated adsorption volume ratios between dry and moisture-equilibrated coal samples at gas pressures 2.07 MPa (300 psi) and 2.8 MPa (400 psi). The same data in U.S. industry standard units are listed in Table 5b. n.d. = no data.

Coal sample	Methane (CH ₄) adsorption capacity (cm ³ /g) and ratio						Carbon dioxide (CO ₂) adsorption capacity (cm ³ /g) and ratio					
	Dry		Moisture-equilibrated		Dry/ moisture-equil. volume ratio		Dry		Moisture-equilibrated		Dry/ moisture-equil. volume ratio	
	2.07 MPa	2.8 MPa	2.07 MPa	2.8 MPa	2.07 MPa	2.8 MPa	2.07 MPa	2.8 MPa	2.07 MPa	2.8 MPa	2.07 MPa	2.8 MPa
4/5/2006	9.4	11.2	4.4	6.1	2.1	1.9	n.d.	n.d.	n.d.	n.d.	n.d.	n.d.
3/31/06 - 4/21/06	12.3	15.2	5.8	7.7	2.1	2.0	n.d.	n.d.	n.d.	n.d.	n.d.	n.d.
20031009-1	8.2	10.6	2.4	3.3	3.4	3.2	22.7	26.6	11.7	14.1	1.9	1.9
20031009-3	9.6	11.9	3.1	3.8	3.1	3.1	19.3	23.1	17.2	21.3	1.1	1.1
20040428-C1	6.3	7.9	3.7	4.9	1.7	1.6	18.4	22.3	13.1	16.6	1.4	1.3
average	9	11	4	5	2.5	2.4	20	24	14	17	1.5	1.4
standard deviation	2.2	2.6	1.3	1.8	0.7	0.8	2.2	2.3	2.8	3.7	0.4	0.4

Table 5b. Calculated adsorption volume ratios between dry and moisture-equilibrated coal samples (ash included) at gas pressures 300 psi (2.07 MPa) and 400 psi (2.8 MPa). Data are presented in U.S. industry standard units. The same data in SI units are listed in Table 5a. n.d. = no data.

Coal sample	Methane (CH ₄) adsorption capacity (scf/ton) and ratio						Carbon dioxide (CO ₂) adsorption capacity (scf/ton) and ratio					
	Dry		Moisture-equilibrated		Dry/ moisture-equil. volume ratio		Dry		Moisture-equilibrated		Dry/ moisture-equil. volume ratio	
	300 psi	400 psi	300 psi	400 psi	300 psi	400 psi	300 psi	400 psi	300 psi	400 psi	300 psi	400 psi
4/5/2006	300	359	140	194	2.1	1.9	n.d.	n.d.	n.d.	n.d.	n.d.	n.d.
3/31/06 - 4/21/06	393	487	186	245	2.1	2.0	n.d.	n.d.	n.d.	n.d.	n.d.	n.d.
20031009-1	263	340	77	105	3.4	3.2	725	850	375	450	1.9	1.9
20031009-3	307	380	100	123	3.1	3.1	618	739	550	682	1.1	1.1
20040428-C1	200	254	117	157	1.7	1.6	590	715	418	530	1.4	1.3
average	293	364	124	165	2.5	2.4	644	768	448	554	1.5	1.4
standard deviation	70.3	83.8	41.6	56.3	0.7	0.8	71.2	72.0	91.2	117.8	0.4	0.4

8.3.3. Effects of moisture loss on high-pressure gas adsorption in coal

Adsorption isotherms of selected coal samples were measured with our small-volume high-pressure volumetric adsorption apparatus at methane gas pressures up to 6.5 MPa (~930 psi) and for carbon dioxide up to 4.5 MPa (~650 psi). These pressure ranges allowed us to obtain experimental adsorption data that are compatible with natural *in situ* hydrostatic gas pressures in Indiana coal seams (i.e., 2.07 to 2.8 MPa; 300 to 400 psi).

Dry coal samples show significantly higher adsorption capacities than moisture-equilibrated coal samples (Figures 5 and 7). These observations are in agreement with results from previous studies indicating that moisture competes with CH₄ and CO₂ for adsorption sites (e.g., Bustin and Clarkson, 1998; Krooss *et al.*, 2002; Levy *et al.*, 1997; Yee *et al.*, 1993). A few studies have investigated the preferential adsorption of CO₂ over CH₄ in gas mixtures on coal and the adsorption ratios between individual gas species in a mixture (e.g., Busch *et al.*, 2003a, b; 2004; 2006; Clarkson and Bustin, 1999a, b). However, a quantification of the gas adsorption ratios between dry and moisture-equilibrated coals has not yet been presented. The adsorption ratios for dry versus moisture-equilibrated coals were estimated from published adsorption isotherms (Clarkson and Bustin, 1999a). They suggest that ~1.5 times more methane can be adsorbed on a dry coal sample than in the moisture-equilibrated coal at 2.8 MPa (400 psi). Similarly, visual inspection of published high-pressure adsorption isotherms (Goodman *et al.*, 2004) suggests that for CO₂ the ratio of dry versus moisture-equilibrated coal samples at 2.8 MPa is ~2.5. On average, our data indicate ratios of 2.4 for methane and 1.4 for CO₂ at comparable pressure ranges.

Gas adsorption data for methane and carbon dioxide in Indiana coals were compared to estimate the adsorption ratios of these two gases at 2.07 and 2.8 MPa (300 and 400 psi, respectively). These pressures were selected to be representative of most coal deposits in Indiana and also to facilitate comparison with published data (e.g., Mastalerz *et al.*, 2004). Eight moisture-equilibrated coals provided high-pressure adsorption data for methane and CO₂ including three samples measured at RMB Earth Science Consultants, Ltd. (Table 3). Additionally, four dry coal samples provided data for CH₄ and CO₂ (Table 4). In all experiments the adsorbed volumes of CO₂ were significantly larger than those of adsorbed CH₄, with CO₂/CH₄ ratios between 2.5 and 5.5 for moisture-equilibrated samples and CO₂/CH₄ ratios between 1.9 and 3.0 for dry samples (Tables 3 and 4). Figure 9 shows the relationship between CO₂ and CH₄ adsorption in coals. These results support the observation of Mastalerz *et al.* (2004) that CO₂/CH₄ ratios of high volatile bituminous coals from Indiana range between 3.5 and 5.3 during high-pressure adsorption on moisture-equilibrated coals at 2.8 MPa (400 psi) and 17°C. The gas adsorption ratios obtained in this study also confirm that the CO₂/CH₄ ratio of adsorbed gases is rank dependent, as suggested earlier by Stanton *et al.* (2001). The Indiana coals of this study are of high volatile bituminous rank. The observed CO₂/CH₄ adsorbed gas ratios are transitional between those of lignites and anthracites (Stanton *et al.*, 2001).

Table 3 shows a decrease in equilibrium moisture content from 12.61 wt. % in ‘zero exposure coal’, to 10.99 wt. % after 10 months of exposure, to 9.99 wt. % after 13 months. These changes, though relatively small, show that CH₄ adsorption is significantly enhanced from ~3.88 cm³/g (~124 scf/ton) to ~6.59 cm³/g (~211 scf/ton) at 2.07 MPa (300 psi) at the end of the 13-month exposure experiment. Similarly, at 2.8 MPa (400 psi)

CH₄ adsorption increases from ~4.75 cm³/g (~152 scf/ton) to ~8.09 cm³/g (~259 scf/ton; all data reported on dry ash-free basis). High-pressure adsorption isotherms for all coal samples measured at Indiana University show a spread that covers the range of the commercially acquired high-pressure isotherms (Figure 6).

The observed reduction in equilibrium-moisture content from 12.61 wt. % in ‘zero exposure coal’ to 9.99 wt. % after 13 months of exposure suggests that storage in dry air affects the coals’ ability to re-equilibrate and re-hydrate to their original moisture content. The reduction in moisture content relates to a ~30% increase in high-pressure methane adsorption capacity for dry coals and a ~40% increase in methane adsorption capacity of moisture-equilibrated coals. Dehydration/hydration hysteresis in coal during dry storage and subsequent incomplete re-hydration of coal is able to significantly bias experimental determinations of gas adsorption capacities, although the differences in moisture content are moderate.

The same adsorption behavior is observed for CO₂ (Figure 8). The influence of moisture loss from the surface area of coals results in higher adsorption over the time of the experiment (~25% higher on dry coals and ~18% higher on coals following moisture equilibration). These results are consistent with observations from experimental work described in Chapter 7. The observed changes in adsorption capacity resulting from moisture loss indicate that special care must be taken during sample collection and preservation of coals until adsorption characteristics are measured in the laboratory. High-pressure isotherms from partially dried coal samples would likely cause over-estimation of gas adsorption capacities, lead to a miscalculation of CBM prospects, and

provide deceptively optimistic prognoses for recovery of CBM or capture of anthropogenic CO₂.

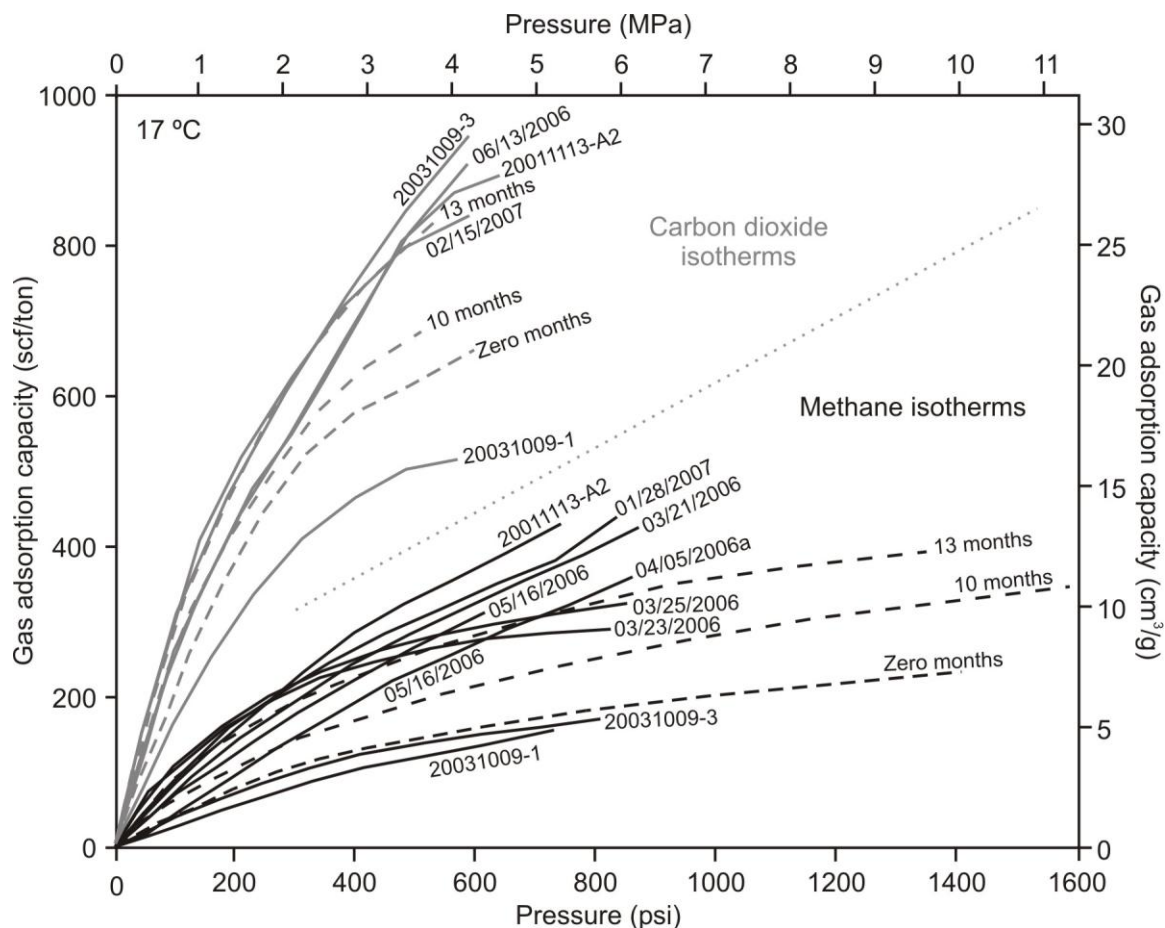


Figure 9. Comparison between carbon dioxide and methane adsorption isotherms determined at 17°C from moisture-equilibrated coal samples. Solid lines correspond to high-pressure methane (black) and carbon dioxide (gray) isotherms measured with our small-volume high-pressure volumetric adsorption apparatus. Dashed lines correspond to high-pressure methane (black) and carbon dioxide (gray) adsorption isotherms determined at RMB Earth Science Consultants, Ltd. CO_2/CH_4 adsorption volume ratios vary between 2.3 and 5.5 for 2.07 and 2.8 MPa (300 and 400 psi, respectively).

8.3.4. Influence of particle size on gas adsorption: results from a large-volume high-pressure volumetric adsorption apparatus

Five CO₂ adsorption experiments were conducted using our large-volume high-pressure volumetric adsorption apparatus described in section 8.2.3.1, simulating reservoir pressure conditions. In this series of 5 experiments, aliquots of a fresh coal sample were crushed and sieved to prepare 5 coals that differ with regard to their particle size distributions. Figure 10 shows the particle size distribution in millimeters vs. weight percent of each sieved coal sample for Experiments 1 – 5. The color coding used in Figure 10 matches the colored adsorption isotherms in Figure 11 and facilitates comparison of data.

High-pressure CO₂ adsorption isotherms suggest a relationship between particle size and CO₂ adsorption capacity of crushed coals (Figure 11). For example, Experiment 1 corresponds to coarser coal particles, whereas Experiment 5 refers to a finer grain size that is equivalent to crushed coal used for adsorption measurements in commercial laboratories. CO₂ adsorption experiments suggest that the adsorption capacity increases with decreasing particle size of coal. An opposite trend to this increase in adsorption with decreasing grain size was found by Siemmons *et al.* (2003) who observed that the CH₄ adsorption capacity increased with increasing grain size of dry coal. These authors, however, did not observe the same behavior for CO₂.

Figure 11 also shows the CO₂ adsorption isotherm obtained at RMB Earth Science Consultants, Ltd. The experiments with our large-volume high-pressure volumetric adsorption apparatus and the measurements by RMB Earth Science Consultants, Ltd. differed with regard to temperature. In our large-volume high-pressure volumetric

adsorption apparatus, the operating temperature was that of the laboratory (~21°C), while the temperature at which data were collected at RMB Earth Science Consultants, Ltd. on crushed (<250 µm) material was 17°C. Such difference in temperature may account for the observed difference in adsorption capacities because higher temperatures decrease the gas adsorption capacity of coal. Nonetheless, the progressive increase in gas adsorption capacity with decreasing grain size shows a consistent trend, with the exception of Experiment 4 which appears to have developed a leak at pressures above 2.8 MPa (400 psi).

Based on the previous observations, it is hypothesized that grinding coal not only enhances diffusion through the coal matrix, but also artificially creates additional surface area that enhances adsorption at sites that otherwise would have not been accessible to gas adsorption. Additional experiments are needed to validate/refute this hypothesis.

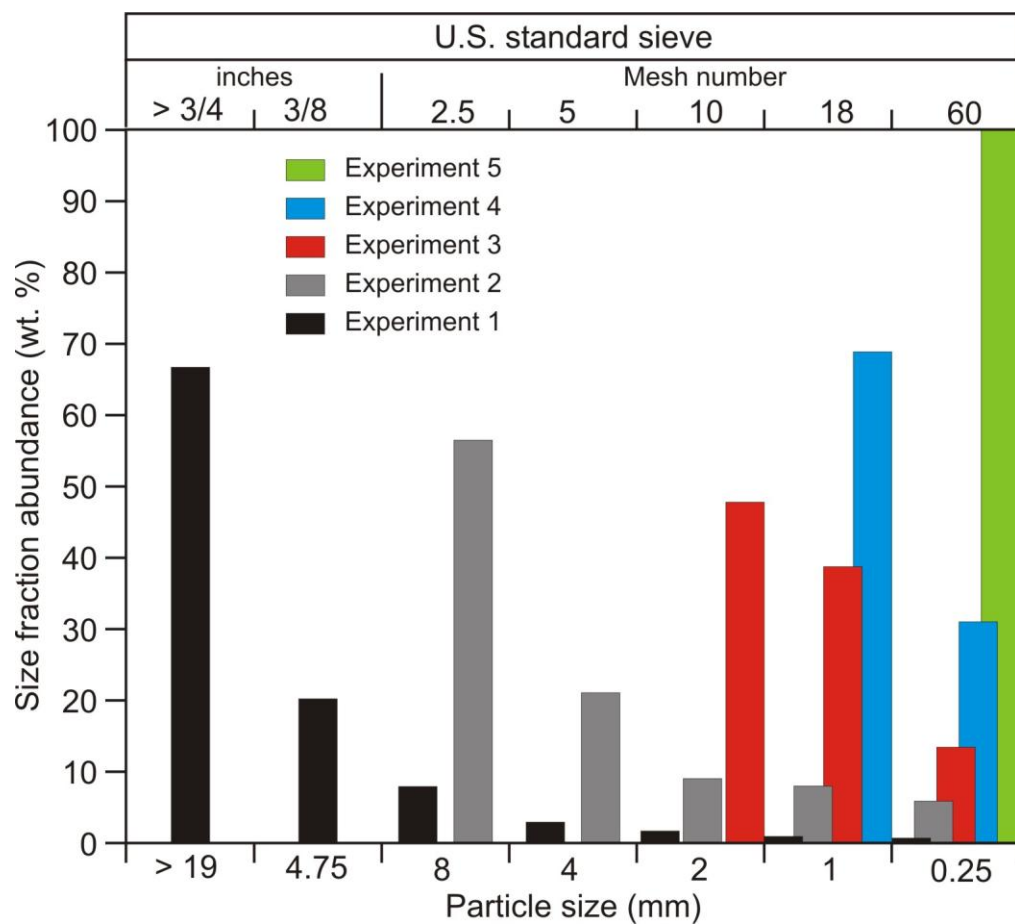


Figure 10. Particle size distributions of coal samples that were crushed to various degrees. The green bar represents a grain size that is typically used for conventional adsorption isotherm work by commercial laboratories.

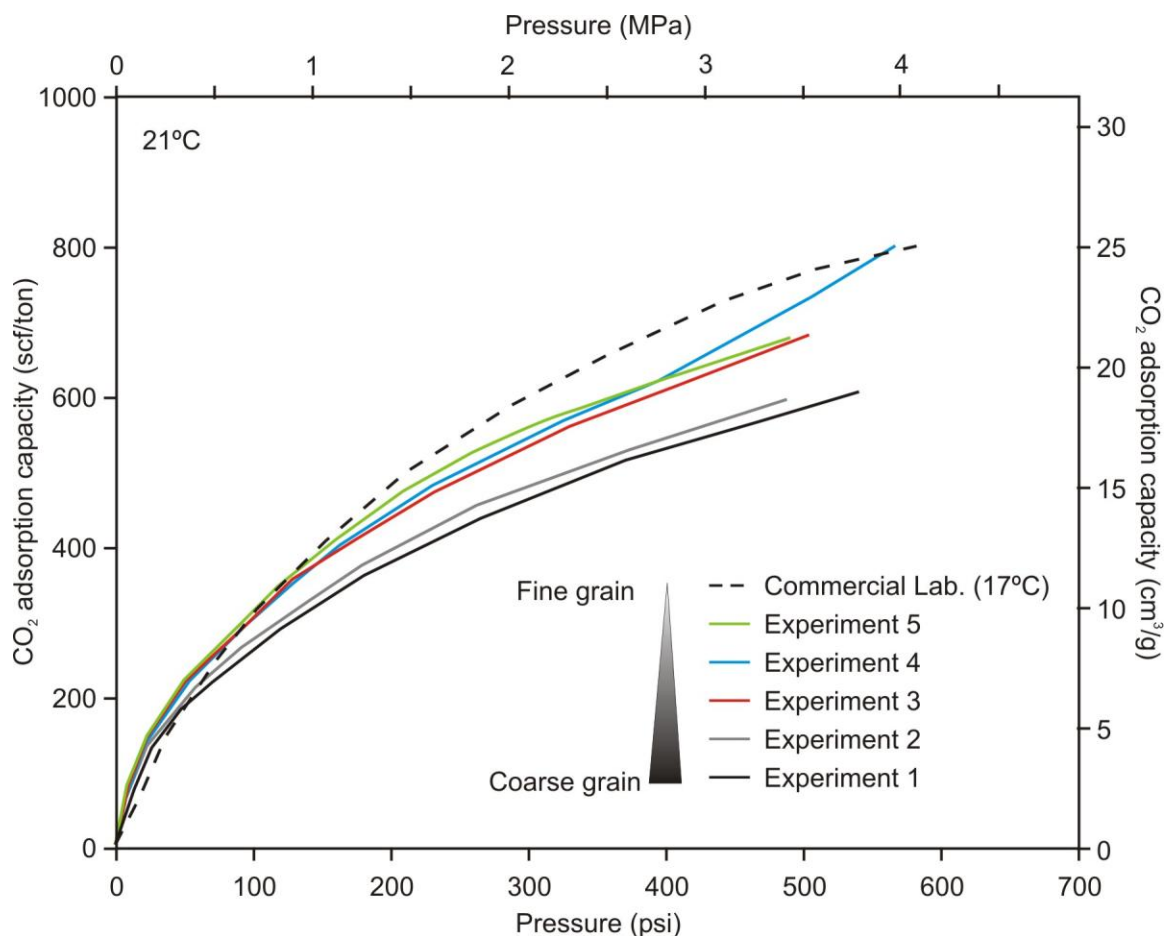


Figure 11. CO₂ adsorption isotherms of crushed coals with distinct particle size distributions. Experiments at Indiana University were conducted at 21°C, whereas data from the commercial laboratory were gathered at 17°C. Note that the adsorption capacity increases with decreasing grain size of crushed coal. Experiment 4 shows a sudden increase in CO₂ adsorption capacity above 2.8 MPa (400 psi) that is expressed as a straight line and is probably due to a leak in the adsorption apparatus.

8.3.5. Petrographic data, ash content, and equilibrium moisture content

Table 6 summarizes petrographic data from all coals with regard to maceral composition and vitrinite reflectance (R_o averaging $\sim 0.58\%$). In addition, ash content and equilibrium moisture content (averaging 8.84 wt. %) are quantified. Figure 12 displays maceral compositions of coal samples and highlights the predominance of vitrinite averaging 77.3 ± 11.7 volume %. The inertinite content averages 13.7 ± 10.2 vol. %, and that of liptinite 7.4 ± 3.5 vol. %, whereas mineral matter ranges between 0.4 and 5 vol. % (average 1.7 ± 1.3 vol. %).

This study considers all coals with < 70 vol. % vitrinite to be “dull” and coals with > 85 vol. % vitrinite to be “bright”. Intermediate coals with vitrinite content between 70 and 85 vol. % are considered either semi-bright or semi-dull. According to this grouping (Figure 12), four coals are dull (7, 9, 10, 12), four coals fall in the intermediate category (4, 6, 8, 11), and four coals are bright (1, 2, 3, 5).

Petrographic analyses reveal intrinsic heterogeneity of coals. Some samples belonging to the same coal member show marked differences in maceral composition, for example in Daviess County between (i) Lower Block Coal Member samples 11 and 12, (ii) Upper Block Coal Member samples 8 and 9, and (iii) Buffaloville Coal Member samples 6 and 7. In contrast, Warrick County coal samples 1 and 2 and Gibson County coal samples 3 to 5 are petrographically more homogeneous.

Table 6. Petrographic characteristics (vol. %) and ash yield and moisture content of coals (wt. %). V = vitrinite, L = liptinite, I = inertinite, MM = mineral matter, R_o = vitrinite reflectance (%), H_2O_{eq} = equilibrium moisture content (wt. %). Coal samples are listed in stratigraphic order by Coal Member. Ash yield reported in wt. % as received (a.r.) and dry basis.

Coal sample	Coal Member	County	Petrography (vol. %)				R_o (%)	Ash yield (wt. %, a.r.)	Ash yield (wt. %, dry)	H_2O_{eq} (wt. %)
			V	L	I	MM				
1. 20011113-A2	Springfield	Warrick	85.2	3.0	10.0	1.8	0.48	11.09	12.65	7.86
2. 20011113-A6	Springfield	Warrick	90.0	5.0	1.6	3.4	0.54	12.05	13.74	n.d.
3. 20031009-1	Springfield	Gibson	85.6	6.8	6.8	0.8	0.62	6.69	7.13	8.38
4. 20031009-2	Springfield	Gibson	81.0	6.8	10.8	1.4	0.62	3.31	3.57	n.d.
5. 20031009-3	Springfield	Gibson	89.8	6.6	2.6	1.0	0.61	4.67	5.05	8.79
6. 20040428-C1	Buffaloville	Daviess	84.0	3.6	10.8	1.6	0.58	5.12	5.82	8.53
7. 20040428-C3	Buffaloville	Daviess	60.8	5.2	29.0	5.0	0.60	9.66	11.09	n.d.
8. 20040428-B1	Upper Block	Daviess	76.4	9.6	12.8	1.2	0.57	4.24	5.03	n.d.
9. 20040428-B2	Upper Block	Daviess	63.4	8.2	28.0	0.4	0.55	3.9	4.7	n.d.
10. Billings	Lower Block	Daviess	69.6	16	13.6	0.8	0.62	2.35	2.73	10.32
11. 20040428-A2	Lower Block	Daviess	84.8	7.2	6.4	1.6	0.59	4.93	5.78	n.d.
12. 20040428-A3	Lower Block	Daviess	56.8	10.6	31.4	1.2	0.60	10.13	11.91	9.18

n.d. = no data

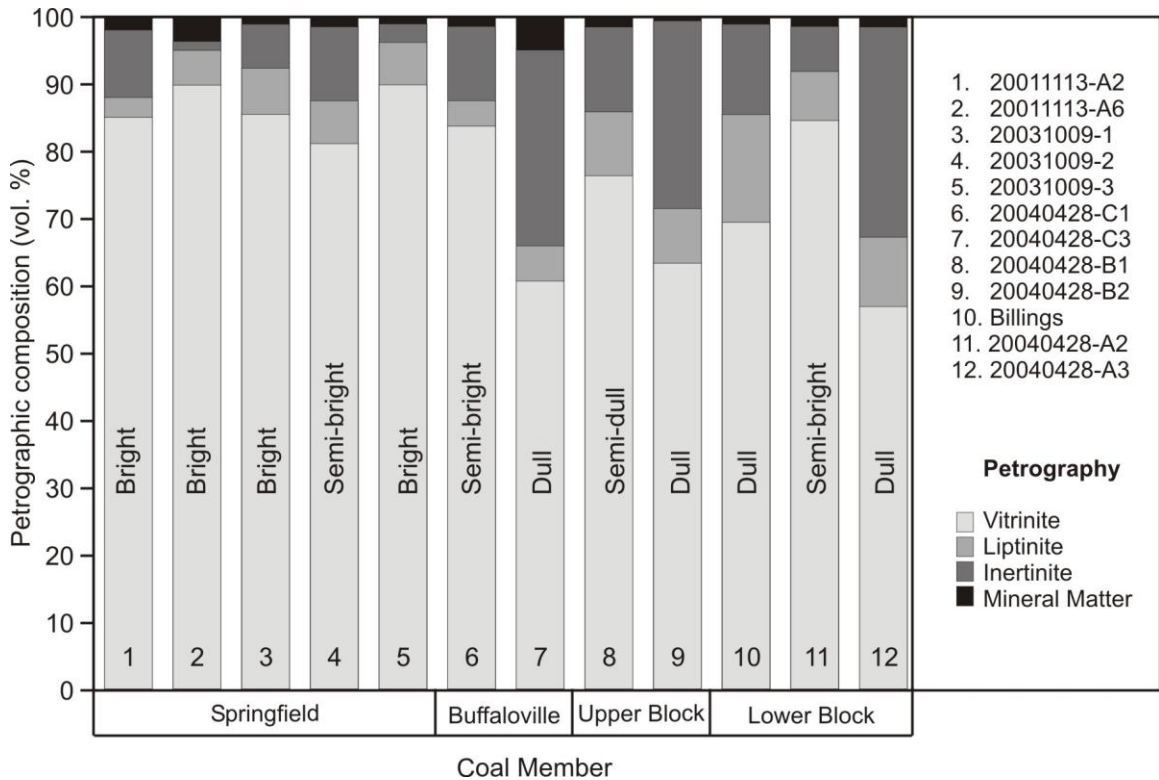


Figure 12. Maceral compositions of selected coal samples.

8.3.6. Grain size analyses

Table 7 summarizes grain size distributions from sieved coal fractions that had been pre-crushed to <3 mm Ø for chemical proximate and ultimate analyses. The samples were sieved and weighed to characterize their particle size distributions. The measured fractions were normalized to 100% of weight to facilitate comparison among all coal samples. The coarsest >1.19 mm Ø fraction was retained on a 16 mesh sieve and averaged ~37 wt. % in all coal samples. The sequence from coarse to fine continued with ~12 wt. % retained on a 20 mesh sieve (840-1189 µm), ~12 wt. % on a 30 mesh sieve (595-839 µm), ~22 wt. % on a 60 mesh sieve (250-594 µm), and finally ~17 wt. % in the pan (<250 µm). All sieved fractions were recombined for each individual coal sample and the coals were stored in the original plastic containers that had been previously used to store the coal at the Indiana Geological Survey's coal laboratory. The samples were kept closed in a dark room before moisture equilibration and measurements of high- and low-pressure adsorption isotherms.

Grain size distributions of coal fractions are shown in Figure 13. The 12 coal samples can be divided into three groups based on visual inspection: (1) samples 1, 2, and 12 with more than 45 wt. % coarse particles >1.19mm, (2) samples 3, 4, 5, 6, 7, 8, 9, and 11 with their coarsest fractions ranging between 30 and 40% wt. %, and (3) sample 10 from Billings Mine with only ~21 wt. % of coarse particles.

Table 7. Particle size distribution of crushed and sieved Indiana coals. The data are presented in stratigraphic order by Coal Member.

Coal sample	Coal Member	Grain size distribution										
		U.S. standard sieve size (mesh)					Net wt. (g)	U.S. standard sieve size (mesh)				
		16	20	30	60	pan		16	20	30	60	pan
		Weight of size fractions (g)						Normalized weight of fractions (%)				
1. 20011113-A2	Springfield	32.7	5.9	7.5	9.7	5.8	61.7	53.1	9.6	12.2	15.7	9.4
2. 20011113-A6	Springfield	31.8	5.3	6.4	9.4	7.2	60.1	52.9	8.9	10.7	15.6	11.9
3. 20031009-1	Springfield	20.8	7.9	10.0	14.9	11.8	65.3	31.9	12.1	15.3	22.7	18.0
4. 20031009-2	Springfield	16.3	6.1	6.9	12.0	8.7	50.1	32.5	12.3	13.9	24.0	17.4
5. 20031009-3	Springfield	26.9	11.0	11.1	17.2	11.5	77.7	34.6	14.2	14.3	22.1	14.8
6. 20040428-C1	Buffaloville	27.1	12.4	12.4	21.5	19.2	92.6	29.2	13.4	13.4	23.3	20.7
7. 20040428-C3	Buffaloville	21.1	8.1	7.7	14.5	13.5	64.8	32.5	12.5	11.9	22.3	20.8
8. 20040428-B1	Upper Block	7.5	2.4	2.2	4.3	3.2	19.7	38.0	12.4	11.3	21.9	16.4
9. 20040428-B2	Upper Block	18.4	6.1	5.8	9.1	9.4	48.9	37.6	12.5	11.9	18.7	19.2
10. Billings	Lower Block	13.7	10.4	10.9	15.8	15.1	65.9	20.7	15.8	16.5	24.0	23.0
11. 20040428-A2	Lower Block	19.0	7.0	7.3	12.5	9.9	55.7	34.2	12.7	13.1	22.4	17.7
12. 20040428-A3	Lower Block	26.1	6.4	6.0	9.3	9.0	56.8	45.9	11.3	10.5	16.4	15.9

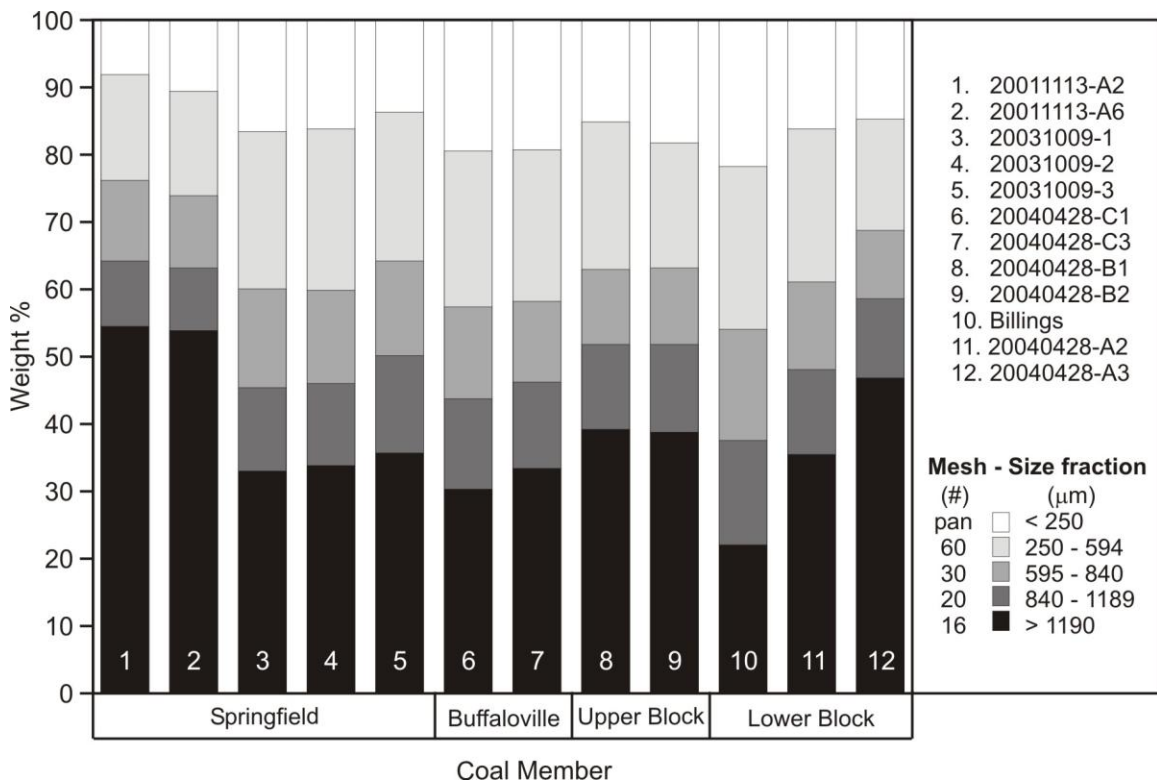


Figure 13. Weight percent distribution of measured coal size fractions from crushed and sieved Indiana coals.

8.3.7. Mesopore characteristics constrained by low-pressure N₂ adsorption

Low-pressure adsorption isotherms were measured on the ASAP-2020 instrument described in Chapter 7 to determine the mesopore characteristics of several coals samples (Table 8). Low-pressure N₂ adsorption isotherms are presented graphically in Figures 14 through 19. Available data were grouped by coal seams for consistency, interpretation, and to facilitate comparison among samples. This study follows Sing *et al.*'s (1985) recommendation that graphs of adsorption isotherm use the Y-axis to display the amount of adsorbed gas and the X-axis to show the relative pressure (P/P_o), where P is the gas pressure at any given incremental measurement and P_o is the saturation gas pressure at equilibrium, at a certain temperature chosen for all measurements.

BET surface area measurements of mesopores range from ~6.1 to ~55.7 m²/g (average 24.0 ± 15 m²/g). Similarly, the BJH cumulative surface area of mesopores ranges from ~5.8 to ~46.6 m²/g (average 21.3 ± 13 m²/g). The average mesopore width of 8.13 nm for sample 13 (Sullivan County; 20052770-T31) is significantly larger than the average mesopore width of 5.9 ± 0.9 nm for the other coal samples.

Figure 14 shows data from the Springfield Coal Member in Gibson and Warrick Counties. Large differences are observed in the adsorption capacities of samples from Gibson County (~4 cm³/g difference between highest and lowest adsorption capacities at 0.5 relative pressure), while a significantly smaller difference of ~0.5 cm³/g is observed for Warrick County samples at the same relative pressure.

Table 8. Low-pressure N₂ adsorption data collected for various coal seams in southwestern Indiana using the Micromeritics ASAP-2020 instrument described in section 8.2.4. The samples are presented in stratigraphic order by Coal Member.

Coal Member	Coal sample number	County	Data from low-pressure N ₂ adsorption		
			BET surface area (m ² /g)	BJH adsorption: cumulative surface area of mesopores (m ² /g)	Average mesopore width (nm)
Springfield	1. 20011113-A2	Warrick	9.7	8.6	6.2
	2. 20011113-A6	Warrick	8.9	8.1	6.6
	3. 20031009-1	Gibson	14.2	12.1	5.4
	4. 20031009-2	Gibson	23.1	19.7	5.1
	5. 20031009-3	Gibson	19.5	16.1	4.9
Seelyville	13. 20052770-T31	Sullivan	6.1	5.8	8.1
Buffaloville	6. 20040428-C1	Daviess	12.9	11.7	6.4
	7. 20040428-C3	Daviess	17.2	15.6	6.3
Upper Block	8. 20040428-B1	Daviess	38.4	35.3	5.8
	9. 20040428-B2	Daviess	33.4	30.9	5.9
Lower Block	10. Billings	Daviess	40.1	36.5	4.8
	11. 20040428-A2	Daviess	55.7	46.6	4.8
	12. 20040428-A3	Daviess	33.2	29.5	5.9

Figures 15, 16, and 17 display the data from Buffaloville, Upper Block, and Lower Block Coal Members, respectively (all from Daviess County, Indiana). The graphs reveal significant differences among nitrogen adsorption capacities in Lower Block coals (~ 10 cm^3/g difference between highest and lowest adsorption capacities measured at 0.5 relative pressure), with smaller differences in gas adsorption capacities at 0.5 relative pressure for the Upper Block (~ 2.8 cm^3/g) and Buffaloville coals (~ 1.9 cm^3/g).

Only one coal sample was available from the Seelyville Coal Member in Sullivan County for determining an adsorption isotherm (Figure 18). The nitrogen adsorption capacity of this coal at 0.5 relative pressure is 3 cm^3/g . Figure 19 compares the nitrogen adsorption capacities of several coals mentioned above. All coals exhibit similar trends in their isotherms except coals from Upper and Lower Block Coal Members where adsorption capacities are far larger than those measured for other coals (i.e., 24 cm^3/g for the Lower Block and 16 cm^3/g for the Upper Block at 0.5 relative pressure).

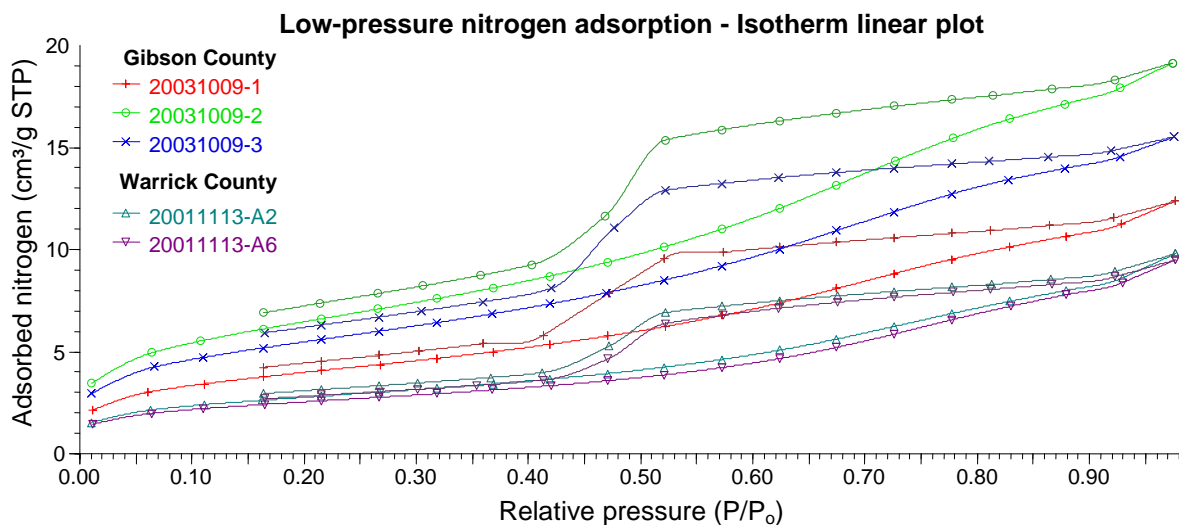


Figure 14. Low-pressure nitrogen adsorption isotherms from coal samples of the Springfield Coal Member from Gibson and Warrick Counties, southwest Indiana. Data graphed at standard temperature and pressure (STP) conditions (0°C and 0.101 MPa).

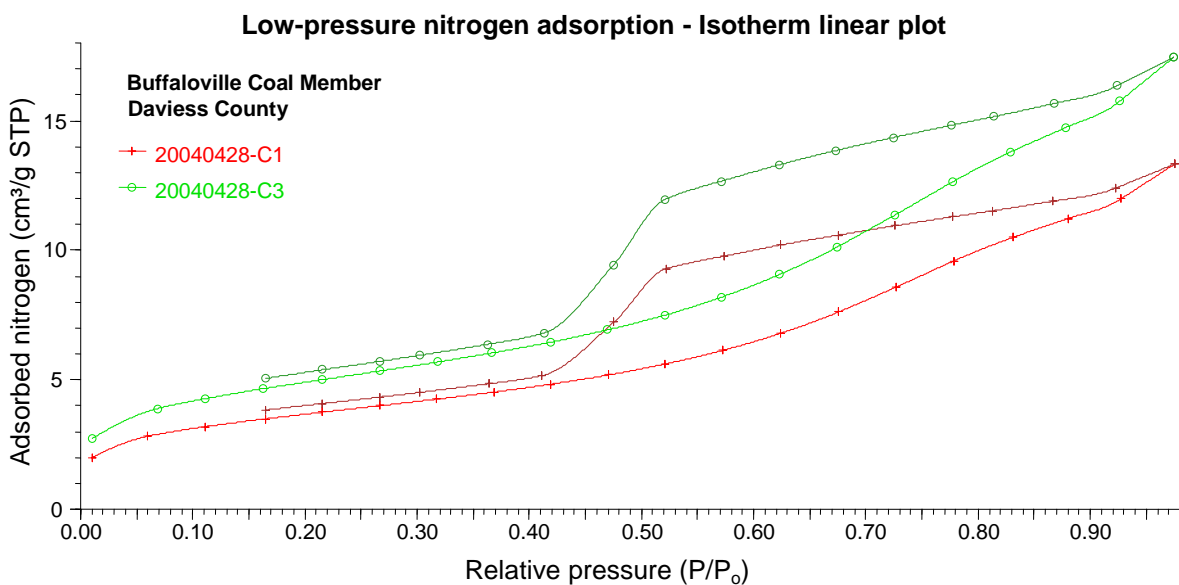


Figure 15. Low-pressure nitrogen adsorption isotherms from coal samples of the Buffaloville Coal Member in Daviess County, Indiana. Data graphed at standard temperature and pressure (STP) conditions (0°C and 0.101 MPa).

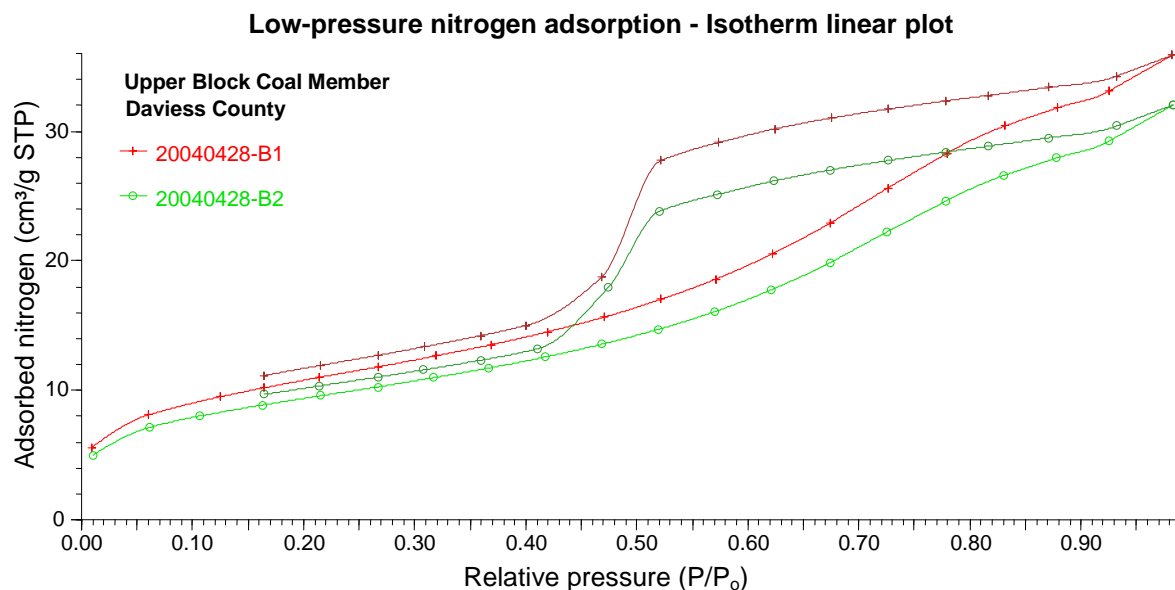


Figure 16. Low-pressure nitrogen adsorption isotherms from coal samples of the Upper Block Coal Member in Daviess County, Indiana. Data graphed at standard temperature and pressure (STP) conditions (0°C and 0.101 MPa).

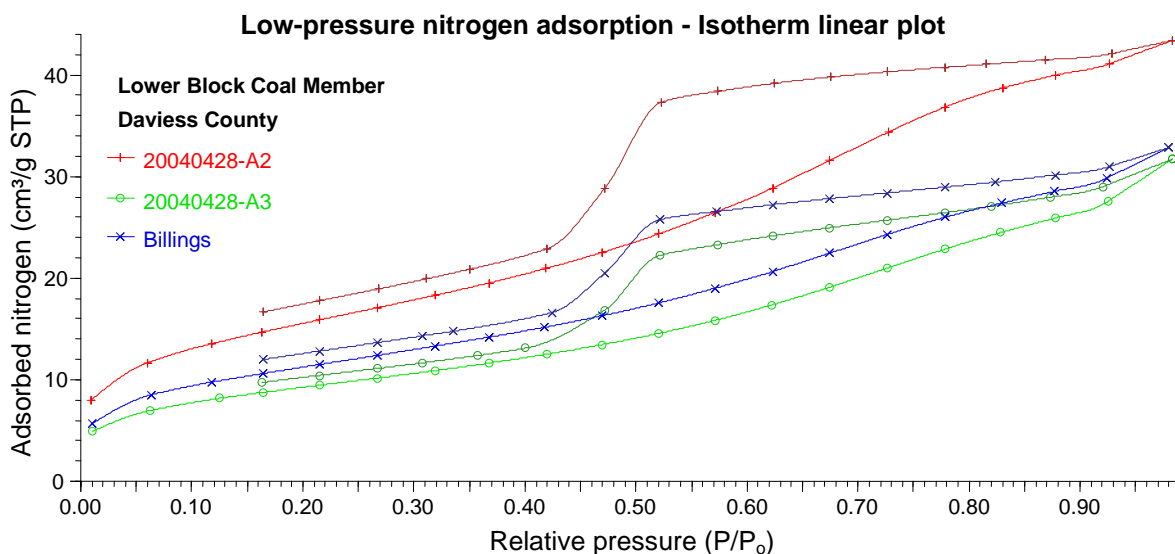


Figure 17. Low-pressure nitrogen adsorption isotherms from coal samples of the Lower Block Coal Member in Daviess County, Indiana. Data graphed at standard temperature and pressure (STP) conditions (0°C and 0.101 MPa).

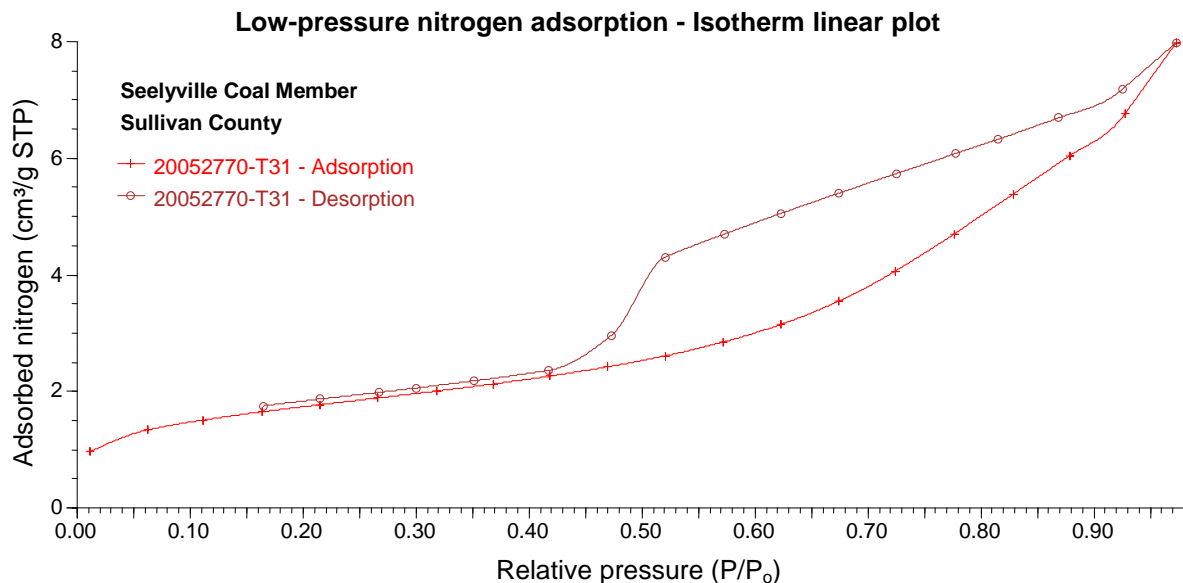


Figure 18. Low-pressure nitrogen adsorption isotherms from coal samples of the Seelyville Coal Member in Sullivan County, Indiana. Data graphed at standard temperature and pressure (STP) conditions (0°C and 0.101 MPa).

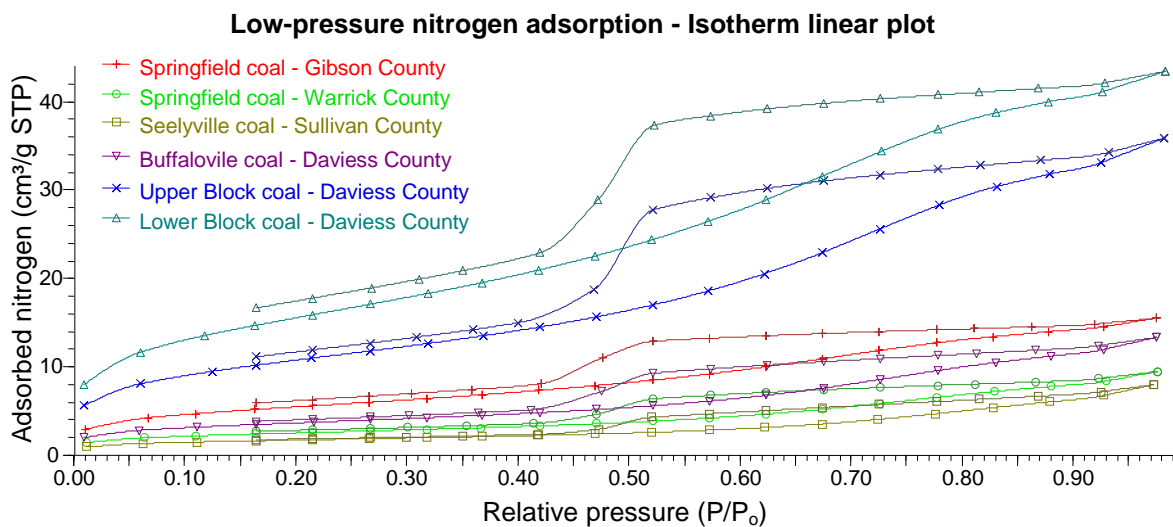


Figure 19. Comparison of low-pressure nitrogen adsorption isotherms from selected coal samples across several coal members and counties in Indiana. Data graphed at standard temperature and pressure (STP) conditions (0°C and 0.101 MPa).

8.3.8. Micropore characteristics constrained by low-pressure CO₂ adsorption

Low-pressure CO₂ adsorption isotherms highlight the adsorption capacity of all coals. Data were measured on a Micromeritics ASAP-2020 instrument to determine the micropore characteristics of several coal samples (Figures 20 through 27; see also Table 9). The data were also grouped by coal seams to facilitate comparison among samples (Figures 20- 23), as described earlier for low-pressure N₂ adsorption data (section 8.3.6).

BET micropore surface areas range between ~55.6 and ~88.4 m²/g (average 76.9 ± 8.8 m²/g). Dubinin-Radushkevich micropore surface areas range from ~87.5 to ~139.5 m²/g (average 120.5 ± 13.9 m²/g). Monolayer capacities range between 19.2 and 30.5 cm³/g (average 26.4 ± 3.1 cm³/g). Limiting micropore volumes range from 0.0410 to 0.0637 cm³/g (average 0.055 ± 0.006 cm³/g).

Figure 20 shows low-pressure CO₂ adsorption isotherms from the Springfield Coal Member in Gibson and Warrick Counties. Slight differences are observed among CO₂ adsorption capacities of coals from the same county. At 0.02 relative pressure, the CO₂ adsorption capacities of Warrick County coals range narrowly from ~10.6 to ~11.1 cm³/g, whereas Gibson County coals exhibit a larger range from ~12.5 to ~13.7 cm³/g.

Figures 21, 22, and 23 illustrate CO₂ adsorption capacities of Daviess County coals. Buffaloville coals exhibit little variance in CO₂ adsorption capacity around 0.3 cm³/g at 0.02 relative pressure (Figure 21), but Upper Block coals are even more similar (Figure 22). CO₂ adsorption capacities of Upper Block coals are ~12.1 cm³/g at 0.02 relative pressure. Lower Block coals (Figure 17) display CO₂ adsorption capacities from ~11 to ~13.2 cm³/g at 0.02 relative pressure.

Only one coal sample was available for the Seelyville Coal Member in Sullivan County for determining a CO₂ adsorption isotherm (Figure 24). The measured CO₂ adsorption capacity of this coal sample at 0.02 relative pressure is 8.8 cm³/g. Figure 25 compares CO₂ adsorption capacities of several coals. The CO₂ adsorption capacities for all coals range between ~8.2 and ~13.7 cm³/g. Springfield coals and Lower Block coals express largest gas adsorption capacities, whereas a sample from the Seelyville Coal Member shows the smallest CO₂ adsorption capacity at 0.02 relative pressure.

Low-pressure CO₂ adsorption capacities display only a moderate variance among coals in this study. Nonetheless, the utility of low-pressure CO₂ adsorption measurements goes beyond estimating the gas saturation capacity of coals at a defined pressure. The advantage of CO₂ as an adsorbent gas is the ease with which it penetrates micropores, therefore providing a means to interpret the size of micropores and establishing the surface area available for adsorption.

Table 9. Low-pressure CO₂ adsorption data collected for various coal seams in southwestern Indiana. The samples are grouped in stratigraphic order by Coal Member.

Coal Member	Sample number	County	Data from low-pressure CO ₂ adsorption				
			BET surface area (m ² /g)	Dubinin-Radushkevich		Dubinin-Astakhov limiting micropore volume (cm ³ /g)	Average micropore size (nm)
				Micropore surface area (m ² /g)	Mono-layer capacity (cm ³ /g)		
Springfield	1. 20011113-A2	Warrick	69.6	108.5	23.74	0.0510	1.35
	2. 20011113-A6	Warrick	72.8	113.4	24.83	0.0535	1.34
	3. 20031009-1	Gibson	82.7	130.0	28.47	0.0580	1.36
	4. 20031009-2	Gibson	86.4	135.4	29.63	0.0608	1.37
	5. 20031009-3	Gibson	88.4	139.5	30.55	0.0608	1.36
Seelyville	13. 20052770-T31	Sullivan	55.6	87.5	19.16	0.0410	1.33
Buffaloville	6. 20040428-C1	Daviess	76.6	123.0	26.92	0.0497	1.30
	7. 20040428-C3	Daviess	73.6	115.2	25.21	0.0519	1.37
Upper Block	8. 20040428-B1	Daviess	77.9	121.8	26.66	0.0592	1.35
	9. 20040428-B2	Daviess	78.0	121.8	26.66	0.0569	1.36
Lower Block	10. Billings	Daviess	81.3	126.9	27.77	0.0581	1.36
	11. 20040428-A2	Daviess	86.2	133.8	29.29	0.0637	1.36
	12. 20040428-A3	Daviess	70.9	109.5	23.97	0.0536	1.37

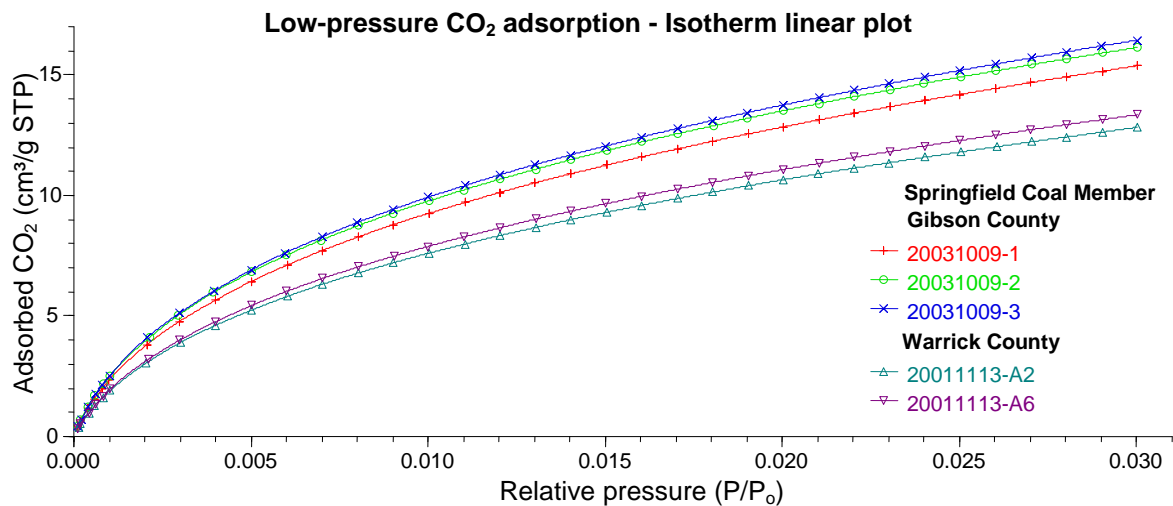


Figure 20. Low-pressure carbon dioxide adsorption isotherms from coal samples of the Springfield Coal Member in Gibson and Warrick Counties, Indiana. Data are graphed at standard temperature and pressure (STP) conditions (0°C and 0.101 MPa).

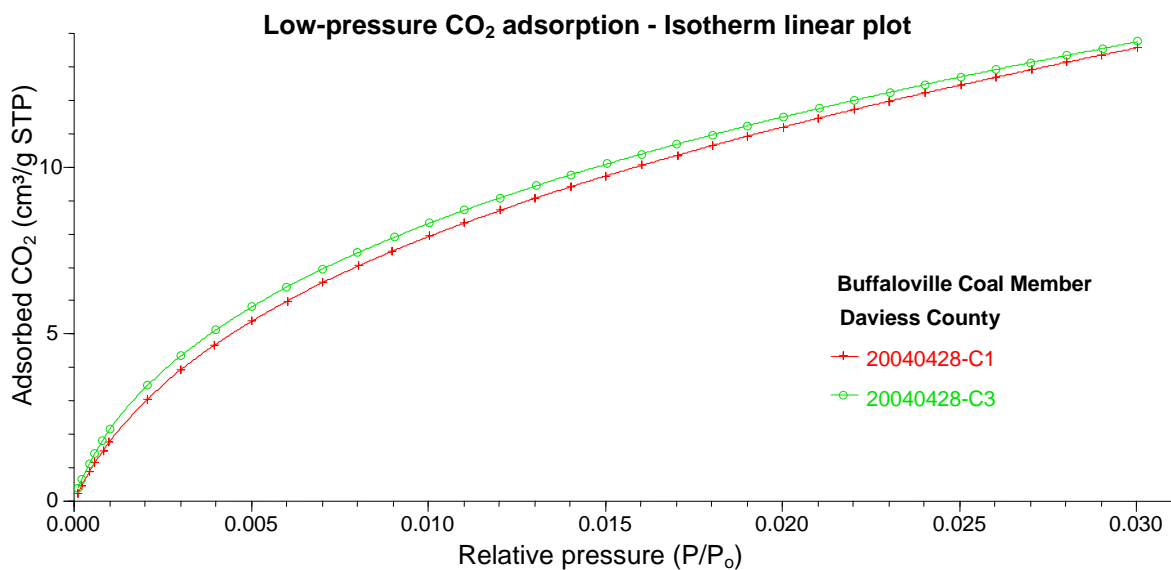


Figure 21. Low-pressure carbon dioxide adsorption isotherms from coal samples of the Buffaloville Coal Member in Daviess County, Indiana. Data are graphed at standard temperature and pressure (STP) conditions (0°C and 0.101 MPa).

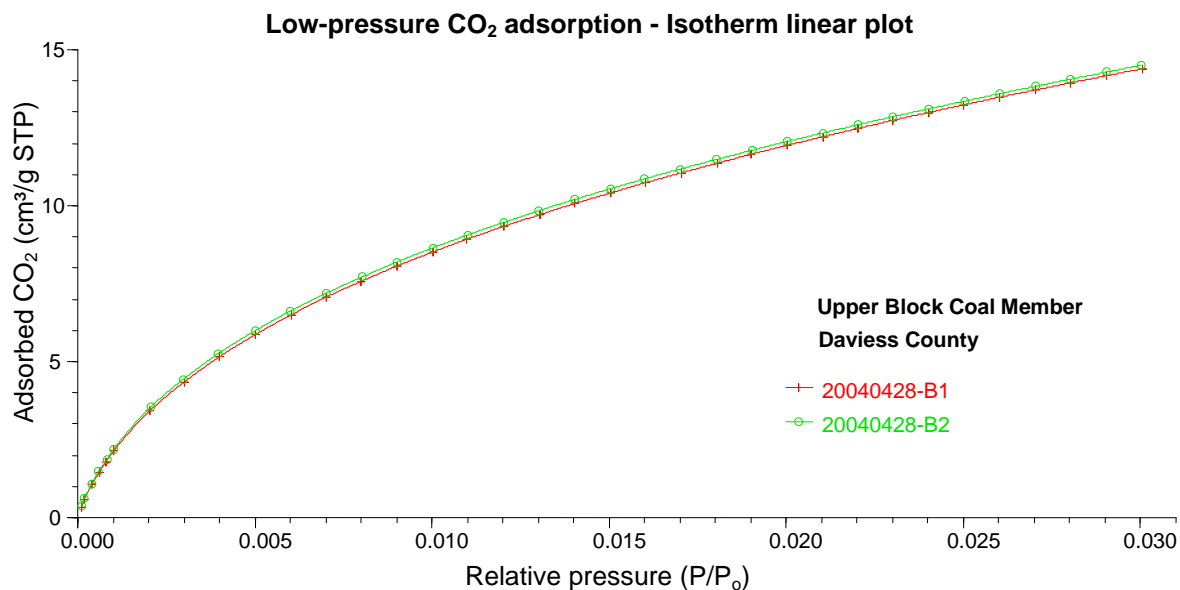


Figure 22. Low-pressure carbon dioxide adsorption isotherms from coal samples of the Upper Block Coal Member in Daviess County, Indiana. Data are graphed at standard temperature and pressure (STP) conditions (0°C and 0.101 MPa).

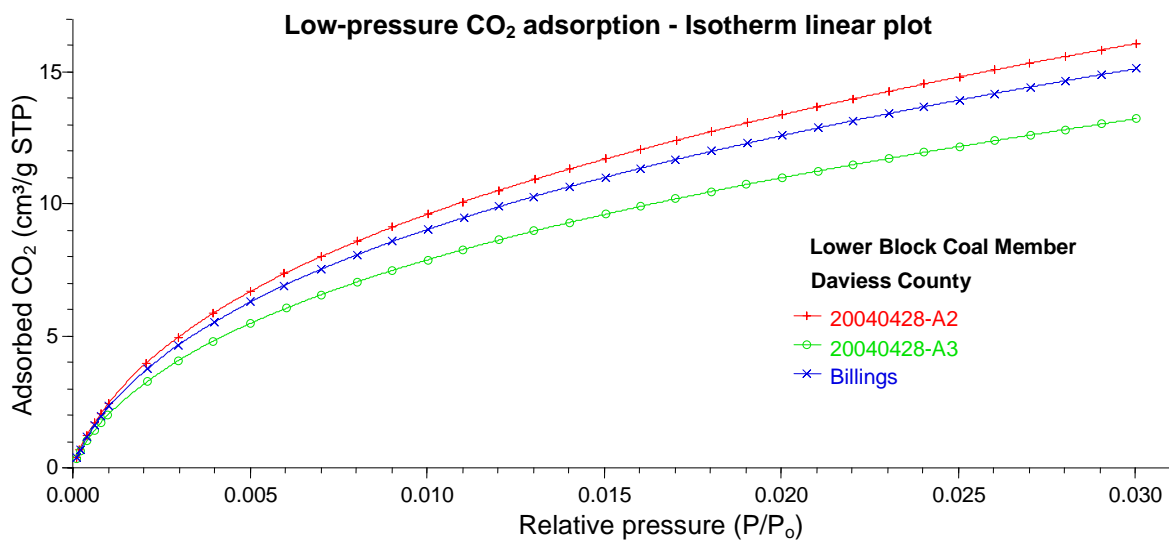


Figure 23. Low-pressure carbon dioxide adsorption isotherms from coal samples of the Lower Block Coal Member in Daviess County, Indiana. Data are graphed at standard temperature and pressure (STP) conditions (0°C and 0.101 MPa).

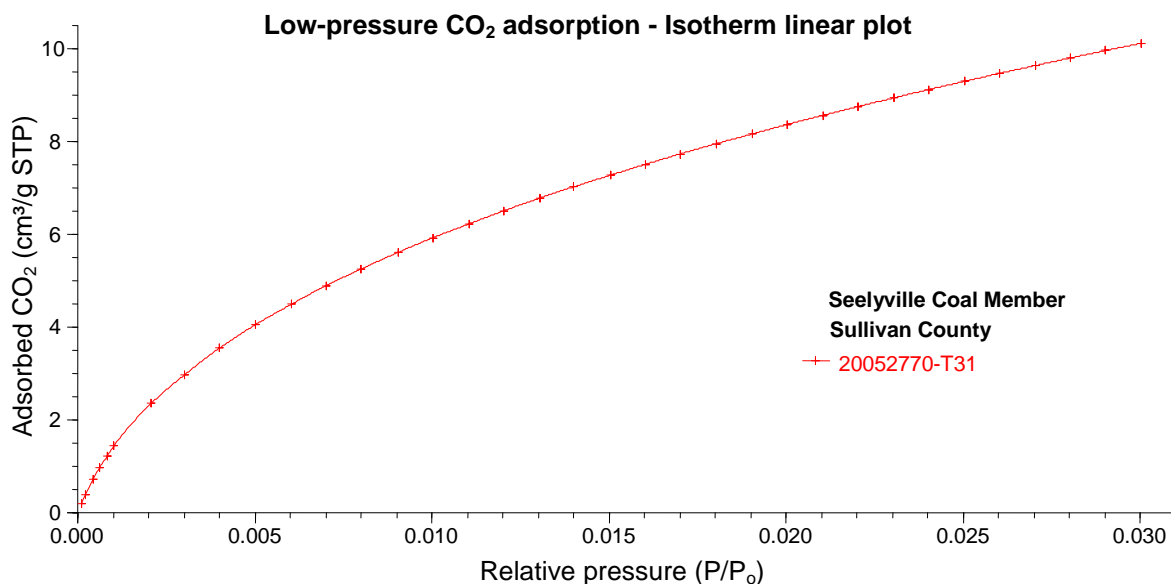


Figure 24. Low-pressure carbon dioxide adsorption isotherm from a coal sample from the Seelyville Coal Member in Sullivan County, Indiana. Data are graphed at standard temperature and pressure (STP) conditions (0°C and 0.101 MPa).

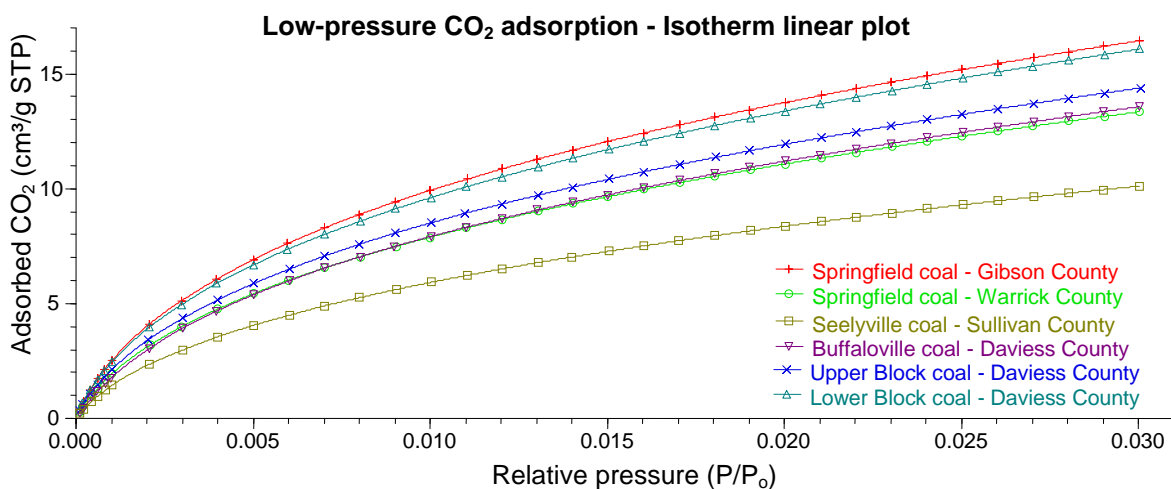


Figure 25. Comparison of low-pressure carbon dioxide adsorption isotherms from selected coal samples across several coal members and counties in Indiana. Data are graphed at standard temperature and pressure (STP) conditions (0°C and 0.101 MPa).

Variabilities in surface areas and micropore distributions in coals of the same rank are compared in graphs of cumulative surface area versus micropore width (Figure 26) and calculated cumulative micropore volume versus micropore width (Figure 27).

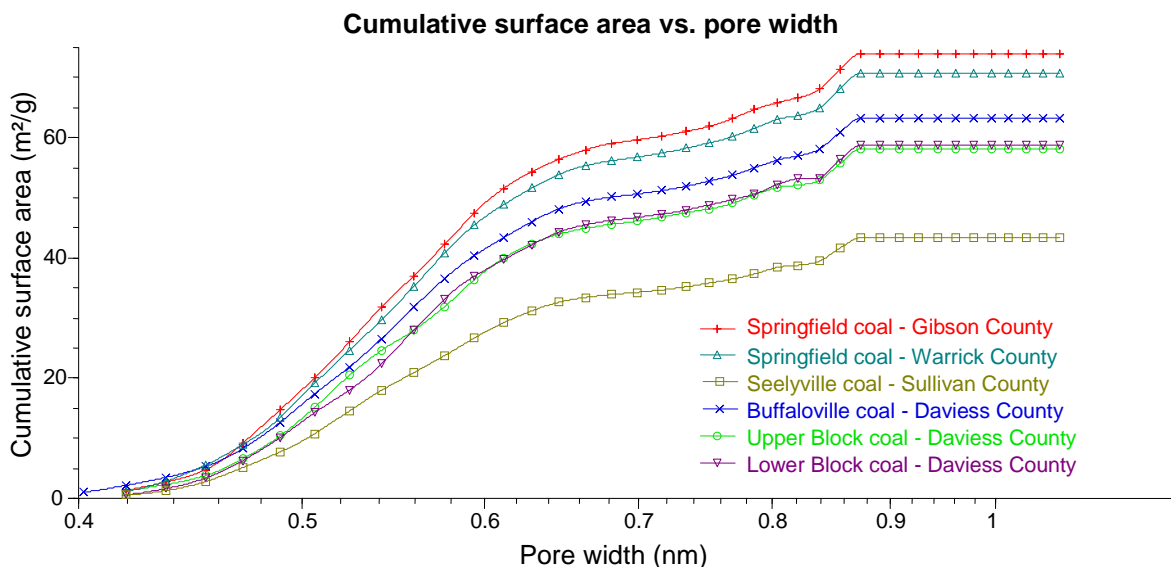


Figure 26. Comparison of cumulative surface areas versus pore widths calculated from low-pressure CO₂ adsorption data for selected coal samples across several coal members and counties in Indiana.

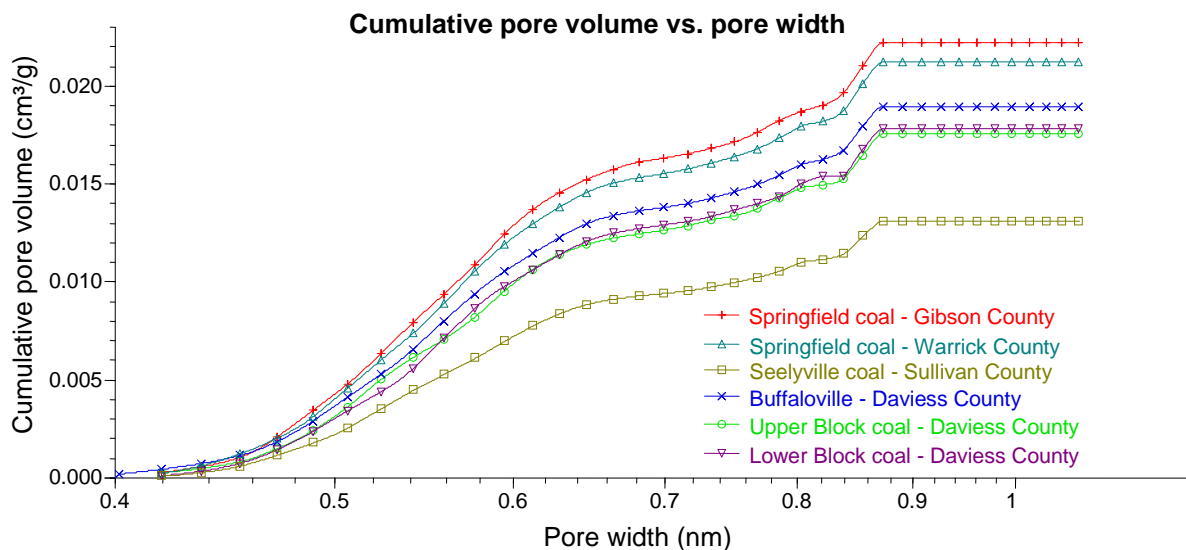


Figure 27. Comparison of cumulative pore volumes versus pore widths calculated from low-pressure CO₂ adsorption data for selected coal samples across several coal members and counties in Indiana.

8.3.9. Effects of grain size and maceral composition on gas adsorption

Two coal samples from the Lower Block Coal Member (samples 11 and 12 in Figures 12 and 13) provide the best evidence for a relationship between maceral composition, particle-size distribution, and gas adsorption capacity. For practical purposes, sample 11 is considered bright (84.8 vol. % vitrinite). The particle-size distribution in this sample is dominated by coarse material (34.2 wt. %) with lesser amounts in smaller size fractions with about equal abundances (Table 6). The low-pressure nitrogen adsorption capacity is $\sim 24 \text{ cm}^3/\text{g}$ at 0.5 relative pressure, whereas for CO_2 the adsorption capacity is $\sim 13.2 \text{ cm}^3/\text{g}$ at 0.02 relative pressure. The other sample is a petrographically dull (56.8 vol. % vitrinite) Lower Block Coal with an even larger abundance of coarse grains (45.9 wt. %) and relatively lower estimated adsorption capacities for nitrogen ($\sim 14 \text{ cm}^3/\text{g}$ at 0.5 relative pressure) and CO_2 ($\sim 11 \text{ cm}^3/\text{g}$ at 0.02 relative pressure). These observations suggest that a positive correlation between vitrinite content, surface area, and adsorption capacity, as well as an inverse correlation between particle-size and adsorption capacity. It is hypothesized that coarse-grained crushed coal tends to exhibit a smaller gas adsorption capacity.

The latter conclusion is rather intuitive because finer materials render a larger surface area available for gas adsorption. The hypothesis is corroborated by the results from our large-volume high-pressure adsorption apparatus. The high-pressure adsorption isotherms of Figures 10 and 11 suggest that an inverse correlation exists between gas adsorption capacity and particle size. Low-pressure adsorption isotherms from CO_2 adsorption experiments (Figures 26 and 27) suggest a positive correlation between gas adsorption, surface area, and micropore width. The coal sample with smallest surface

area and micropore width (i.e., Seelyville Coal; sample 13. 20052770-T31) also exhibits the smallest gas adsorption capacities for both nitrogen and CO₂ (Figures 19 and 25).

Figure 12 shows the relative ‘brightness’ or ‘dullness’ of coal according to the proportion of macerals present in each sample. These characteristics were compared with the particle-size distribution of crushed coal samples (Figure 13) and the adsorption data from high- and low-pressure adsorption experiments in an attempt to establish relationships and to provide a better understanding of the role of maceral composition and particle-size distribution on gas adsorption.

Coal sample 6 from the Buffaloville Coal Member is classified as semi-bright (84 vol. % vitrinite) whereas coal sample 7 from the same coal member falls into the dull category (60.8 vol. % vitrinite; Figures 12 and 13). The percentages of coarse particles are not very different from one another (29.2 and 32.5 wt. %; Table 7). Low-pressure nitrogen adsorption measurements show a trend that is opposite than that observed for Lower Block Coals (Figure 17). In the Buffaloville Coal Member, the sample with the highest vitrinite content and lowest abundance of coarse particles (i.e., sample 6; 20040428-C1; Figures 12 and 15) has the lowest gas adsorption capacity and the lowest surface area (Table 8). This observation is counterintuitive, but the same behavior was observed for low-pressure CO₂ adsorption results for the same pair of coal samples.

The consistent results from low-pressure CO₂ adsorption experiments for Lower Block Coal samples support the hypothesis that adsorption capacity is a function of particle size. However, the same trend was not observed for other samples (i.e., from Springfield and Buffaloville Coal Members). CO₂ adsorption data allow an adequate estimation of adsorption capacity because CO₂ is able to access pore spaces regardless of

maceral composition. For this reason, future investigations of the particle-size influence on low-pressure gas adsorption capacity of pure macerals are recommended. Such studies would allow constraining the preferential adsorption of gases in coal.

8.4. Conclusions

This study reveals that the adsorption of water on coal (i.e., the moisture content) critically influences the adsorption capacity of CH₄ and CO₂ gases in coal. The particle size distribution of crushed coal and its maceral composition seem to be directly correlated with the gas adsorption capacity. Measurements from a large-volume high-pressure volumetric adsorption apparatus at Indiana University suggest a positive relationship between decreasing grain size and increasing adsorption capacity. However, additional studies are needed to corroborate this hypothesis.

The ratio of CO₂ and CH₄ adsorption capacities in coal can help to estimate the CO₂ sequestration potential of coal seams with otherwise limited data coverage. These results have important implications for CBM exploration, the prediction of potential coalbed methane reservoirs, as well as for estimation of the potential gas storage capacity of coal seams for CO₂ sequestration. The ratios between experimentally determined CO₂ and CH₄ adsorption capacities from high-pressure experiments in moisture-equilibrated high volatile bituminous coals range between 2.3 and 5.5 at 2.8 MPa (400 psi), which is in agreement with previous studies on Indiana coals.

The average methane adsorption capacity of dry coal samples at 2.8 MPa (400 psi) is 2.4 times larger than the average methane adsorption capacity of moisture-equilibrated coal samples. For CO₂ the respective factor is 1.4. The calculated ratios of CO₂ and CH₄ adsorption capacities from high-pressure gas adsorption isotherms of dry coal samples range between 1.9 and 2.8 at 2.8 MPa (400 psi). Therefore, a significant bias in data from

experimental adsorption assays can be introduced when coal samples have not been adequately preserved and no longer reflect *in situ* moisture conditions in coal seams.

The most significant finding of this work involves the effect of irreversible moisture loss on the adsorption capacities of (i) coal that was exposed to dry air and (ii) the same coal that has subsequently been moisture-equilibrated. At high gas pressure, moisture loss accounts for up to ~30% increased methane adsorption capacity of dry coal samples relative to coals that have never experienced drying. Even after moisture-equilibration of previously dried coals, the adsorption capacity remains up to ~40% enhanced. A clear relationship exists between the duration of coal's exposure to dry air and the ability of coal to become re-equilibrated with moisture. In other words, samples that have been exposed to air drying after collection, or have not been properly "sealed" to prevent moisture loss, are likely to produce adsorption data that do not correspond to the gas adsorption potential of *in situ* moisture-saturated coal.

Similar to CH₄, a qualitative increase in high-pressure adsorption capacity with increasing loss of moisture was observed for CO₂ as an adsorbent gas, although the relative increase in CO₂ adsorption capacity was significantly lower than that of methane, i.e., ~25% for dry coal samples and about ~18% for moisture-equilibrated coal samples.

The results from this study urge the reader to pay utmost attention to collection and preservation of coal samples. Even slight changes of the coal's original reservoir conditions, in particular with regard to the loss of moisture from coal, will likely result in artificially enhanced gas adsorption capacities. This bias can lead to erroneous over-estimates in exploration, namely with regard to the potential capacities of coals to

produce coalbed methane (CBM), and also in terms of reservoir capacities for capture and permanent storage of sequestered anthropogenic CO₂.

References

- ASTM, 2006. Annual Book of ASTM Standards. Section 5. Petroleum Products, Lubricants, and Fossil Fuels. Volume 05.06. Gaseous fuels; coal and coke. American Society for Testing and Materials Standards, West Conshohocken, Pennsylvania, 705 p.
- Bachu, S., Michael, K., 2003. Possible controls of hydrogeological and stress regimes on the producibility of coalbed methane in Upper Cretaceous - Tertiary strata of the Alberta basin, Canada. American Association of Petroleum Geologists, Bulletin 87, 1729-1754.
- Brunauer, S., Deming, L.S., Deming, W.E., Teller, E., 1940. On a theory of the van der Waals adsorption of gases. Journal of the American Chemical Society 62, 1723-1732.
- Brunauer, S., Emmett, P.H., Teller, E., 1938. Adsorption of gases in multimolecular layers. Journal of the American Chemical Society 60, 309-319.
- Busch, A., Gensterblum, Y., Siemons, N., Krooss, B.M., van Bergen, F., Pagnier, H.J.M., David, P., 2003a. Investigation of preferential sorption behaviour of CO₂ and CH₄ on coals by high pressure adsorption/desorption experiments with gas mixtures. International Coalbed Methane Symposium, Tuscaloosa, Alabama, Paper 0350.
- Busch, A., Krooss, B.M., Gensterblum, Y., van Bergen, F., Pagnier, H.J.M., 2003b. High-pressure adsorption of methane, carbon dioxide, and their mixtures on coals with a special focus on the preferential sorption behaviour. Journal of Geochemical Exploration 78-79, 671-674.

- Busch, A., Gensterblum, Y., Krooss, B.M., Littke, R., 2004. Methane and carbon dioxide adsorption-diffusion experiments on coal: upscaling and modeling. *International Journal of Coal Geology* 60, 151-168.
- Busch, A., Gensterblum, Y., Krooss, B.M., Siemons, N., 2006. Investigation of high-pressure selective adsorption/desorption behavior of CO₂ and CH₄ on coals: An experimental study. *International Journal of Coal Geology* 66, 53-68.
- Busch, A., Gensterblum, Y., Krooss, B.M., 2007. High-pressure sorption of nitrogen, carbon dioxide, and their mixtures on Argonne Premium coals. *Energy & Fuels* 21, 1640-1645.
- Ceglarska-Stefanska, G., Zarebska, K., 2002. The competitive sorption of CO₂ and CH₄ with regard to the release of methane from coal. *Fuel Processing Technology* 77-78, 423-429.
- Clarkson, C.R., Bustin, R.M., 1996. Variation in micropore capacity and size distribution with composition in bituminous coal of the Western Canadian sedimentary basin. *Fuel* 75, 1483-1498.
- Clarkson, C.R., Bustin, R.M., 1999a. The effect of pore structure and gas pressure upon the transport properties of coal: a laboratory and modeling study. 1. Isotherms and pore volume distributions. *Fuel* 78, 1333-1344.
- Clarkson, C.R., Bustin, R.M., 1999b. The effect of pore structure upon the transport properties of coal: a laboratory and modeling study. 2. Adsorption rate modeling. *Fuel* 78, 1345-1362.

- Clarkson, C.R., Bustin, R.M., 2000. Binary gas adsorption/desorption isotherms: effect of moisture and coal composition upon carbon dioxide selectivity over methane. *International Journal of Coal Geology* 42, 241-271.
- Cloke, M., Lester, E., Belghazi, A., 2002. Characterisation of the properties of size fractions from ten world coals and their chars produced in a drop-tube furnace. *Fuel* 81, 699-708.
- Crosdale, P.J., Beamish, B.B., Valix, M., 1998. Coalbed methane sorption related to composition. *International Journal of Coal Geology* 35, 147-158.
- Cui, X., Bustin, R.M., Dipple, G., 2004. Selective transport of CO₂, CH₄, and N₂ in coals: insights from modeling of experimental gas adsorption data. *Fuel* 83, 293-303.
- Dubinin, M.M., 1960. The potential theory of adsorption of gases and vapors for adsorbents with energetically nonuniform surfaces. *Chemical Reviews* 60, 235-241.
- Ettinger, I., Eremin, I., Zimakov, B., Yanovskaya, M., 1966. Natural factors influencing coal sorption properties I - Petrography and the sorption properties of coals. *Fuel* 45, 267-275.
- Gamson, P.D., Beamish, B.B., Johnson, D.P., 1993. Coal microstructure and micropermeability and their effects on natural gas recovery. *Fuel* 72, 87-99.
- Gan, H., Nandi, S.P., Walker, P.L., 1972. Nature of the porosity in American coals. *Fuel* 51, 272-277.
- Goodman, A.L., Busch, A., Bustin, R.M., Chikatamarla, L., Day, S., Duffy, G.J., Fitzgerald, J.E., Gasem, K.A.M., Gensterblum, Y., Hartman, C., Jing, C., Krooss B.M., Mohammed, S., Pratt, T., Robinson, R.L. Jr., Romanov, V., Sakurovs, R.,

- Schroeder, K., White, C.M., in press. Inter-laboratory comparison II: CO₂ isotherms measured on moisture-equilibrated Argonne premium coals at 55°C and up to 15 MPa. *International Journal of Coal Geology*, doi:10.1016/j.coal.2007.01.005.
- Goodman, A.L., Busch, A., Duffy, G.J., Fitzgerald, J.E., Gasem, K.A.M., Gensterblum, Y., Krooss B.M., Levy, J., Ozdemir, E., Pan, Z., Robinson, R.L. Jr., Schroeder, K., Sudibandriyo, M., White, C.M., 2004. An Inter-laboratory comparison of CO₂ isotherms measured on Argonne premium coal samples. *Energy & Fuels* 18, 1175-1182.
- Goodman, A.L., Campus, L.M., Schroeder, K., 2005. Direct evidence of carbon dioxide sorption on Argonne premium coals using attenuated total reflectance - Fourier Transform Infrared Spectroscopy. *Energy & Fuels* 19, 471-476.
- Gurdal, G., Yalcin, M.N., 2001. Pore volume and surface area of the Carboniferous coals from the Zonguldak basin (NW Turkey) and their variations with rank and maceral composition. *International Journal of Coal Geology* 48, 133-144.
- Hartman, C., Pratt, T.J., 2005. A preliminary study of the effect of moisture on the carbon dioxide storage capacity in coal. 2005 International Coalbed Methane Symposium, Tuscaloosa, Alabama, Paper 0533.
- Karacan, C.O., Mitchell, G.D., 2002. Carbon dioxide storage properties of different coal lithotypes in relation to geological sequestration into coalbeds. 19th Annual International Pittsburgh Coal Conference, Pittsburgh, PA, pp. 1-8.

- Karacan, C.O., Mitchell, G.D., 2003. Behavior and effect of different coal microlithotypes during gas transport for carbon dioxide sequestration into coal seams. *International Journal of Coal Geology* 53, 201-217.
- Krooss, B.M., van Bergen, F., Gensterblum, Y., Siemons, N., Pagnier, H.J.M., David, P., 2002. High-pressure methane and carbon dioxide adsorption on dry and moisture-equilibrated Pennsylvanian coals. *International Journal of Coal Geology* 51, 69-92.
- Lamberson, M.N., Bustin, R.M., 1993. Coalbed methane characteristics of Gates Formation coals, Northeastern British Columbia: Effect of maceral composition. *American Association of Petroleum Geologists, Bulletin* 77, 2062-2076.
- Langmuir, I., 1918. The adsorption of gases on plane surfaces of glass, mica, and platinum. *Journal of the American Chemical Society* 40, 1361-1403.
- Levy, J., Day, H., Killingley, J.S., 1997. Methane capacities of Bowen basin coals related to coal properties. *Fuel* 76, 813-819.
- Low, M.J.D., 1960. Kinetics of chemisorption of gases on solids. *Chemical Reviews* 60, 267-312.
- Mastalerz, M., Gluskoter, H., Rupp, J.A., 2004. Carbon dioxide and methane sorption in high volatile bituminous coals from Indiana, USA. *International Journal of Coal Geology* 60, 43-55.
- Mavor, M.J., Nelson, C.R., 1997. Coalbed Reservoir Gas-In-Place Analysis, Chapter 3. Gas Research Institute, Report No. GRI-97/0263, Chicago, Illinois.
- Mavor, M.J., Owen, L.B., Pratt, T.J., 1990. Measurement and evaluation of coal sorption isotherm data. *Society of Petroleum Engineers SPE* 20728, 157-170.

- Mazumder, S., van Hemert, P., Bruining, J., Wolf, K.H.A.A., 2003. A preliminary numerical model of CO₂ sequestration in coal for improved coalbed methane production. 2003 International Coalbed Methane Symposium, Tuscaloosa, Alabama. Paper 0331.
- Mazumder, S., van Hemert, P., Bruining, J., Wolf, K.H.A.A., Drabe, K., 2006. In situ CO₂-coal reactions in view of carbon dioxide storage in deep unminable coal seams. Fuel 85, 1904-1912.
- Medek, J., 1977. Possibility of micropore analysis of coal and coke from the carbon dioxide isotherm. Fuel 56, 131-133.
- Nandi, S.P., Walker, P.L., 1975. Activated diffusion on methane from coals at elevated pressures. Fuel 54, 81-86.
- Olague, N.E., Smith, D.M., 1989. Diffusion of gases in American coals. Fuel 68, 1381-1387.
- Pashin, J.C., McIntyre, M.R., 2003. Temperature-pressure conditions in coalbed methane reservoirs of the Black Warrior basin: Implications for carbon sequestration and enhanced coalbed methane recovery. International Journal of Coal Geology 54, 167-183.
- Pratt, T.J., Baez, L.R.G., 2003. Critical data requirements for coal and gas shale resource assessment. 2003 International Coalbed Methane Symposium, Tuscaloosa, Alabama, Paper 0367.
- Saunders, J.T., Tsai, B.M.C., Yang, R.T., 1985. Adsorption of gases on coals and heat-treated coals at elevated temperature and pressure. 2. Adsorption from hydrogen-methane mixtures. Fuel 64, 621-626.

- Scott, A.R., Kaiser, W.R., Ayers, W.B.J., 1994. Thermogenic and secondary biogenic gases, San Juan basin, Colorado and New Mexico - Implications for coalbed gas producibility. American Association of Petroleum Geologists, Bulletin 78, 1186-1209.
- Siemons, N., Busch, A., Bruining, H., Krooss, B., Gensterblum, Y., 2003. Assessing the kinetics and capacity of gas adsorption in coals by a combined adsorption / diffusion method. Society of Petroleum Engineers SPE 84340, 1-9.
- Sing, K.S.W., Everett, D.H., Haul, R.A.W., Moscou, L., Pierotti, R.A., Rouquérol, J., Siemieniewska, T., 1985. Reporting physisorption data for gas/solid systems with special reference to the determination of surface area and porosity (IUPAC Recommendations 1984). Pure & Applied Chemistry 57, 603-619.
- Slater, J.C., Kirkwood, J.G., 1931. The van der Waals forces in gases. Physical Reviews 37, 682-697.
- Stanton, R., Flores, R., Warwick, P.D., Gluskoter, H., Stricker, G.D., 2001. Coal bed sequestration of carbon dioxide. First National Conference on Carbon Sequestration, U.S. Department of Energy, DOE/NETL-2001/1144 (CD-ROM), 12 p.
- Taylor, G.H., Teichmüller, M., Davis, A., Diessel, C.F.K., Littke, R., Robert, P., 1998. Organic Petrology. Berlin, Gebrüder Borntraeger, 704 p.
- Testa, S.M., Pratt, T.J., 2003. Sample preparation for coal and shale gas assessment. 2003 International Coalbed Methane Symposium, Tuscaloosa, Alabama, Paper 0356.
- Toda, Y., Hatami, M., Toyoda, S., Yoshida, Y., Honda, H., 1971. Micropore structure of coal. Fuel 50, 187-200.

- Unsworth, J.F., Fowler, C.S., Jones, L.F., 1989. Moisture in coal. 2. Maceral effects on pore structure. *Fuel* 68, 18-26.
- van Bergen, F., Pagnier, H.J.M., van der Meer, L.H.G., van den Belt F.J.G., Winthaegen, P.L.A., Krzystolik, P., 2003. Development of a field experiment of ECBM in the Upper Silesian coal basin of Poland (RECOPOL). 2003 International Coalbed Methane Symposium, Tuscaloosa, Alabama. Paper 0320.
- Walker, P.L., Verma, S.K., Rivera-Utrilla, J., Davis, A., 1988. Densities, porosities and surface areas of coal macerals as measured by their interaction with gases, vapours and liquids. *Fuel* 67, 1615-1623.
- White, C.M., Strazisar, B.R., Granite, E.J., Hoffman, J.S., Pennline, H.W., 2003. Separation and capture of CO₂ from large stationary sources and sequestration in geological formations - coalbeds and deep saline aquifers. *Journal of Air & Waste Management Association* 53, 645-715.
- Yee, D., Seidle, J.P., Hanson, W.B., 1993. Gas sorption on coal and measurement of gas content. In: Law, B.E., Rice, D.D. (Eds.), *Hydrocarbons from Coal*. American Association of Petroleum Geologists, *Studies in Geology* 18. Tulsa, OK, pp. 203-218.
- Zwietering, P., van Krevelen, D.W., 1954. Chemical structure and properties of coal. IV - Pore structure. *Fuel* 33, 331-337.

CHAPTER 9

Summary

The increasing demand for energy has renewed interest in coal resources worldwide. Industrialized and developing countries are optimizing the use of coal to provide energy necessary for their technological advancement. The increased use of coal requires more effective emission control from energy-producing facilities. Given the social responsibilities associated with the use of coal as an energy source for future generations, this study aims to address options available for beneficial and environmentally sound use of Indiana coal resources, namely 1) potential coalbed methane (CBM) recovery and 2) sequestration of carbon dioxide.

This study includes both field and laboratory components. Field studies were conducted to understand the distribution of potential CBM resources in coal seams from Indiana and their relationships with depth and lithology of adjoining strata. Coal maps were generated for Danville, Springfield, Houchin Creek, and Seelyville Coal Members because of their widespread occurrence, thickness of seams, and coal quality. New canister-desorption data from these coal seams were obtained and incorporated into a gas content database. These data show an overall increase in gas content with increasing depth for Gibson and Sullivan Counties, but no distinct trends could be recognized in other areas.

Cleats and fractures in coal control permeability and offer gas migration routes out of the coal network, two of the most critical aspects for CBM producibility. Cleats and fractures in Pennsylvanian coals of Indiana were described, statistically analyzed, and subsequently interpreted in terms of their origin, relation to geologic lineaments, and significance for permeability and coalbed gas generation and storage. An important contribution of this study is the integration of cleat and fracture data across different

scales and their implications for permeability and gas migration. Cleat and fracture data indicate a power-law distribution between spacing and aperture of cleats at meso- and microscopic scales. Azimuth directions of mineral-filled cleats show good agreement with geologic lineaments. Cleat, fracture, and lineament data suggest possible avenues for groundwater migration through Indiana coals, which may have facilitated transport of microbial consortia and subsequent biogenic generation of coalbed methane.

The occurrence of diagenetic minerals in cleats and fractures provides evidence to constrain the timing of mineralization and coalbed gas generation. Cleats and fractures in southwestern Indiana coal seams are often filled with authigenic kaolinite and/or calcite. New carbon and oxygen stable isotope data generated in this study from cleat-filling kaolinite and calcite indicate that these mineral phases precipitated at different reservoir conditions (i.e., 1600 m depth at 78°C for kaolinite and 500 to 1300 m depth at 43°C for calcite). The data also reveal that diagenetic calcite mineralization must have preceded the inoculation of coal seams with microbes that reduce carbon dioxide (CO₂) because modern microbially-influenced ¹³C-enriched coalbed CO₂ is out of isotopic equilibrium with ¹³C-depleted calcite in cleats.

Experimental aspects of this study focused on factors that influence gas adsorption capacities in coal, such as oxidation during storage, maceral composition, gas species and pressure, and particle size distribution of crushed coal samples. Laboratory data suggest a correlation between moisture loss and the decrease in calorific value of coal during oxidative storage in air at low temperature. Low-pressure gas adsorption experiments were conducted to investigate the changes in porous structure of coals resulting from storage in the laboratory. Drying of coal over the duration of coal storage reduces

moisture content, adsorption capacity for nitrogen, and mesopore surface area available for gas adsorption. Drying also increases the surface area of micropores and the CO₂ adsorption potential in coal.

High-pressure adsorption data from this study suggest relationships between gas adsorption capacity and particle size distribution of crushed coal, as well as between gas adsorption capacity and maceral composition. An increase in CO₂ adsorption capacity was observed with decreasing particle size.

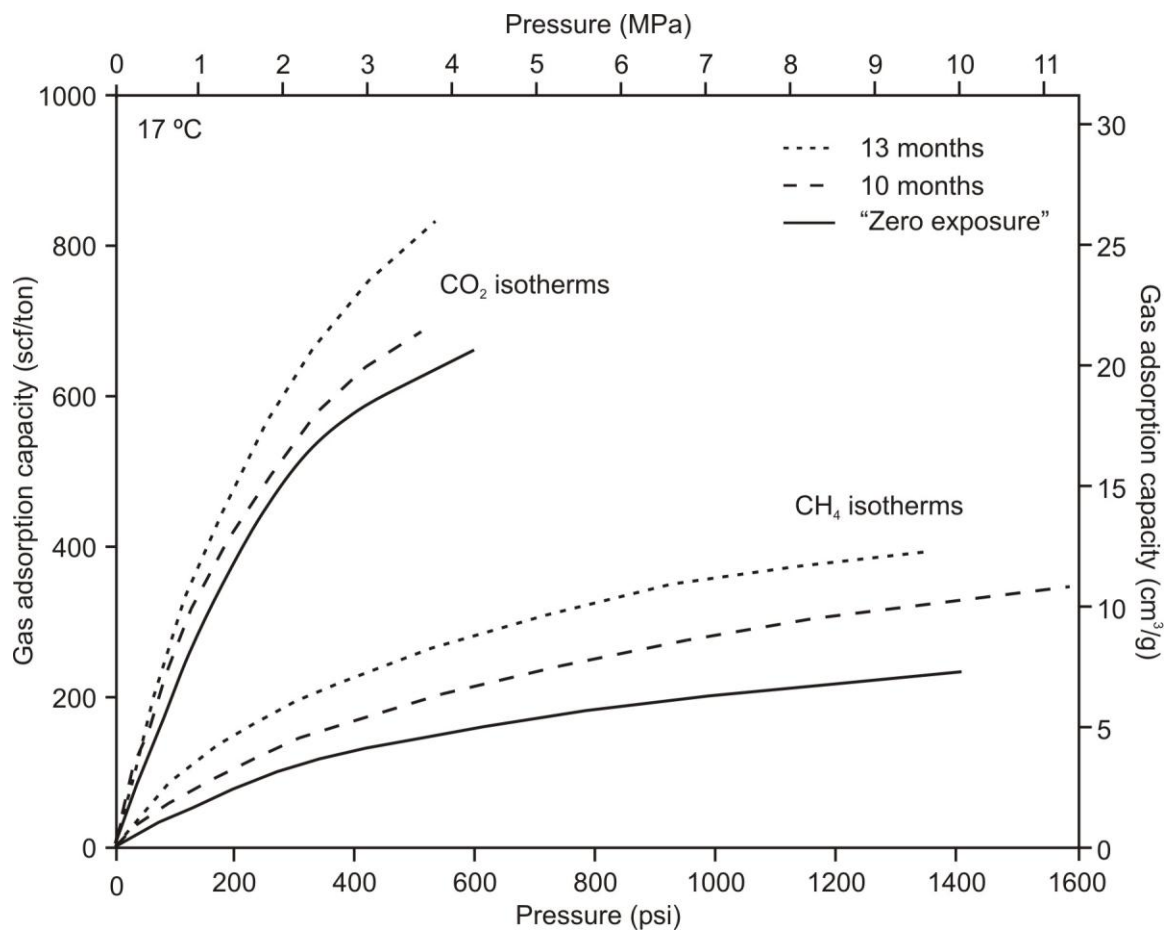
This study reveals that the adsorption of water on coal (i.e., the moisture content) critically influences the adsorption capacity of methane and CO₂ in coal. Noteworthy is the effect of irreversible moisture loss on the adsorption capacities of (i) coal that was exposed to dry air and (ii) the same coal that has subsequently been moisture-equilibrated. Maximum adsorption capacities in coal are determined from high-pressure adsorption isotherms and are used to predict CBM and CO₂ sequestration potentials. At high gas pressure, moisture loss accounts for up to ~30% increased methane adsorption capacity of dry coal samples relative to coals that have never experienced drying. Even after moisture-equilibration of previously dried coals, the methane adsorption capacity remains up to ~40% enhanced. For CO₂, an increase in high-pressure adsorption capacity with increasing loss of moisture was also observed. However, the relative increase in CO₂ adsorption capacity was significantly lower than that of methane, i.e., ~25% for dry coal samples and about ~18% for moisture-equilibrated coal samples.

These and other experimental results of this study indicate that adequate preservation of freshly mined or cored coal samples is critical for accurate assessment of resource gas-in-place evaluations, and therefore, for estimating the adsorption potential

for applications such as CO₂ sequestration. Even slight changes of the coal's original reservoir conditions, in particular with regard to the loss of moisture from coal, will likely result in artificially enhanced gas adsorption capacities.

Appendix

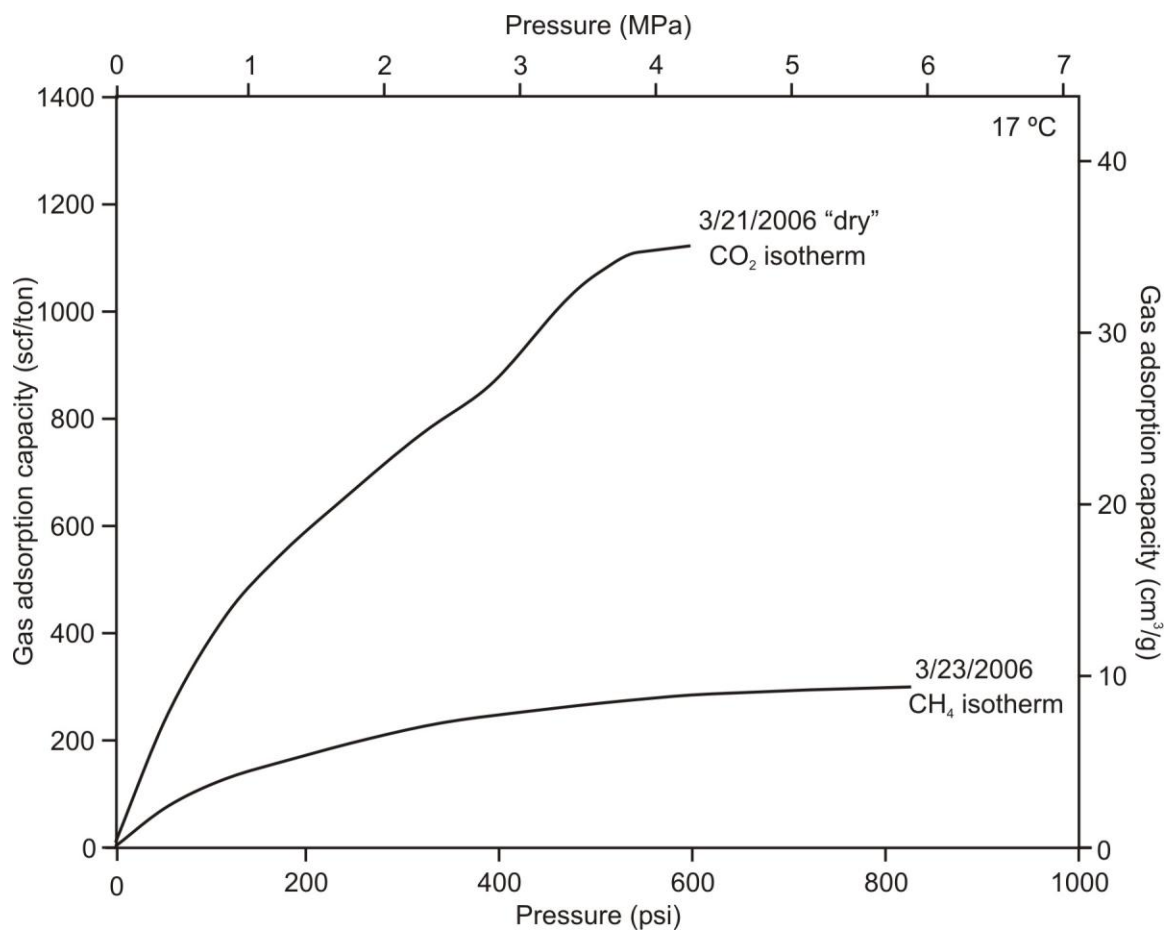
This section contains graphical and experimental raw data corresponding to all high-pressure adsorption isotherms collected on dry and moisture-equilibrated conditions with small-volume high-pressure volumetric apparatus. Most data were grouped by collection date, but in some instances data are presented together to facilitate comparisons.



Billings mine "zero exposure"									
Equilibrium pressure		CH ₄ adsorption		Equilibrium pressure		CO ₂ adsorption		CO ₂ /CH ₄ ratio	
psi	Mpa	scf/ton	cm ³ /g	psi	Mpa	scf/ton	cm ³ /g		
71	0.50	31.4	0.98	86	0.60	165.6	5.18		5.3
129	0.90	51.3	1.60	124	0.87	246.5	7.70		4.8
195	1.37	76.7	2.40	179	1.25	343.3	10.73		4.5
270	1.89	99.8	3.12	247	1.73	435.7	13.62		4.4
340	2.38	115.9	3.62	322	2.26	510.8	15.96		4.4
414	2.90	130.1	4.07	402	2.81	568.7	17.77		4.4
506	3.54	145.1	4.54	498	3.48	609.5	19.05		4.2
609	4.26	160.4	5.01	603	4.22	656.4	20.51		4.1
781	5.47	182.0	5.69						
982	6.87	201.5	6.30						
1191	8.34	217.6	6.80						
1404	9.83	232.3	7.26						

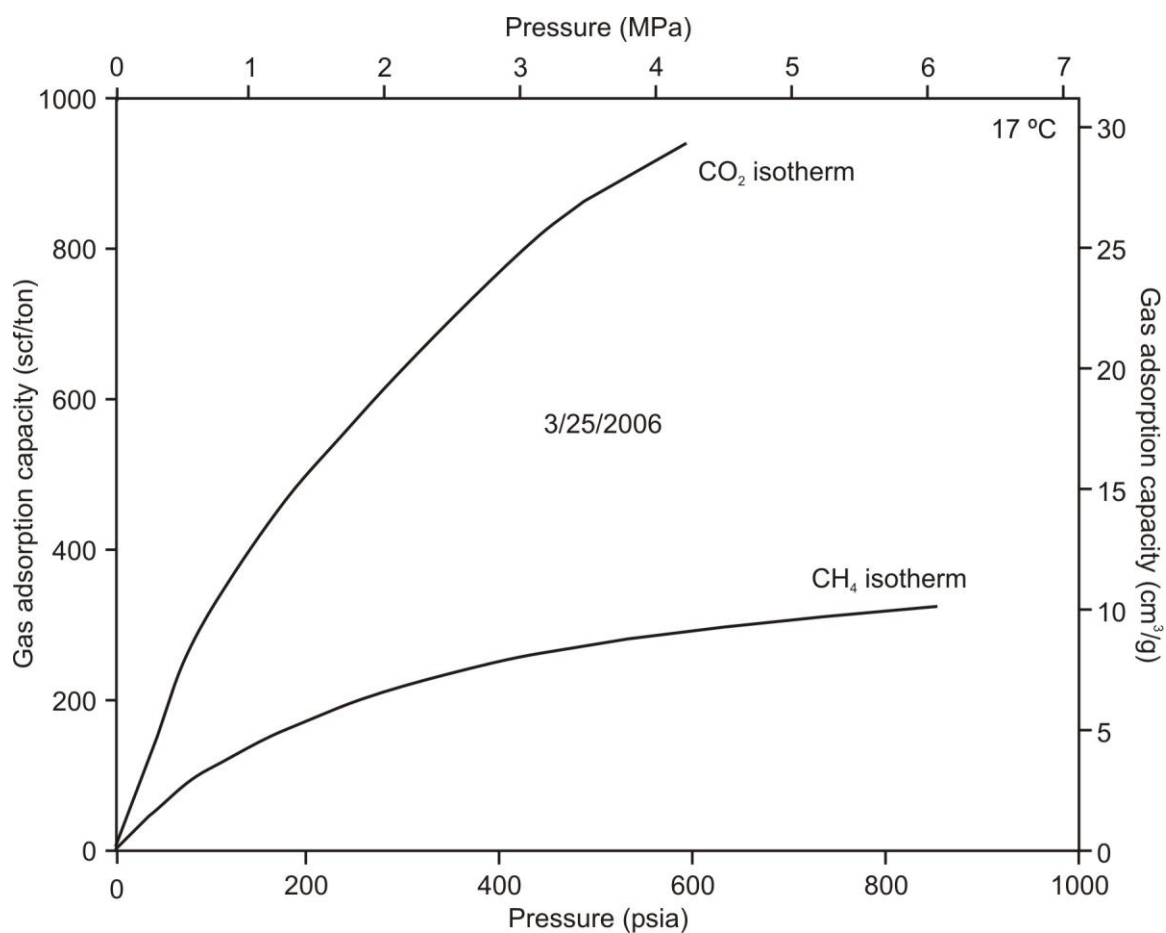
Billings mine "after 10 months"									
Equilibrium pressure		CH ₄ adsorption			Equilibrium pressure		CO ₂ adsorption		CO ₂ /CH ₄ ratio
psi	Mpa	scf/ton	cm ³ /g		psi	Mpa	scf/ton	cm ³ /g	
42	0.29	23.3	0.73		5	0.03	18.2	0.57	0.8
94	0.66	56.8	1.77		16	0.11	48.7	1.52	0.9
160	1.12	89.5	2.80		34	0.24	92.9	2.90	1.0
232	1.62	118.0	3.69		55	0.38	148.6	4.64	1.3
306	2.14	142.5	4.45		83	0.58	218.2	6.82	1.5
379	2.65	163.1	5.10		128	0.90	305.5	9.55	1.9
541	3.78	202.5	6.33		189	1.33	399.8	12.49	2.0
738	5.16	241.0	7.53		261	1.83	487.4	15.23	2.0
947	6.63	275.3	8.60		424	2.97	631.2	19.72	2.3
1156	8.09	305.4	9.54		514	3.60	678.1	21.19	2.2
1328	9.30	321.7	10.05						
1579	11.06	347.7	10.86						

Billings mine "after 13 months"									
Equilibrium pressure		CH ₄ adsorption			Equilibrium pressure		CO ₂ adsorption		CO ₂ /CH ₄ ratio
psi	Mpa	scf/ton	cm ³ /g		psi	Mpa	scf/ton	cm ³ /g	
13	0.09	17.9	0.56		32	0.23	87.2	2.72	4.9
41	0.29	52.2	1.63		65	0.46	193.8	6.05	3.7
90	0.63	92.8	2.90		116	0.81	324.9	10.15	3.5
165	1.15	138.9	4.34		181	1.27	450.3	14.07	3.2
230	1.61	168.3	5.26		255	1.79	561.7	17.55	3.3
301	2.11	195.4	6.11		333	2.33	656.8	20.53	3.4
371	2.60	219.9	6.87		427	2.99	753.0	23.53	3.4
523	3.66	266.3	8.32		538	3.77	830.0	25.94	3.1
715	5.01	313.5	9.80						
920	6.44	354.8	11.09						
1133	7.93	377.0	11.78						
1346	9.42	396.4	12.39						

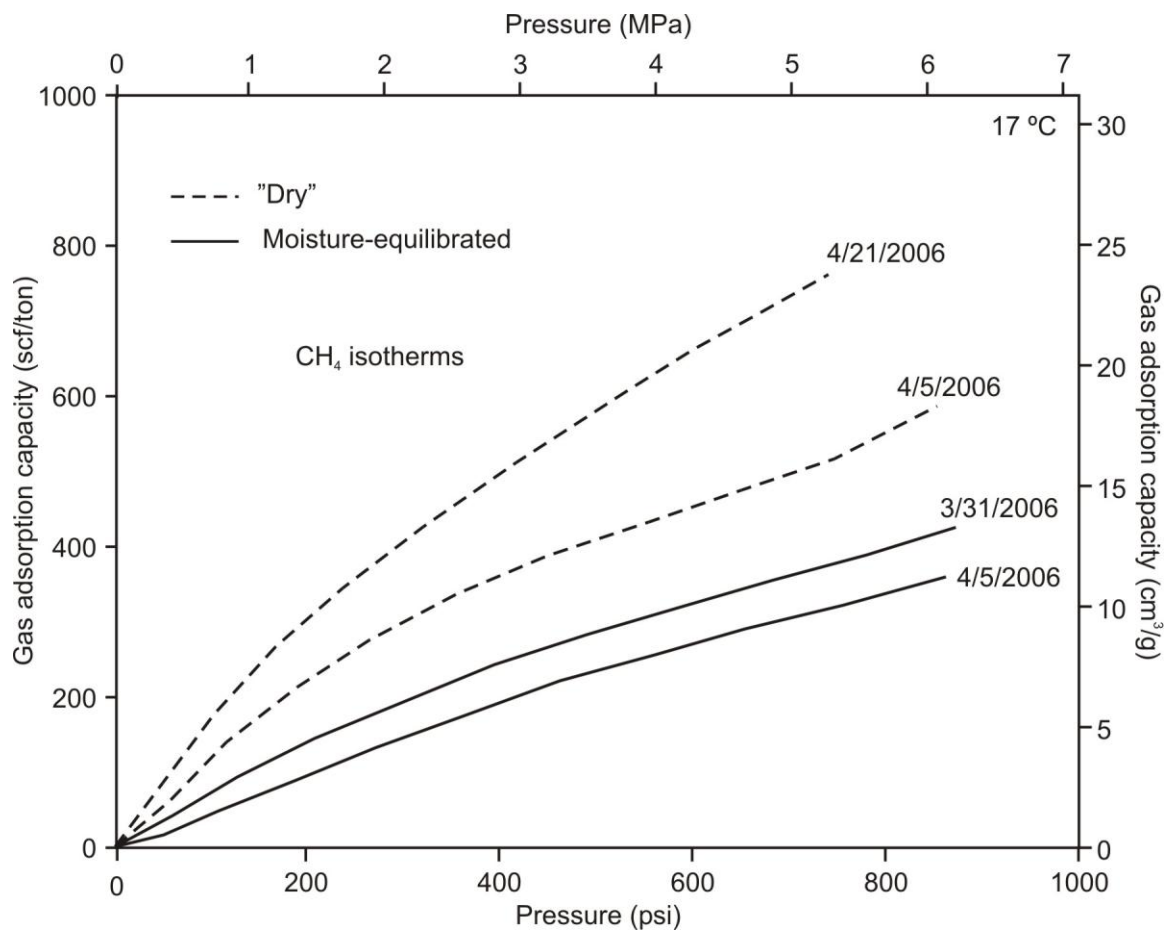


Billings mine (3/21/2006) "dry"									
Equilibrium pressure		CH ₄ adsorption			Equilibrium pressure		CO ₂ adsorption		CO ₂ /CH ₄ ratio
psi	Mpa	scf/ton	cm ³ /g		psi	Mpa	scf/ton	cm ³ /g	
					42	0.29	193.6	6.05	
					115	0.81	431.9	13.50	
					220	1.54	617.7	19.30	
					312	2.18	764.3	23.88	
					387	2.71	840.9	26.28	
					468	3.28	1033.7	32.30	
					544	3.80	1098.9	34.34	
					597	4.18	1106.9	34.59	

Billings mine (3/23/2006)									
Equilibrium pressure		CH ₄ adsorption			Equilibrium pressure		CO ₂ adsorption		CO ₂ /CH ₄ ratio
psi	Mpa	scf/ton	cm ³ /g		psi	Mpa	scf/ton	cm ³ /g	
62	0.43	63.7	1.99						
118	0.82	115.9	3.62						
184	1.29	160.7	5.02						
263	1.84	197.4	6.17						
340	2.38	227.0	7.10						
428	3.00	250.5	7.83						
523	3.66	266.1	8.32						
616	4.31	276.5	8.64						
720	5.04	285.0	8.91						
822	5.75	290.7	9.09						



Billings mine (3/25/2006)								
Equilibrium pressure		CH ₄ adsorption		Equilibrium pressure		CO ₂ adsorption		CO ₂ /CH ₄ ratio
psi	Mpa	scf/ton	cm ³ /g	psi	Mpa	scf/ton	cm ³ /g	
53	0.37	60.5	1.89	44	0.31	137.8	4.31	2.3
100	0.70	110.9	3.47	105	0.74	319.4	9.98	2.9
178	1.24	164.0	5.13	189	1.32	477.0	14.91	2.9
256	1.79	201.8	6.31	288	2.01	618.9	19.34	3.1
343	2.40	235.7	7.37	390	2.73	742.7	23.21	3.2
437	3.06	263.3	8.23	490	3.43	850.0	26.56	3.2
534	3.74	283.7	8.87	596	4.17	930.3	29.07	3.3
635	4.44	298.5	9.33					
733	5.13	312.4	9.76					
852	5.96	324.3	10.13					

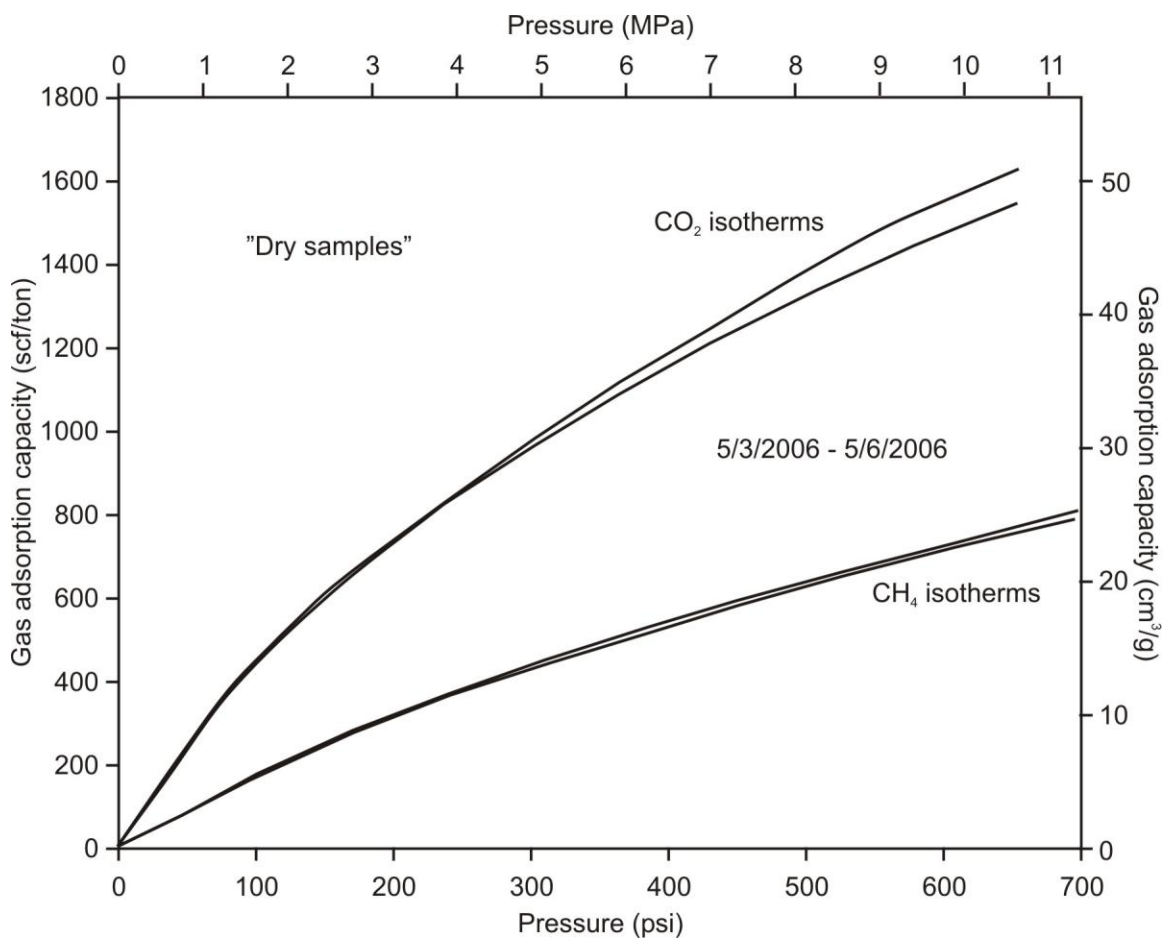


Billings mine (3/31/2006)									
Equilibrium pressure		CH ₄ adsorption			Equilibrium pressure		CO ₂ adsorption		CO ₂ /CH ₄ ratio
psi	Mpa	scf/ton	cm ³ /g		psi	Mpa	scf/ton	cm ³ /g	
58	0.41	38.0	1.19						
124	0.87	93.4	2.92						
207	1.45	143.6	4.49						
297	2.08	187.6	5.86						
390	2.73	242.5	7.58						
489	3.42	282.8	8.84						
589	4.13	322.4	10.07						
681	4.77	354.3	11.07						
775	5.43	389.5	12.17						
866	6.06	426.5	13.33						

Billings mine (4/5/2006)									
Equilibrium pressure		CH ₄ adsorption			Equilibrium pressure		CO ₂ adsorption		CO ₂ /CH ₄ ratio
psi	Mpa	scf/ton	cm ³ /g		psi	Mpa	scf/ton	cm ³ /g	
51	0.36	12.2	0.38						
108	0.75	47.2	1.47						
189	1.32	91.1	2.85						
273	1.91	133.3	4.16						
366	2.56	175.3	5.48						
457	3.20	221.2	6.91						
559	3.91	256.0	8.00						
654	4.58	289.8	9.06						
752	5.26	324.8	10.15						
855	5.99	361.1	11.28						

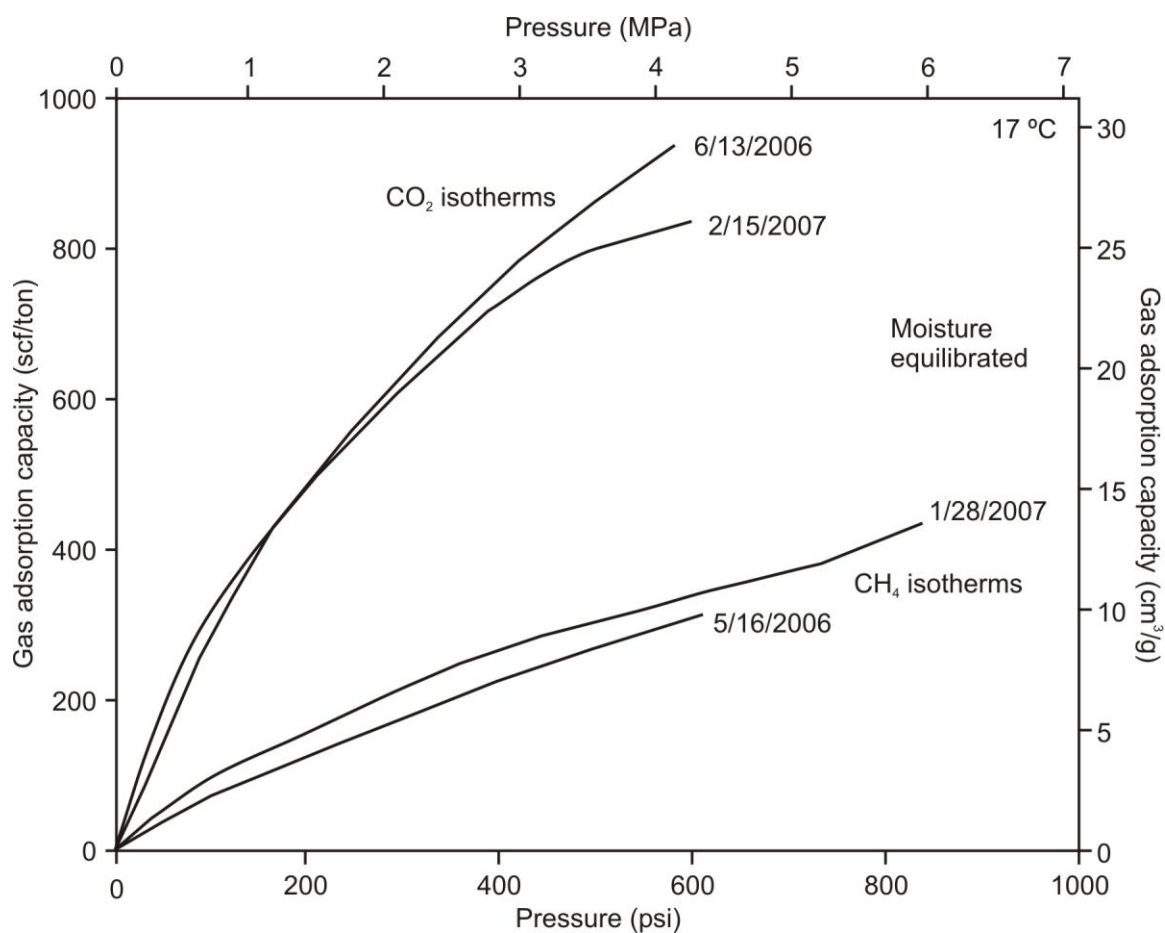
Billings mine (4/5/2006) "dry"									
Equilibrium pressure		CH ₄ adsorption			Equilibrium pressure		CO ₂ adsorption		CO ₂ /CH ₄ ratio
psi	Mpa	scf/ton	cm ³ /g		psi	Mpa	scf/ton	cm ³ /g	
43	0.30	54.9	1.72						
95	0.67	130.9	4.09						
175	1.22	208.1	6.50						
260	1.82	275.7	8.61						
354	2.48	335.4	10.48						
447	3.13	387.5	12.11						
549	3.84	432.0	13.50						
646	4.52	472.7	14.77						
744	5.21	514.3	16.07						
848	5.93	585.0	18.28						

Billings mine (4/21/2006) "dry"									
Equilibrium pressure		CH ₄ adsorption			Equilibrium pressure		CO ₂ adsorption		CO ₂ /CH ₄ ratio
psi	Mpa	scf/ton	cm ³ /g		psi	Mpa	scf/ton	cm ³ /g	
50	0.35	75.3	2.35						
99	0.69	162.4	5.08						
163	1.14	251.8	7.87						
235	1.64	333.5	10.42						
320	2.24	418.3	13.07						
416	2.91	503.2	15.72						
512	3.58	581.0	18.16						
591	4.14	646.2	20.19						
647	4.53	686.1	21.44						
738	5.16	751.8	23.50						



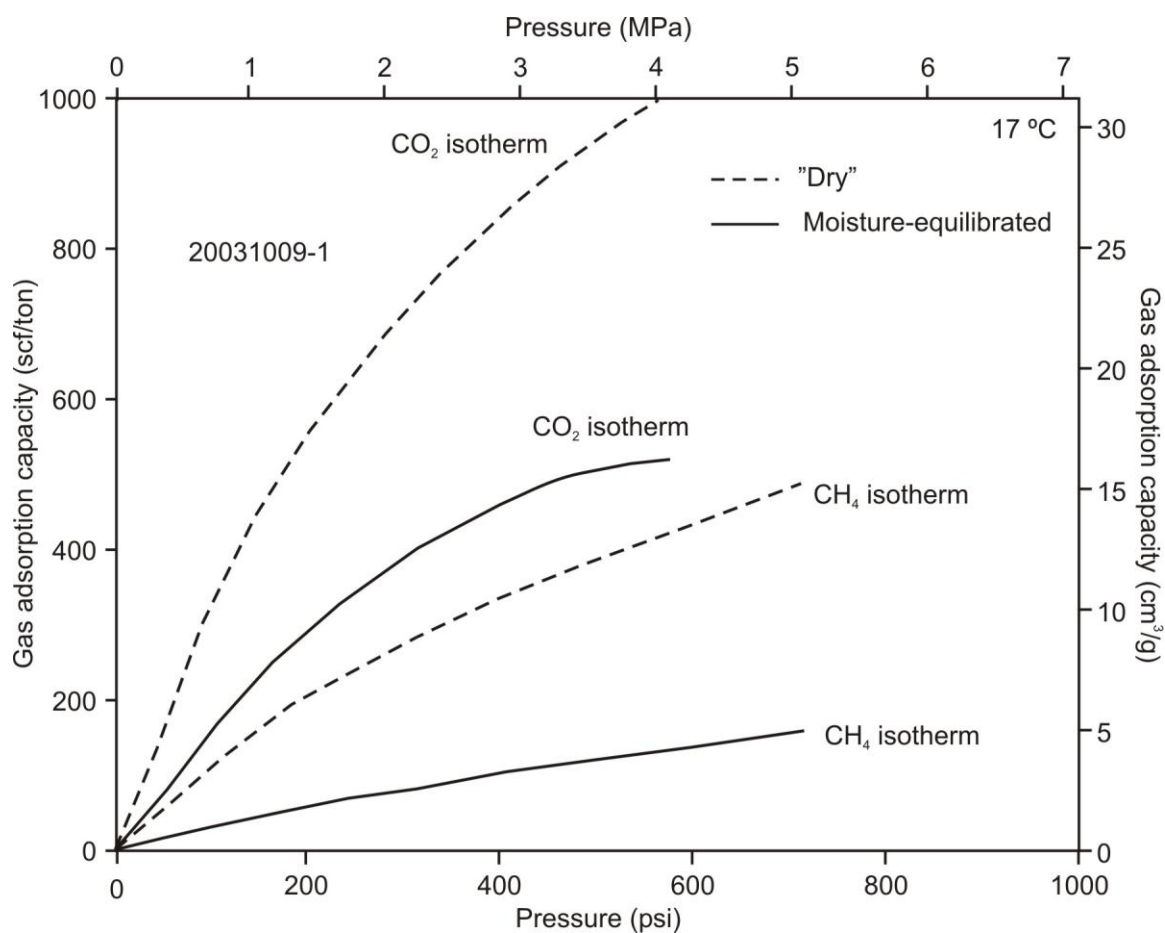
Billings mine (5/3/2006) "dry"									
Equilibrium pressure		CH ₄ adsorption			Equilibrium pressure		CO ₂ adsorption		CO ₂ /CH ₄ ratio
psi	Mpa	scf/ton	cm ³ /g		psi	Mpa	scf/ton	cm ³ /g	
49	0.35	78.4	2.45		38	0.26	158.2	4.94	2.0
101	0.71	173.9	5.44		82	0.57	381.5	11.92	2.2
167	1.17	266.6	8.33		157	1.10	615.4	19.23	2.3
238	1.67	355.8	11.12		238	1.67	820.8	25.65	2.3
309	2.16	435.3	13.60		302	2.11	983.3	30.73	2.3
384	2.69	512.7	16.02		365	2.55	1107.4	34.61	2.2
451	3.16	577.0	18.03		432	3.02	1238.4	38.70	2.1
526	3.69	650.5	20.33		503	3.52	1380.7	43.15	2.1
612	4.29	725.5	22.67		579	4.05	1517.5	47.42	2.1
701	4.90	803.0	25.09		655	4.58	1608.5	50.27	2.0

Billings mine (5/6/2006) "dry"									
Equilibrium pressure		CH ₄ adsorption			Equilibrium pressure		CO ₂ adsorption		CO ₂ /CH ₄ ratio
psi	Mpa	scf/ton	cm ³ /g		psi	Mpa	scf/ton	cm ³ /g	
50	0.35	82.8	2.59		38	0.27	162.8	5.09	2.0
102	0.72	178.2	5.57		83	0.58	382.9	11.97	2.1
168	1.17	274.0	8.56		158	1.10	617.8	19.31	2.3
239	1.67	359.3	11.23		239	1.68	812.0	25.38	2.3
310	2.17	435.9	13.62		304	2.13	959.0	29.97	2.2
385	2.69	512.3	16.01		367	2.57	1079.3	33.73	2.1
452	3.16	575.5	17.99		434	3.04	1203.4	37.61	2.1
527	3.69	645.6	20.18		505	3.54	1333.9	41.68	2.1
613	4.29	716.5	22.39		581	4.06	1459.5	45.61	2.0
701	4.91	788.7	24.65		656	4.59	1536.7	48.02	1.9



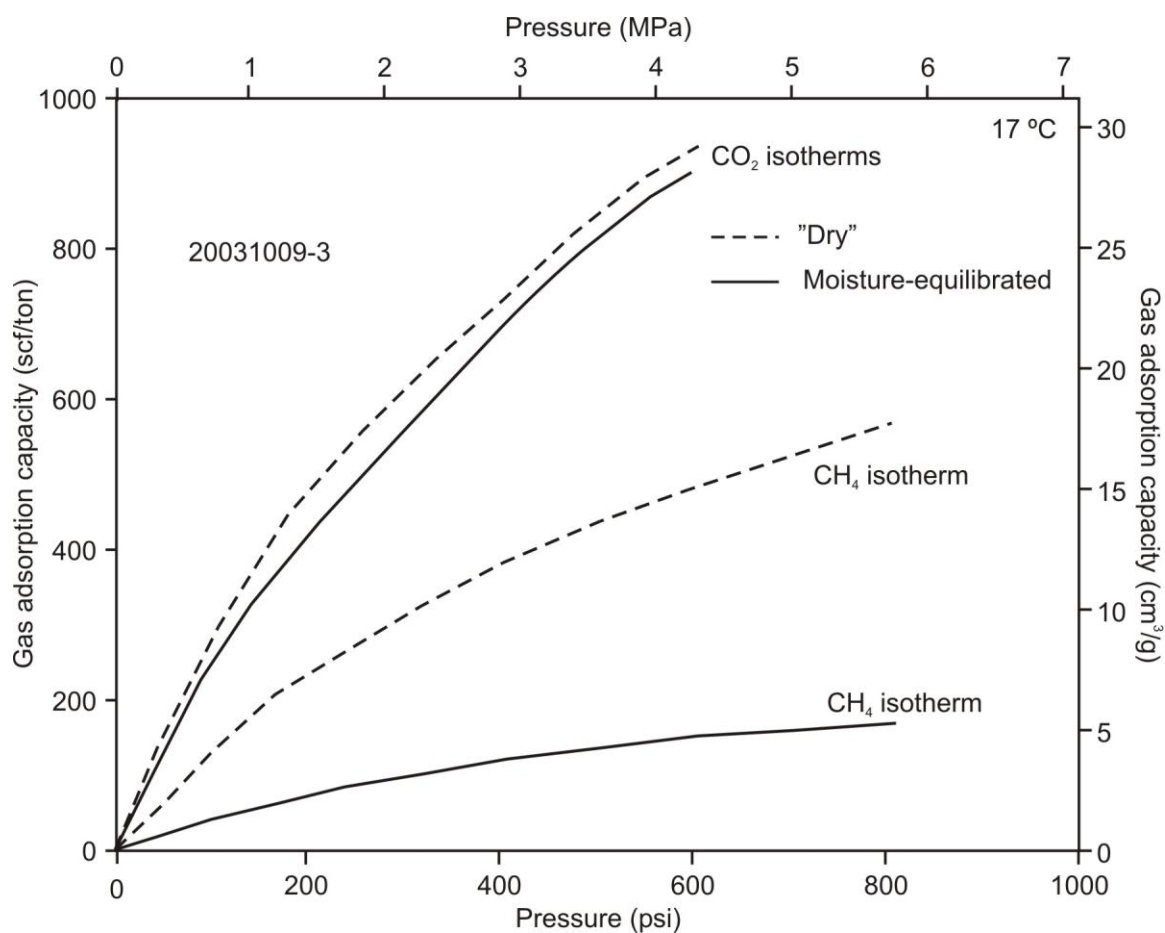
Billings mine (5/16/2006 - 6/13/2006)								
Equilibrium pressure		CH ₄ adsorption		Equilibrium pressure		CO ₂ adsorption		CO ₂ /CH ₄ ratio
psi	Mpa	scf/ton	cm ³ /g	psi	Mpa	scf/ton	cm ³ /g	
51	0.36	30.0	0.94	38	0.27	98.4	3.07	3.3
101	0.70	70.5	2.20	89	0.62	258.6	8.08	3.7
167	1.17	104.5	3.26	160	1.12	419.0	13.09	4.0
233	1.63	140.1	4.38	244	1.70	556.5	17.39	4.0
305	2.13	178.5	5.58	331	2.32	678.1	21.19	3.8
400	2.80	224.0	7.00	417	2.92	782.7	24.46	3.5
496	3.47	265.4	8.29	498	3.48	861.5	26.92	3.2
613	4.29	311.9	9.75	580	4.06	936.5	29.27	3.0

Billings mine (1/28/2007 - 2/15/2007)									
Equilibrium pressure		CH ₄ adsorption			Equilibrium pressure		CO ₂ adsorption		CO ₂ /CH ₄ ratio
psi	Mpa	scf/ton	cm ³ /g		psi	Mpa	scf/ton	cm ³ /g	
55	0.39	55.8	1.74		39	0.27	141.5	4.42	2.5
110	0.77	107.2	3.35		86	0.60	280.5	8.77	2.6
189	1.32	159.2	4.98		141	0.98	391.5	12.24	2.5
272	1.90	200.0	6.25		211	1.48	502.9	15.71	2.5
356	2.49	244.0	7.63		296	2.07	608.5	19.02	2.5
444	3.11	283.0	8.84		387	2.71	712.4	22.26	2.5
539	3.77	316.5	9.89		488	3.41	801.1	25.04	2.5
635	4.45	352.7	11.02		594	4.16	834.4	26.08	2.4
732	5.13	380.4	11.89						
833	5.83	440.0	13.75						



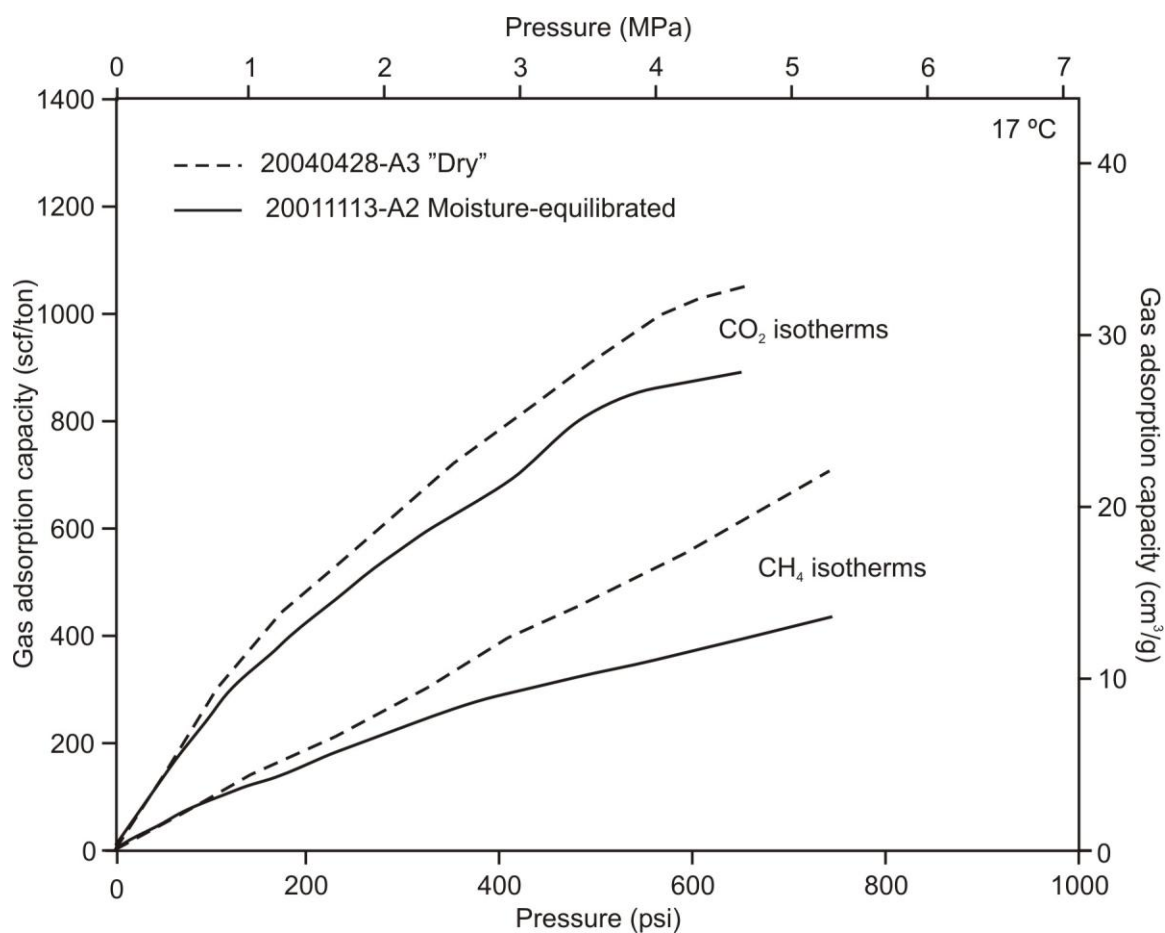
20031009-1								
Equilibrium pressure		CH ₄ adsorption		Equilibrium pressure		CO ₂ adsorption		CO ₂ /CH ₄ ratio
psi	Mpa	scf/ton	cm ³ /g	psi	Mpa	scf/ton	cm ³ /g	
51	0.35	10.2	0.32	50	0.35	72.1	2.25	7.1
99	0.69	27.9	0.87	99	0.69	162.2	5.07	5.8
168	1.18	48.1	1.50	163	1.14	246.2	7.69	5.1
241	1.69	68.2	2.13	234	1.63	326.3	10.20	4.8
319	2.23	87.6	2.74	314	2.20	402.5	12.58	4.6
404	2.83	106.6	3.33	404	2.83	460.3	14.39	4.3
500	3.50	121.7	3.80	493	3.45	502.6	15.71	4.1
602	4.22	136.0	4.25	574	4.02	513.5	16.05	3.8
720	5.04	158.3	4.95					

20031009-1 "dry"									
Equilibrium pressure		CH ₄ adsorption			Equilibrium pressure		CO ₂ adsorption		CO ₂ /CH ₄ ratio
psi	Mpa	scf/ton	cm ³ /g		psi	Mpa	scf/ton	cm ³ /g	
49	0.34	46.5	1.45		44	0.31	131.5	4.11	2.8
94	0.66	105.2	3.29		88	0.61	299.3	9.35	2.8
160	1.12	173.0	5.40		150	1.05	462.3	14.45	2.7
232	1.62	224.2	7.01		221	1.55	596.2	18.63	2.7
310	2.17	278.4	8.70		303	2.12	722.6	22.58	2.6
395	2.76	333.1	10.41		394	2.76	837.9	26.18	2.5
490	3.43	384.5	12.01		483	3.38	934.2	29.19	2.4
592	4.14	434.3	13.57		565	3.96	995.9	31.12	2.3
709	4.97	489.4	15.30						



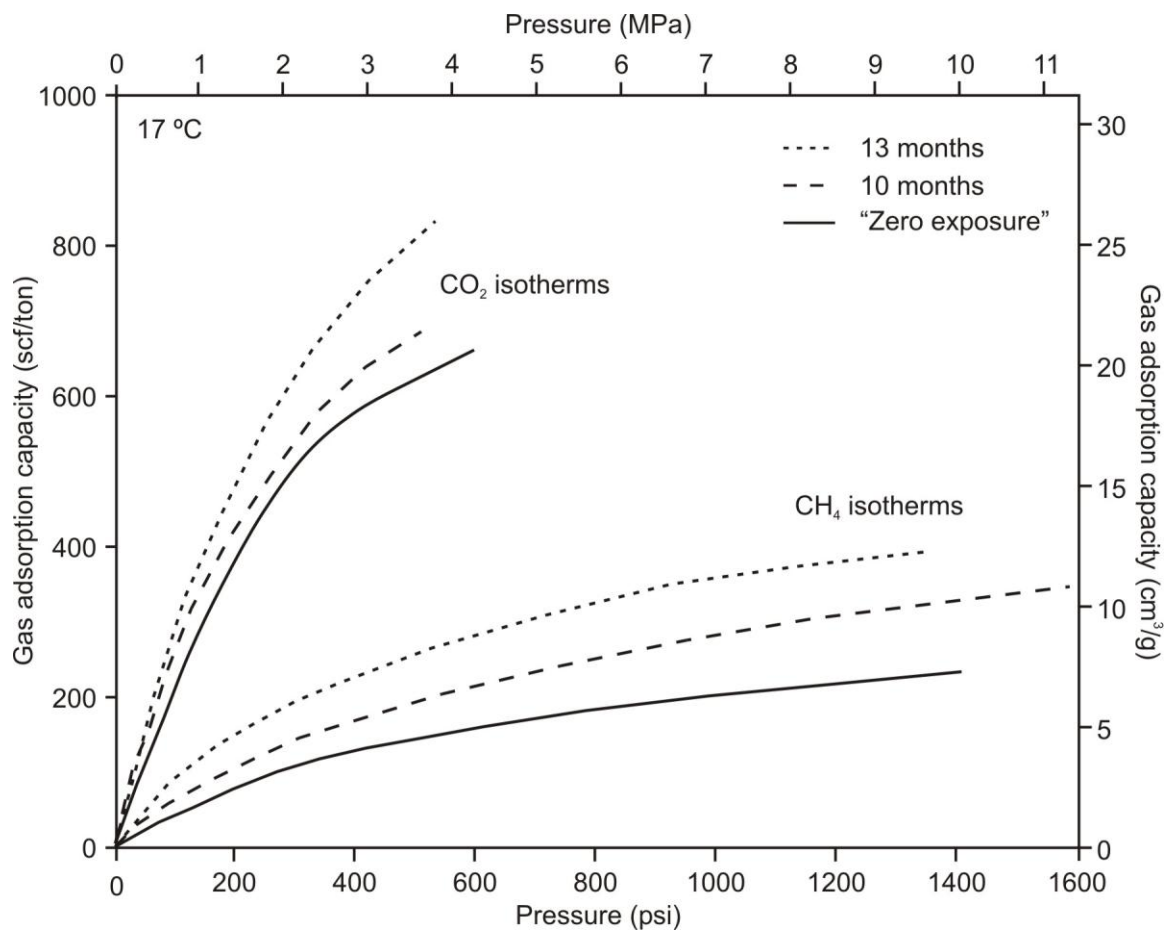
20031009-3									
Equilibrium pressure		CH ₄ adsorption			Equilibrium pressure		CO ₂ adsorption		CO ₂ /CH ₄ ratio
psi	Mpa	scf/ton	cm ³ /g		psi	Mpa	scf/ton	cm ³ /g	
49	0.34	17.6	0.55		39	0.27	106.0	3.31	6.0
101	0.71	41.1	1.28		86	0.60	221.1	6.91	5.4
171	1.20	61.8	1.93		141	0.98	321.4	10.05	5.2
242	1.69	83.1	2.60		211	1.48	431.2	13.48	5.2
322	2.25	104.8	3.28		296	2.07	547.4	17.11	5.2
407	2.85	123.1	3.85		387	2.71	670.8	20.96	5.4
512	3.58	138.1	4.31		488	3.41	797.0	24.91	5.8
605	4.24	150.2	4.69		594	4.16	902.5	28.20	6.0
706	4.94	158.6	4.96						
806	5.64	169.5	5.30						

20031009-3 "dry"									
Equilibrium pressure		CH ₄ adsorption			Equilibrium pressure		CO ₂ adsorption		CO ₂ /CH ₄ ratio
psi	Mpa	scf/ton	cm ³ /g		psi	Mpa	scf/ton	cm ³ /g	
46	0.32	51.6	1.61		44	128.69	131.5	4.11	2.5
94	0.66	123.4	3.86		105	301.16	299.3	9.35	2.4
162	1.13	199.7	6.24		189	454.90	462.3	14.45	2.3
232	1.63	260.6	8.14		288	597.38	596.2	18.63	2.3
313	2.19	321.1	10.03		390	725.49	722.6	22.58	2.3
401	2.81	380.4	11.89		490	840.25	837.9	26.18	2.2
506	3.54	434.5	13.58		596	934.86	934.2	29.19	2.1
599	4.20	477.3	14.92						
700	4.90	520.4	16.26						
800	5.60	562.9	17.59						



20011113-A2								
Equilibrium pressure		CH ₄ adsorption		Equilibrium pressure		CO ₂ adsorption		CO ₂ /CH ₄ ratio
psi	Mpa	scf/ton	cm ³ /g	psi	Mpa	scf/ton	cm ³ /g	
53	0.37	43.6	1.36	48	0.34	118.3	3.70	2.7
100	0.70	89.3	2.79	98	0.69	254.4	7.95	2.8
154	1.08	125.7	3.93	165	1.15	364.3	11.38	2.9
233	1.63	178.2	5.57	230	1.61	460.8	14.40	2.6
311	2.17	230.0	7.19	294	2.06	541.1	16.91	2.4
401	2.80	286.8	8.96	348	2.43	610.5	19.08	2.1
478	3.35	322.5	10.08	422	2.96	696.1	21.75	2.2
560	3.92	354.1	11.07	486	3.40	805.7	25.18	2.3
652	4.56	391.6	12.24	569	3.98	867.3	27.10	2.2
742	5.19	431.6	13.49	643	4.50	883.5	27.61	2.0

20040428-A3 "dry"									
Equilibrium pressure		CH ₄ adsorption			Equilibrium pressure		CO ₂ adsorption		CO ₂ /CH ₄ ratio
psi	Mpa	scf/ton	cm ³ /g		psi	Mpa	scf/ton	cm ³ /g	
57	0.40	58.1	1.82		51	128.69	157.1	4.91	2.7
113	0.79	119.4	3.73		108	301.16	314.4	9.83	2.6
187	1.31	182.2	5.69		181	454.90	455.3	14.23	2.5
267	1.87	258.9	8.09		270	597.38	600.9	18.78	2.3
358	2.50	347.8	10.87		357	725.49	726.1	22.69	2.1
471	3.30	455.5	14.24		447	840.25	840.6	26.27	1.8
598	4.18	564.7	17.65		502	934.86	912.2	28.51	1.6
747	5.23	718.2	22.44		567	934.86	1011.3	31.60	1.4
					649	934.86	1052.4	32.89	



20040428-C1									
Equilibrium pressure		CH ₄ adsorption			Equilibrium pressure		CO ₂ adsorption		CO ₂ /CH ₄ ratio
psi	Mpa	scf/ton	cm ³ /g		psi	Mpa	scf/ton	cm ³ /g	
52	0.37	16.1	0.50		53	0.37	78.6	2.46	4.9
106	0.74	39.9	1.25		100	0.70	163.4	5.11	4.1
175	1.22	65.8	2.06		159	1.11	250.8	7.84	3.8
246	1.72	93.9	2.93		236	1.65	352.5	11.02	3.8
333	2.33	129.0	4.03		317	2.22	439.2	13.73	3.4
419	2.93	158.6	4.96		401	2.81	517.9	16.18	3.3
513	3.59	191.6	5.99		489	3.42	587.1	18.35	3.1
615	4.30	230.7	7.21		566	3.96	627.2	19.60	2.7
711	4.97	265.5	8.30						
816	5.71	304.7	9.52						

20040428-C1 "dry"									
Equilibrium pressure		CH ₄ adsorption			Equilibrium pressure		CO ₂ adsorption		CO ₂ /CH ₄ ratio
psi	Mpa	scf/ton	cm ³ /g		psi	Mpa	scf/ton	cm ³ /g	
51	0.36	30.0	0.94		48	0.33	111.9	3.50	3.7
102	0.71	76.2	2.38		91	0.63	237.4	7.42	3.1
169	1.18	126.6	3.96		148	1.04	364.6	11.39	2.9
240	1.68	169.2	5.29		225	1.58	491.5	15.36	2.9
327	2.29	215.6	6.74		308	2.16	600.2	18.75	2.8
414	2.90	255.9	8.00		394	2.76	700.6	21.89	2.7
509	3.56	297.3	9.29		483	3.38	793.0	24.78	2.7
610	4.27	337.8	10.56		561	3.93	860.8	26.90	2.5
706	4.94	374.0	11.69						
811	5.68	412.7	12.90						

OFFICE ADDRESS

Indiana Geological Survey, Indiana University
611 North Walnut Grove, S-123
Bloomington, IN 47405, USA

Phone: (812) 855-9992
Fax: (812) 855-2862
E-mail: wsolano@indiana.edu

EDUCATION:

- Ph.D. Geology Indiana University Bloomington, Indiana, U.S.A., 2007
Advisors: Dr. Maria Mastalerz and Dr. Arndt Schimmelmann
Major: Coal Geology
Minor: Geomorphology
- M.S. Geology Indiana State University, Terre Haute, Indiana, U.S.A., 2001
Major: Sandstone Diagenesis Advisor: Dr. Prodip K. Dutta
Minor: Geography
- B.S. Geology Universidad Nacional de Colombia, Bogotá, Colombia, 1998
Major: Sedimentology and Stratigraphy Advisor: Dr. Fernando Etayo

EMPLOYMENT

- | | | |
|----------------|--|--|
| 2004 - Present | Reservoir Geologist - Research Scientist | Evaluate mechanisms that govern potential accumulations of coalbed gas in the Illinois Basin. Investigate the physical and chemical aspects of CO ₂ sorption in low-rank coals. Collect and measure drill samples for desorption and isotopic analyses. Interpret depositional environments from the evaluation of geophysical well-logs for regional assessment and the characterization of unconventional reservoirs, shales, depleted oil and gas reservoirs, and deep-saline aquifers. ILLINOIS BASIN CONSORTIUM - U.S. DEPARTMENT OF ENERGY - COALBED METHANE PROJECT AND MIDWEST REGIONAL CARBON SEQUESTRATION PARTNERSHIP (MRCSP) – PHASE II |
| Summer 2006 | Geoscientist - Internship | Chevron Energy Technology Company, Houston, TX. Quartz cementation along deformation bands in deepwater Gulf of Mexico. Reservoir characterization using Touchstone modeling. |
| Summer 2005 | Geoscientist - Internship | Chevron Co., CIEP, NMA Deepwater New Ventures, Houston, TX. Interpretation of a combined 2D-3D seismic survey in offshore west Africa using Landmark Seisworks. Mapped channels, seismic facies, and structural attributes for the subsurface assessment of an oil prospect. Applied depth-time conversions to seismic data and performed amplitude extractions to identify hydrocarbon indicators. |
| 2001 - 2003 | Reservoir Geologist MIDCARB Project | Conduct assessments and compilations of reservoir properties of conventional and unconventional reservoirs (oil, gas and saline aquifers). Map oil and gas pools/fields; interpret depositional environments; evaluate geophysical well-logs for regional assessment and reservoir characterization of potential sinks for carbon dioxide sequestration. |
| Summer 2001 | Support Geologist | Assisted in the development and construction of the Energy Resources Petroleum database (PDMS) for the Indiana Geological Survey. Coordinated input of geologic and drilling information of petroleum wells. |

2001 - 1999	Associate Instructor	Indiana State University. Coordinator of associate instructors in undergraduate geology and instructor for geology laboratory.
1998 - 1999	Consultant Geologist	HOCOL - Nimir Petroleum Co. Prepared exploration reports, maps, seismic interpretation, well-log correlation, and field data acquisition.
Summer 1998	Consultant Field Geologist	DUNIA Consultores Ltda. Mapped and acquired field data along seismic lines for delineation of geologic structures in subsurface. Measured stratigraphic sections, collected samples, and acquired surface gamma-ray data for SIPETROL S.A.
Spring 1998	Consultant Geologist	IGL - Ingenieria y Geotecnia Ltda. Mapped and delineated unstable zones along an alternate railroad pathway in the Department of Antioquia.
Fall 1997	Assistant Production geologist - Internship	OXY - Occidental Petroleum Co. Edited and prepared stratigraphic and structural cross-sections for production in the Caño Limón oil field. Also prepared well-log correlations, described well samples, and assisted in mud-logging and electric logs acquisition.
Spring 1997	Associate Instructor	Universidad Nacional de Colombia - Photogeology. Revised the historical record of flooding of the Magdalena River in the Departments of Santander, Cesar and Bolivar using aerial photographs for the environmental assessment of the Zapatos and Chilloa swamps.
Fall 1996	Assistant Instructor	Universidad Nacional de Colombia - Petrology. Prepared samples (hand specimens and thin sections) for igneous and metamorphic petrology laboratory and assisted the geology majors in rock-type identifications.
Summer 1996	Assistant Exploration geologist - Internship	OXY - Occidental Petroleum Co. Collected data for exploration prospects and prepared well-log correlations. Interpreted seismic data and prepared stratigraphic and structural cross-sections. Assisted in the estimation of OOIP and calculated possible and probable oil-reserves.
1996 - 1995	Assistant Instructor	Universidad Nacional de Colombia - Petrography and Optical mineralogy. Prepared samples (hand specimens and thin sections) for the igneous and metamorphic petrography and optical mineralogy classes and assisted the geology majors in rock-type and mineral identifications.
Summer 1995	Research Assistant	Universidad Nacional de Colombia -Crystallography and mineralogy. Prepared samples and cured the mineralogy collection.

PEER-REVIEWED PUBLICATIONS

1. Solano-Acosta, W., Schimmelmann, A., Mastalerz, M., and Arango, I., 2007. Diagenetic mineralization in Pennsylvanian coals from Indiana, USA: $^{13}\text{C}/^{12}\text{C}$ and $^{18}\text{O}/^{16}\text{O}$ implications for cleat origin and coalbed methane generation. International Journal of Coal Geology, in press.
2. Solano-Acosta, W., Mastalerz, M., and Schimmelmann, A., 2007. Cleats and their relation to geologic lineaments, and coalbed methane potential in Pennsylvanian coals in Indiana. International Journal of Coal Geology, in press.
3. Solano-Acosta, W., and Dutta, P.K., 2005. Unexpected trend in the compositional maturity of second-cycle sand. Sedimentary Geology, v.178:275-283.
4. Solano-Acosta, W., Mastalerz, M., Rupp, J.A., Schimmelmann, A., and Strapoc, D., 2005, Coal-bed gas potential in Pennsylvanian coal beds of Indiana. Proceedings of the 2005 International Coalbed Methane Symposium, Tuscaloosa, AL. Paper 0526.

CONFERENCE ABSTRACTS

1. Solano-Acosta, W., Mastalerz, M., and Rupp, J.A., 2004, Controls for Coalbed Methane Occurrence in Indiana. 1st Annual Illinois Basin Coalbed Symposium. November 2004. Evansville, IN.
2. Solano-Acosta, W., Mastalerz, M., Drobniak, A., and Rupp, J.A., 2004, Geologic Controls for CO₂ Sequestration and Coalbed Methane in Indiana Coals. GSA (Annual Meeting). November 2004. Denver, CO, USA.
3. Solano-Acosta, W., Mastalerz, M., and Schimmelmann, A., 2004, Experimental CO₂ Adsorption in Coal versus Particle Size: Implications for CO₂ Sequestration. AAPG-NE section meeting. October 2004, Columbus, OH, USA.
4. Radhakrishnan, P., Solano-Acosta, W., and Rupp, J.A., 2004, Sequestration of CO₂ in Various Geological Media: An Assessment of Potential Volumes in Indiana Using GIS Tools. AAPG-NE section meeting, October 2004. Columbus, OH, USA.
5. Solano-Acosta, W., Rupp, J.A., Mastalerz, M., and Schimmelmann, A., 2004, Enhanced coalbed methane recovery and CO₂ sequestration options in Indiana coals. 32nd International Geological Congress. August 2004, Florence, Italy.
6. Seyler, B., Frailey, S.M., Carr, T.R., Drahovzal, J.A., Nuttall, B.C., Rupp, J.A., Solano-Acosta, W., and Wickstrom, L.H., 2004, Use of Relational Database and GIS Tools to Assess Carbon Sequestration Volumes: The MIDCARB Database. AAPG (Annual Meeting). April 2004, Dallas, TX, USA.
7. Solano-Acosta, W., Radhakrishnan, P., and Rupp, J.A., 2004, An Assessment of Potential Carbon Sequestration Volumes in Indiana's Petroleum Fields, Aquifers, Unminable Coal Seams, and Shales. Third Annual Conference on Carbon Capture & Sequestration. May, 2004, Alexandria, VA, USA.
8. Solano-Acosta, W., Mastalerz, M., Rupp, J.A., and Schimmelmann, A., 2004, Sorption behavior of Indiana coals and their CO₂ sequestration potential. (Invited Speaker for Theme Session 8: Geological Carbon Sequestration: Analogs, Opportunities, and Risks) NE-SE GSA Joint Meeting 2004, Tyson's Corner, VA, USA.
9. Solano-Acosta, W., Hawkes, L., Mastalerz, M., Schimmelmann, A., Fong, J., Walker, R., and R. Burruss, 2003, Sorption behavior of Helium and Nitrogen in uncrushed coal cores under controlled pressure and temperature. GSA (Annual Meeting). November 2003, Seattle, WA, USA.
10. Walker, R., Mastalerz, M., Schimmelmann, A., Hawkes, L., Fong, J., and W. Solano-Acosta, 2003, Prediction of CO₂ sorption in coal seams using uncrushed coal cores under realistic P, T, and moisture conditions. TSOP (Annual Meeting). September 2003, Washington, D.C., USA.
11. Solano-Acosta, W., Rupp, J.A., Drobniak, A., and M. Mastalerz, 2003, Pennsylvanian System in Indiana: A complex target for CO₂ sequestration and coal bed methane recovery. AAPG-NE and SPE (joint meeting). September 2003, Pittsburgh, PA, USA.
12. Solano-Acosta, W., Zuppann, C.W., and J.A Rupp, 2003, Assessment of oil and gas fields in Indiana for CO₂ sequestration. AAPG (Annual Meeting). May 2003, Salt Lake City, UT, USA.
13. Wickstrom, L.H., McDonald, J., Riley, R.A., Carr, T.R., Nuttall, B., Rupp, J.A., Solano-Acosta, W., Zuppann, C.W., and B. Seyler, 2003, Online tools to evaluate oil and gas fields for CO₂ sequestration. AAPG (Annual Meeting). May 2003, Salt Lake City, UT, USA.
14. Carr, T.R., Wickstrom, L.H., Korose, C.P., Fisher, S., and W. Solano-Acosta, 2003, Online tools to evaluate saline aquifers for CO₂ sequestration. AAPG (Annual Meeting). May 2003, Salt Lake City, UT, USA.
15. Solano-Acosta, W., Rupp, J.A., and C.W. Zuppann, 2002, Estimating the CO₂ sequestration capacity of deep saline aquifers in southwestern Indiana. GSA (Annual Meeting). October 2002, Denver, CO, USA.
16. Solano-Acosta, W., Zuppann, C.W., Eaton, N.K., and R. Escolar, 2002, Estimating carbon dioxide sequestration potential in mature, multi-pay petroleum fields in Indiana. AAPG (North-Eastern Section). October 2002, Champaign-Urbana, IL, USA.
17. Eaton, N.K., Escolar, R., C.W. Zuppann, and W. Solano-Acosta, 2002, Petroleum well location maps: A geographic Information System (GIS) approach to petroleum mapping in Indiana. AAPG (North-Eastern Section). October 2002, Champaign-Urbana, IL, USA.

18. Solano-Acosta, W., and Eaton, N.K., 2002, Characterization of a deep saline aquifer for CO₂ sequestration in Indiana: an integrated Geology-GIS approach. GSA (North-Central and South Eastern Sections joint meeting). April 2002, Lexington, KY, USA.
19. Solano-Acosta, W., and Dutta, P.K., 2001, Chemical trends between cutler sandstone, precursor sand, and granitic source rock. GSA (Annual Meeting). Nov. 2001. Boston, MA, USA.
20. Solano-Acosta, W., and Dutta, P.K., 2000, First vs. second cycle sand: Does recycling always lead to maturity? GSA (Annual Meeting). November 2000. Reno, NV, USA.
21. Solano-Acosta, W., 2000, Climatic influence in controlling the authigenic mineralogy of volcanolithic sandstones. AAPG (Northeastern section). September 2000. London, ON, Canada.
22. Solano-Acosta, W. 2000, The Yaví Formation: an example of climatically induced poor quality reservoir. Sigma Xi Poster competition. Indiana State University, Terre Haute, IN, USA.
23. Solano-Acosta, W., 2000, Petrographic evidence for climatic and tectonic control on the arenites of the Yaví Formation in Colombia, South America. GSA (North-Central Section). April 2000. Indianapolis, IN, USA.

SHORT COURSES AND SEMINARS

- | | |
|------|---|
| 2007 | Deepwater reservoirs of California. Davis Miner and Don Lowe, April 1, 2007 AAPG Annual Meeting, Long Beach, CA. |
| 2005 | Basic Openhole Log Interpretation. Daniel Krygowski, September 16-17, 2005 AAPG-ES, Morgantown, WV. |
| 2005 | Devonian Stratigraphy and Hydrocarbon geology near U.S. Route 250 in West Virginia and Virginia. John M. Dennison, September 20-22, 2005 AAPG-ES, Field Trip. |
| 2005 | Coalbed Reservoir Gas-in-Place Analysis. Charles R. Nelson, May 17, 2005 International Coalbed Methane Symposium, Tuscaloosa, AL. |
| 2003 | Trenton and Black River carbonates in the Union Furnace area of Blair and Huntigdon Counties, Pennsylvania. September 10, AAPG-ES & SPE Joint Meeting, Field Trip. |
| 2003 | Coalbed Methane: Geologic and Engineering Principles. John P. Seidle (Sproule and Associates, Inc.) and George Hampton (Hampton and Associates), May 10, AAPG Annual Meeting, Salt Lake City, UT, USA. |
| 2003 | Coalbed Methane Exploration Strategies: Hydrogeologic Controls Critical for Exploration, Development, and Resource Assessment. Andrew R. Scott, May 5-6, International Coalbed Methane Symposium, The University of Alabama, Tuscaloosa, AL, USA. |
| 2003 | MSHA Training – James Craig, April 8. Indiana Geological Survey, Bloomington, IN. |
| 2003 | Creating ArcView Layouts and Printing with ArcPress (ArcGIS 8.2) - Infoshare. Nathan Eaton. January 24, Indiana University, Bloomington, IN. |
| 2002 | Access - Workshop. IT Training and Education. November 19-21, Dec 3-4. Indiana University, Bloomington IN. |
| 2002 | Migrating to ArcGIS - Infoshare. Nathan Eaton and Anna Radue. September 13. Indiana University, Bloomington, IN. |
| 2002 | Techniques in Sedimentology. Todd Thompson and Erik Kvale, November 7 – December 19, Department of Geological Sciences, Indiana University, Bloomington, IN. |
| 2002 | Applied Digital Subsurface Mapping. Petroleum Technology Transfer Council – Midwest Region, April 18-19, Mount Carmel, IL. Timothy Carr (Kansas University) and Hannes Leetaru (Illinois State Geological Survey) |
| 2002 | Pore Pressure Prediction in Practice. AAPG Department of Education, Richard Swarbrick and Martin Traugott (University of Durham, UK), March 14-15, Houston, TX. |

- 2002 Advanced Carbonate Seminar. Todd Thompson and Brian Keith, Department of Geological Sciences, Indiana University Bloomington.
- 2002 Carbonate Petrology Seminar. Robert Dodd, Department of Geological Sciences, Indiana University Bloomington.
- 2002 MSHA Training – James Craig, January 19. Indiana Geological Survey, Bloomington, IN.
- 2002 ARCGIS 8.1. ESRI Virtual Campus. Indiana Geological Survey, Bloomington, IN.
- 2001 Geological Society of America, Sequence Stratigraphy for Graduate Students, November 3-4, GSA Annual Meeting, Boston, MA.
- 1998 Fundamentación Geofísica (Geophysics Fundamentals - short course), Sep 28 - Oct 16, Universidad Nacional de Colombia, Bogotá – Colombia.